THE UNIVERSITY *of* EDINBURGH

Calcium phosphate substrate-directed osteogenic differentiation of mesenchymal stem cells

Kate Cameron

B.Sc Hons

University of Edinburgh

2013

Abstract

An increase in degenerative bone disease in an ageing population, combined with a rise in the number of patients suffering from bone defects caused by physical trauma, makes the repair of bone an issue of growing clinical relevance. Current treatments such as autografts and allografts have major drawbacks, including donor site morbidity, limited availability, disease transmission and immune rejection. To overcome these issues synthetic bone grafts have been developed to mimic the mineral phase of bone. Given the significant roles of silicon in bone growth and development there has been great interest in introducing silicon into synthetic bone grafts to enhance their bioactivity. Calcium phosphate based silicate containing grafts have demonstrated enhanced bioactivity, improved physical properties, enhanced protein adsorption and greater bone formation, when compared to non-silicated calcium phosphates such as hydroxyapatite. However, is not clear whether the increased bone formation associated with these materials is the result of greater osteoblast activity or a rise in numbers of osteoblasts resulting from activation and differentiation of stem/ progenitor cells. To answer this question, multipotent stem cells were cultured on silicate substituted calcium phosphate (Si-CaP) and hydroxyapatite (HA). Si-CaP promoted greater cell adhesion and enhanced proliferation when compared to HA. Cells differentiated along the osteogenic lineage on both substrates as evidenced by up regulation of osteoblast specific genes and proteins. However, cells on Si-CaP showed earlier and greater gene expression of all osteoblast genes examined, and greater protein production as detected by immunohistochemistry. Integrin gene expression analysis revealed up regulation of α and β subunits on both substrates during differentiation. Integrins α5 and β1 expression were greater on Si-CaP than on HA, suggesting preferential binding of fibronectin. The implication of these findings for tissue engineering is clear, suggesting these substrates may be utilized to control stem cell fate *in vivo* and *in vitro* without the need for osteogenic supplementation. Furthermore, the increased rate of differentiation seen on Si-CaP may enable the development of novel substrates for osteogenic differentiation of MSC, which may have significant impact in regenerative medicine.

Declaration

This thesis is the result of my own work and includes nothing that is the outcome of work done in collaboration, except where indicated in the text.

The work in this thesis has not been submitted for any other degree or professional qualification.

Kate Cameron

Table of Contents

List of figures and tables

Abbreviations

+OS	Osteogenic supplementation
ACAN	Aggrecan
ADMSC	Adipose derived mesenchymal stem cell
ALP	Alkaline phosphatase (enzyme)
ALPL	Alkaline phosphatase, tissue-nonspecific isozyme (gene)
APC	Allophycocyanin
B2M	β2 microglobulin
BGLAP	Bone gamma-carboxyglutamate (gla) protein
BMP	Bone morphogenetic protein
Ca^{2+}	Calcium
CD	Cluster of differentiation
CD105	Endoglin
CO_2	Carbon dioxide
COL10A1	Collagen, type X, alpha 1
COL1A1	Collagen, type I, alpha 1
COL2A1	Collagen, type II, alpha 1
DAPI	4',6-diamino-2-phenylindole
DMEM	Dulbecco's modified Eagle's medium
DMP1	Dentin matrix protein 1
DNA	Deoxyribonucleic acid
ECM	Extracellular matrix
FA	Focal adhesion
FACS	Fluorescence-activated cell sorting
FBS	Fetal bovine serum
FITC	Fluorescein isothiocyanate
HA	Hydroxyapatite
hES	Human embryonic stem cell
hES-MP	Human embryonic derived mesenchymal progenitor cell
M-CSF	Monocyte-colony stimulation factor 1
MFI	Mean fluorescence intensity
MPa	Megapascal
MSC	Bone marrow derived mesenchymal stem cell
OPG	Osteoprotegerin
OSX	Osterix / Sp7 transcription factor 7
PBS	Phosphate buffered saline

PCR	Polymerase chain reaction
PE	R-Phycoerythrin
PE Cy 5.5	R-Phycoerythrin cyanine dye conjugate
PerCP	Peridinin chlorophyll protein
PL	Tissue culture polystyrene
PPARG	Peroxisome proliferator-activated receptor gamma
PTH1R	Parathyroid hormone receptor 1
RANKL	Receptor activator of NF-kappa-B ligand
RGD	Arginyl glycyl aspartic acid
RNA	Ribonucleic acid
RUNX2	Runt related transcription factor 2
SD	Standard deviation
SEM	Scanning electron microscopy
SEM*	Srandard error of mean
Si-CaP	Silicate substituted calcium phosphate
SOX9	SRY-box containing gene 9
SSEA	Stage-specific embryonic antigen
TGF-β	transforming growth factor-β
TRA	keratan sulfate antigen

Acknowledgments

Firstly, I would like to thank my initial supervisors Dr Brendon Noble and Dr Tom Buckland for giving me the opportunity to study for a PhD and for providing the freedom to let me do it my way and learn from my own mistakes.

I've had the good fortune to receive support and guidance from others, particularly my second supervisor Dr Paul Travers for making my PhD a more enjoyable and rewarding experience, for providing support, the answers to many questions, asking many more and ensuring my sanity with an abundant supply of delicious bacon rolls.

I would like to thank the Engineering and Physical Sciences Research Council, not only for providing the funding which allowed me to undertake this research, but also for giving me the chance to attend exotic conferences and meet so many interesting people. I also wish to thank Apatech, my industrial collaborator, for funding, the supply of materials and providing the fantastic opportunity to work with them on industrial placement. Particular thanks go to Charlie, Agi and Egle, who helped to make it an extremely productive and entertaining experience, and to the Casal-Dominguez family for looking after me in London and making me feel at home in theirs.

To all the people in the labs at the University of Edinburgh who have helped me out over the years, especially Balta, Claire, Antonello, Kay, Ronnie, Stewart, Allison, Sudeh, Angela and Asim for their expertise and for making the lab a fun place to work. I would also like to thank Dr Steve Morely who inspired me to continue my academic career and for his continual support and advice.

Special thanks to my amazing family; to my grandparents most of whom are not around to see this day, I hope I have made you proud, and to Granddad Cameron for sticking around to see this finished. To my mum and dad for their moral support through the many ups and downs over the

past few years, thanks for keeping me going and for believing that I could do it, eventually! Thanks to Shona for being a competitive and hugely supportive big sister, for all her amazing cakes and for actually listening when I talk about science.

To all my friends, whom have all helped me in so many ways over the years, a massive thank you, particularly to Naomi, Fiona, Aoife, Dave, Solveig, Jo, Stu, Roddy, Agnes and Marta.

Thank you, to the staff and locals at the Victoria and A Room In The Town for being there at the start and the end and ensuring wine was always to hand!

Last but not least, thank you to Ben, who wouldn't let me quit, your support and encouragement, was worth more than I can express on paper.

Publications

Cameron K, Travers P, Chander C, Buckland T, Noble B. 2012. Directed osteogenic differentiation of human mesenchymal stem/ precursor cells on silicate substituted calcium phosphate. *Journal of Biomedical Materials Research Part A*. (Published 26th June 2012)

CHAPTER ONE: GENERAL INTRODUCTION

1.1 Regenerative medicine

As a consequence of ageing in the overall population, the number of people with degenerative diseases has increased significantly (Karen A Hing et al. 2001; Anon n.d.) with disease and injury of the skeletal system becoming a relevant and demanding biomedical issue. The regeneration of damaged skeletal tissues is therefore a major challenge in the field of regenerative medicine.

Defined as a "therapeutic intervention which replaces or regenerates cells, tissues or organs, to restore or establish normal function" (Ducheyne & Qiu 1999; Mason 2007) regenerative medicine is not one discipline alone, but instead covers a number of fields or strategies. Merging aspects of engineering and biology, the goal of regenerative medicine is to encompass the use of biomaterials, growth factors, and stem cells to restore function to failing organs.

Currently, many aspects of medicine are not truly "regenerative", instead they offer repair of damaged tissue or organs through surgery, surgical implantation of artificial tissue, replacement of the organ function e.g. insulin injections in diabetes or dialysis in kidney failure, or replacement of the damaged organs themselves through transplantation. These strategies though are far from ideal. For example, organ transplantation often involves immunosuppressant drugs, and artificial metal hips can induce inflammation in addition to becoming loose. Furthermore the demand for organs required for transplantation continues to outstrip supply (Fujita et al. 2003; NHS 2012a; Florence Barrère 2006). One method to replace the need for transplanted organs is to utilise biomaterials either to prevent further damage or, in combination with cells, to replace organs entirely (Habraken et al. 2007; Barrère et al. 2008).

Biomaterial scaffolds are being developed to provide mechanical support, serve as cell carriers, and also to actively influence cellular responses such

as cell attachment, proliferation and differentiation. Chemical modifications can be used to enhance the physical and biological properties of biomaterials (Nair et al. 2008; Zippel et al. 2010; Pietak & Sayer 2006; Fujita et al. 2003; Langstaff et al. 2001). Through the use of such biomaterials, it is hoped that damaged or diseased organs could be restored and allow the tissue to return to normal function.

1.2 Normal tissue homeostasis

Multiple cellular processes, including cellular proliferation, differentiation and death, maintain healthy tissue function in a process known as tissue homeostasis.

One of the most important means of tissue homeostasis is the on going removal and replacement of certain differentiated cells. This is described as cell turnover and is composed of three key stages:-

1. selected differentiated cells are continually eliminated,
2. adult stem cells or their daughter cells divide to replace the eliminated cells,
3. the new cells become functionally integrated with the tissue (Ramaswamy et al. 2008; Robbins & Cotran 1974; Tamai et al. 2007).

1.2.1 Bone homeostasis

Bone is a perfect example of a tissue that appears to be homeostatic, yet it is actually highly dynamic. In a process known as remodelling, bone is constantly resorbed and renewed in response to a variety of physical and chemical factors (Ponader et al. 2008; Wolff 1870; Atilgan et al. 2007).

This dynamic process occurs throughout the many different types of bone, and is coordinated by osteoclasts (cells that destroy bone) and osteoblasts (cells that form bone) as well as osteocytes within the bone matrix. This process is depicted in Figure 1.

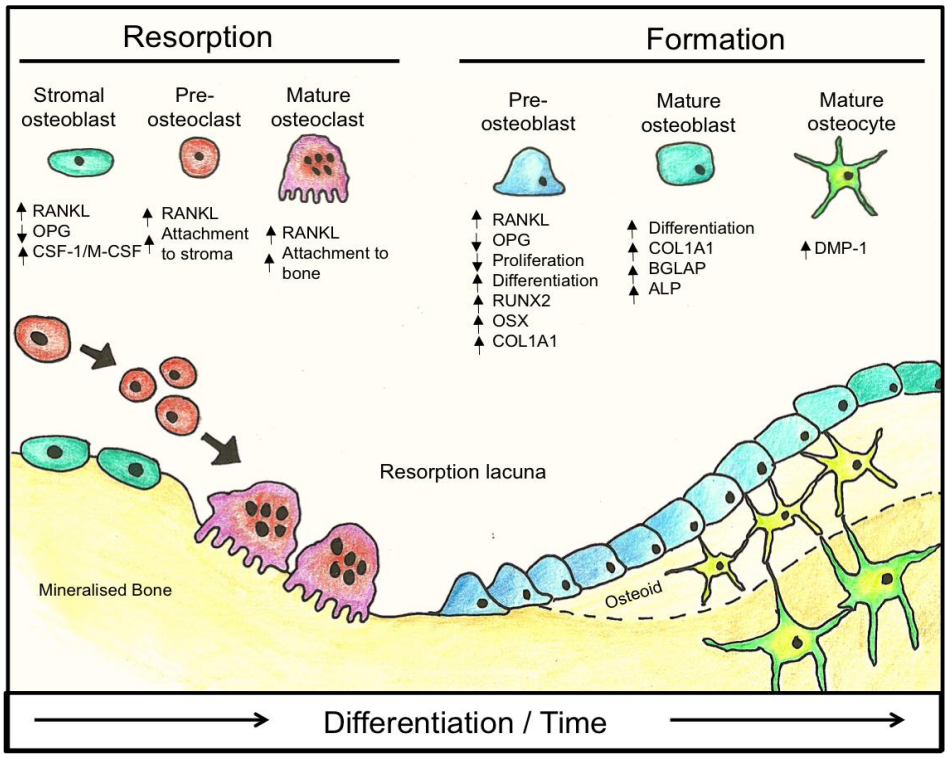

Figure 1: Illustration depicting bone remodelling.

Osteoclast and osteoblast differentiation from precursor cells, bone resorption and bone formation over time. RANKL - Receptor activator of nuclear factor κB ligand, OPG – osteeoprotegerin, RUNX2 - runt related transcription factor 2, OSX - osterix, COL1A1 - collagen type I, BGLAP - osteocalcin, ALP - alkaline phosphatase, DMP-1 - dentin matrix protein 1. Hand drawn image, annotated in Microsoft PowerPoint 2007.

During bone remodelling the activity of these cell types are matched, so that the amount of bone removed by osteoclasts is equal to the amount of bone formed by osteoblasts. This process occurs throughout adult life, maintaining the structure and strength of bone (Hench et al. 1971; Sims & Gooi 2008). However, like any other organ or tissue, this process can be disrupted through disease or injury. One of the most common and prevalent diseases of bone is osteoporosis, affecting approximately 3 million people in the UK (Shi 2004; NHS 2012b). Osteoporosis is caused by an imbalance in bone resorption and bone formation, where too much bone is resorbed and not renewed (Kolf, Cho & Tuan 2007b; Chamberlain et al. 2007; Crisan et al. 2008; Vodyanik et al. 2010; Haasters et al. 2009; Sanchez-Guijo et al. 2009; Yoshimura et al. 2006; Kozhevnikova et al. 2008; Jack et al.

2002; Dominici et al. 2006; Ohgushi et al. 2005; Orciani et al. 2010). Paget's disease of bone is also a result of over active bone resorption, but unlike osteoporosis, is followed by a compensatory increase in new bone formation, resulting in structurally disorganised bone (Kolf, Cho & Tuan 2007b; Chamberlain et al. 2007; Crisan et al. 2008; Barry & J. M. Murphy 2004; Boyd et al. 2009; Haasters et al. 2009; Kozhevnikova et al. 2008; Pittenger 1999; Jack et al. 2002; Dominici et al. 2006; Orciani et al. 2010). Osteopetrosis is an inherited disease affecting osteoclast differentiation and is characterised by an increase in skeletal mass, due to lack of resorption (Chamberlain et al. 2007; Kolf, Cho & Tuan 2007b; Crisan et al. 2008; Barry & J. M. Murphy 2004; Boyd et al. 2009; Haasters et al. 2009; Kozhevnikova et al. 2008; Pittenger 1999; Yoshimura et al. 2006; Blitterswijk et al. 2007; Foster et al. 2005; Jack et al. 2002; Dominici et al. 2006; Orciani et al. 2010).

Non-bone specific disorders, such as autoimmune disease and cancer can also affect bone. Although it is relatively uncommon for cancer to originate in bone, cancer can spread from another part of the body- termed metastatic cancer (Kolf, Cho & Tuan 2007b; Vodyanik et al. 2010; Jack et al. 2002; Tare et al. 2012). Bone can also be damaged through injury; it can be broken or fractured, usually caused by high force impact or stress. Being highly dynamic, in most cases bone can repair itself after minor fractures. Yet, in some cases bone cannot regenerate itself extensively or effectively enough, and additional assistance is needed. Bone itself is a highly complex organ, containing a variety of cell types and is composed of organic and inorganic matter. In order to successfully repair/ regenerate bone, its structure, formation and composition must be understood.

1.3 Bone

Bone achieves a variety of function through its complex structure:-

1. providing protection for vital organs including bone marrow,
2. serving mechanically as a support for soft tissue and attachment sites for the muscles,
3. being the major organ responsible for the maintenance of serum homeostasis (due to its ability to store several ions, especially calcium and phosphate), also functioning as the most abundant site of haematopoiesis (Crisan et al. 2008; Boyd et al. 2009; Jack et al. 2002).

The structure of bone is complex, both externally and internally, providing an extremely strong yet lightweight frame to keep the body supported. It is a composite of mineral and organic matrix, which confer structure and strength respectively. The mineral phase of bone is composed of calcium phosphate, largely in the form of hydroxyapatite ($Ca_{10}(PO_4)_6OH_2$) and the organic matrix of bone consists of a highly organised network of proteins, of which collagen type I is the main constituent.

1.3.1 Bone development

During embryonic development bone is formed via two separate processes, either intramembranous or endochondral ossification.

In intramembranous bone formation, mesenchymal progenitors condense and differentiate directly into osteoblasts. This process is closely coordinated by osteoclasts selectively resorbing bone, maintaining the proportions and structure of the marrow cavity and cortical bone as it grows

Occurring simultaneously is endochondral ossification, where the same progenitor cells first form cartilage, which undergoes mineralisation, vascular and osteoprogenitor invasion and extensive apoptosis. This sequential coordination of growth leads to the longitudinal lengthening of the bone.

Both endochondral and intramembranous ossification occur not only in long bones but also in the short, flat and irregular varieties. Although derived from a different embryonic origin (neural crest) the skull and facial bones are formed by both endochondral and intramembranous ossification in a similar manner (Chamberlain et al. 2007; Kolf, Cho & Tuan 2007b; Barry & J. M. Murphy 2004; Boyd et al. 2009; Haasters et al. 2009; Yoshimura et al. 2006; Pittenger 1999; Crisan et al. 2008).

1.3.2 Bone structure

Anatomically, long bones can be divided into different zones, which are shown in Figure 2:-

1. epiphysis (the rounded ends of long bones),
2. diaphysis (or midshaft) and the
3. metaphysis (development zone).

The epiphyses and methaphyses are formed at two independent ossification centres, separated by a layer of cartilage known as the epiphyseal plate or line. This layer is responsible for the longitudinal growth in long bones and is produced by proliferative cells and expanding cartilage. Below the epiphyseal plate, immature bone grows in the methaphysis. Extending between the methaphyses is the diaphysis, which provides mechanical stability. Within the diaphysis is the medullary cavity, filled with bone marrow. This cavity has two surfaces: the periosteal surface (external surface) and the endosteal surface (internal surface) covered by the periosteum and endosteum, respectively.

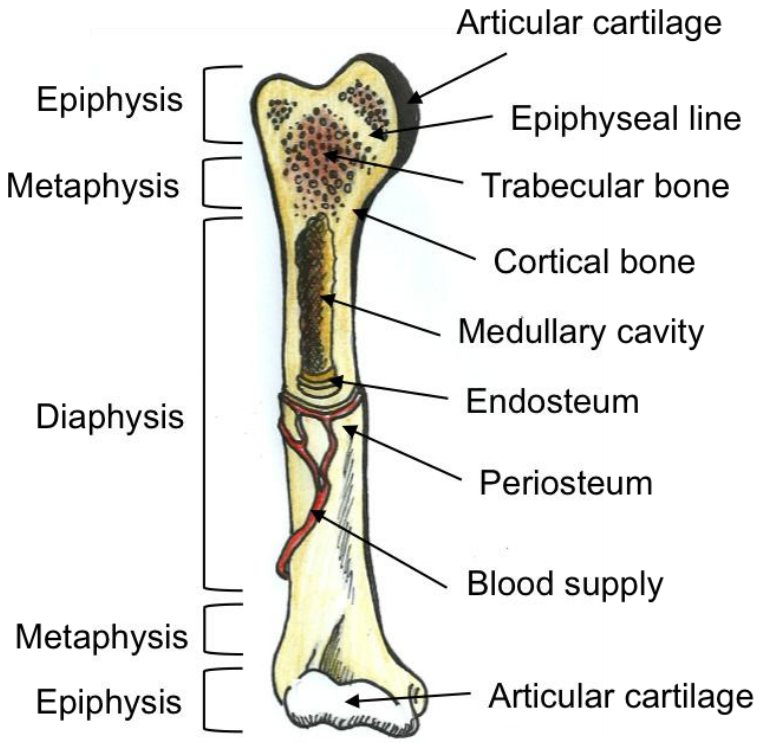

Figure 2: Illustrated anatomy of a long bone.

Anatomical depiction of a long bone structure and zones, highlighting the bone marrow filled medullary cavity, trabecular and cortical areas, the surrounding connective tissue layer (endosteum), vascular periosteum and articular cartilage. Hand drawn illustration annotated in Microsoft PowerPoint 2007.

Bone exists in two distinct forms, cortical and trabecular. Cortical bone is denser (5-10% porosity) than trabecular bone (50-90% porosity); hence its function is mainly mechanical and protective (Oishi & Ito-Dufros 2006). It exists in the outer shafts (diaphyses) of the long bones, and on the surface of small and flat bones.

Cortical bone is composed of densely packed collagen fibers that form concentric lamellae around central spaces called Haversian canals; each unit of Haversian canal and surrounding concentric lamellae is termed an osteon, as shown in Figure 3. Within Haversian canals are blood vessels, lymphatics, nerves and connective tissue (see Figure 3 inset). Between the lamellae and canals are lacunae that contain osteocytes, which are

connected to each other and the central canal by many smaller canal-like structures termed caniculi (Banas et al. 2007; Mitchell et al. 2005).

Trabecular or cancellous bone is less abundant but it is metabolically more active, being located near the epiphyses of long bones and the interior structure of small bones. Within cancellous bone there are interconnecting plates and bars called trabeculae, interconnected by marrow in a honeycomb like structure. The trabeculae are aligned along the lines of stress or mechanical force, adding considerably to its strength.

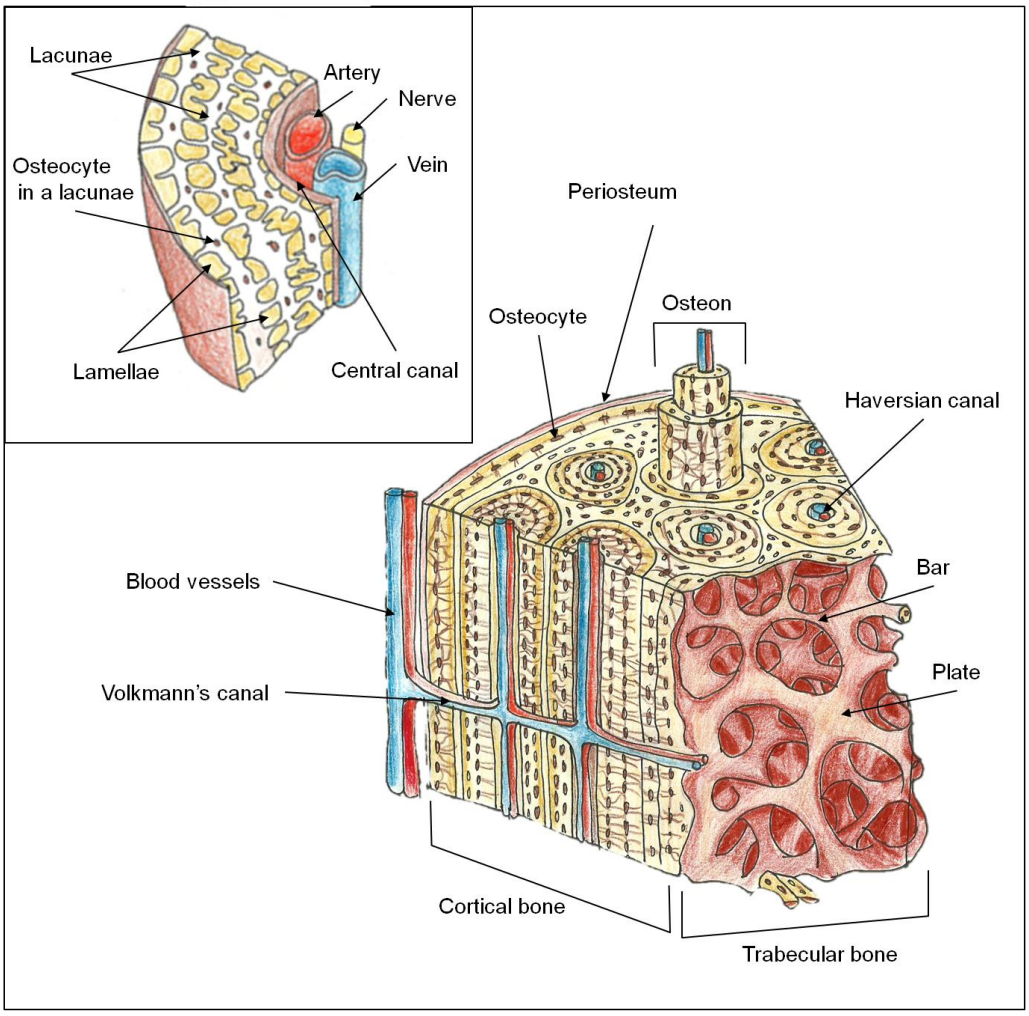

Figure 3: Illustrated cross section of compact and trabecular bone.

Bone microstructure, indicating osteons blood supply and cell types. Hand drawn figure annotated in Microsoft PowerPoint 2007. (Gronthos et al. 2003)

1.3.3 Periosteum and Blood supply

Surrounding most bones is a dense, fibrous, connective tissue called the periosteum. Beneath the periosteum exists a network of capillaries and vessels, which supply blood to the bone. Blood vessels penetrate the bone, through Volkmann's canals, which supply both cortical and trabecular bone forming a dense capillary network. Endothelial pericytes surround these vessels, these cells of mesenchymal origin are found throughout the microvasculature of connective tissue, nervous tissue and the lungs. Pericytes have the ability to contract and therefore regulate blood flow, but more recently it has been demonstrated that these cells can differentiate into a wide variety of cell types including bone-forming cells (osteoblasts) (Peister 2004).

1.3.4 Bone composition

Bone material itself is composed of two distinct phases: an organic matrix, mostly made of collagen, along with proteoglycans and several non-collagenous proteins, and the mineral phase which strengthens the organic phase with calcium salts.

1.3.4.1 Organic matrix

The organic matrix or 'osteoid' is composed of collagenous (90%) and non-collagenous proteins, synthesised by osteoblasts. The most abundant protein is collagen type I, which is characterized by its fibrous nature, with the fibrils in bone generally about 80–100 nm in diameter. Each fibril is made up of three polypeptide chains roughly 1000 amino acids long, wound together in a triple helix composed by two $\alpha 1$ chains and one $\alpha 2$ chain. Between these molecules there are small spaces (37.5nm) that are filled with hydroxyapatite crystals. The collagen fibrils are stabilised by inter and intra-molecular crosslinks, and the number and distribution of these crosslinks are thought to determine whether the tissue will mineralise (Chamberlain et al. 2007). In classic Ehlers-Danlos syndrome, mutations in the collagen type I gene *COL1A1* results in disruption of the stability of

triple helix formation, and as consequence can cause osteopenia or bone fragility (Péault et al. 2007).

Other constituents of the organic phase include proteoglycans and non-collagenous bone matrix proteins such as osteocalcin, osteopontin, osteonectin and fibronectin (Bentmann et al. 2010). Osteopontin and bone sialoprotein have an RGD (Arginyl, glycyl, aspartic acid) sequence that can be recognized by the $\alpha v\beta 3$ integrin receptor, which is involved in mediating cell attachment, activating cell signalling pathways and also involved in binding hydroxyapatite. *In vitro,* bone sialoprotein nucleates the formation of hydroxyapatite crystals whereas osteopontin inhibits the mineral growth (Pampena et al. 2004; Hunter et al. 1994). Osteocalcin is thought to play a role in mineralisation, is an inhibitor of osteoclast function, and is highly expressed by mature osteoblasts (Caetano-Lopes et al. 2007).

1.3.4.2 Bone Mineral

Several decades ago, De Jong demonstrated the similarities between synthetic apatite (hydroxyapatite) and mineral bone, using X-ray diffraction (de Jong 1926).

Since then, several differences have been demonstrated between hydroxyapatite (HA; $Ca_{10}(PO_4)_6 OH_2$), and the biological apatite that is present in bone tissue including composition, crystallinity, stoichiometry, physical and mechanical properties. Natural bone mineral incorporates numerous substitutions within the calcium phosphate lattice, including carbonate (CO_3^{2-}), sodium (Na^+), magnesium (Mg^{2+}), potassium (K^+), fluoride (F^-), chloride (Cl^-) ions and, also some trace elements such as silicon (Si^{4-}) strontium (Sr^{2+}), lead (Pb^{2+}), and barium (Ba^{2+}). These substitutions appear to be crucial to the biological activity and surface chemistry of bone (Pietak et al. 2007). In particular, trace levels of silicon in the form of silicate (SiO_4^{4-}) are known to be essential for normal growth and development of bone (Carlisle 1972; Schwarz & Milne 1972). The incorporation of these ions and elements have considerable influence on the physical, chemical, and physiological properties of bone (Kannan et al. 2008).

1.3.4.3 Bone cells and their origin

Three key cell types exist within bone: osteoblasts, osteocytes and osteoclasts, which are respectively involved in bone formation, maintenance and resorption.

1.3.4.3.1 Osteoblasts

Osteoblasts are responsible for producing the bone matrix, during embryonic bone formation and constantly facilitate the maintenance of new bone deposited in adults. Osteoblasts arise from multipotent mesenchymal stem cells (MSC) (Caplan 1991; Owen 1988), which prior to commitment to the osteoblast lineage, are capable of differentiation into other mesenchymal cells lineages such as adipocytes, and chondrocytes (Pittenger 1999). In vivo, MSC are induced to differentiate into osteoblasts through a variety of factors, including bone morphogenic proteins and other supporting cytokines (Lavery et al. 2009; Maegawa et al. 2007). As MSC differentiate along the osteogenic lineage they express a range of stage specific genes, shown in Figure 4

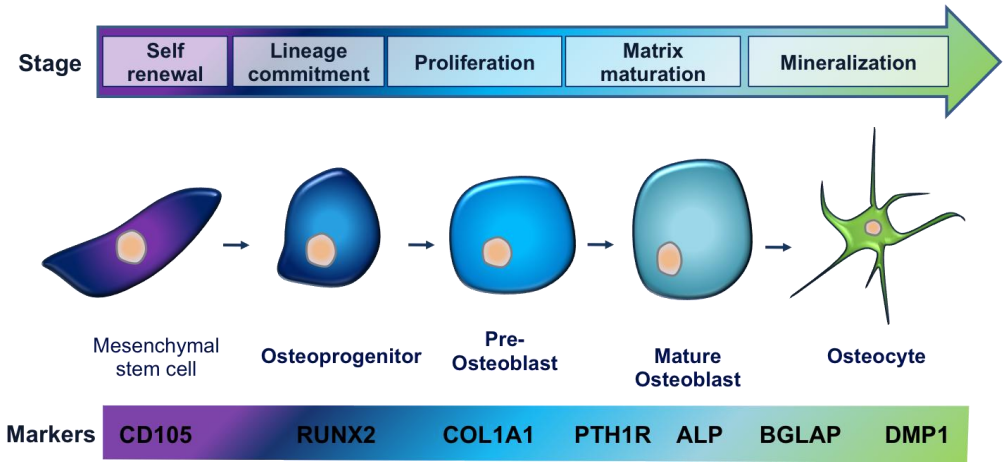

Figure 4: Diagram representing stages and markers of osteogenic differentiation.

Schematic diagram of growth and differentiation of osteoblasts, created using Microsoft PowerPoint 2007. CD105 – endoglin RUNX2 – runt-related transcription factor 2, COL1A1 – collagen type I, PTH1R- parathyroid hormone 1 receptor, ALP - alkaline phosphatase, BGLAP – Osteocalcin, DMP1 – dentin matrix protein 1.

Over a decade ago RUNX2 (also known as Cbfa-1) was identified as the key transcription factor controlling osteoblastogenesis. RUNX2, a member of the runt family of transcription factors, is expressed at the onset of skeletal development and is present in osteoblasts throughout their differentiation. RUNX2 has been shown to be both necessary and sufficient to direct MSC toward the osteoblast lineage (Marie 2008).

RUNX2 operates by binding to a Run consensus sequence; this sequence is present in the promoter of all major osteoblast genes (*COL1A1*, *OPN*, *BSP* and *BGLAP*) and regulates their expression (Yamaguchi et al. 2000). RUNX2 also inhibits the differentiation of MSC into adipocytic and chondrocytic lineages and also negatively controls osteoblast proliferation by acting upon the cell cycle by modulating expression of key kinases such as p85 PI3K (Caetano-Lopes et al. 2007; Komori 2006). Osterix is a zinc finger transcription factor, that acts downstream of RUNX2. Critical for osteoblast differentiation, osterix deficient mice show a complete absence of osteoblasts resulting in defective bone formation (Nakashima et al. 2002). Both RUNX2 and osterix act together to mediate the expression of collagen type I and alkaline phosphatase (Marie 2008; Datta et al. 2008). Pre-osteoblast and mature osteoblasts synthesise and secrete bone matrix proteins of which collagen type I is the major component, constituting up to 90% of the organic matrix (Mackie 2003). Along with collagen, osteoblasts manufacture various non-collagenous proteins such as bone sialoprotein (*BSP*), osteopontin (*OPN*) and osteocalcin (*BGLAP*). Osteocalcin is an osteoblast-specific protein that is characterized by 3-gammacarboxyglutamic acid residues; 1,25 OH Vitamin D3 enhances its synthesis and its expression reflects metabolic cellular activity. Of the *de novo* synthesized osteocalcin, 60%–90% is incorporated into the bone matrix where it binds to hydroxyapatite during matrix mineralisation. The remainder is released into the circulation where it can be measured as a sensitive marker of bone formation (Cantatore et al. 2004).
Tissue non-specific alkaline phosphatase is produced by osteoblasts, and is highly expressed prior to mineralisation (Robison 1923). Alkaline phosphatase is activated by several transcription factors, including RUNX2 and osterix, and is commonly used to quantify osteoblast differentiaton *in*

vitro (E. E. Golub & Boesze-Battaglia 2007).

1.3.4.3.2 Osteoclasts

Osteoclasts are large multinucleated cells, uniquely capable of resorbing bone, and remodeling its structure. Originating from circulating haematopoietic myelomonocytic precursors, which undergo differentiation, multinucleation and activation in a process termed osteoclastogenesis (Sims & Gooi 2008; Yavropoulou & Yovos 2008). The process of osteoclastogenesis is a complex sequence of events, which cannot take place in the absence of osteoblasts (Civitelli 2008). In a similar manner to osteoblastogenesis, osteoclast differentiation is regulated by a number of both systemic and locally produced hormones and cytokines. Osteoclastogenesis is crucially dependent upon two key cytokines; RANKL (receptor activator of nuclear factor κB ligand) and M-CSF (monocyte-colony stimulation factor). M-CSF is critical for the proliferation of osteoclast progenitors, while RANKL directly controls the differentiation process by binding to its receptor, RANK. The precise mechanism by which RANK induces osteoclastogenesis is not fully understood, but it is known to trigger an internal cascade resulting in the expression of new receptors (Katagiri & Takahashi 2002; Datta et al. 2008). Osteoblasts can produce a decoy receptor, osteoprotegerin (OPG), which blocks RANK/ RANKL interaction by binding RANKL, and therefore prevents osteoclast differentiation and activation; this negative feedback loop is essential in controlling bone remodelling (Theoleyre et al. 2004). In a further level of regulation, the osteoclast, can release its own cytokines, which then feedback to control its own activity, or control the activity of osteoblasts as they deposit new bone (Civitelli 2008).

1.3.4.3.3 Osteocytes

Until recently the role osteocytes has been enigmatic and contentious, however the existing view is that the osteocytes are responsible for detecting and responding to mechanical loading and initiating the bone adaptation process (You et al. 2008). Osteocytes are non-proliferative, yet

are the most abundant cell type in bone, constituting 90% of all adult bone cells (Tate et al. 2004).

Osteocytes are formed when terminally differentiated osteoblasts are left behind during osteoid production then encased in the mineralised osteoid, a process that occurs relatively infrequently (10-20%). As the osteocyte is entombed it maintains contact with advancing osteoblasts by extending cellular processes, whilst the osteoid becomes mineralised under the control of enzymes (Palumbo et al. 1990; Datta et al. 2008). Significant changes occur, as an osteoblast becomes an osteocyte. Initially its shape changes considerably, from a rounded cobblestone like cell into a stellate shape with multiple long processes. Despite being encased in individual lacunae, osteocytes form an impressive network connected to each other through these dendritic processes in canaliculi. These canaliculi are fluid filled spaces containing a mesh of proteoglycans and extra cellular proteins, and are thought to permit signalling between osteocytes. This system of fluid filled canals allows the osteocytes to detect mechanical loading and respond to this external stimulus by sending signals to osteoclasts and osteoblasts, regulating bone remodelling (You et al. 2008; Noble 2008; Kurata et al. 2007). Osteocytes are thought to orchestrate local bone remodelling through the action of local and systemic, stimulatory and inhibitory signals (Tate et al. 2004). A number of matrix proteins, including dentin matrix protein 1 (DMP1), increase in expression once the osteoblast begins to transform into an osteocyte (Mikami et al. 2008; Toyosawa et al. 2001; Hao et al. 2004). DMP1 is an extracellular matrix protein member of the SIBLING family and has been implicated in osteocyte function and signalling. It is also critical for matrix mineralisation, and mutations in the gene can lead to rickets and osteomalacia (Feng et al. 2006).

1.4 Bone tissue engineering

Successful tissue engineering must integrate principles of engineering and life sciences to develop functional biological substitutes that restore, maintain or improve tissue functions (Zippel et al. 2010).

The first documented attempt at tissue engineering was bone grafting, described by a Dutch surgeon in 1668 when a bone defect in a soldier's

cranium was filled with a piece of skull from a dog. The bone was removed 2 years later at the patients request, so that he could be allowed back to church, which had denounced him because of the xenotransplant (van Meekeren 1730).

1.5 Bone grafting

Bone grafting is a surgical procedure where missing or damaged bone is repaired or replaced using natural or synthetic materials; from the patient's own body, from a donor, or using synthetic or natural substitutes such as hydroxyapatite, collagen or coral. Bone grafts can be used to repair fractures that fail to heal properly or voids that are extremely complex.

In order to critically evaluate bone grafts, biocompatibility must first be addressed. The biocompatibility of a bone graft or bone graft substitute refers to the ability to perform as a substrate that will support the appropriate cellular activity, including the facilitation of molecular and mechanical signalling systems, whilst allowing integration and conduction of new bone growth, without eliciting any undesirable local or systemic responses in the eventual host (Williams 2008).
The biocompatibility of any bone graft material can be determined by the following factors:-

1. Osteogenic potential, or the presence of osteogenic cells, which have the unique potential to differentiate and form new bone. Graft materials that contain cells or act as cell carriers, contain the ability to form bone *de novo.* This new bone formation utilises the transplanted cells' ability to initiate early healing uniting the graft and existing bone. This osteogenic potential is commonly seen in autogenously transplanted bone and bone marrow (Lucarelli et al. 2004).

2. Osteoinduction is the ability of a matrix or scaffold to initiate new bone formation. Generally, this occurs through neovasculature ingrowth and infiltration of osteogenic precursor cells then the graft becomes completely

resorbed in a process known as 'creeping substitution' (Yaszemski et al. 1996).
Materials such as allograft bone, demineralised bone matrix, collagen and calcium phosphate based ceramics are all examples of osteoinductive bone substitutes that can be completely resorbed (Giannoudis et al. 2005).

3. Osteoconduction, an osteoconductive surface is one that permits bone growth on its surface or within pores or channels (Albrektsson & Johansson 2001).
Some bone and cartilage graft substitutes encourage such ingrowth through the inclusion of factors or biochemical substances, such as bone morphogenic proteins (Giannoudis & Einhorn 2009), transforming growth factors (Nicoll et al. 1997), and fibroblast growth factors (Joung et al. 2008).

4. Structural integrity provides support for the bone as it encounters natural mechanical stresses. Biomechanical strength is a key element for bone grafts, due to the daily stresses, which the skeleton undergoes.
Metal implants composed of titanium, provide excellent structural integrity yet possess no osteogenic properties. Cancellous bone grafts provide initial poor structural strength, but this changes as a result of osteointegration. Cortical bone grafts provide excellent initial structural integrity, which once remodelled and osteointegration occurs, can lose up to one third of its strength (Williams 2008; Schimandle & Boden 1997).

1.5.1 Autografts

Autografts are considered the gold standard for bone grafting, due to their osteogenic potential, osteoconductivity, osteoinductivity and if cortical bone is used, structural strength. Furthermore, there are minimal immunological issues associated as a result of complete histo-compatibility (Marsh 2003).
Autografts can be cancellous, cortical, cortico-cancellous or free vascularised bone; each type of autograft can contain viable cells and proteins within the bone matrix.

Cancellous autografts are the most common bone grafts used due to their superior osteoinduction and osteoconduction. They promote rapid revascularisation and incorporation, have a strong osteogenic potential due to viable cells and bone inducing growth factors contained within. Cancellous autografts also exhibit good moulding characteristics, but must be used alongside either internal or external fixation as they are lacking in support (Drosse et al. 2008).

Cortico-cancellous autografts, also harvested from the iliac crest, but in strips or small chips, contain some cortical component. This element provides more support and structure, often used to bridge a small defect (Marsh 2003).

Structural or cortical autografts, commonly from the fibula, are used to fill discrete defects, providing immediate mechanical and structural support until bone can regenerate, restoring structural integrity. Despite the advantage of mechanical strength, cortical bone is biologically less desirable as it contains fewer osteogenic cells, due to the absence of bone marrow. Furthermore, the cells that are present are less likely to survive, as they are embedded in a more compact matrix and are shielded from factors and nutrients (Dinopoulos et al. 2012). The lower surface area, per weight of cortical bone also limits the amount of new bone that can form, and from which proteins can pass. Finally, cortical bone is more resistant to vascularisation and remodelling, necessary factors for healing and developing strength (Drosse et al. 2008; Marsh 2003; Schimandle & Boden 1997).

Despite the excellent success rate and low risk of disease transmission of autologous cancellous grafts, they have several disadvantages: including issues of resorption and viability, associated donor-site morbidity, limited availability, risk of infection and fracture, the need for a second procedure with potential increased blood loss, prolonged operating time and poor aesthetic outcome (Dinopoulos et al. 2012).

1.5.2 Allografts

Allografts, or bone grafts from a different patient, are most frequently used for spinal fusion surgery. In recent years the use of allograft has increased, due to improvements in the methods of procurement, preparation and storage, and also through the desire to avoid donor site morbidity associated with autogenous bone. Often used as large structural sections or smaller cortico-cancellous chips, allografts provide an osteoconductive scaffold for new repair. The abundant supply, varying shape and volume has also fuelled its recent increase in use, with larger allografts being possible where autografting would not be considered.

Unlike autografts, allografts do not contain osteogenic cells and therefore undergo a much slower incorporation. Issues also exist concerning the possibility of infection and even infectious disease transmission (Drosse et al. 2008; Marsh 2003; Schimandle & Boden 1997).

Allogeneic bone is available in many forms including: demineralised bone matrix, small cancellous fragments or chips, cortico-cancellous and cortical grafts, and osteochondral and various bone segments. Due to the removal of live cells via irradiation or freeze-drying processing, allografts have little or no osteogenicity. But they do have osteoconductive and reduced osteoinductive properties (Keating & McQueen 2001).

However, there are issues of transmission of viral, especially human immunodeficiency virus (HIV), hepatitis B and C, bacterial infections, malignancy, immunogenicity and rejections reactions, as well as high cost of harvesting, processing and conservation of allogeneic grafts (Dinopoulos et al. 2012). The overall infection rates using structural allograft have been reported to be as high as 12.8% (Dick & Strauch 1994).

1.5.3 Demineralised bone matrix

Demineralised bone matrix (DBM), is a form of allograft in which the mineral phase has been extracted, leaving proteins, growth factors and collagen. Available widely as powders, pastes or putties and can be moulded into deficient areas: both within fractures and non-union sites (areas of bone which have failed to heal a significant time after injury). The

presence of low molecular weight glycoproteins such as bone morphogenic protein (BMP) underlies the osteoconductivity of demineralised bone matrix. Residing in the extracellular matrix of bone and constituting only 0.1% by weight of all bone proteins, BMP is known to simulate the migration, differentiation and activity of osteoprogenitors. Along with BMP, demineralised bone matrix also contains a number of other growth factors known to stimulate osteoprogenitors, such as transforming growth factor-β (TGF-β). Numerous studies have shown TGF-β is of significant importance in the control of differentiation of marrow precursor cells, which are capable of forming chondrocytes, adipocytes and osteoblasts (Drosse et al. 2008; Marsh 2003; Massagué 1998). However, demineralised bone matrix can be variable in osteoinductive and osteoconductive properties due to donor variability and also provides no structural support.

1.5.4 Cell based strategies

1.5.4.1 Bone marrow aspirate

Bone marrow aspirate can be utilised to stimulate bone formation alone, or in combination with a bone graft. Aspirate can be obtained from the iliac crest in a minimally invasive process (Schade & Roukis 2008).
Bone marrow aspirate contains osteogenic and haematopoetic progenitor cells and once transplanted is capable of enhancing bone formation, and revascularisation respectively. However, concentration and quality of progenitor cells vary significantly between individuals, especially in elderly patients (Huibregtse et al. 2000; D'Ippolito et al. 1999).

1.5.4.2 Mesenchymal stem cells

Bone marrow aspirate can be centrifuged to separate cells from plasma, reducing the volume of material that is replaced. Within the fractionated aspirate are multiple cell types of the osteo-progenitor lineage and all are implicated in bone repair (Drosse et al. 2008). Mesenchymal stem cells are the key stem cells involved in bone regeneration and can be readily isolated from bone marrow (Pittenger 1999). Once purified these cells can be expanded, differentiated and delivered together with a bone graft to

enhance repair. The process of MSC differentiation into osteoblasts and ultimately osteocytes, also known as osteogenesis, is activated and regulated by a variety of soluble factors and physical environment *in vivo*.

1.5.4.3 Soluble factor based osteogenesis

Mesenchymal stem cells can be induced to differentiate into osteoblasts *in vitro* through the addition of soluble factors such as; glucocorticoids, growth factors, hormones, and vitamins (Pittenger. 1999). The most commonly used combination of soluble factors to promote osteogenic differentiation *in vitro* is dexamethasone, ascorbic acid and β-glycerophosphate. Each constituent stimulates or supports osteogenic differentiation of mesenchymal stem cells *in vitro*.

1.5.4.3.1 Dexamethasone

Dexamethasone is a synthetic corticosteroid, although not found naturally in the body, imitates the actions of various glucocorticoids such as cortisol, oestradiol, testosterone, vitamin D3 (B et al. 2001). Glucocorticoids influence the expression of many genes, through binding to specific activator proteins. In the absence of a glucocorticoid, activator proteins are kept in the cytosol and cannot bind DNA. *In vitro* dexamethasone can stimulate osteogenic differentiation of MSC and acts at multiple points in the differentiation process to stimulate osteoblastic maturation; transforming MSC morphology from spindle-shaped to cuboidal, increasing alkaline phosphatase (ALP) activity and enhancing mineralisation (R. M. Porter et al. 2003b). It was previously thought that dexamethasone was required for MSC differentiation *in vitro* however; multiple studies have demonstrated it enhances osteogenic differentiation but is not essential (Bellows et al. 1990; Benayahu et al. 1989; Kamalia et al. 1992). Long-term intake of dexamethasone *in vivo* can result in osteoporosis, through decreased osteoblast activity (Mazziotti et al. 2006). This contradictory effect is thought to be due to the anti-proliferative effects of this corticoid (Jaiswal et al. 1998).

1.5.4.3.2 Ascorbic acid

Ascorbic acid is an essential component in the synthesis of hydroxyproline and hydroxylysine, two key components required to stabilize the collagen triple helix and to form intermolecular crosslinks within collagen (Murad et al. 1981). Several studies have shown that ascorbic acid concentration is correlated with collagen production by osteoblasts (Aronow et al. 1990; Franceschi & Iyer 1992) and also linked to enhanced ALP activity (Franceschi et al. 2009). However, a contradictory study has found that ALP expression by MSC cultured in presence of ascorbic acid was no different than the same cells cultured in the absence of ascorbic acid (Gronthos et al. 1994).

1.5.4.3.3 βglycerophosphate

βglycerophosphate provides a source of organic phosphate ions that promote mineralisation *in vitro* (Chung et al. 1992). Despite several studies, the exact mechanism behind this mineralisation remains unclear, but may be related to the ability of ALP to hydrolyse organic phosphate and release inorganic phosphate (Y. L. Chang et al. 2000).

1.5.4.3.4 Other soluble factors

Numerous soluble factors are also known to activate or have a significant effect on osteogenic differentiation, a summary of the most commonly studied factors are listed in Table 1.

Table 1: Soluble factors known to influence osteogenic differentiation

Factor	**Effect(s)**
Bone morphogenic proteins	A family of cytokines that stimulates proliferation of osteoblasts and causes increased matrix production and have also been seen to induce MSC differentiation to osteoblasts.
Fibroblast growth factors	A family of growth factors that stimulates proliferation of MSCs and osteoblasts.
Insulin-like growth factors	A family of growth factors that stimulates proliferation of osteoblasts and induces matrix production.
Platelet-derived growth factor	A growth factor, it stimulates proliferation osteoblasts, it has also been implicated in bone resorption.
Transforming growth factor-β	A growth factor, can initiate differentiation of MSCs to chondrocytes, and may also induce chondrocyte and osteoblast proliferation. Since, like PDGF, it has been seen to enhance bone resorption at certain concentrations, it may play a role in coupling formation and resorption activities.
Epidermal growth factor	A growth factor, it stimulates chondrocyte proliferation while decreasing the cells' ability to synthesise matrix components.
Parathyroid hormone	A single chain polypeptide, it causes the release of calcium from the bone matrix as well as induces osteoclast differentiation from precursor cells. It is also thought to inhibit osteoblast function.
Estrogen	A hormone, it has a complex effect on bone, with the final outcome being decreased bone resorption by osteoclasts.
Vitamin D	A vitamin that has a complex effect on bone formation, thought to regulate the synthesis of other molecules, and has been reported to influence both bone resorption and matrix mineralisation.

Adapted from (Sikavitsas et al. 2001)

3.1.1.1 . Non-soluble factor driven osteogenesis

A complex extracellular matrix (ECM) composed of multiple proteins surrounds MSC and osteoblasts *in vivo,* and can modulate cellular interactions and receptor binding (Mathews et al. 2012). The composition and mechanics of this microenvironment also plays a vital role in MSC maintenance and osteogenesis.

1.5.4.3.5 Physical forces

The skeleton is constantly exposed to physical forces, including compression, strain and shear stress. These physical stimuli have long known to play a role in bone remodelling. In 1982, Wolff found mechanical loading of bone ensures that the bone is constantly renewed and repaired (Wolff & Wessinghage 1991).

Osteocytes are thought to be the major cell type involved in translating external mechanical strain into biochemical signals, and are known to orchestrate bone remodelling (Bonewald 2006). However, osteoblasts are also mechanically receptive. Several studies have shown increased proliferation and differentiation of osteoblasts in response to mechanical strain and shear stress (Sikavitsas et al. 2001). In the absence of mechanical loading, osteoblast proliferation and matrix production decreases and osteoclast activity increases (Nabavi et al. 2011). Such studies in microgravity and simulated microgravity may explain the significant bone loss associated with spaceflight (Vico et al. 1998).

Electromagnetic fields and ultrasound have also been shown to enhance fracture repair, although the molecular mechanism responsible is not yet fully understood (Dyson 1983; Li et al. 2006).

1.5.4.3.6 Engineered substrates

Recent advances in material synthesis and processing have enabled a wide range of synthetic and natural materials to examine the effect of physical forces on MSC and osteogenesis. Using a variety of techniques and

materials including; lithography, micro printing and nano-tubes, researchers have investigated the influence of patterned surfaces on cell adhesion and differentiation. MSC on disordered patterned surfaces differentiated into osteoblasts in the absence of soluble osteogenic factors (Dalby et al. 2007). The shapes of nano-islands were also shown to direct cell fate (Kilian et al. 2010), through control over the cellular cytoskeleton; MSC attached to larger islands of adhesive ligands, which permitted greater cell spreading preferentially differentiated into osteoblasts, whereas cells on smaller islands preventing cell spreading differentiated into adipocytes (McBeath et al. 2004). This work indicated that lineage commitment was regulated by RhoA-ERK-MAPK pathway. Altering the dimensions of cross-sectional nanotubes affected osteogenic differentiation of MSC, in the absence of osteogenic inducing media. Larger tubes induced cell spreading, cytoskeletal stress and osteoblast differentiation (S. Oh et al. 2009).

In a landmark study, MSC assumed differential morphology and gene expression when cultured on polyacrylamide gels with varying moduli. MSC showed lineage specification depending on the substrate mechanics, in the absence of any known inducing soluble factors. Reflecting the *in vivo* matrix elasticity - soft substrates supported differentiation along the neural lineage, intermediate substrates resulted in cells of the myogenic lineage, and stiffer substrates differentiated cells along the osteogenic lineage (Engler et al. 2006). Cues provided by the matrix mechanics were thought to occur via the cells ability to sense the matrix elasticity and generatinon of intracellular signals based on this force.

Altering the surface chemistry of surfaces has been also shown to be sufficient to direct MSC differentiation (Benoit et al. 2008). Unmodified and methyl ($–CH_3$) modified surfaces maintained MSC multipotency, hydroxyl (–OH) and carboxyl (–COOH) modified surfaces promoted chondrogenic differentiation, and amino ($–NH_2$), silane ($–SH_4$) modified surfaces promoted ostegengenic differentiation (Curran et al. 2006). These engineered substrates that contain cues to facilitate MSC differentiation along the osteoblastic pathway provide insight into the molecular mechanisms controlling cell fate but also may enable the further development of novel substrates for tissue engineered bone regeneration.

1.5.5 Bone graft substitutes

Both synthetic materials and alternative natural matrices have been utilised in the design and manufacture of bone graft substitutes, making it largely possible to incorporate many properties of an ideal biomaterial. This has led to a superior class of tissue-engineered products, with enhanced biocompatibility. Manufactured bone grafts represent a much more abundant source of graft materials that do not depend upon bone banks, and are not limited by the volume of tissue that can be removed autonomously. Furthermore, this approach eliminates many of the problems associated with traditional bone grafts, such as infection, or disease transmission.

1.5.5.1 *Natural materials*

Natural bone graft substitutes largely consist of components found in bone, such as the extracellular matrix, collagen, hyaluronic acid and hydroxyapatite. These biodegradable materials have the advantage of being bioactive, biocompatible and represent natural body constituents providing adhesive surfaces for cells.
Other natural materials are derived from plants, animals or insects: cellulose, chitosan and silk respectively (Muzzarelli 2009).
Some disadvantages of using natural materials over synthetic products include limited control over physicochemical properties; degradation is difficult to control along with sterilisation and purification. There is also the risk of pathogenic or viral infection when isolating from differing sources. Despite these drawbacks, recently chitosan and hyaluronic have become commercially available and appear to possess well-characterised and reproducible properties (Stoop2008; Dawson et al 2008).

1.5.5.2 Collagen

Bone is naturally very rich in collagen, known to contribute to mineralisation, vascular ingrowth and has excellent growth factor binding

capacity. As a result, collagen has become one of the most exploited natural polymers for orthopaedic applications and combined with hydroxyapatite, is clinically available under the trade names SunMax, Legato and Collagraft (SunMax n.d.; Legato n.d.; Zimmer n.d.).
Collagen alone is a poor bone graft material; however, when combined with growth factors, hydroxyapatite, or osteoprogenitor precursors, it can significantly enhance the incorporation of grafts. These commercially available collagens are traditionally extracted from animal tissues and can contain different types of collagen. Therefore, these products can be contaminated with potential immunogenic and infective agents (Xu et al. 2011).

1.5.5.3 Synthetic bone graft substitutes

Synthetic bone graft substitutes represent a much larger class of biomaterials. This group encompasses metals, synthetic polymers and synthetically altered ceramics. Major advantages include design flexibility and elimination of disease transmission. Moreover, synthetic materials can be processed into many different forms to suit their use, such as scaffolds, fibers, sheets, blocks or even microspheres (Drosseet al. 2008; Marsh 2003).

1.5.5.4 Synthetic polymer based bone graft substitutes

Widely variable in design, structure and composition, synthetic polymers represent a vast group of bone graft substitutes. The most commonly used synthetic polymers are the poly-hydroxyl acids; these include polylactic acid (PLA), polyglycolic acid (PGA) and polylactide-co-glycoride (PLGA). These materials gradually degrade by hydrolysis into water and soluble oligomers, both of which are removed from the implant site. PLA/ PGA/ PLGA scaffolds are currently used in orthopaedics and tissue engineering technologies. Several types of cells have been successfully grown on PLA/ PLGA scaffolds including MC3T3-E1 osteoprogenitor cells; osteoblasts, chondrocytes and bone marrow derived stromal cells. Nonetheless, synthetic polymers inherently have low bioactivity and

require biological, chemical or physical modification to achieve an appropriate cellular response (Dawson 2008).

1.5.5.5 Drug Release Polymers

Growth factors can be introduced into polymers to improve their biocompatibility and bioactivity. Growth factors can be delivered either through direct incorporation or through encapsulation. A variety of scaffold materials have been used to deliver growth factors including natural and synthetic polymers. This approach has shown great promise, with increased cell proliferation and differentiation leading to increased biocompatibility (Quaglia 2008; Sokolsky-Papkov et al. 2007; Habraken et al. 2007). Growth factors however, are expensive and several doses may be required to achieve any therapeutic effect (Kumada & Zhang 2010). Furthermore, the effects of long-term implantation of materials containing supra-physiologic doses of growth factors remain unknown (Kretlow et al. 2009).

1.5.5.6 Calcium phosphate based synthetic ceramics

Calcium phosphate based ceramics are considered to be one of the most promising materials for bone tissue engineering due to their bone-like composition and mechanical properties. Synthetically manufactured calcium phosphate based bone grafts provide an osteoconductive and inductive material without any of the disadvantages associated with autografts and allografts.

1.5.5.7 Hydroxyapatite

Synthetic hydroxyapatite (HA) and β-tricalcium phosphate (β-TCP) are two forms of calcium phosphate currently used in fracture fixing, spinal fixation, the treatment of bone defects (Karin A Hing et al. 2007; Ogose et al. 2006) and also as coatings on metallic and polymeric substrates to promote osseointegration and firm implant fixation (Shepperd & Apthorp

2005). Both compounds can be artificially synthesised through low temperature aqueous chemistry (Langstaff et al. 2001).

In vitro, both HA and β-TCP have been shown to promote the proliferation and differentiation of osteoblasts (Huan & J. Chang 2009; K A Hing et al. 1998), and to encourage osteogenic differentiation of bone marrow derived (Arinzeh et al. 2005) and adipose derived mesenchymal stem cells (Q. Liu et al. 2008). Both compounds have been shown to encourage new bone ingrowth *in vivo* (Anon n.d.; Karen A Hing et al. 2001), forming a strong bond with existing bone, a property that is unique to bioactive ceramics (Mason 2007; Ducheyne & Qiu 1999). β-TCP is reported to have greater bioactivity due to enhanced biodegradation rates when compared to stoichiometric HA, which has a more limited reactivity (NHS 2012a; Fujita et al. 2003; Florence Barrère 2006). Without cellular or cortical support HA is naturally brittle, with low fracture resistance due to its chemical and structural, crystalline composition. This can make it inefficient in applications requiring significant impact, torsional, bending or shear stress. Furthermore, HA has an extremely low resorbability, which can affect stability in the long term, as it is not properly remodelled (Barrère et al. 2008; Habraken et al. 2007).

Biological apatite is not stoichiometric, instead it has multiple ionic substitutions (as described previously in section 1.3.4.2) which disrupt the lattice, making it unstable. HA's qualities can be improved through the addition of compounds or ionic substitution. These modifications have been the focus of many scientific studies (Zippel et al. 2010; Nair et al. 2008; Pietak & Sayer 2006; Fujita et al. 2003; Langstaff et al. 2001).

The addition of ions, such as Niobium and Zinc has been shown to lower toxicity and promotes calcification of hydroxyapatite-based materials (Robbins & Cotran 1974; Ramaswamy et al. 2008; Tamai et al. 2007). Other studies have incorporated compounds such as Pamidronate and sulphate particles with some success (Wolff 1870; Ponader et al. 2008; Atilgan et al. 2007).

Bioactive glass ceramics are calcium phosphate based, and contain specific proportions of SiO_2 Na_2O CaO and P_2O_5. The inclusion of these compounds results in a bioactive substrate, capable of forming intimate bonds to bone. Larry Hench originally developed Bioglass in 1971, as a bone graft substitute for Vietnam veterans (Sims & Gooi 2008; Hench et al. 1971).

Since then Bioglass is clinically used in multiple forms, each containing varying proportions of ions (NHS 2012b; Shi 2004). These different compositions result in varying bioactivity, allowing degradation rates and bonding capabilities to be tightly controlled. *In vitro* studies of Bioglass have shown its dissolution products contain high levels of silicon, known to stimulate osteogenesis and protein production (Marie & Kassem 2011; Valerio et al. 2004; Xynos et al. 2001). The key disadvantage of Bioglass is its mechanical weakness and low bending strength. As a result Bioglass is not appropriate for load bearing applications (Krane 1977; Shi 2004).

1.5.5.8 Silicon

After oxygen, silicon is the next most abundant element in the earth's crust. The presence of silicon in mammalian systems is relatively variable, yet essential for multiple organ functions (Tolar et al. 2004; Schwarz & Milne 1972). In particular, silicon is present in high levels in extracellular components, implying a role in biological cross-linking that could contribute to the resilience and structure of connective tissue (Theill et al. 2002; Pietak et al. 2007; Bagi 2005). Silicon is essential in early bio-mineralisation and calcification (Rodan 1992; Carlisle 1972; Yaszemski et al. 1996). Silicon deficiencies in chicks and rats showed deformities in skeletal development and regulation (Shapiro 2008; Duivenvoorden et al. 2008; Gans & Northcutt 1983; Pietak et al. 2007). Furthermore, low dietary intake of silicon has been linked to low bone mineral density, whilst dietary supplementation of silicon shows stimulatory effects on cartilage and inhibits the physiological resorption process (Schulmerich 2008; Ramaswamy et al. 2008). Aqueous silicon has been demonstrated to increase osteoblast proliferation, differentiation and protein production *in vitro* (Datta et al. 2008; Reffitt et al. 2003; Keeting et al. 1992).

1.5.5.9 Silicate substituted calcium phosphate

Given the significant roles of silicon in bone growth and development there has been great interest in introducing silicon into synthetic bone grafts to enhance their bioactivity (Weiner & Traub 1986; Pietak et al. 2007). Silicon

in the form of silicate (SiO_4^{4-}) can be introduced to these materials in a variety of concentrations.

Wet chemical methods involve silicon as a chemical carrier, such as tetraethyl-, propyl- or ortho- silicate. Solid state or hydrothermal methods apply extremely high temperatures, exceeding 700°C, sintering the materials together (Malfait et al. 2007; Tang et al. 2005; Reid et al. 2006). Either of these processes can result in differing forms of silicon substitution, including octo-calcium phosphate, and tri-calcium phosphate, either in α or β forms (Langstaff et al. 2001). The content can also be carefully regulated, resulting in reproducible and accurate percentage weight.

The biological performance of silicate-substituted calcium phosphates has been well studied, *in vivo* and *in vitro*.

Actifuse is a commercially available and clinically used silicon substituted calcium phosphate (Si-CaP). It was specifically designed to incorporate silicon at a similar level to that seen in bone (0.8% wt) (K A Hing et al. 2004a).

In vivo studies on Si-CaP demonstrated (up to 14.5% compared to HA) greater, more dense (Wheeler et al. 2007) bone ingrowth (Patel et al. 2002; Patel et al. 2005), more stable (Karin A Hing et al. 2007) bone graft and enhanced bone remodelling (A. E. Porter, Patel, et al. 2004b), no inflammatory response (Wheeler et al. 2007)

In vitro studies have shown to enhance osteoblast adhesion, proliferation, protein production, and enhanced mineralisation (Thian et al. 2007; Bjerre et al. 2008; Zou et al. 2009; Ponader et al. 2008; Balamurugan et al. 2008).

1.5.5.10 Biological reactivity of calcium phosphates

When a calcium phosphate based bone graft is implanted, a series of reactions occur at the graft–tissue interface that will determine the bioactivity and ultimately how well the material is integrated into the surrounding bone. The dynamic reactions required to result in successful remodelling of a bone graft are shown in Table 2.

Table 2: Stages of bone graft integration upon implantation

Implantation
Dissolution of ions
Biomimetic apatite layer formation
Protein adsorption
Cell migration
Cell attachment
Cell proliferation
Cell differentiation
Matrix production
Matrix mineralisation
Graft remodelling

Shortly after implantation, both HA and Si-CaP based bone grafts lose calcium and phosphate ions from their structure in a process known as dissolution. This results in an enhanced concentration of ions next to the graft-bone interface that react to form a biologically equivalent, carbonated HA layer on the graft materials surface, termed an apatite layer. The bioactivity of a substrate can be directly linked to the rate and composition of this biomimetic layer (Chou et al. 2004). Multiple *in vitro* and *in vivo* studies, have examined dissolution rates and apatite layer formation of both Si-CaP and HA (LeGeros et al. 2003; A. E. Porter, Botelho, et al. 2004a; A. E. Porter et al. 2003a). Stoichiometric HA has an extremely slow dissolution rate, the slowest of all calcium phosphates (Ducheyne et al. 1993), and as a result forms an apatite layer much later when compared to substituted calcium phosphates (Ducheyne & Qiu 1999). Substitution in the form of silicate, in particular (Si-CaP), decreases the time taken to form an apatite layer (Gibson et al. 2009). Studies have demonstrated that the silicon ions released form Si-CaP were capable of stimulating apatite precipitation, even in the presence of bacterial inhibitors known to prevent calcium phosphate precipitation (Damen & Cate 1992). Dissolution of Si-CaP not only releases calcium and phosphate into the surrounding environment, but also silicate ions (Botelho et al. 2002). This release of silicate into the extracellular environment may play an additional role in promoting

biological activity. As discussed previously, silicate has dose-dependent effects on osteoblast differentiation, proliferation and protein synthesis, and mineralisation. This silicate release, coupled with an enhanced apatite formation rate, may lead to enhanced binding of key proteins involved in cell attachment.

1.5.6 Protien adsorption

Protein adsorption is the process of accumulation and binding of protein to a surface. This occurs rapidly in implanted calcium phosphate bone grafts, which adsorb proteins from blood. Protein adsorption aids the recruitment and osteoblastic differentiation of MSC, which ultimately results in remodelling of newly synthesised bone at the implant site. This biological response of a bone graft is dependent upon the species, quantity and conformation of the proteins adsorbed (K A Hing 2005). A wide variety of proteins have been shown to adsorb onto biomaterials *in vivo*, including bone sialoprotein, collagens, fibrinogen, fibronectin, laminin, osteopontin, thrombin, thrombospondin and vitronectin (Combes & Rey 2002; Alford & Hankenson 2006).

In order to examine the effect of proteins on MSC and osteoblast adhesion, proliferation and differentiation, experiments consisting of cell cultures on dishes coated with extracellular matrix proteins are currently used. Results have shown that cells adhere to proteins with differing affinity; osteoblasts adhere preferentially to fibronectin, compared to collagen type I and vitronectin (Gronthos et al. 1997). Furthermore, studies have demonstrated that collagen; fibronectin and vitronectin in particular are readily adsorbed onto Si-CaP and HA *in vivo* (Guth, Campion, Buckland & Hing 2010b; Blunn n.d.). Although both substrates adsorb proteins, studies have shown that a greater quantity of protein is adsorbed in a preferential binding conformation on Si-CaP, compared to HA (Pietak et al. 2007; Botelho 2005; Karin A Hing et al. 2006). The adsorbed protein layer will subsequently mediate the interaction of the implanted graft with local cells and migrating progenitor cells and attachment of these cells are dependent upon adhesion molecules present on the cell surface. Integrins are the

predominant receptor involved in cell adhesion to extracellular proteins (Siebers et al. 2005).

1.6 Integrins

Integrins are membrane-spanning proteins that couple the cell to its extracellular environment and allow signalling across the cell membrane in both directions. Integrins are composed of two glycoprotein subunits, the α chain and the βchain, which are non-covalently bound. Each chain spans the cell membrane, containing cytoplasmic, transmembranous and intracellular domains. Each αand βchain contains disulfide bridges, but can differ vastly in length. The αchain is 1008-1152 amino acids long, and the β chain 770, amino acids in length (Siebers et al. 2005). The basic structure of an integrin and its subunits are depicted in Figure 5.

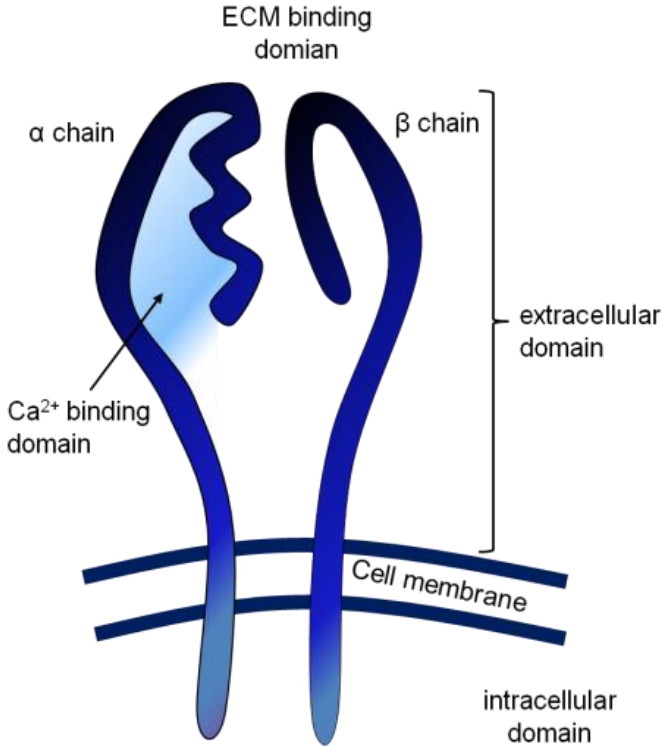

Figure 5: Integrin subunit structure and domains.

Illustration depicting the extracelluar and intracellular areas of integrin subunits, highlighting calcium (Ca2+) binding domain, and extracelluar matrix (ECM) binding domain. Integrins allow bidirectional signalling, transducing information from the external environment into the cell and from within the cell to its surroundings. Figure was created using Microsoft PowerPoint 2007.

1.6.1 Integrin signalling

Integrins bind to specific recognition sequences in proteins, such as the arginine, glycine, aspartic acid (RGD) binding domain of fibronectin or the glycine-phenylalanine-hydroxyproline-glycine-glutamine-arginine (GFOGER) binding domain of collagen type I (García & Reyes 2005). These binding sites are also affected by the proteins structure and many integrins also require secondary binding sites to achieve maximum signal function (Danen et al. 1995). Individually, integrin binding to the ECM is relatively weak however; ligand binding activates clustering of multiple integrins, forming a larger signalling complex. Within this complex, a variety of adapter proteins connect integrins to the cytoskeleton, shown in Figure 6.

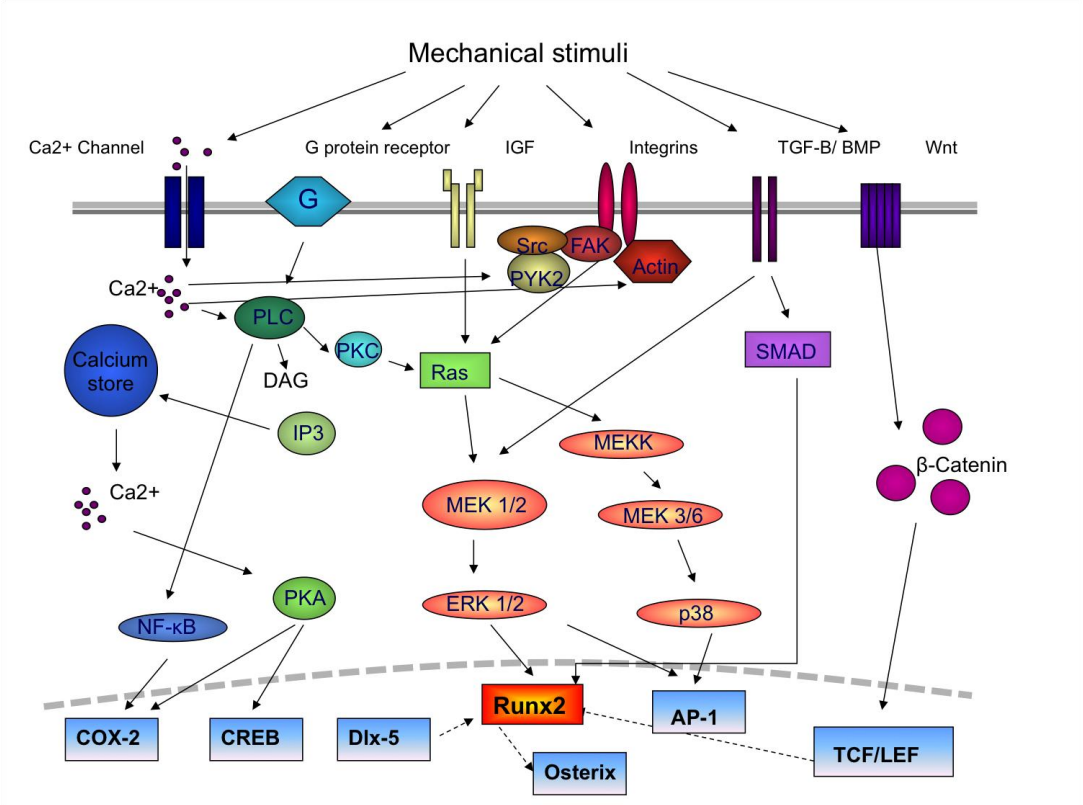

Figure 6: Major signalling pathways involved in mechanical stimulation of osteogenic differentiation.

Figure drawn using Microsoft powerpoint 2007, adapted from (Papachroni et al. 2009). Membrane-bound receptors including Ca2+ channels, G-proteins, integrins, IGF, TGF-β, BMP and Wntreceptors can be stimulated by extracellular forces, inducting activation of several transcription factors, which regulate osteoblast differentiation. AP-1 and RUNX2 are induced mainly through MAPK and SMADs pathways. RUNX2 is also stimulated via the Wnt pathway, involving β-catenin and TCF or LEF factors. PLC–PKA pathway contributes to NF-κB, Cox-2 and CREB induction. Abbreviations: IGF – insulin like growth factor receptor, AP-1- activator protein-1, FAK - focal adhesion kinase, IP3 - inositol (1,4,5)-trisphosphate, MEKK - MAPK kinase kinase, PKA - protein kinase A, PKC - protein kinase C, PLC - phospholipase C, PYK2 - proline-rich tyrosine kinase 2.

Large clusters of integrins and signalling molecules form focal adhesion complexes, which are essential to cell attachment (Eleniste & Bruzzaniti 2012). Focal adhesions these are the contact points between cells and the substrate and dynamically link the ECM to intracellular actin, facilitating cell spreading and migration. Figure 7shows an osteoblast attached to Si-

CaP with mature focal adhesions directly connected to actin filaments. In combination with other receptors, these adhesive clusters can activate intracellular pathways critical to proliferation, migration, and differentiation (Giancotti 1999).

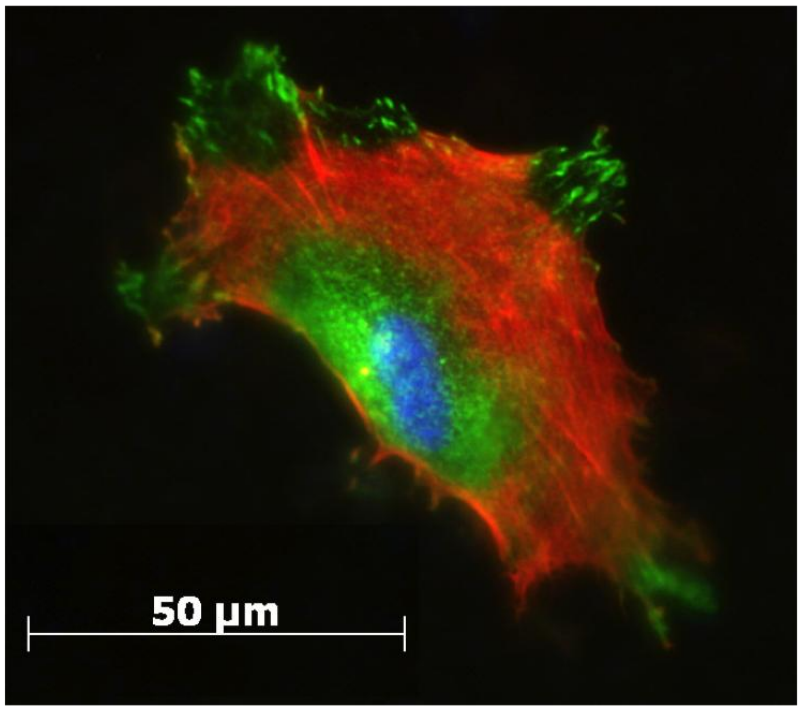

Figure 7: Osteoblast attached to Si-CaP with multiple focal adhesions.

Immunostained osteoblast attached to silicate substituted calcium phosphate (Si-CaP), actin (red), Vinculin (green) DAPI (blue) scale bar represents 50 µm.

Due to these multifunctional properties integrins have been extensively studied and as a result have become one of the best understood cell adhesion receptors since their recognition around 15 years ago (Hemler 1999). The mammalian set of integrins is composed of 18 αand 8 βsubunits, which assemble to form 24 distinct integrins, shown in Table 3.

Table 3: Selected integrins, subunits, ligands and expression.

Subunits		Binds to	Expression
β1	α1	Collagens, Laminins	Bone cells, cultured osteoblastic cells, activated T-cells, monocytes, melanoma cells and smooth muscle cells
	α2	Collagens, Laminins	Bone cells, cultured osteoblastic cells, B and T lymphocytes, platelets, fibroblasts, endothelial cells and melanoma cells
	α3	Laminins, Fibronectin, Thrombospondin	Cultured osteoblastic cells, B- lymphocytes, kidney glomerulus and most cultured cell lines
	α4	Fibronectin VCAM	Cultured osteoblastic cells, lymphocytes, monocytes, eosinophils, NK-cells and thymocytes
	α5	Fibronectin	Bone cells, cultured osteoblastic cells, memory-T-cells, monocytes, platelets and fibroblasts
	α6	Laminins	Platelets, lymphocytes, monocytes, thymocytes and epithelial cells
	α7	Laminins	Skeletal and cardiac muscle at specific stages during muscle development and melanoma cells
	α8	Fibronectin, Tenascin	Adult skeletal muscle, visceral smooth muscle, skin and corneal epithelial cells, hepatocytes
	α9	Tenascin	
	α10	Collagens	
	α11	Collagens	
β3	αv	Fibronectin, Vitronectin, Fibrinogen, Thrombospondin	Bone cells, cultured osteoblastic cells, endothelial cells, some B-cells, platelets and monocytes
β4	α6	Laminins	Immature thymocytes, squamous epithelia, subsets of endothelial cells, Schwann cells and fibroblasts in the peripheral nervous system
β5	αv	Tenascin	Cultured osteoblastic cells, hepatoma cells, fibroblasts and carcinoma cells
β6	αv	Vitronectin	Carcinoma cells
β7	α4	Fibronectin, Tenascin	Leukocytes (directed to the Peyer's patches of the gut)
β8	αv	Collagens, Fibronectin, Laminins	Mature synapses of central nervous system

1.7 Aims and Objectives

Understanding the interaction between bone grafts and stem cells has a key role in improving the success of orthopedic devices. Ideally, a substrate should not only support, but actively drive osteogenic differentiation. Silicon is known to play an essential role in bone formation and can stimulate gene and protein expression in osteoblasts. The inclusion of silicon into calcium phosphates, in particular silicate substituted calcium phosphate (Si-CaP), has shown enhanced bone formation *in vivo*, when compared to hydroxyapatite (HA).
This thesis will therefore examine the hypothesis that the superior bone formation associated with Si-CaP is a result of activating osteogenic differentiation of mesenchymal stem cells.

This will be achieved by the following:

- The optimisation of dense disc manufacture of Si-CaP and HA for in vitro testing.
- Characterisation of mesenchymal stem cells from three different sources.
- An investigation into the effects of Si-CaP and HA upon these mesenchymal stem cells, compared to soluble factors known to drive osteogenic differentiation.
- The evaluation of possible mechanisms behind how stem cells transduce signals from Si-CaP and HA.

CHAPTER TWO: MATERIALS AND METHODS

Unless otherwise stated, all chemicals were purchased from Sigma-Aldrich, UK. All tissue culture reagents were purchased from Invitrogen, UK and all tissue culture plastics from Corning, UK. All tissue culture procedures were performed in a Class 2, HEPA filtered, laminar flow hood, using sterile equipment.

2.1 General solutions

All solutions are made in distilled water unless otherwise stated.

50 X TAE:	24.2 % (w/ v) Tris base 5.71 % (v/ v) Glacial acetic acid 1.86 % (w/ v) EDTA
10 X loading dye:	0.25% (w/ v) Bromophenol blue 0.25% (w/ v) Xylene cyanol 25% (v/ v) Ficoll
Digestion solution:	1 mg/ ml Collagenase II 3.5 % BSA in un-supplemented DMEM
Red blood lysis buffer: chloride	Solution A: 0.83 % (w/ v) ammonium Solution B: 2.059 % (w/ v) Tris base 9 parts of solution A are added to 1 part of solution B and the pH is adjusted pH to 7.65 with 1M hydrochloric acid
EDTA solution:	37.2 % (w/ v) EDTA (pH 7.4)
PBS-EDTA:	50 % (v/ v) PBS, 50 % (v/ v) EDTA solution

2.2 Cell Culture

The media referred to as 'growth media' consists of Dulbecco's Modified Eagle's Medium – high glucose (DMEM), supplemented with 10% (v/ v) Fetal bovine serum (FBS), L-glutamine (2 mM) (Gibco, UK), penicillin (100 IU/ ml) and streptomycin (100 µg/ ml) (Gibco, UK).

2.2.1 Human Bone Marrow Derived Mesenchymal Stem Cell Isolation And Culture

Following written consent from the patients and approval from the local ethical committee, (study number: 2002/ R/ OST/ 02). Human femoral head tissue was obtained from a total of five patients who had undergone elective arthroplasty, who did not have viral infections (Hepatitis or AIDS), and where tissue was not suitable for bone banking. The tissue samples were allocated an anonymous number based on the chronological order of the sample collection, shown in Table 4.

Table 4: Patient details and passage at which cells were used.

Patient number	Age at date of surgery	Sex	Passage
559	50	Female	P3 - P10
582	79	Female	P2 - P11
596	74	Female	P3 - P9
623	57	Male	P3 - P10
633	70	Male	P3 -P7

Tissue samples were stored in sterile phosphate buffered saline (PBS) at 4°C, directly after surgery. The MSC isolation protocol used was as previously described by (Tremoleda et al. 2008) with minor modifications from (Gronthos & Zannettino 2008) and (Gundle & Joyner 1995) and was started within 4 hours post-surgery.

Using bone cutters and a blunt ended scalpel, the trabecular bone was removed from the femoral head and placed in a 50 ml Falcon tube. Then 9

ml of growth media was added to the bone chips, which were pipetted up and down for approximately 1 minute with a 5 ml pipette (Corning, USA). Large bone fragments were allowed to settle to the bottom of the 50 ml Falcon tube and the supernatant, containing cells, was transferred to a 50 ml Falcon tube. This process was repeated twice using 5 ml of growth media and the supernatants combined. The tube containing the supernatants was allowed to settle and the upper layer containing fat was removed. The remaining portion was transferred to a 25 cm^2 tissue culture flask (Corning, USA). The cells were maintained undisturbed for 4 days, in a humidified air incubator at 37°C with 5% (v/ v) carbon dioxide (CO_2). After this time, non-adherent cells were removed by washing twice with 5 ml of PBS, before 5 ml of fresh growth media was added.

The growth media was refreshed every two or three days. Once the cells reached approximately 80% confluence, they were washed twice with PBS, and passaged by adding 1 ml of trypsin solution (2.5 mg/ ml) in PBS (Invitrogen, UK). After up to 15 minutes incubation with trypsin at 37°C, 9 ml of growth media was added to the flasks. The flasks were tapped hard on each side to lift cells off the bottom of the flask, once in suspension the cells were centrifuged at 1000 rpm for 5 minutes and media removed. The cells were resuspended in 10 ml of growth media and were added to new tissue culture flasks (75 cm^2). The flasks were then incubated and refreshed with new growth media as before.

2.2.2 Human Embryonic Derived Mesenchymal Progenitor Cells

Human embryonic Stem Cell derived Mesenchymal Progenitor cells (hES-MP) (Cellartis, UK) were cultured according to methods provided by Cellartis. Cells were cultured on 0.1% gelatin coated 75 cm^2 flasks in growth media, with the addition of 1µg/ ml of basic fibroblast growth factor (bFGF) and incubated at 37°C with 5% (v/ v) CO_2. The media was changed with fresh growth media at regular intervals three times every 7 days. When the cells were confluent, they were washed twice in PBS and passaged by adding 1 ml of 2.5 mg/ ml trypsin solution in PBS. After 5 minutes incubation at 37°C, 9 ml of growth media was added to each of the flasks. The cell suspension was centrifuged at 1000 rpm for 5 minutes and media

removed. The cells were counted and resuspended in accordance with recommendations given by Cellartis, flasks were then incubated and media changed as before.

2.2.3 Human adipose derived mesenchymal stem cell isolation and culture

All human adipose derived cells were extracted and processed by Dr Christopher West, and were received at P1 or P3.
After written consent from the patients and approval from the local ethical committee (South East Scotland Research Ethics Committee 03 (SESREC03), Study number: 10/ S1103/ 45), human lipoaspirate or whole fat was obtained from patients who had undergone plastic surgery for cosmetic reasons. Tissue was collected from two patients. The tissue samples were allocated an anonymous number based on the chronological order of the sample collection, shown in Table 5.

Table 5: Patient details and passage at which cells were used.

Patient number	Age at time of surgery	Sex	Type of tissue	Passage
ADP 14	43	Female	Whole fat	P1-P10
ADP 17	23	Female	Lipoaspirate	P3-P10

All tissue samples were stored at 4°C, directly after surgery and processed within 24 hours.
The growth media was refreshed every two to three days. Once the cells were approximately 80 % confluent, they were washed twice with PBS, and passaged by adding 1 ml of trypsin solution (2.5 mg/ ml) in PBS (Invitrogen, UK). After up to 15 minutes incubation at 37°C, 9 ml of growth media was added to the flasks. The cell suspension was centrifuged at 1000 rpm for 5 minutes and the supernatant removed. The cells were resuspended in 10 ml of growth media and were added to new tissue culture flasks (75 cm^2). The flasks were then incubated and refreshed with new growth media as before.

2.2.4 Differentiation conditions

All cell types were induced along the adipogenic, osteogenic and chondrogenic lineages using the following differentiation media.

2.2.4.1 Adipogenic differentiation

DMEM supplemented with 10% FBS, 1 μM dexamethasone, 100 μM indomethacin, 1 μg/ ml of insulin, and 500 μM 3-isobutyl-l-methylxanthine. The cultures were maintained for 3 weeks and the culture medium was replaced every two to three days.

2.2.4.2 Osteogenic differentiation

DMEM containing 100 nM dexamethasone, 50 μg/ ml L-ascorbic acid 2-phosphate, and 10 mM βglycerophosphate. The cultures were maintained for 3 weeks and the culture medium was replaced every two to three days.

2.2.4.3 Chondrogenic differentiation

DMEM supplemented with 10 ng/ ml of recombinant human TGF-β, 100 nM dexamethasone, 6 μg/ ml of insulin, 50 μg/ ml L- ascorbic acid 2-phosphate, 1 mM sodium pyruvate, 6 μg/ ml of transferrin, and 0.40 mM proline. The cultures were maintained for 3 weeks and the culture medium was replaced every two to three days.

2.3 Flow cytometry

Cells were trypsinised, resuspended in PBS containing 1% FBS, and incubated with the appropriate antibodies (shown in Table 6) for 30 minutes at 4°C. Then 1 ml of PBS was added per tube and centrifuged at 1000 rpm for 5 minutes, excess liquid was removed and cells resuspended in 0.1% sodium azide in PBS and run through the flow cytometry machine. Cells were gated by their forward- and side-scatter characteristics and to exclude dead cells. A minimum of ten thousand events was acquired using a FACS Calibur Flow Cytometry System (Becton, Dickinson and Company, Biosciences, San Diego, CA) and analysed using FlowJo (Treestar, Inc., San Carlos, CA).

Table 6: Antibodies for Flow cytometry and isotype controls.

Antibody Specificity	Conjugate	Supplier	Catalogue number	Dilution	Isotype
CD90	Biotin	BD Pharmingen	555594	1/ 50	IgG_1 κ
	FITC	BD Pharmingen	561969	1/ 50	IgG_1 κ
CD73	PE	BD Pharmingen	550257	1/ 20	IgG_1 κ
	APC	BD Pharmingen	560847	1/ 20	IgG_1 κ
CD105	APC	eBioscience	17-1057	1/ 50	IgG_1 κ
	FITC	BD Pharmingen	56443	1/ 50	IgG_1 κ
Stro-1	APC	R& D systems	340104	1/ 20	IgM
CD146	FITC	eBioscience	11-1469	1/ 50	IgG_1 κ
CD34	FITC	BD Pharmingen	555821	1/ 50	IgG_1 κ
CD14	PE	BD Pharmingen	557154	1/ 50	IgG_{2a} κ
CD45	PerCP	BD Pharmingen	557513	1/ 50	IgG_1 κ
StreptAvidin	PE Cy 5.5	Caltag	SA1018	1/ 800	N/ A
SSEA-1	FITC	BD Pharmingen	551376	1/ 50	IgM, κ
SSEA-3	APC	BD Pharmingen	561145	1/ 50	Rat IgM
SSEA-4	FITC	BD Pharmingen	560308	1/ 50	IgG_3
TRA-1-81	PE	BD Pharmingen	560161	1/ 50	IgM, κ
TRA 1-60	APC	BD Pharmingen	560850	1/ 50	IgM, κ
OCT 4	FITC	BD Pharmingen	560307	1/ 50	IgG_1, κ

2.4 Molecular techniques

2.4.1 RNA extraction

Cultured cells were washed twice in PBS, 1 ml of Trizol (Invitrogen) was added and the cell lysate passed several times through a pipette. Then 0.2 ml of chloroform was added and tubes vortexed for 15 seconds and centrifuged at 13 000 rpm for 15 minutes at 4°C. The aqueous phase was transferred to a fresh tube and an equal volume of phenol chloroform (1:1) was added, the tubes were vortexed briefly and centrifuged at 13 000 rpm for 3 minutes at room temperature, the upper aqueous phase was transferred to a new tube and an equal volume of chloroform added, vortexed and centrifuged as before. The upper aqueous phase was transferred to a new tube and mixed with an equal volume of isopropyl alcohol and centrifuged at 13 000 rpm for 50 minutes at 4°C. The supernatant was removed and the pellet washed with 0.8 ml 70% ethanol, and centrifuged at 13 000 rpm for 2 minutes at 4°C. The ethanol was removed and the pellet air-dried for 5 minutes before it was dissolved in RNase free water. The RNA was stored at -80°C or immediately used for reverse transcription into cDNA.

2.4.2 cDNA synthesis

RNA was reverse transcribed to cDNA using SuperScript III First-Strand Synthesis System (Sigma-Aldrich, UK). Up to 8 µl of total RNA, 1 µl of 50 µM Oligo (dT) Primer, and 1 µl of 10 mM dNTP mix was incubated at 65°C for 5 min, then placed on ice for 1 min. The reaction mix for cDNA synthesis consisted of 2 µl of 10X RT buffer (200 mM Tris-HCl, pH 8.4, 500 mM KCl), 4 µl of 25 mM $MgCl_2$, 2 µl of 0.1 M DTT, 1 µl of RNaseOUT (ribonuclease inhibitor), and 1 µl of SuperScript III Reverse Transcriptase. The synthesis reaction was incubated at 50°C for 50 min, and then at 85°C for 5 minutes to terminate the reaction. The tubes were centrifuged and 1 µl of RNase H (non-specific endonuclease) added and incubated at 37°C for 20 minutes. cDNA was then stored at -20°C or used for PCR immediately.

The quality of the RNA and cDNA was assessed my measuring the ratio of absorbance at 260 *versus* 280 nanometres using a NanoVue spectrophotometer (GE Lifesciences, UK) that measures 2 µl samples with high accuracy. For RNA values greater than 2.0 indicated adequate purity, and for cDNA values greater than 1.8 were deemed acceptable.

2.4.3 Polymerase chain reaction

All quantitative polymerase chain reactions (PCR) was performed using a Rotor-Gene 6000 series (Corbett Life Sciences) and analysed using Rotor-Gene (version 1.7.34). For routine PCR, a PTC-225 Peltier Thermal cycler (MJ research, Watertown, MA, USA) was used. Specific oligonucleotides were designed to amplify each DNA fragment of interest, and are shown in Table 7 and

Table 8.

The following standard reaction was used:

Component	Volume
DNA template (50 ng/ µl)	Up to 8 µl
Forward primer (10 pmol/ µl)	1 µl
Reverse primer (10 pmol/ µl)	1 µl
2 X Thermoscript master mix ***or***	
2 X GoTaq Promega qPCR master mix	10µl
DNase free distilled water	Up to a final volume of 20 µl

Standard PCR cycle parameters were as follows; initialisation (required for hot start polymerases to be heat activated) at 95°C for 15 minutes, denaturation at 95°C for 15 seconds, annealing at (50- 65°C) for 1 minute, extension at (60-72°C) for 5 minutes final elongation 72°C and final hold at 4°C. Denaturation, annealing and extension steps were repeated between

30-40 cycles. Annealing and elongation temperatures and times were altered according to the primers used and product length respectively.
The polymerase in both master mixes (*Taq* DNA polymerase) acts by extending the annealed oligonucleotides to synthesise DNA from 3' end of the oligonucleotide. This process of denaturation, annealing and synthesis is repeated numerous times, with each newly synthesised DNA acting as a template for the next reaction. Agarose gel electrophoresis (section 2.4.4) was used to ensure that the PCR product was the correct size.

2.4.4 Agarose gel electrophoresis

Agarose gel electrophoresis was used for analytical or preparative separation of DNA. A 1 % (w/ v) agarose gel solution in 1 x Tris / Acetic acid / EDTA (TAE) buffer was prepared by heating to dissolve the agarose. Once the solution had cooled, ethidium bromide (Invitrogen, Paisley, UK) was added (final concentration of 0.5 µg/ ml) and the mixture poured into the gel tray containing an appropriate gel comb. 10 X loading dye of the appropriate volume was added to the DNA sample and the samples loaded, along with a 1 Kb GeneRuler marker (Fermentas, UK). DNA gels were run at 120 mA in 1 x TAE buffer, and imaged using a UV light source.

Table 7: Primers used to identify mesenchymal lineage specific genes.

Gene	Forward primer 5'-3'	Reverse primer 5'-3'	Annealing temp (ºC)	Product size (bp)
βACTIN	CATGTACGTTGCTATCCAGGC	CTCCTTAATGTCACGCACGAT	55	250
B2M	TGCTGTCTCCATGTTTGATG	CAACCATGCCTTACTTTATC	55	332
CD105	TGCCACTGGACACAGGATAA	GATGAGGACGGCATCGAGAT	50	807
RUNX2	CCGCACGACAACCGCACCAT	CGCTCCGGCCTACAAATCTC	57.5	289
COL1A1	ATCGAGCTGACCTTCCTGCG	TCGAAGCCGAATTCCTGGTC	55	323
BGLAP	CGCAGCCACCGAGACACCAT	GGGCAAGGGCAAGGGGAAGA	65	405
PTH1R	GCATCTCATAGTGCATCTGG	CACAGCCTCATCTTCATGG	60	418
ALP	GGGGGTGGCCGGAAATACAT	GGGGGCCAGACCAAAGATAG	60	543
PPARG	AAACTCTGGGAGATTCTCCT	TCTTGTGAATGGAATGTCTT	50	248
SOX9	CACACTACAGCCCCTCCTAC	CCTCCTCAAGGTGGAGTGAG	55	259
COL2A1	GAAACCATCAATGGTGGGTTC	CGATAACAGTCTTGCCCCAC	55	301

Table 8: Integrin primers

Integrin	Forward primer 5'-3'	Reverse primer 5'-3'	Product size (bp)
ITGA1/ α1	TCAGCCAAGTCAATGTTTCG	CAAAAGCACTCAGCAGGATG	216
ITGA2/ α2	CGGTTGATGGGACAGAAGTAA	GGCTTGGAAACTGAGAGACG	167
ITGA3/ α3	CCCAACTACAGGCGAAACA	GCATCCGCAAAGGTAAAGAG	226
ITGA4/ α4	GTTTTCCAGAGCCAAATCCA	GCCAGCCTTCCACATAACAT	185
ITGA5/ α5	CAGGGTGGTGCTGTCTACCT	GCTCAGTGGCTCCTTCTCTG	237
ITGA6/ α6	GATAAACTGCGTCCCATTCC	TCGTCTCCACATCCCTCTTT	164
ITGA7/ α7	CCTTTGATGGTGATGGGAAA	CAGCAGGTCAGGGTATTGGT	164
ITGA9/ α9	AAGCCGACCACATCCTACC	TCCAGCCCAATAAAATGACC	203
ITGA10/ α10	CCCAGAACAAGGAAACAGGA	CACAGCCACATCAGCAAAAC	167
ITGA11/ α11	GAAGGGTGGAAGGAAAGGAG	GGGTCACTGGCGATGTATTT	207
ITGAV/ αV	ATGGCAAACTCCAAGAGGTG	GAGATGGGACTGCGTTCAAG	249
ITGB1/ β1	CTGCCTTGGTGTCTGTGCT	CCTCGTTGTTCCCATTCACT	233
ITGB2/ β2	TGGTGTTTGCCACTGATGAC	GATGGGCTGGATGTTGTTTT	182
ITGB3/ β3	GCGGCAAGTGTGAATGTG	ACTGAGAGCAGGACCACCAG	367
ITGB4/ β4	CACCAGCAGTCGCTCTACAC	CTCGTCCACCATCTTGACCT	171
ITGB5/ β5	TCTACAAAACCGCCAAGGAC	AAGCCCAACAAGGAGGATG	161
ITGB6/ β6	GTGAGACACAAAGGGCTGCT	AACACACTTGCCACAAACACA	177
ITGB7/ β7	ACCGTGACCCTTGAACACTC	GCTTGGAGAGAAACCCAGAA	161
ITGB8/ β8	ATTAGCATCCACCCCGAAA	CCAGCAGCAATCTTTTAGCC	247

All integrin primers anneal at 60°C. Primer sequences taken from ***(Wong et al. 2010) .***

2.5 Histology

2.5.1 Cell fixation

For immunofluorescence imaging, cells were either fixed with 4 % (w/ v) paraformaldehyde (PFA) or 100 % methanol. The 4 % PFA solution was prepared by adding PFA powder (4 g) to PBS (100 ml), heated to 60°C, and cleared by the addition of 1 M NaOH.

The culture medium was removed and the cells were gently washed twice with PBS and fixed with either 4% (w/ v) PFA for 15 minutes at room temperature or with 100% methanol at -20°C for 10 min. The fixative was removed by aspiration and the cells were washed twice with PBS before immunofluorescence staining.

Table 9: Antibodies used for direct immunofluorescence imaging.

Antibody	Host	Clone	Source
Anti-human RUNX2/ CBFA1	Rat	232902	R&D systems
Anti-human Collagen type I	Mouse	COL-1	Sigma Aldrich
Anti-human Osteocalcin	Mouse	190125	R&D systems
Anti-human Vinculin	Mouse	hVIN-1	Sigma Aldrich
Rhodamine conjugated Phalloidin	N/ A	N/ A	Invitrogen
Anti-human endoglin/ CD105	Mouse	166707	R&D systems
Anti-human Stro-1	Mouse	#STRO-1	R&D systems
Anti-rat Alexa Fluor IgG 488	Goat	N/ A	Invitrogen
Anti-mouse Alexa Fluor IgG 488	Goat	N/ A	Invitrogen

Table 10: Direct immunofluorescence information.

Fixation	Permeabilsation/Blocking buffer	Primary antibody	Secondary antibody
100 % methanol	5% goat serum 0.1 % BSA (30 minutes)	Rhodamine conjugated **Phalloidin** 1:200	N/ A
100 % methanol	5% goat serum (30 minutes)	Mouse monoclonal anti-**vinculin** 1:200 in 1% goat serum	Goat anti mouse Alexa Fluor 488 1:200 1% goat serum
100 % methanol	10% goat serum (30 minutes)	Mouse monoclonal anti-**CD105** 1:50	Goat anti mouse Alexa Fluor 488 1:200
100 % methanol	10% goat serum (30 minutes)	Mouse monoclonal anti-**Stro-1** 1:50	Goat anti-mouse Alexa Fluor 488 1:200
4 % PFA	10% goat serum, 1% BSA 0.1% Triton X-100 (1 hour)	Anti-human **RUNX2** 1:200 in 1% blocking buffer	Goat anti-rat Alexa Fluor 488 1:500
4 % PFA	Dako protein block (30 minutes)	Mouse monoclonal anti-**collagen** type I 1:200 in Dako antibody diluent	Goat anti-mouse Alexa Fluor 488 1:1000 antibody diluent
4 % PFA	10% goat serum, 1% BSA, 0.1% Triton X-100 (1 hour)	Anti-human **osteocalcin** 1:200	Goat anti-mouse Alexa Fluor 488 1:1000

All solutions and antibodies were diluted in PBS unless otherwise stated.

2.5.2 Direct immunofluorescence

After fixation cells were immunostained using the appropriate antibodies (shown in Table 9). Following the protocols shown in Table 10. If required, cell membranes were permeabilised by incubation with detergent diluted in PBS. To prevent non-specific antibody binding cells were 'blocked' with serum diluted in PBS or Dako protein block (Dako, UK). Primary antibodies were incubated at 4°C overnight with the exception of F-actin and vinculin which were incubated at 37°C for 1 hour. Cells were incubated with secondary antibodies for 1 hour, at room temperature in the dark. Cells were washed three times with PBS in between each step, and counterstained with DAPI as described in section 2.5.3 and mounted using fluorescent mounting medium (Dako, UK) prior to imaging.

2.5.3 DAPI counterstaining

All cells stained for immunofluorescence were counterstained with 4',6-diamino-2-phenylindole (DAPI) at a concentration of 2 µg/ ml in PBS, for 20 minutes at room temperature, in the dark. DAPI binds to DNA, allowing visualisation of the cell nucleus.

2.5.4 Alkaline Phosphatase staining

Tissue non-specific alkaline phosphatase (ALP) activity was measured by histochemical staining using an alkaline phosphatase kit (Leukocyte Alkaline Phosphatase Kit, Sigma-Aldrich Ltd., Poole, UK) following manufacturer's instructions. Briefly, cells were fixed in 4% PFA as described in (section 2.5.1), and washed several times with PBS. A diazonium salt solution was prepared by adding 500 µl of sodium nitrate solution (0.1 M) to 500 µl of Fast Blue base-alkaline solution (5 mg/ ml). The solution was inverted and allowed to stand at room temperature for 2 minutes. Distilled water (22.5 ml) was added to 500 µl of naphthol AS-BI alkaline solution (4 mg/ ml), and combined with the diazonium salt solution. After mixing, 250 µl of the solution was added to each well. The plates were then incubated in the dark at room temperature for 15 minutes,

before each well was washed with PBS. The cells were counterstained with DAPI as described in section 2.5.3. Rat femoral sections were used as a positive control, an example of ALP staining (blue) seen in bone marrow and bone matrix, shown in Figure 8 (A).

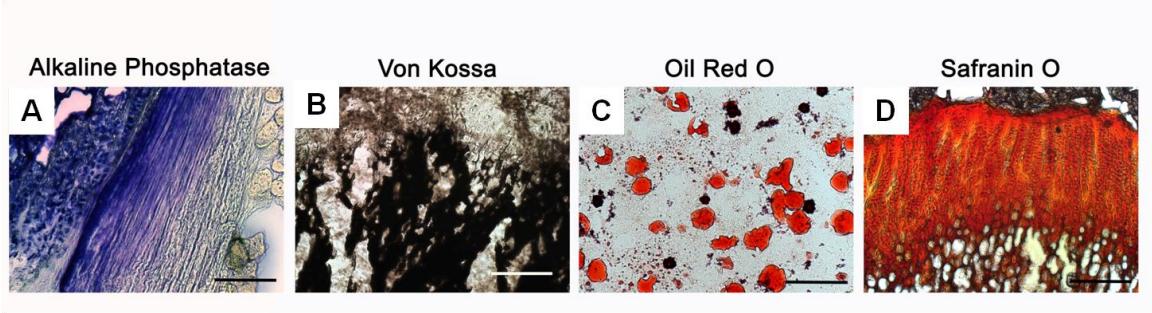

Figure 8: Positive controls for lineage specific staining.

Sections of rat tibia were fixed and stained for (A) alkaline phosphatase, (B) mineralisation (Von Kossa), (C) oil droplets (Oil red O), and for (D) glycosaminoglycans (Safranin O) scale bars represents 100μm.

2.5.5 Von Kossa staining for phosphate

Von Kossa staining was carried out to assess mineralisation in the form of phosphate crystals. The principle of this stain is the silver ions react with phosphate and precipitate as metallic silver under bright light, resulting in black staining (Kossa 1901). Briefly cells were fixed in 4% PFA, washed three times with distilled water, then incubated with 5% (w/ v) silver nitrate solution before being exposed to a 60 watt light bulb for 10-15 minutes. This allowed staining of any mineralised matrix produced, but not of the substrates that also contain calcium phosphate. Following exposure, cells were washed in distilled water and incubated in 5% (w/ v) sodium thiosulphate solution for 5 minutes to remove any unreacted silver nitrate. Cells were washed three times in distilled water and the cells counterstained with DAPI (section 2.5.3). Rat femoral sections were used as a positive control; mineralised areas (black deposits) of trabecular bone are shown in Figure 8 (B).

2.5.6 Oil Red O staining for lipid droplets

Oil red O can be used to detect lipid droplets produced by adipocytes, due to high solubility in lipids. Cells were fixed with 4% PFA and washed three times with distilled water, then once with 60 % isopropyl alcohol. Stock solution (oil red O 0.5% (w/ v) in isopropyl alcohol) was diluted 3:2 in distilled water, allowed to stand for 10 minutes then filtered through a 0.22 μm filter. This 'working' solution of oil red O was added to cells and allowed to incubate for 15 minutes at room temperature. Then the cells were rinsed briefly with 60% isopropyl alcohol, then washed three times with water and counterstained with DAPI, (section 2.5.3). Rat femoral sections were used as a positive control; oil red O stained lipid droplets red, within the bone marrow, and is shown in Figure 8 (C).

2.5.7 Safranin O staining for cartilage

Safranin O is a dye that binds to glycosaminoglycans, which make up a large proportion of extracellular matrix found in cartilage (Camplejohn & Allard 1988). Cells were fixed with 4% PFA and washed three times with distilled water and once with 1% acetic acid for 10 seconds. Safranin O 0.1% (w/ v) solution was added to cells and allowed to incubate for 5 minutes at room temperature. Then the cells were washed three times with water and counterstained with DAPI, (section 2.5.3). Rat femoral sections were used as a positive control; patellar articular cartilage was stained orange with safranin O shown in Figure 8 (D).

2.5.8 Imaging and image analysis

2.5.8.1 Image acquisition

All images were collected using a Zeiss Axio Observer.Z1 microscope with LD Plan-Neofluar objective lenses (Carl Zeiss Ltd. Welwyn Garden City, UK). The microscope was coupled to a Zeiss AxioCamMR3 camera. The image acquisition and processing software used was Zeiss Axiovison Rel 4.8. and Axiovison Version 4.7.1.0, respectively. When visualising immunofluorescence staining, Dako fluorescent imaging medium (Dako UK Ltd, Cambridgeshire, UK) was used. All images were collected at room temperature.

2.5.8.2 Semi-automated cell counting

To calculate the number of cells attached to each substrate, cells were stained with DAPI (section 2.5.3) the entire well was imaged and cell number counted using a self-created macro (cell count macro) in ImageJ (National Institute of Health, USA) (see appendix). Figure 9 shows how the cell macro operates, and full details of the macro are shown in the appendix, part A.

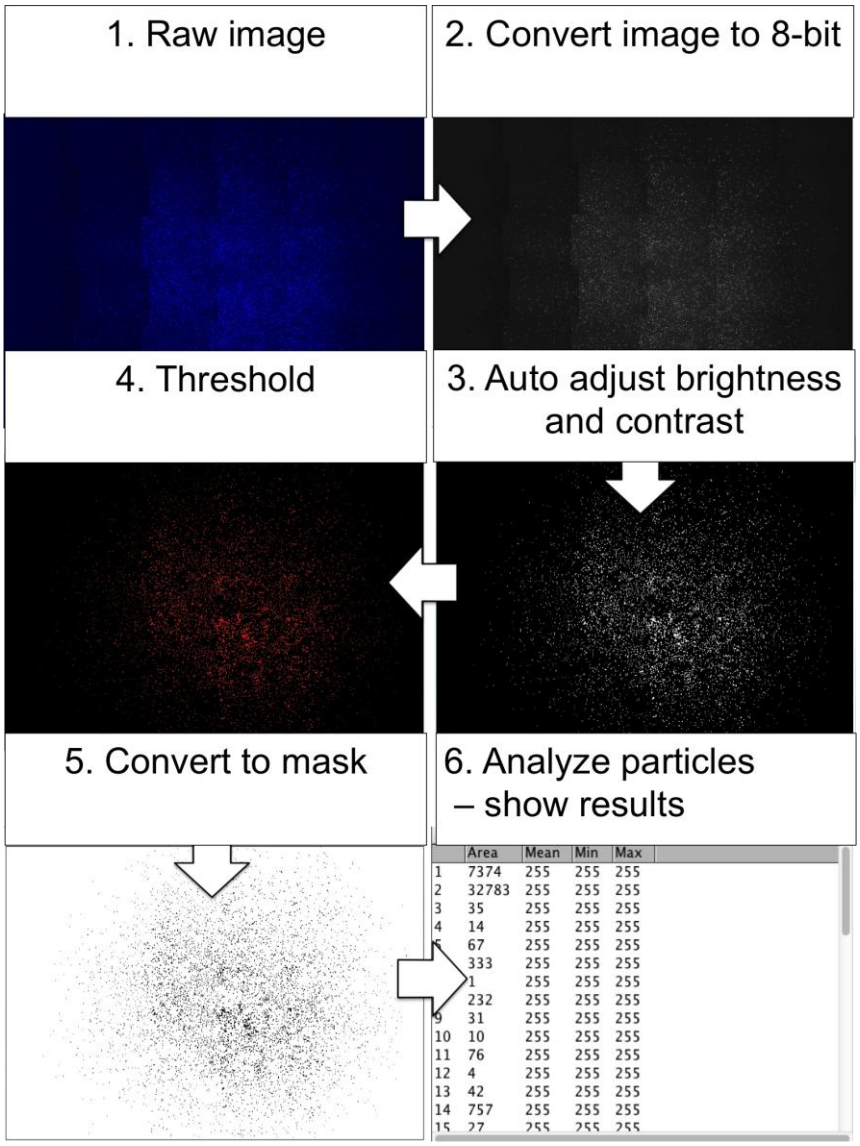

Figure 9: Diagram of how the cell counter macro operates.

1. A mosaic image was taken of the entire well, where cell nuclei are stained with DAPI, shown here in blue. 2. The image was converted to an 8-bit image, in Image J. 3. The brightness and contrast were adjusted automatically. 4. An automatic theshold was set. 5. The image was converted to mask. 6. The number of particles were counted, including all particles between 10 and 100 pixels in size, and the number of particles shown in a summary table.

2.5.8.3 Area of staining quantification

To quantify the area of alkaline phosphatase staining or area of mineralistion (Von Kossa) on each substrate, the cells were stained, imaged and the area was quantified using a self- created macro (Area quant macro) using ImageJ (see appendix). An example of how images were processed in the macro is shown in Figure 10 and Figure 11.

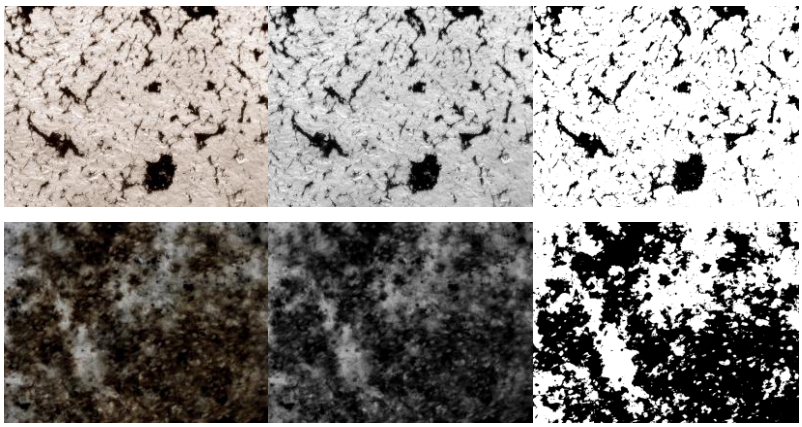

Figure 10: Von Kossa staining and quantification.

Example of how Von Kossa staining is quantified by area, the image was converted to an 8-bit image, an automatic threshold set and the area analysed using an automated area quantification macro. The upper image is 18.5% lower image is 60.5%

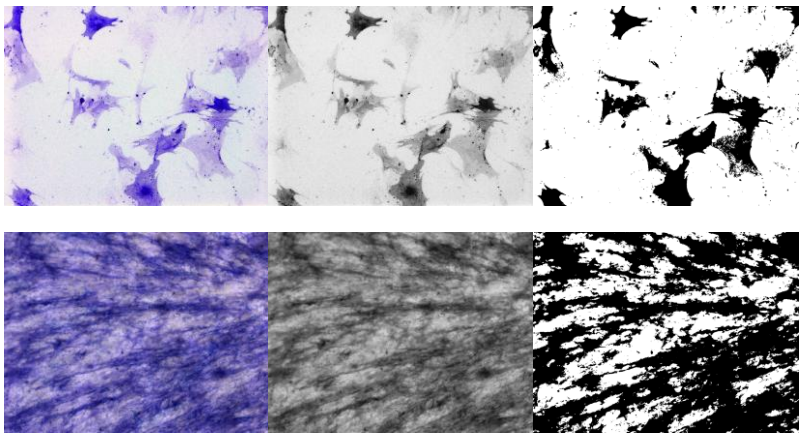

Figure 11: Alkaline phosphatase staining and quantification.

Example of how alkaline phosphatase is quantified by area of staining, the image was converted to an 8-bit image, an automatic threshold set and the area analysed using an automated area quantification macro. The upper right image is 16.8% lower right image is 54.5%

2.6 Silicate substituted calcium phosphate and hydroxyapatite disc manufacture

Hydroxyapatite was prepared using the precipitation reaction between calcium hydroxide ($Ca(OH)_2$) and orthophosphoric acid (H_3PO_4) with molar ratios described in Table 11 below. This precipitation method is based on the method described by (Akao et al. 1981). Silicate-substituted calcium phosphate (Si-CaP) was prepared as described by (Gibson et al. 1999). Briefly, Si-CaP was prepared by an acid-base neutralisation reaction, the precipitation reaction was carried out at room temperature, and the pH maintained at 10.5 through the addition of ammonium hydroxide solution. The precipitation reaction was mixed for several hours then left undisturbed overnight. The solution was then filtered though a filtration press at 600 bar for approximately 30 min, then dried for 4 days at 40°C. The dried precipitate was ground by hand into 10 mm^2 pieces, passed through a milling machine, which ground the precipitate into a powder with grains approximately 400 μm in diameter, then calcined at 700°C for 4 hours.

Table 11: Quantities of reactants used and calculated molar ratios

Sample	No. of Moles $Ca(OH)_2$	No. of Moles H_3PO_4	No. of Moles $Si(CH_3COO)_4$	Expected Ca/P Ratio	Expected Ca/(P + Si) Ratio
Stoichiometric Hydroxyapatite (HA)	0.5	0.297	0	1.68	1.68
Silicate -substituted Calcium Phosphate (Si-CaP)	0.5	0.289	0.008	1.73	1.68

Calcined powder was pressed into discs 20 mm in diameter, using a die and pellet set and a Manual Hydraulic Press (both Specac, UK). Samples were pressed for 5 seconds at 2 MPa, removed from the pellet and then sintered at 1260°C for 1 hour and 33 minutes prior to analysis.

2.6.1 Disc analysis

Sintered disc height and diameter were measured using digital callipers (0.01mm) and weighed using digital scales (0.0001g).

2.6.2 Mercury intrusion porosimetry

The term "porosimetry" is frequently used to include the measurements of pore size, volume, distribution and density. Porosity is particularly important in understanding the formation, structure, and potential use of many materials as porosity can affect a material's adsorption, permeability, strength, and density (Abell et al. 1999). Mercury is a non-wetting liquid (one having a contact angle greater than 90°) and therefore, will only intrude capillaries under pressure. The required pressure is inversely proportional to the size of the pores, only slight pressure being required to intrude mercury into large macropores, whereas much greater pressures are required to force mercury into smaller pores (micropores). Mercury intrusion porosimetry involves the progressive intrusion of mercury into a porous structure under strictly controlled pressures. From the pressure versus intrusion data, the instrument generates volume and size distributions using the Washburn equation (Washburn 1921), below.

Equation 1

$$r = \frac{-2\gamma cos\theta}{p}$$

Where r is the radius of the pore, p is pressure, γ is the contact angle between the mercury and a surface of the solid material tested and θ is the surface tension of mercury.

The pore size distribution is determined from the volume intruded at each pressure increment, and total porosity was determined from the total volume intruded. Porosity measurements were performed using a mercury intrusion porosimeter (Poremaster GT, Quantachrome UK Ltd. Hook, UK**)**

using pressures from 1 to 10^5 psi. Briefly, samples were weighed and loaded into penetrometers (see Figure 12 the upper rim of the penetrometer was lubricated using heat stable, silicone grease (Dow Corning, Belgium) and contacts placed on top, ensuring a tight seal, and the caps were firmly screwed onto the contact. Two penetrometers were placed into the low-pressure stations of the machine and set to run. Once the low pressure run was complete the two penetrometers were removed, the capillary opening was filled with up with hydraulic oil and then placed into metal casings, and into the high-pressure chamber for the next run.

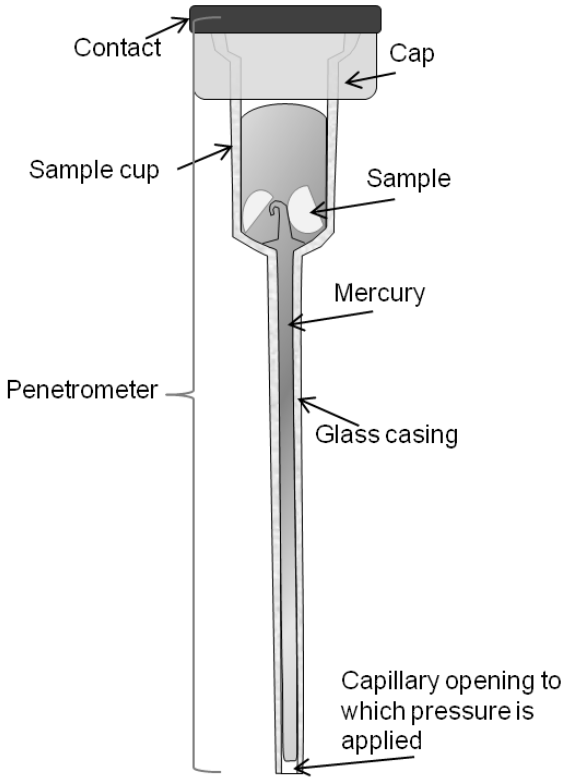

Figure 12: Diagram of a mercury penetrometer containing sample and mercury.

Mercury penetrometers were used with a intrusion porosimeter to determine porosity of discs. Under high pressures the mercury is forced into the pores of the disc and the volume of liquid displaced allows calculation of the volume of a range of pore sizes and total porosity of each disc.

The data was integrated from the low pressure and high pressure runs and raw and volume *vs.* Pressure was graphed as shown in Figure 13. This was then converted to –dV/ logD *vs.* Pore size, shown in Figure 14. This graph

shows the distribution of pore size in relation to the intruded volume of mercury. The pore size to be analysed was chosen (0.1-5 µm), shown in Figure 15. A standard report summary was generated and the intruded volume (g/ cc) calculated and converted to strut porosity, using the formula in Equation 2.

Equation 2

$$(\%)\text{Strut porosity} = \frac{intruded\ volume}{\left(\left(\frac{1}{3.08}\right) + intruded\ volume\right) x100}$$

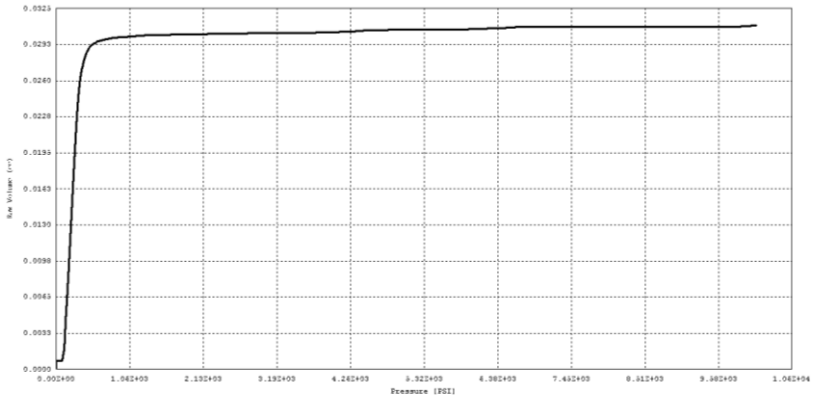

Figure 13: Raw voiume (cc) Vs.pressure (psi).

The change in volume is shown at different pressures, increasing until all the pores are filled. After this point the pressure continues to increase but volume does not.

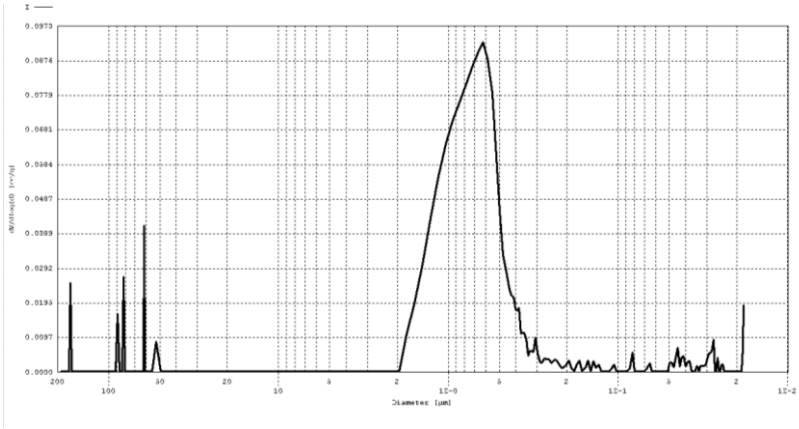

Figure 14: dV/dlogD Vs. Pore size.

The intruded volume is converted to pore size and the pore size, the peak indicates the greatest number of pores were within 5 - 0.1 µm.

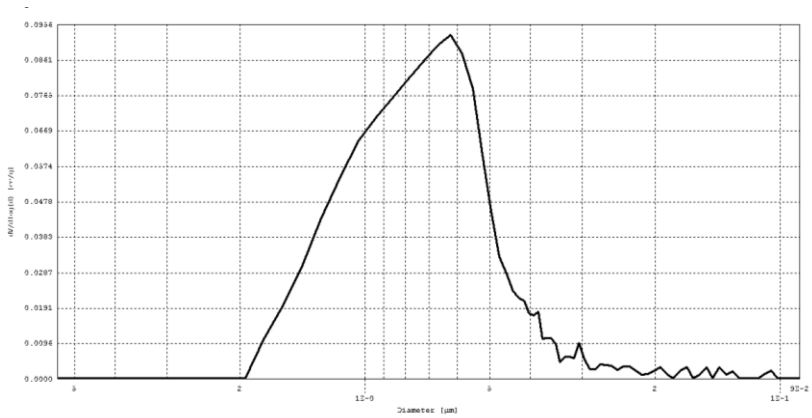

Figure 15: dV/dlogD Vs. Pore size (5- 0.1 µm).

Indicating selected pore size to be analysed.

2.6.3 Helium pycnometry

Helium pycnometry is a method used to determine the density of a material. A chamber is filled with gas, generally helium; the object to be measured is then placed in the chamber and filled with gas again. The pycnometer then calculates density based on gas displacement (Furuse 1989).

Pycnometric densities were measured using a helium pyconometer (Ultrapycnometer 1200e, Quantachrome UK Ltd. Hook, UK**).** Prior to each analysis the pycnometer was calibrated twice, once with an empty chamber and secondly with a reference volume. Two discs were selected and weighed, they were placed inside the pycnometer and run 18 times, with 10 pulses at a pressure of 17 psi, a minimum of 6 runs were averaged to achieve a standard deviation of ≤0.0005.

Equation 3

$$V_s = V_c + \frac{V_r}{1 - \frac{P_1}{P_2}}$$

The volume of the samples was calculated using the formula above. Where *Vs.*is the sample volume, V_c is the volume of the empty sample chamber, V_r is the volume of the reference volume, P_1 is the first pressure (sample chamber) and P_2 is the second (lower) pressure after expansion of the gas into the combined volumes of sample chamber and reference chamber.

The density was then calculated using the following equation, where *p* is the density, *m* is the mass and *V* the volume of the sample ($V=\pi r^2 h$ $\pi r^2 h$) where (*r* = radius, *h* = height of disc).

Equation 4

$$\rho = \frac{m}{V}$$

2.6.4 Embedding and polishing

Embedding and polishing of specimens was performed prior to analysis of density using Scanning Electron Microscopy. Discs were split in half using sharp-ended pliers and dried at 50-70°C for 12 hours; each sample was then cooled at room temperature in a desiccator cabinet for 30 minutes. Samples were then placed into numbered moulds inside a vacuum impregnation cabinet (Struers Epovac, Struers, Rotherham, UK) and held under vacuum at approximately 200 Mbar for 15 minutes. Embedding resin was composed of 50 g epoxy resin (EpoFix, Struers), 8 g hardener (EpoFix hardener) and < 0.5 g Sudan blue dye (Sigma Aldrich). All components were mixed thoroughly for 5 minutes then applied in stages, under vacuum, to each mould until each sample was fully covered. After all the resin was added the samples remained under vacuum for a further 10 minutes. To remove excess bubbles the pressure in the vacuum was increased to 700 Mbar then decreased back to 200 Mbar three times. The samples were then removed from the vacuum cabinet and left to 'cure' overnight in a fume hood. Once the resin had fully hardened the sample were extruded from the moulds using a toggle press, and labelled accordingly, an illustration of a emedded disc is shown in

Figure 16.

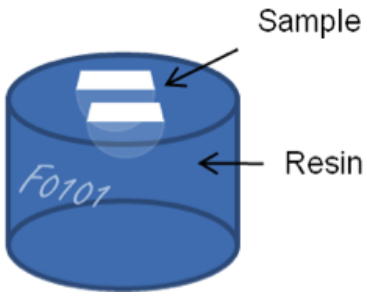

Figure 16: Diagram of embedded and polished disc.

All embedded discs were then polished using a polishing machine (Struers TegraPol-21 and a Struers Tegraforce-5 sample holder) using the regime shown in Table 12. The first step of grinding is used to flatten the base of

the sample. The following steps are to smooth and polish the upper face of the sample. In between each step, samples were washed in water to remove dirt or polishing lubricant. Once polishing was complete samples were dried thoroughly using compressed air. All samples were then stored in a desiccator cabinet prior to scanning electron microscopy analysis.

Table 12: Grinding and polishing parameters

	Pad	Lubricant	Pressure (Newtons)	Speed (rpm)	Duration (minutes)	Dosing rate (drops per minute)
Grinding	120	Water	15	150	1	N/A
	120	Water	15	300	2	N/A
	220	Water	15	300	3	N/A
	600	Water	15	300	5	N/A
	1200	Water	15	150	10	N/A
Polishing	MD Dac	6μm DiaDuo	25	150	10	9
	MD Nap	1μm DiaDuo	30	150	12	10

2.6.5 Scanning Electron Microscopy

Scanning Electron microscopy was used to analyse the internal structure and surface of discs and was performed using a Jeol, Neoscope JCM-500 (Hertfordshire, England).

Samples were plasma-sprayed with gold, to prevent the accumulation of electrostatic charge, using a gold coater (NeoCoater MP-19020NTCR) and a silver strip painted to ground the charge. Five images were taken for each sample and the number of artefacts were measured and quantified. Artefacts were classed as pits or objects and measured using NIS Elements BR 2.30.

2.6.6 Data analysis

Design expert software (Design Expert, version 7.1.6; Stat-Ease Inc. US) was used to analyse all data. One-way Analysis of variance (ANOVA) was used to test differences between test group sets. For all analyses a 95% confidence interval was used and significance level $P<0.005$.

CHAPTER THREE: DISC MANUFACTURE AND OPTIMISATION

3.2 Introduction

Silicon substituted calcium phosphate (Si-CaP) is commonly used as a substrate to encourage and support new bone formation in clinical situations such as spinal fusion, fractures and small bone defects as a structure to encourage and support new bone formation. Si-CaP has been demonstrated to possess superior bone regenerative capacity and resorbability when compared to traditional hydroxyapatite (HA). The bioactivity of Si-CaP has been established by scientific research in vivo and in clinical studies (Patel et al. 2002; Reid et al. 2006; Karin A Hing et al. 2007; Patel et al. 2005). However, it remains unclear if the improved bone formation results from activation of stem/ progenitor cells (MSC) that differentiate preferentially into osteoblasts. Thus in order to understand fully the influence of Si-CaP and HA on mesenchymal stem cells in vivo, extensive in vitro studies are needed.

Si-CaP and HA can be produced in many forms for orthopaedic applications. Both materials are commonly used as granules, which can be mixed with blood or bone marrow aspirate, to form a cohesive graft. Bone marrow aspirate provides a source of osteoprogenitors and mesenchymal stem cells, and has been shown to enhance de novo bone formation when combined with bone graft substitutes (Block 2005). New bone formation must always be preceded by the formation of a vascular network. This can be encouraged through the mixing of bone graft granules with autologous blood. The extent of vascularisation and has been shown to be strongly influenced by the degree of structural interconnectivity between pores (K A Hing et al. 2005). Si-CaP granules are specifically manufactured to contain interconnected pores of varying size, to enhance attachment, vascularisation, (Mastrogiacomo et al. 2006), osseointegration (Karageorgiou & Kaplan 2005) and resorbability (K A Hing 2005). In particular strut porosity, defined as 'the fraction of porosity within the scaffold struts, <10 μm in diameter' has been shown to be directly linked

to vascularisation of bone grafts and enhanced osseointegration (K A Hing et al. 2005).

In order to examine the response of MSC to the surface properties of Si-CaP and HA without the influence of surface porosity or strut porosity the materials were pressed into dense discs.

Dense discs have previously been used to analyse the response of osteoblasts to calcium phosphate based substrates (Rosa et al. 2003; Courteney-Harris et al. 1995; Kumar et al. 2010). However, the response of mesenchymal stem cells to HA and Si-CaP in dense disc form has not yet been examined.

The preparation of calcium phosphates with different compositions and morphology has been investigated over recent years. Others have focused on the impact of different production methods, reporting wide variation in structural and chemical properties (X. Liu & Ei-Ghannam 2010; G.-J. Oh et al. 2010; Wu et al. 2008; Rosa et al. 2003; Botelho et al. 2006; Pontier et al. 2001; Juang 1996; Rodríguez-Lorenzo et al. 2001). When comparing these studies, confusion arises not only from the different compositions of powder but also from the different production methods. However, in each methodology dense disc manufacture can be divided into three distinct stages: Powder processing, disc pressing and post pressing processing.

Powder processing

Calcium phosphate is commonly produced by precipitation, filtration, then dried and ground into a powder. This powder can be processed to produce granules, mixed with other components to make bone graft composites or pressed into dense discs. Prior to processing, powder is commonly calcined to remove unwanted volatile fractions. Altering the temperature of calcination has been shown to significantly affect the sintering properties of discs. Firstly, by decreasing grain size, making it finer than un-calcined powder, which can lead to increased powder packing. Secondly, calcining at high temperatures can delay the initiation of sintering, causing a reduction in shrinkage, resulting in larger discs (Juang 1996).

Disc pressing

Powder is commonly pressed into discs using a hydraulic press, die and pellet set. Different compaction pressures have been studied, ranging from 70 MPa (Rodríguez-Lorenzo et al. 2001) to 1100 MPa (Pattanayak et al. 2005). Increasing applied pressure has produced comparable results, and as expected, as pressure increases, the density of disc increases. Results from multiple groups confirm this effect, with increased pressure resulting in discs with both lower porosity and increased density. However, above a compaction pressure greater than 1100 MPa density was shown to decrease, thought to be due to the formation of cracks in the discs (Pattanayak et al. 2005).

Duration of pressure also differed between studies, varying from 30 seconds (Kumar et al. 2010; Rodríguez-Lorenzo et al. 2001) to 1 minute (Rodríguez-Lorenzo et al. 2001). Nonetheless, the impact of the duration of pressure discs on structure and mechanical properties within one study has not yet been examined.

Post pressing processing

Sintering is one of the final stages of ceramic production, where granules or discs are heated until particles adhere together. This process is well documented and can have significant effects on material properties, depending upon the temperature and duration of heating. Rodriguez-Lorenzo et al studied the effect of different sintering temperatures (600-1300°C) on HA discs, and found total pore area decreased whereas density and compressive strength increased with increasing temperature up to 1200°C (Rodríguez-Lorenzo et al. 2001). Calcined human enamel hydroxyapatite studies revealed similar results; that low densification (increase in density) is seen after sintering at low temperatures (1000°C, 1100°C) and high densification is achieved after sintering at higher temperatures (1200°C, 1300°C) (Oktar 2007).

Conversely, a silica-calcium phosphate nanocomposite behaved very differently; as sintering temperature increased from 900°C to 1100°C, compressive strength and modulus of elasticity decreased (X. Liu & Ei-Ghannam 2010). In the same study, sintering was shown to alter the phases

of material. Prior to sintering, silica-calcium phosphate was composed of α- and β-cristobalite and after sintering temperature increased, the intensity of characteristic peaks of α-cristobalite decreased gradually (X. Liu & Ei-Ghannam 2010).

The aim of this chapter was to optimise production yield of dense discs whilst maintaining the desired physical properties, described below.

Optimising production yield

Dense disc manufacture involves the use of a manual hydraulic press; this is a time-consuming and labour intensive process. Therefore reducing the amount of effort (lowest pressure) and decreasing production time (duration of pressure/ lubrication) could lead to improved production yield.

Desired physical properties

Dense discs must be strong enough to resist cracking upon handling; discs must also contain little or no surface or strut porosity and should be as smooth as possible without irregularities on the surface- all factors that could influence cellular response.

3.3 Results

3.3.1 Disc manufacture and optimisation

Input parameters were identified as factors, which could affect the discs mechanical properties and disc production, these were divided into the three stages of disc production: Powder processing, disc pressing and post-pressing processing. At least one parameter was chosen per stage and several variables were selected for disc pressing. The input parameters identified and the parameters selected for investigation are shown in Table 13. These parameters were put into Design Expert software (Design Expert, version 7.1.6; Stat-Ease Inc. Minneapolis, US) and a study comprising a five factor; two level design with midpoints for numerical factors was generated. Details of variables investigated and the values to be tested are described in Table 14.

Table 13: Critical input parameters of disc production and parameters selected to be investigated.

Powder processing	Investigated	Disc pressing	Investigated	Post-press processing	Investigated
Calcination of powder	Yes	Powder weight	Yes	Sintering temperature	Yes
Powder composition	No	Pressure	Yes	Polishing discs	No
Powder grain size	No	Duration of pressure	Yes		
		Lubrication of die and pellets	Yes		
		Number of discs pressed	No		

The standard conditions previously used to manaufacture dense discs of Si-CaP were: 1 g of calcined powder, pressed at 200 MPa, for a duration of 5 seconds, without lubrication of the die and pellet. Therefore, points above and below were selected to investgate the effects on dense disc production, and are shown in Table 14.

Table 14: Selected process parameters and variables to be investigated.

Powder weight (g)	Pressure (MPa)	Press duration (seconds)	Powder	Lubrication
0.5	100	5	Calcined	Stearic acid
1.25	200	17.5	Un-calcined	None
2	300	30		

Si-CaP powder was prepared as described in materials and methods section 2.6 and was then heated dry at 700°C for 4 hours (this process is called calcination –and is used to remove volatile fractions) or left un-calcined. Si-CaP powder (0.5 g, 1.25 g or 2 g) was pressed into discs using a 20 mm diameter die and pellet set and a Specac Manual Hydraulic Press, shown in Figure 17.

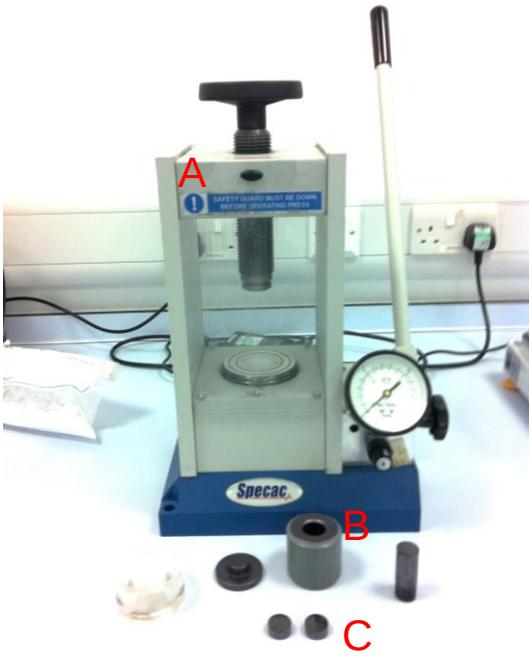

Figure 17: Specac Manual Hydraulic Press and die and pellet set.

Hydraulic press (A), with pressure gauge, and coated pellet (B) and die set (C) used to manufacture all dense discs.

Samples were pressed at 100, 200 or 300 MPa for 5, 17.5 or 30 seconds either with or without lubrication in the form of 4 % w/ v stearic acid (Sigma Aldrich, Poole, Dorset) in acetone. Each sample was produced in triplicate and all discs were sintered at 1260°C for 1 hour and 33 minutes prior to analysis. Once sintered the following properties of each disc were examined: height, diameter, calculated density, measured density, intruded volume, strut porosity and the number of irregularities on the disc surface. Microsoft Excel was used to generate graphs showing relationships between investigated parameters. Design Expert software was used to analyse all data. One-way Analysis of variance (ANOVA) was used to test differences between test group sets. For all analyses all five factors were included and for all graphs standard error (SEM*) of mean is shown A summary of results is shown in Table 15. It was found that disc height and diameters were influenced by several factors, significant results were graphed and are discussed below.

Table 15: Summary of results.

Batch number	Powder weight (g)	Pressure (MPa)	Press duration (seconds)	Calcination	Lubrication	Calculated density (kg/ m^3)	Density (kg/ m^3)	Intruded volume (kg/ m^3)	Intruded strut porosity %	Total number of irregularities
A	0.5	100	5	Calcined	Stearic acid	2.4451	3.1365	0.0285	8.07	16
B	2	100	5	Calcined	None	2.7704	3.1008	0.0383	10.55	5
C	0.5	300	5	Calcined	None	3.0466	3.1890	0.0000	0.00	2
D	2	300	5	Calcined	Stearic acid	2.9954	3.0914	0.0000	0.00	19
E	0.5	100	30	Calcined	None	2.8660	2.9489	0.0205	5.94	23
F	2	100	30	Calcined	Stearic acid	2.9167	3.0789	0.0292	8.25	12
G	0.5	300	30	Calcined	Stearic acid	3.1180	3.0737	0.0000	0.00	2
H	2	300	30	Calcined	None	2.9921	3.1070	0.0003	0.09	3
I	0.5	100	5	Un-calcined	None	2.9814	3.3148	0.0127	3.76	6
J	2	100	5	Un-calcined	Stearic acid	2.9643	3.1066	0.0227	6.53	1
K	0.5	300	5	Un-calcined	Stearic acid	2.7909	3.0060	0.0120	3.56	1
L	2	300	5	Un-calcined	None	2.9611	3.0874	0.0084	2.52	3
M	0.5	100	30	Un-calcined	Stearic acid	2.9439	3.0152	0.0157	4.61	0
N	2	100	30	Un-calcined	None	2.8217	3.2662	0.0192	5.58	4
O	0.5	300	30	Un-calcined	None	2.1781	3.0454	0.0007	0.22	3
P	2	300	30	Un-calcined	Stearic acid	3.0735	3.1650	0.0002	0.06	5
Q	1.25	200	17.5	Calcined	None	2.5823	3.0505	0.0005	0.15	4
R	1.25	200	17.5	Un-calcined	None	2.8280	3.0678	0.0029	0.89	3
S	1.25	200	17.5	Calcined	Stearic acid	3.2722	3.0067	0.0012	0.37	39
T	1.25	200	17.5	Un-calcined	Stearic acid	3.2209	3.1064	0.0000	0.00	49

3.3.1.1 Disc height

Disc height was directly related to powder weight and pressure. The relationship between weight and height of discs is shown in

Figure 18. As expected the weight was directly proportional to disc height in all batches, height in mm was approximately double the weight in grams, this relationship was highly significant (P<0.001).

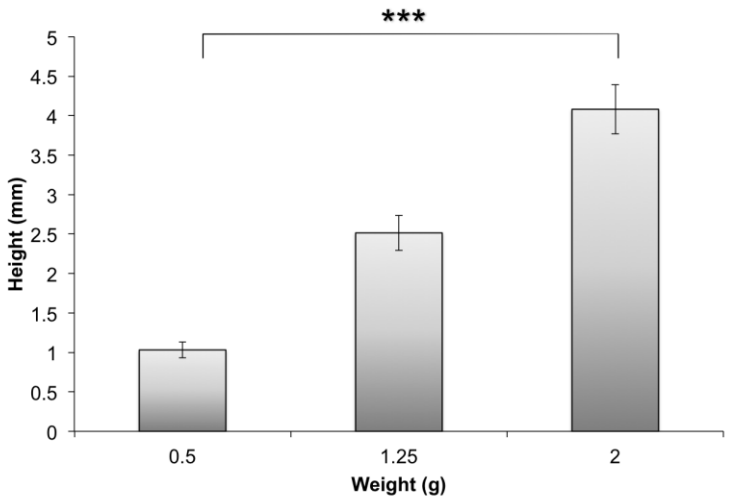

Figure 18: Relationship between powder weight and disc height.

Effect of powder weight on disc height, the average height is shown and error bars represent standard error of mean SEM. Key: ns (P>0.05), *(P≤ 0.05), **(P≤ 0.01), *** (P≤ 0.001), ****(P ≤ 0.0001).*

Similarly, as expected, when pressure was increased, disc height decreased, this relationship was significant (P<0.001) and is depicted in Figure 19. The effect of pressure on height was notably different in discs pressed using different powder weights. The effect of pressure on disc height was most apparent in discs made varied with 2 g of powder by 0.57 mm on average, compared to a variation of 0.11 mm in discs made with 0.5 g of powder. Discs made of 1.25 g of powder were pressed at 200 MPa, and varied by as much as 0.75 mm. Generally, increased pressure results in increased density however, above a certain threshold density cannot increase, and

would limit the height of discs. This was not observed in the range of pressures examined here.

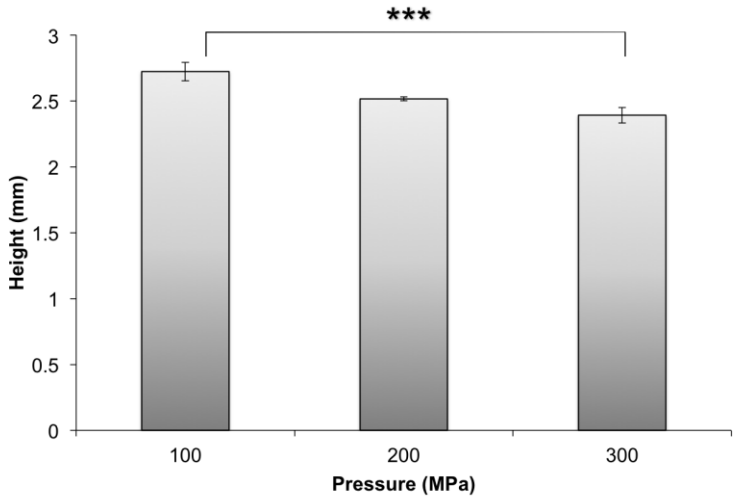

Figure 19: Relationship between pressure and disc height.

Average height of all discs pressed at different pressures, error bars represent SEM. Key: ns (P>0.05), * (P≤ 0.05), ** (P≤ 0.01), *** (P≤ 0.001), **** (P ≤ 0.0001).*

3.3.1.2 Disc diameter

The diameter of discs was limited during pressing by the die and pellet set, and therefore disc diameter was never greater than 20 mm immediately after pressing. However, significant changes in diameter were observed post processing/ after sintering. Several parameters significantly influenced disc diameter including; pressure, calcination and lubrication.

Powder weight affected disc diameter; increased weight of powder resulted in discs of a smaller diameter, but this was not found to be statistically significant (P=0.0881). Pressure significantly influenced disc diameter (P<0.0001) as shown in Figure 20. Increased pressure lead to discs with increased diameter. Discs pressed at 300 MPa were on average 0.34 mm larger in diameter compared to discs pressed at 100 MPa.

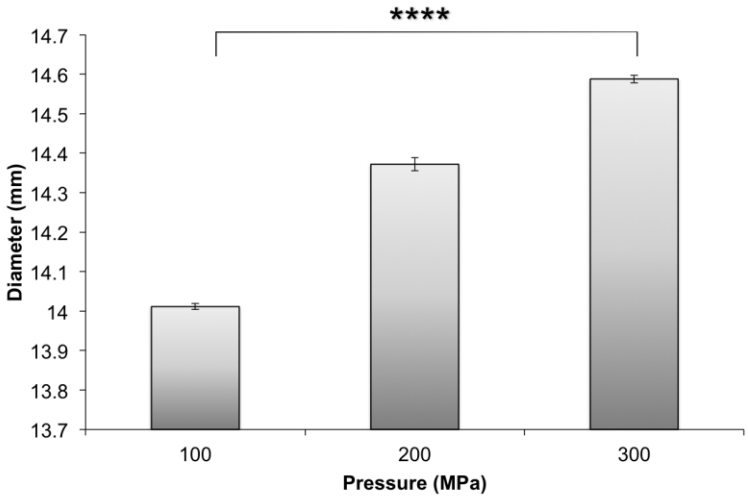

Figure 20: Effect of pressure on diameter of discs.

Average diameter of discs, error bars represent SEM. Key: ns (P>0.05), *(P≤ 0.05), ** (P≤ 0.01), *** (P≤ 0.001), **** (P ≤ 0.0001).*

Prior to pressing discs, powder is commonly calcined to remove unwanted volatile fractions. Figure 21 shows the effect of calcination on disc diameter. Calcination of powder produced discs of significantly greater diameter than un-calcined powder; although diameter only varied by 1.18 mm (P<0.001).

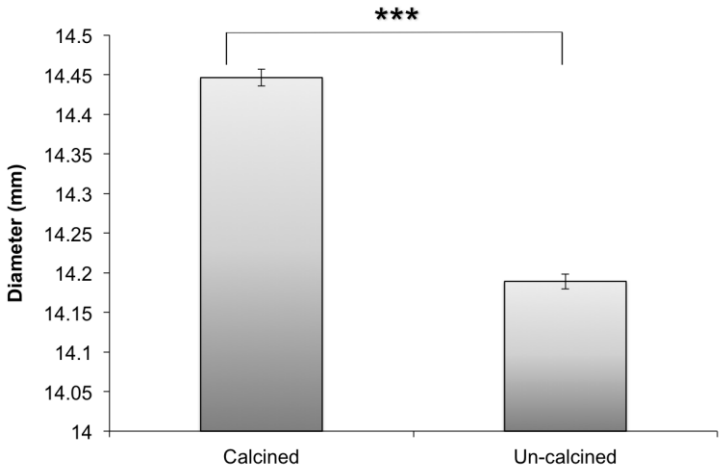

Figure 21: Effect of calcination on diameter.

Average diameter of discs, error bars represent SEM. Key: ns (P>0.05), *(P≤ 0.05), ** (P≤ 0.01), *** (P≤ 0.001), **** (P ≤ 0.0001).*

Lubrication in the form of stearic acid also influenced disc diameter, shown in Figure 22. Discs produced with lubrication were significantly larger in diameter compared to discs made without a lubricant (P= 0.0119).

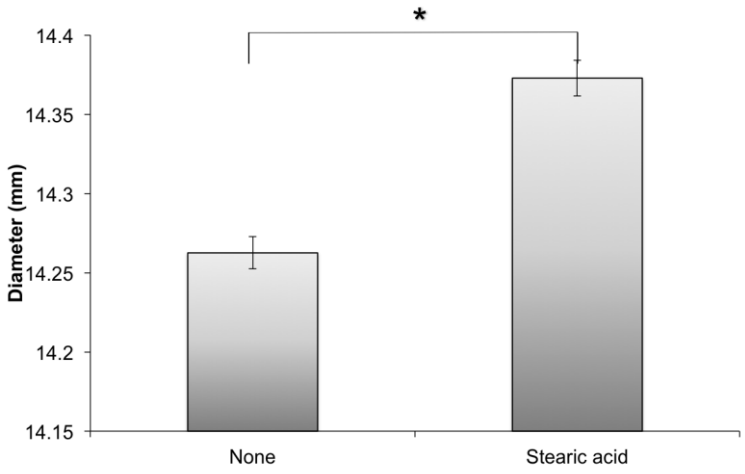

Figure 22: Effect of lubrication on diameter of discs.

Average diameter of discs, error bars represent SEM. Key: ns (P>0.05), *(P≤ 0.05), ** (P≤ 0.01), *** (P≤ 0.001), **** (P ≤ 0.0001).*

3.3.1.3 Intruded strut Porosity

Strut porosity is also described as microporosity and strut pores are formed from the interconnected spaces existing between the struts in the scaffold of calcium phosphate biomaterials (Campion et al. 2011). Intruded strut porosity was calculated from intruded volume measured by mercury intrusion porosimetry, as described in materials and methods section 2.6.2. Figure 23: Effect of pressure on porosity.

(A) shows the relationship between intruded strut porosity and pressure in all discs. Porosity varied greatly, even when discs were formed at the same pressure. At several data points porosity was unexpectedly high, in partiular, there were two instances where the porosity of discs pressed at 300 MPa, was higher than in discs pressed at 100 MPa. Prior to MIP discs were broken, these discs may have been broken into smaller pieces, providing a greater surface area for intrusion, thus explaining these unexpected results. However, when a subset of discs were examined (excluding discs made with 0.5 g of powder, calcined powder and

lubricated), the relationship between intruded strut porosity and pressure follows a more logical trend.Figure 23: Effect of pressure on porosity.

(B) shows in this section of discs where increased pressure resulted in decreased porosity, a result that was statistically significant (P<0.001).

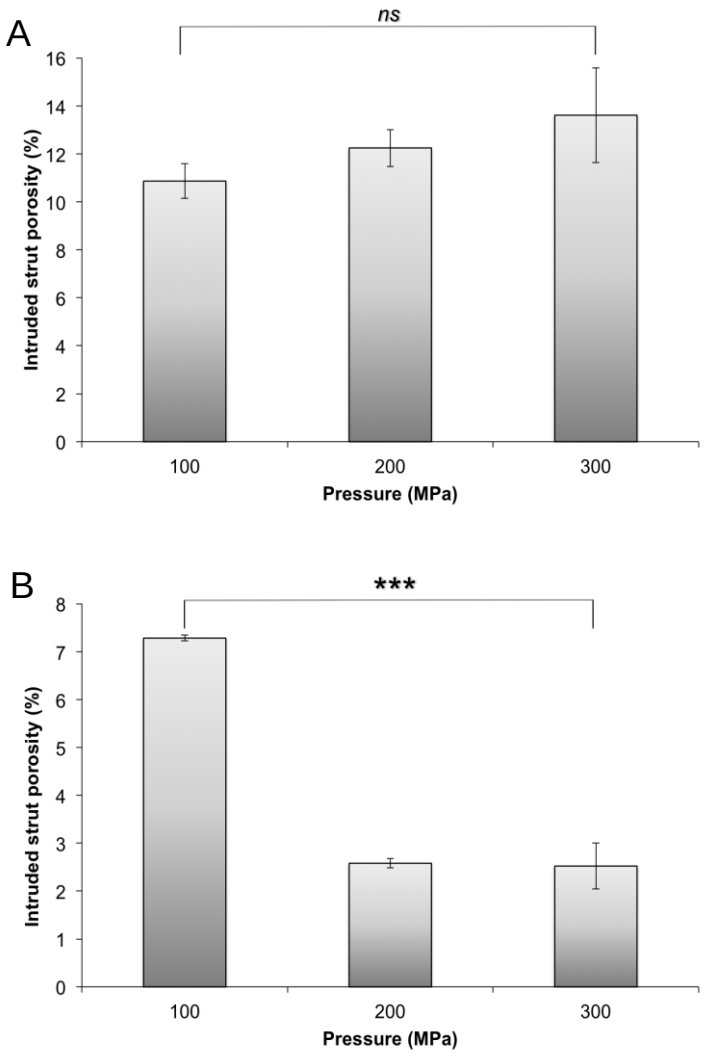

Figure 23: Effect of pressure on porosity.

(A) Effect of pressure on intruded strut porosity of all discs (B) Effect of Pressure on intruded strut porosity on selected discs. Average intruded strut porosity of discs (<0.5 g of powder, un-calcined and without lubrication) As measured by mercury intrusion porosimetry, error bars represent SEM. Key: ns (P>0.05), *(P≤ 0.05), **(P≤ 0.01), *** (P≤ 0.001), ****(P ≤ 0.0001).*

3.3.1.4 Density

Results from pycnometry and calculated densities are shown in Table 15. All calculated densities were lower than measured pycnometric density values, and neither set of values were significantly correlated to the studied process parameters (see Table 16).

Table 16: Process parameters, pycnometric density and calculated density p values.

Process parameters	Pycnometric density P value	Calculated density P value
Powder weight	0.3286	0.1916
Pressure	0.4652	0.7028
Duration of pressure	0.2400	0.9571
Calcination	0.2104	0.6059
Lubrication	0.3259	0.4549

3.3.1.5 Surface analysis- Scanning Electron Microscopy

Irregularities in the form of pits or objects, examples of which can be seen in Figure 24, were observed on the surface of most discs. The number, type, and size of irregularities were quantified, and the data depicted in Figure 25: Type and size of irregularities on discs.

. More irregularities were seen on discs pressed with stearic acid as a lubricant, however this did not reach statistical significance (P=0.07) despite apparent differences (see Figure 24 A and E). Discs pressed with stearic acid had more pits and objects than discs pressed with no lubricant; again this was not statistically significant (P=0.06). There was also a larger number of large objects and pits (500 µm and 100 µm in size) on discs produced with stearic acid (P=0.08).

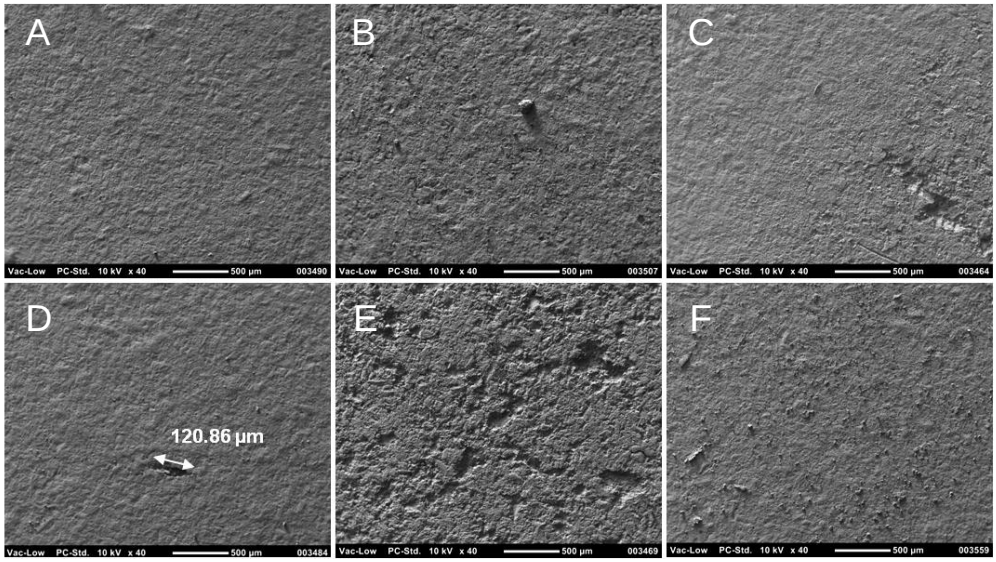

Figure 24: Scanning elctron microscopy images of sintered disc surfaces.

(A) Surface with no irregularities, (B) irregularity classified as an object, (C) irregularity classified as a pit, (D) example of how objects/pits were quantified (E) pitted surface and (F) multiple objects <100 µm in diameter.

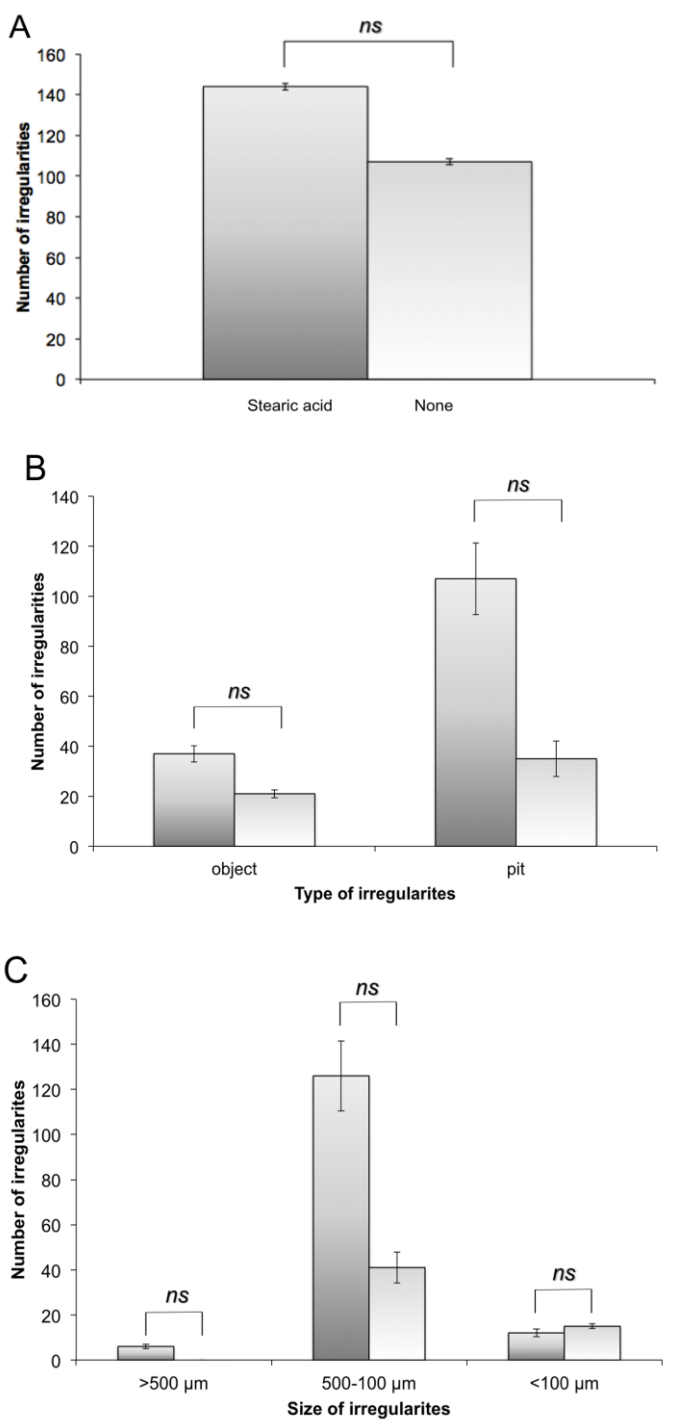

Figure 25: Type and size of irregularities on discs.

(A) Total number, (B) type and (C) size of irregularities on discs produced with stearic acid (light grey) or with no lubricant (dark grey) A total of ten discs were examined for each group and five images taken per disc.

3.3.1.6 Internal structure analysis -scanning electron microscopy

The internal structures of each disc was examined using SEM, the images below were taken near the edge of the disc so the microstructure near the surface is visible. Figure 26 shows the effect of pressure on density; discs pressed at lower pressures (100 MPa) had loosely packed particles, with large spaces between the powder clearly seen (A). In discs pressed at 300 MPa, the disc was much more dense and no spaces were seen between powder particles (B). Less apparent was the effect of calcination, which also affected disc structure; discs are less dense when made with calcined powder (C), compared to a disc made of un-calcined powder (D).

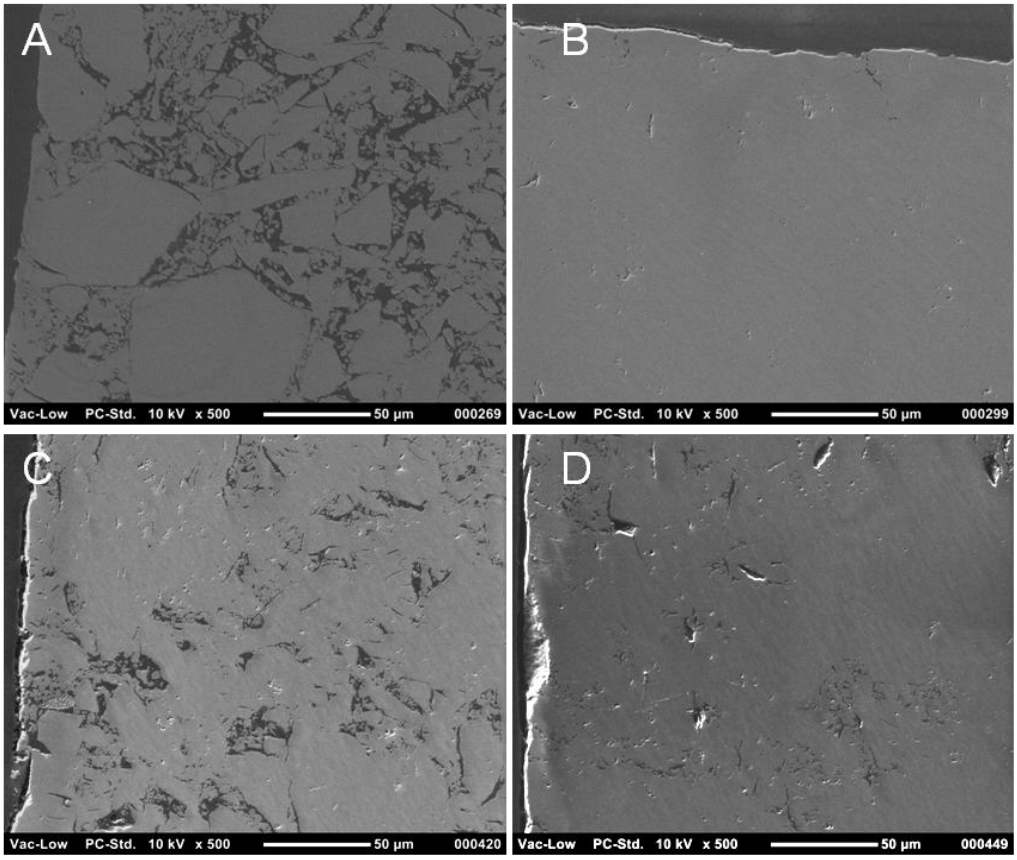

Figure 26: Effect of pressure and calcination on internal structure of discs.

Disc pressed at (A) 100 MPa and (B) 300 MPa (C) calcined powder (D) un-calcined powder.

The surface of the discs was also affected by calcination, as seen in Figure 27, calcined powder appeared to be more dense, and grains more rounded

compared to the irregular grains seen in the un-calcined sample. The surface of the calcined disc also appeared to be smoother, with fewer irregularities such as pits and objects, than the un-calcined disc.

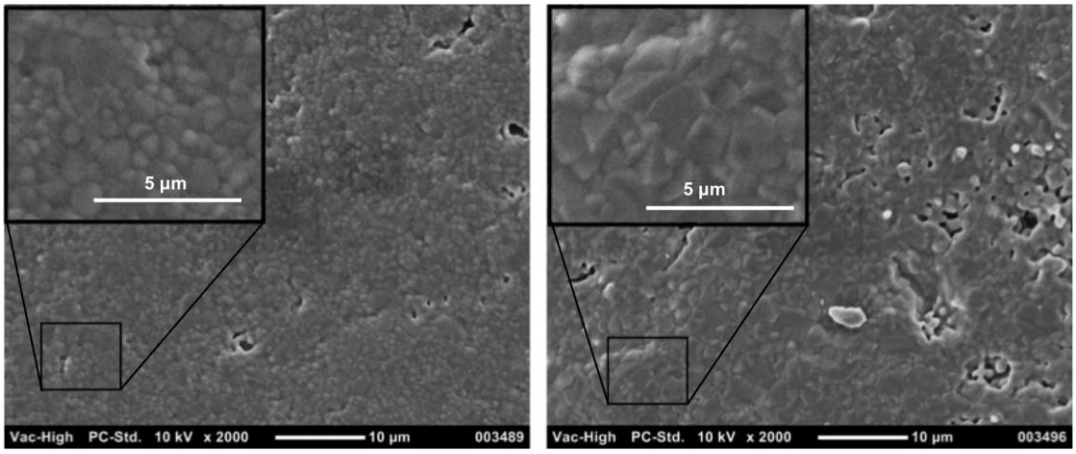

Figure 27: Effect of calcination on grain surface microstructure.

Large image- scale bar represents 10 µm, inset- scale bar represents 5 µm. Discs made using calcined powder (left) and un-calcined powder (right)

Figure 28: Effect of press duration and powder weight on internal structure of discs.

shows the internal structure of discs pressed for different lengths of time (press duration) and powder weight. Press duration and powder weight did not appear to significantly affect the internal structure of discs. Discs pressed for both 5 and 30 seconds appeared similar in density, with little or no space between powder particles, and the edge of the disc appeared to be smooth, seen in (A) and (B) respectively. Discs made with more powder (D) appeared to be slightly more dense than discs made with 0.5 g (C). In both discs spaces between particles can be seen, but also large areas of densely packed powder.

SEM analysis determined the internal structure of discs was influenced by several factors, but most significantly by calcination of powder and the strength of pressure applied.

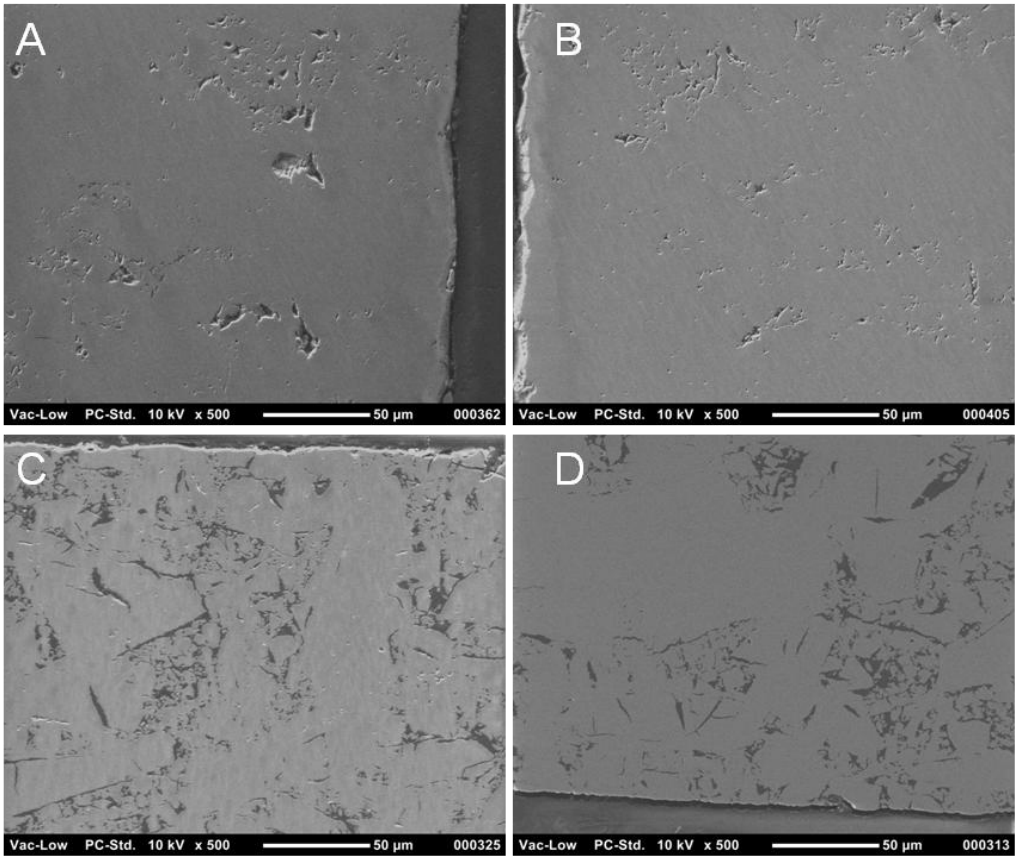

Figure 28: Effect of press duration and powder weight on internal structure of discs.

(A) Disc pressed for 5 seconds, (B) 30 seconds, (C) disc made with 0.5 g of powder, (D) 2 g powder, scale abr represents 50 µm.

3.3.1.7 Sintering

Sintering is one of the final stages of ceramic production, where powder or discs are heated until the particles adhere together. The effect of sintering temperature on disc surface, diameter and height was investigated on both HA and Si-CaP. Figure 29 shows the surfaces of discs sintered at 1260°C, 1000°C, 800°C, and un-sintered discs. The surface of both HA and Si-CaP were smooth when sintered at 1260°C, and appear rougher as sintering temperature decreases. At lower temperatures (1000-800°C and un-sintered) there are more small objects on the surface, and larger areas of deeply pitted surface. The surfaces of the discs sintered at lower temperatures also appear to be more granular and rough.

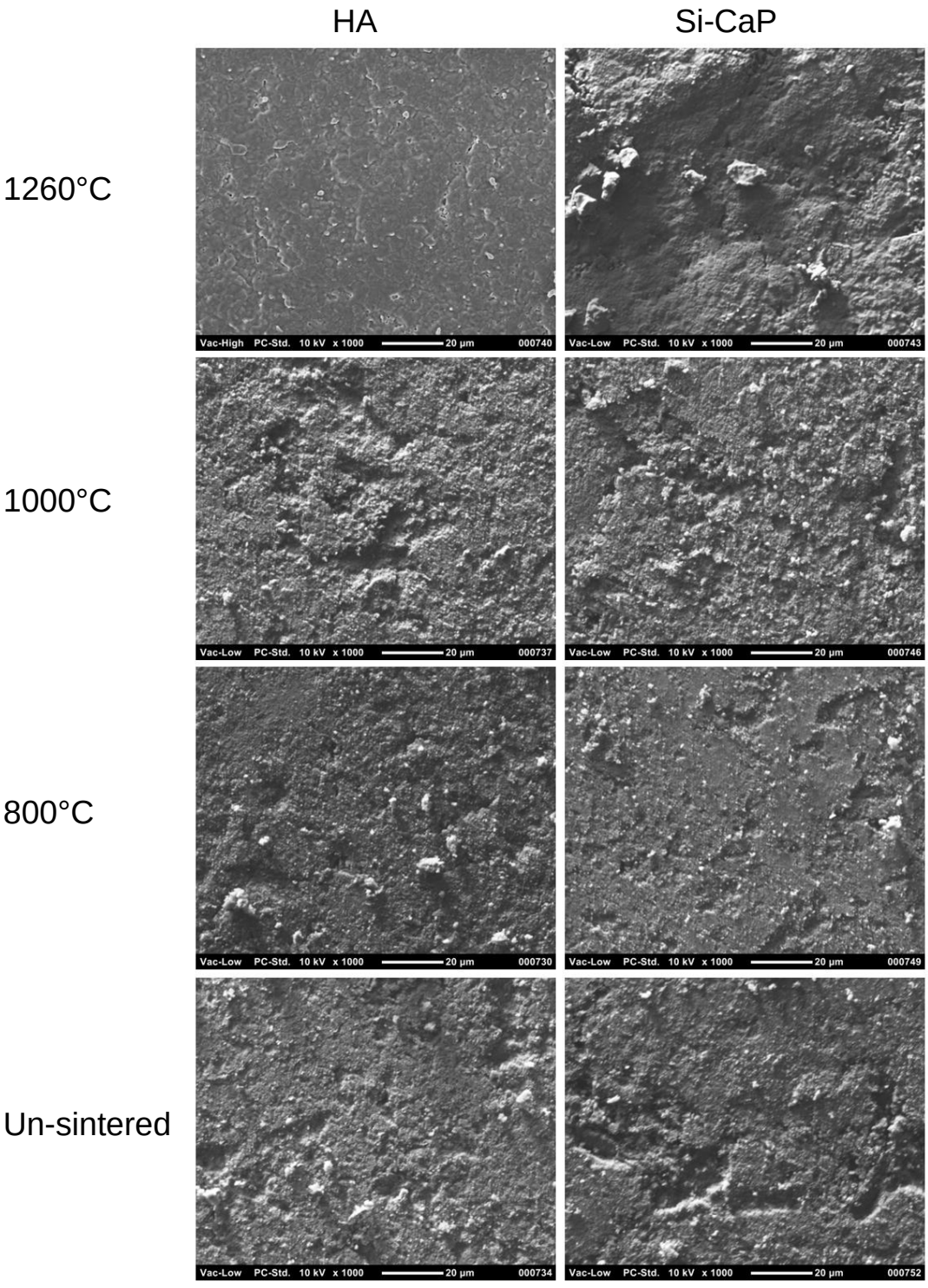

Figure 29: Surface of discs sintered at different temperatures,

Left column- hydroxyapatite (HA), right column Silicate-substituted calcium phosphate(Si-CaP). Scale bar represents 20 µm.

Figure 30 shows how sintering temperature altered height and diameter of discs made with HA or Si-CaP. Disc height decreased as sintering temperature increased, and varied by only 1 mm. Both HA and Si-CaP were similar in height at 1260°C, 800°C and when un-sintered. However, at 1000°C the difference in height is significant (P=0.0016), with HA discs lower in height compared to Si-CaP (2.02 and 2.295 mm respectively). A similar trend is seen in disc diameter, with the only significant difference between HA and Si-CaP occurring at 1000°C (P=0.0001). Overall, the height and diameter of discs decreased as sintering temperature increased, this was more apparent with the diameter varying by as much as 5 mm in both HA and Si-CaP (n=3).

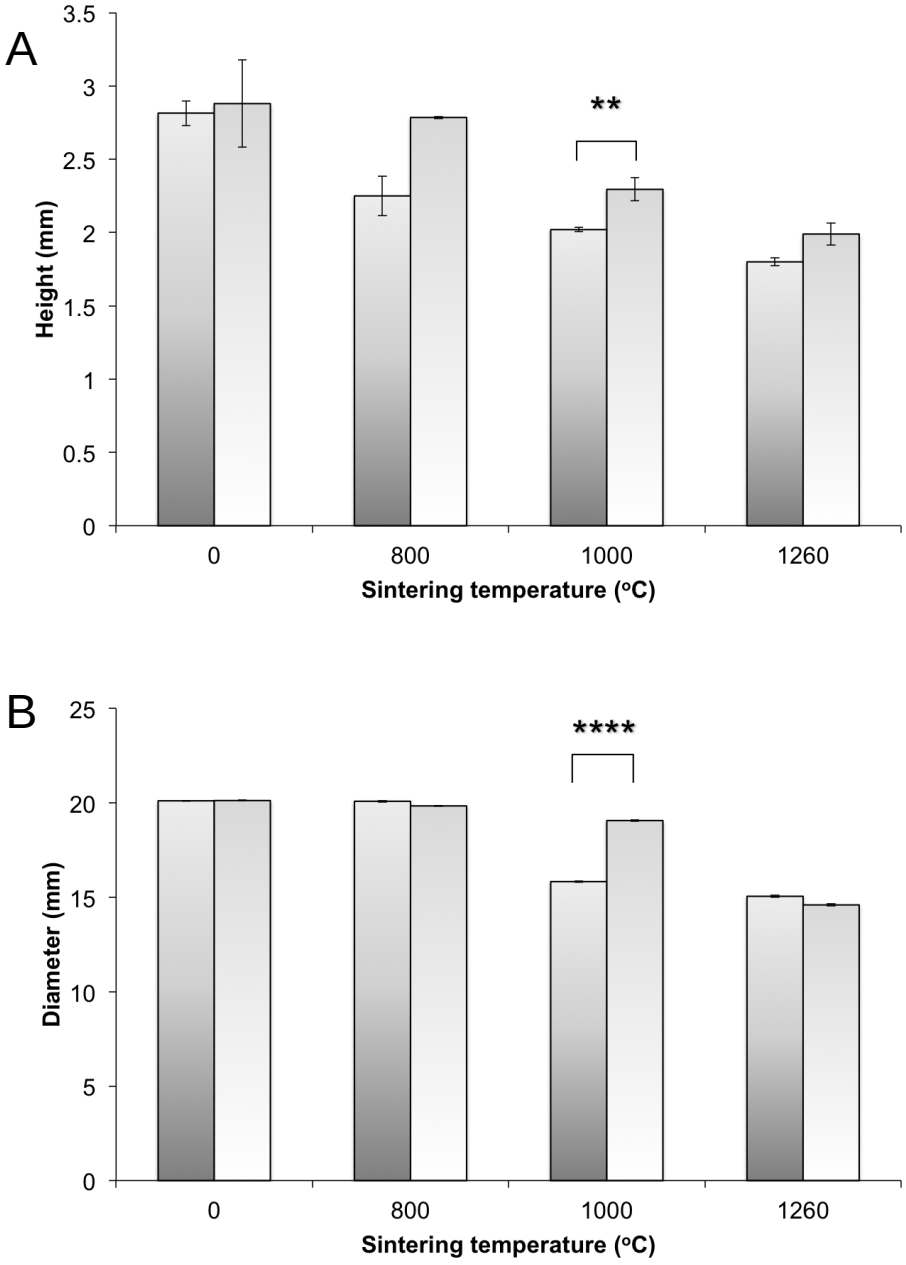

Figure 30: Effects of sintering on (A) disc height and (B) diameter.

*Temperature ranged from 0 (un-sintered) to 1260°C, Three discs were analysed at each temperature. Key: ns (P>0.05), *(P≤ 0.05), **(P≤ 0.01), ***(P≤ 0.001), ****(P ≤ 0.0001).*

Figure 31 shows the grain boundaries of Si-CaP after sintering for 1 hour and 33 minutes at 1260°C. Silicate grains appear much smaller, <1 μm in diameter, and are more rounded when compared to the larger calcium phosphate grains which are up to 2 μm in diameter and are more hexagonal in shape.

The grain boundaries shown here suggest the surface is not uniform; the disc surface is composed of multiple silica grains close together, interspersed with large calcium phosphate grains. HA has an organised crystal lattice structure, whereas the surface of Si-CaP at this scale appears to be disordered, and composed of areas of negative and positive charge.

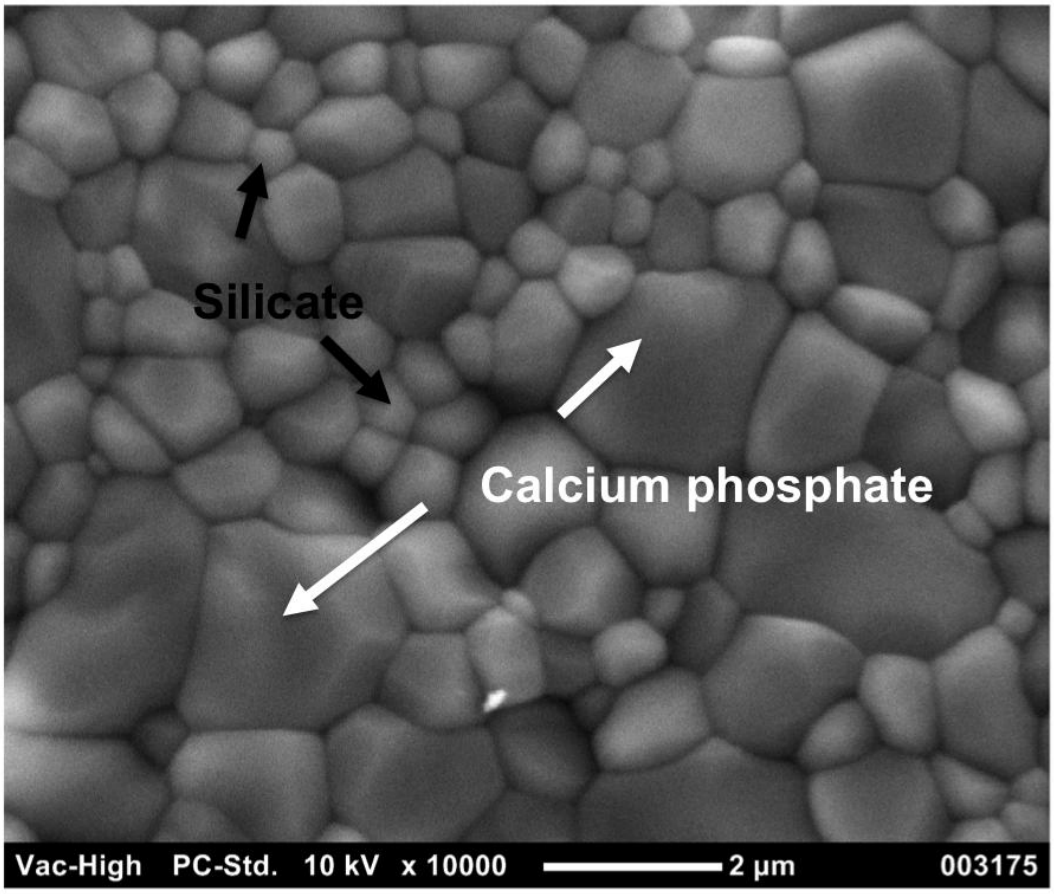

Figure 31: Grain boundaries of sintered Si-CaP disc.

Large grains (white arrow) calcium phosphate, smaller rounded grains are silicate (black arrows). Scale bar represents 2 μm.

3.4 Discussion

3.4.1 Physical properties and production yield

The aim of this chapter was to investigate critical process parameters in production of Si-CaP discs with desired physical properties and optimised production yield.

Pressure greatly influenced disc height and was particularly significant in discs made with 2 g of powder ($P<0.001$), or 0.5 g powder ($p=0.02$). High pressure (300 MPa) resulted in lower disc height. Conversely, lower compaction pressures (100 MPa) produced discs of greater height. Different compaction pressures have been studied with similar results, ranging from 70 MPa (A. Sinha et al. 2001) to 1100 MPa (Pattanayak et al. 2005), suggesting high compaction pressure increases density of discs, and in other studies, increases compressive strength and modulus of elasticity (X. Liu & Ei-Ghannam 2010).

Results in this study demonstrated increased pressure significantly reduced porosity ($P<0.001$), but did not find a significant relationship between density and pressure. Calculated densities ranged from 2.18 to 3.11 kg/m^3 slightly below the maximum theoretical density of hydroxyapatite (3.156 kg/m^3). Pycnometric densities were much higher and in certain cases (samples I, N and P in Table 15) were in excess of this maximum theoretical density. This is likely due to the small sample size and increasing error potential for this measurement technique, and may be avoided in future studies by increasing sample size to reduce error.

Pressure also significantly affected disc diameter ($P<0.001$). Disc diameter increased as pressure increased, which could be due to the discs pressed at high pressures being denser and therefore more resistant to densification (increase in density) upon sintering.

Differing pressure and press duration have been studied, ranging from 30 seconds to 1 minute (Rosa et al. 2003; Kumar et al. 2010; X. Liu & Ei-Ghannam 2010; Pattanayak et al. 2005). However, until now the effect of

altering duration of pressure on physical properties of dense discs had not yet been examined. Press duration did affect strut porosity and density, but neither reached statistical significance (P=0.187 and P=0.2400 respectively).

Discs were successfully manufactured and sintered with as little as 0.5 g of powder. However, these discs cracked easily, whereas discs produced with 1.25 g and 2 g were more resistant to strain on handling. It may be useful in the future to investigate compressive strength and modulus of elasticity to evaluate the strength of discs quantitatively.

Powder weight directly affected several parameters; including disc height, diameter and strut porosity. As expected height was increased in discs made with greater powder weight and this relationship was found to be significant (P=0.0156). Discs made with 2 g of powder resulted in discs with smaller diameters than discs made with 0.5 g of powder, but this was not significant (P= 0.0881). This may due to discs made of 2 g are less dense and therefore more likely to shrink on sintering. Data from strut porosity and SEM images, confirm this, and show that discs made from 0.5 g of powder were denser after sintering.

Prior to pressing discs, powder is commonly calcined to remove unwanted volatile fractions. Altering the temperature of calcination has been shown to significantly affect the sintering properties of discs. Calcined powder was found to produce discs with greater diameters when compared to un-calcined powder (P= 0.016). Calcination makes the powder finer, and denser, therefore less susceptible to shrinking on sintering. The use of un-calcined powder in disc manufacture however, may not be desirable as some volatile fractions and chemical impurities would not be removed if the discs were left un-sintered.

Several studies have utilised lubricants in disc manuafcture, commonly stearic acid (Juang 1996; A. Sinha et al. 2001), to coat the die and pellet. Stearic acid greatly improved the ease with which the discs were removed from the pellet and die set; as such this was expected to improve production rates. However, the time taken to clean the pellet and die set

meant the rate of production was either unaffected or prolonged. Furthermore, it did not significantly affect any parameters, except diameter. Which was likely caused due to the stearic acid contributing to internal density and therefore preventing shrinkage. Notably, when compared to discs manufactured with no lubricant there was a greater frequency of large irregularities in the form of both pits and objects ($p=0.170$). It has also been shown that stearic acid can affect the surface chemistry of calcium based materials (Rungruang et al. 2006). This is far from desirable as it may influence the cellular response.

SEM analysis of gold sputtered discs demonstrated that the sintered disc surface is not typically smooth at micrometer scale; many discs have a pitted surface or may contain objects greater than 500 μm in length. Analysis of sectioned discs revealed internal structures and variations in particle packing and whilst this was not quantified, gave insight into the density and structure of the discs. It is recommended that any future studies quantify the amount of strut-porosity using image analysis of embedded sections.

Sintering is one of the final stages of ceramic production, where powders or discs are heated until particles adhere together. This process can have significant effects on material properties, depending upon the temperature and duration of heating and has been extensively studied (Rosa et al. 2003; Kumar et al. 2010; Wu et al. 2008; Rodríguez-Lorenzo et al. 2001; Pattanayak et al. 2005; Gibson et al. 1999).

Here it was demonstrated that altering the sintering temperatures could significantly affect height, diameter and surface properties of dense discs. Sintering at low temperatures (800-1000°C) produced discs of a greater height and diameter, compared to higher temperatures (1260°C) and resulted in a rough surface with multiple objects and pits. This is consistent with similar studies, which have shown low densification is seen after sintering at low temperatures (1000-1100°C) and high densification is achieved after sintering at higher temperatures (1200-1300°C) (Oktar 2007).

Sintering not only affects the structural and mechanical properties of calcium phosphate but can alter the phases of material (X. Liu & Ei-Ghannam 2010) and at very high temperature can result in melting of grains. This was not detected in Si-CaP sintered at 1260°C, suggesting this is the optimal sintering temperature.

It was demonstrated that disc height and diameter were influenced by the input parameters, but that intruded strut porosity, calculated and pycnometric densities were not affected by input parameters.

Discs could be successfully produced with 0.5 to 2 g of powder, yet the minimum weight of powder required to manufacture discs of sufficient handling strength was 1.25 g.

The minimum pressure needed was found to be 100 MPa; however discs pressed at 200 MPa or above contained substantially less strut porosity.

Press duration was not found to be critical to disc manufacture, therefore the lowest press time investigated (5 seconds) is suggested to be optimal for greatest throughput.

Un-calcined powder was more readily compacted, however the use of un-calcined powder in disc manufacture may not be desirable, as volatile fractions and chemical impurities would not be removed if left un-sintered.

Stearic acid improved ease of extrusion of disc from the die, however resulted in a greater frequency of surface irregularities compared to discs manufactured without a lubricant.

Sintering temperature affected disc height, diameter and surface characteristics of dense discs.

The final recommendations for all parameters based on data provided in this study are shown in Table 17.

Table 17: Recommended final parameters.

Parameter	Specification	Tolerance
Powder weight	1.25g	+/ - 0.1g
Pressure	200 MPa	+/ - 10MPa
Press duration	5 seconds	+/ -1 second
Lubrication	None	N/ A
Calcination	calcined	N/ A
Sintering temperature	1260 °C	N/ A

3.4.2 Influence of disc on cell response

Disc manufacture was optimised with regard to physical properties and production yield. These dense discs were then used to analyse cellar response to the surface chemistry of Si-CaP and HA, without the influence of porosity and with minimal variation in surface topography.

It has been demonstrated that surface chemistry of biomaterials can greatly influence cell adhesion, proliferation and differentiation.

Whether *in vitro* or *in vivo*, cells do not interact directly with the biomaterial, instead proteins in surrounding fluid condition the biomaterial. This process of protein adsorption, where proteins adhere to the surface of a substrate, can be altered by many variables including surface energy, topography, temperature and pH. The orientation and conformation of protein absorption has a direct influence on cell attachment, proliferation and differentiation (Boyan 1996). Surface charge has shown to be particularly influential in protein adsorption (Combes & Rey 2002).

The surface of Si-CaP was shown here to be heterogeneous, composed of different grains with positive and negative surface charge. This is consistent with previous studies (Botelho et al. 2002).

The effect of the surface charge of Si-CaP and HA on protein adsorption has previously been investigated (Botelho 2005). It was demonstrated that

Si-CaP had a higher binding capacity for total human serum proteins, particularly collagen type I due to its overall positive charge, when compared to HA (Botelho et al. 2004). This preferential binding of positively charged proteins was due to the of overall electronegative charge of Si-CaP (Botelho et al. 2002). The more electronegative Si-CaP surface was shown to enhance the nucleation of an amorphous calcium phosphate apatite layer than the HA surface, known as an apatite layer –considered to be an important factor for osseointegration (Botelho 2005).

Many studies have closely examined the surface charge of Si-CaP and its subsequent effect on protein adsorption and nucleation. As such this thesis will focus on the attachment, proliferation and differentiation of mesenchymal stem cells on Si-CaP.

CHAPTER FOUR: CHARACTERISATION OF MESENCHYMAL STEM CELLS

4.1 Introduction

Multipotent mesenchymal stem cells (MSC) are well established as a source of cells for tissue engineering and cellular therapy. *In vivo*, a population of MSC are known to reside within bone marrow (Kolf, Cho & Tuan 2007a; Nombela-Arrieta et al. 2011; Chamberlain et al. 2007; Crisan et al. 2008; Barry & J. M. Murphy 2004; Boyd et al. 2009; Haasters et al. 2009; Yoshimura et al. 2006; Pittenger 1999; Jack et al. 2002).

MSC are thought to migrate to sites of damage, (Chamberlain et al. 2007; Haasters et al. 2009; Yoshimura et al. 2006; Pittenger 1999), where they are capable of differentiating into, and repairing mesenchymal tissues including bone, cartilage and adipose tissue (Augello et al. 2010). MSC represent a very small fraction of the total population of cells in bone marrow, 0.001-0.01% (Pittenger 1999). Despite this, they can be isolated and readily expanded in culture (Dominici et al. 2006).

Under defined conditions *in vitro*, MSC have been shown to differentiate into osteoblasts (in the presence of serum, ascorbic acid, beta glycerophosphate and dexamethasone), chondrocytes (in serum free medium containing TGF-β1, TGF-β2 or TGF-β3), and adipocytes (in the presence of isobutylmethylxanthine) (Barry & J. M. Murphy 2004). This multipotent differentiation potential, plastic adherence, and specific surface antigen expression, are considered to be the minimal criteria for MSC *in vitro* (Dominici et al. 2006). Despite many attempts to develop a robust cell-surface antigen profile for the identification and purification of MSC (Kolf, Cho & Tuan 2007a), the defining characteristics of MSC are still debated amongst investigators and therefore definitive MSC surface antigen expression remains a contentious issue (Dominici et al. 2006). As such, a combination of multiple surface markers should be used to positively identify MSC.

It is generally accepted that MSC express (amongst others) the cell surface markers CD90, CD73, CD105, Stro-1, and are negative for haematopoietic progenitor markers CD34, CD45 and CD14. The reported expression of these markers by a number of studies is reviewed in Table 18.

Table 18: Reported cell surface marker expression in mesenchymal stem cells.

Expression	Antigen	References
Positive	CD90	(Kolf, Cho & Tuan 2007b; Chamberlain et al. 2007; Crisan et al. 2008; Vodyanik et al. 2010; Haasters et al. 2009; Sanchez-Guijo et al. 2009; Yoshimura et al. 2006; Kozhevnikova et al. 2008; Jack et al. 2002; Dominici et al. 2006; Ohgushi et al. 2005; Orciani et al. 2010)
	CD73	(Kolf, Cho & Tuan 2007b; Chamberlain et al. 2007; Crisan et al. 2008; Barry & J. M. Murphy 2004; Boyd et al. 2009; Haasters et al. 2009; Kozhevnikova et al. 2008; Pittenger 1999; Jack et al. 2002; Dominici et al. 2006; Orciani et al. 2010)
	CD105	(Chamberlain et al. 2007; Kolf, Cho & Tuan 2007b; Crisan et al. 2008; Barry & J. M. Murphy 2004; Boyd et al. 2009; Haasters et al. 2009; Kozhevnikova et al. 2008; Pittenger 1999; Yoshimura et al. 2006; Blitterswijk et al. 2007; Foster et al. 2005; Jack et al. 2002; Dominici et al. 2006; Orciani et al. 2010)
	Stro-1	(Kolf, Cho & Tuan 2007b; Vodyanik et al. 2010; Jack et al. 2002; Tare et al. 2012)
	CD146	(Crisan et al. 2008; Boyd et al. 2009; Jack et al. 2002)
Negative	CD34	(Chamberlain et al. 2007; Kolf, Cho & Tuan 2007b; Barry & J. M. Murphy 2004; Boyd et al. 2009; Haasters et al. 2009; Yoshimura et al. 2006; Pittenger 1999; Crisan et al. 2008)
	CD45	(Nombela-Arrieta et al. 2011; Kolf, Cho & Tuan 2007b; Chamberlain et al. 2007; Crisan et al. 2008; Barry & J. M. Murphy 2004; Boyd et al. 2009; Haasters et al. 2009; Yoshimura et al. 2006; Pittenger 1999; Jack et al. 2002)
	CD14	(Chamberlain et al. 2007; Haasters et al. 2009; Yoshimura et al. 2006; Pittenger 1999)

Each of these surface markers is thought to play a role in maintaining multipotency of mesenchymal stem cells or in identifying haematopetic progenitor cells.

- CD90 (Thy-1) is a glycosylphosphatidylinositol (GPI)-anchored, extracellular surface, protein found on mesenchymal stem cells, and is thought to be related to mutipotency (Oishi & Ito-Dufros 2006).
- CD73 or lymphocyte-vascular adhesion protein 2 is a nucleotidase expressed on many cell types, including lymphocytes, and is not specific to mesenchymal stem cells. Nonetheless, it does not react with osteoblasts or osteocytes, which may contaminate MSC cultures and its persistence throughout culture supports its utility as an MSC marker (Kolf, Cho & Tuan 2007b).
- CD105 is a transmembrane, transforming growth factor (TGF)-beta receptor associated with mesenchymal stem cells (Barry et al. 1999): it has been shown to play a role in proliferation, differentiation and migration (Banas et al. 2007; Mitchell et al. 2005).
- The best-known MSC marker by far is Stro-1, cells negative for Stro-1 are not capable of forming colonies (Simmons & Torok-Storb 1991b). However, Stro-1 is a contentious MSC marker for several reasons: first, no mouse counterpart of Stro-1 has been found; second, Stro-1 expression is not exclusive to MSC; third, its expression in MSC is gradually lost during culture expansion (Gronthos et al. 2003), and fourth, the exact function of the Stro-1 antigen is unknown.
- CD34 is a primitive haematopoietic stem cell marker, rarely expressed in human MSC, although it is positive in mice MSC (Peister 2004). CD45 and CD14 are found in cells of the haematopoietic lineage (Chamberlain et al. 2007).

Despite this confusion around antigen expression, the most defining property of MSC is their capacity for multi-lineage differentiation.

Bone marrow derived MSC can be used to study osteogenic differentiation *in vitro*; induced through the addition of soluble factors known to stimulate differentiation, and also cultured on substrates engineered to direct cell fate. However, they have several potential drawbacks, including limited

availability, donor genetic variability, variability in age and condition of the tissue at the time of donation, and heterogeneity in culture. To date, multipotent stem cells have been extracted from a variety of organs, such as skeletal muscle (Péault et al. 2007), bone marrow (Pittenger 1999), skin (Toma et al. 2001), pancreas, fat (Zuk et al. 2001), dental pulp (Gronthos 2000), placenta (Scherjon et al. 2004), and umbilical cord (Erices et al. 2000).

One of the most promising sources of multipotent adult stem cells is from adipose tissue, largely due to the ease by which adipose tissue can be accessed. Initial enzymatic digestion of extracted adipose tissue yields a combination of stromal and vascular cells often referred to as the stromal-vascular fraction. These adipose derived multipotent stromal cells (ADMSC) appear to be very similar to bone marrow derived MSC with similar cell surface marker expression (Gronthos, D. M. Franklin, et al. 2001a), hold comparable differentiation potential (Guilak et al. 2005; Zhang et al. 2011), and possess a similar proliferative capacity (Crisan et al. 2008).

Ideally a population of healthy, homogenous cells with unlimited expansion potential would be optimal to study osteogenic differentiation *in vitro* and the route to obtaining these may be through the growth and differentiation into MSC of human embryonic stem cells (hES).

hES have an infinite proliferative capacity *in vitro* (Wang et al. 2008) and have the potential to differentiate into derivatives of all three germ layers; however, a major drawback of these cells is the risk of tumour formation *in vivo* (Pera et al. 2000). An alternative is to use hES to derive lineage restricted progenitor cells, which do not form teratomas. Human Embryonic stem cell derived mesenchymal progenitors (hES-MP) are a commercially available (Cellartis, Dundee, UK) source of homogenous cells with extensive proliferative capacity. These cells do not express markers associated with hES, and have a similar gene expression pattern to MSC data (de Peppo, Sjovall, et al. 2010a). It has been demonstrated that hES-MP express MSC associated surface markers, can differentiate along osteo-, chondro- and adipogenic lineages and have an MSC-like morphology in culture (Karlsson et al. 2009).

Despite the potential therapeutic benefits of pluripotent hES cells, legal and ethical controversies concerning their use still remain. As a result, sources of multipotent cells from within adult tissue continue to be explored.

In this thesis, three different sources of cell types; MSC, hES-MP and ADMSC, were utilised to analyse the osteogenic influence of Si-CaP and HA.

The aim of this chapter was to determine similarities and differences of cells from different sources.
Each cell type was examined with regard to: morphology in culture, expression of cell surface markers, expression of transcription factors and the ability to differentiate into multiple lineages *in vitro*.

4.2 Results

MSC supply was limited due to a variety of logistical reasons; the priority for tissue samples was for clinical bone banking, and only tissues not suitable for this purpose were made available for research use. In addition, a number of groups were in competition for these samples, further restricting access to clinical samples. Consequently, when samples were obtained, cells were expanded for several passages to ensure sufficient cell number for experimental purposes.

In order to ensure the MSC used at later passages were equivalent to cells used at earlier passages characterisation was carried out at both early (P2) and later passages (P6). The effect of passage number on cell characteristics was also examined in hES-MP and in ADMSC.

4.2.1 Morphology

Cells displayed similar morphology despite originating from different sources. All three cell types adhered strongly to tissue culture plastic and displayed a fibroblast-like morphology as shown in Figure 32, where all three cell types are compared.

MSC (A) had a relatively small cell body with long thin processes; the population appeared to be relatively homogenous with all cells similar in length and shape. hES-MP (B) were more heterogeneous, in length, width and size. They tended to grow in clusters, which was most apparent when cells became confluent. ADMSC (C) morphology was very similar to MSC, but cells were slightly larger, with a less pronounced nucleus.

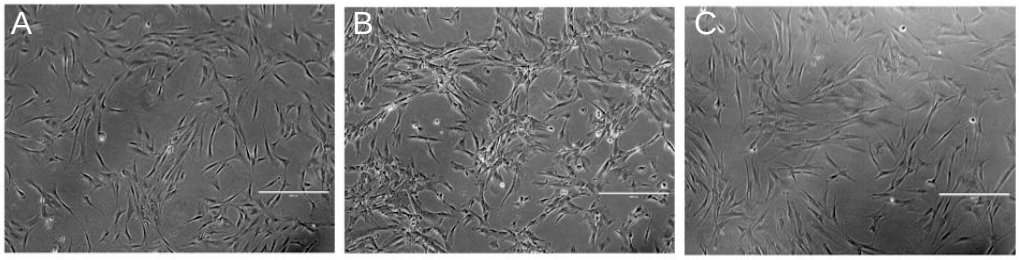

Figure 32: Typical morphology of cells in culture

Representative images of cell morphology cultured on tissue culture plastic (A) MSC, (B) hES-MP, (C) ADMSC. Scale bars represent 400 μm.

4.2.2 Proliferation

Cells of each of the three MSC types were allowed to proliferate over 21 days, and at regular intervals were fixed, counted and the average number of attached cells per mm^2 calculated; these counts were used to produce growth curves for each cell type, and these are shown in Figure 33. These data were used to calculate cell-doubling rates, using the formula below where N_1 is the number of cells on Day 1 and N_{21} is the number of cells on Day 21.

$$\text{Doubling rate (Days)} = [\log10(N_{21}) - \log10(N_1)]/ \log10(2),$$

ADMSC proliferated the fastest and most consistently, with a doubling rate of 1.7 ± 0.09 days (mean±SD). MSC doubling rate was less than half that of ADMSC (4.1 ± 1.6 days). Doubling rates of different MSC isolates were relatively consistent between donors (4.3, 3.89, and 4.1 days) and similar variation was observed (SD of 2.0, 1.2, and 1.6 days respectively). In hES-MP, the average doubling rate was 4.9 ± 3.5 days, and was also relatively consistent between passages (4.8, 4.8, and 4.9 days) but at the latest passage (P11) greater variation was observed (SD of 4.9, compared to 2.5 and 2.8 days for P9 and P10 respectively).

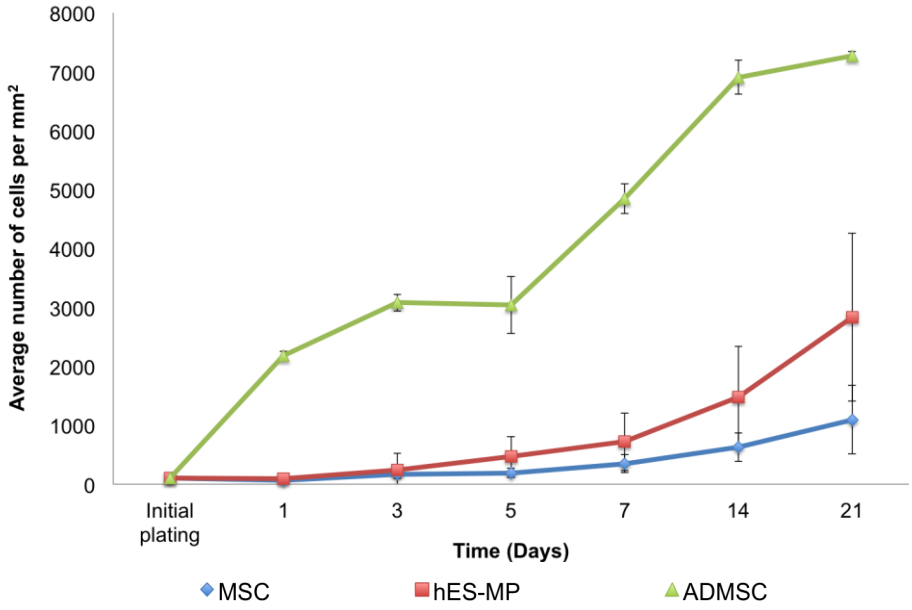

Figure 33: Proliferation of different mesenchymal cell types.

Cells on tissue culture plastic over 21 days, for MSC three donors were used, for ADMSC two donors were used and each sample was run in triplicate.

4.2.3 Flow cytometric analysis

Flow cytometry was used to determine expression of surface markers associated with mesenchymal stem cells: CD90, CD73, CD105 and Stro-1.
Cells were gated according to their side scatter *vs.* forward scatter properties, in order to eliminate dead, differentiated or cell aggregates, as shown in Figure 34.
Each cell type displayed different forward scatter (FSC) and side scatter (SSC) profiles. MSC had a high FSC, suggesting these cells are larger than both hES-MP and ADMSC. hES-MP had low SSC suggesting these cells were less granular compared to MSC. They also appeared to be the most homogenous, which would be expected from a cell line. ADMSC had a lower FSC compared to MSC, suggesting they are smaller; SSC was higher and more diverse, suggesting these cells were more heterogeneous and complex in granularity, which could be due to either intracellular or extracelluar (i.e cell shape) complexity.

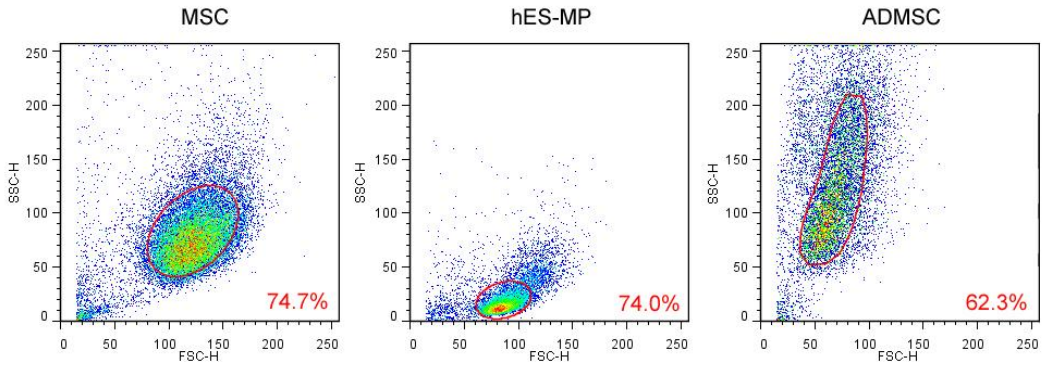

Figure 34: Flow cytometry gated populations

Cell gates defined based on forward scatter (FSC) and side scatter (SSC).

The expression of a number of cell surface markers of MSC (outlined in Table 18) was analysed on each of the gated populations and the histograms obtained are shown in Figure 35.

MSC MSC highly expressed CD90 (99.6%), CD73 (100%), CD105 (96.1%), and had moderate expression of Stro-1 (20.8%). All cells appeared to be homogenous as evidenced by a clear shift of the whole population to the right.

hES-MP hES-MP highly expressed CD90, CD73, CD105; (83.9, 98.5, 99.9%, respectively) and had slightly more Stro-1 positive cells (65.2%) compared to MSC. Similarly, most markers were homogenous within the population of cells, with the exception of CD90, which appeared to contain two distinct subpopulations, both of which were positive, termed CD90 ^{high} and CD90 ^{low}. Subsequently these distinct populations were sorted by fluorescence-activated cell sorting (FACS), and examined for differences in transcription factor expression prior to and after culture for 1 week. These results will be discussed in a later section (see section 4.2.6).

ADMSC A high percentage of ADMSC were positive for CD90 (99.3%) CD73 (94.2%) and CD105 (92.2%). The Stro-1 positive population appears to be slightly lower (46.9%) but this may

be an artifact of a higher level of nonspecific background staining seen with this cell type.

Despite the homogeneity of hES-MP apparent in the forward and side scatter profiles shown in Figure 34, MSC appear to be the most homogenous in marker expression, as evidenced by the narrow window of expression seen in the histograms in Figure 35.

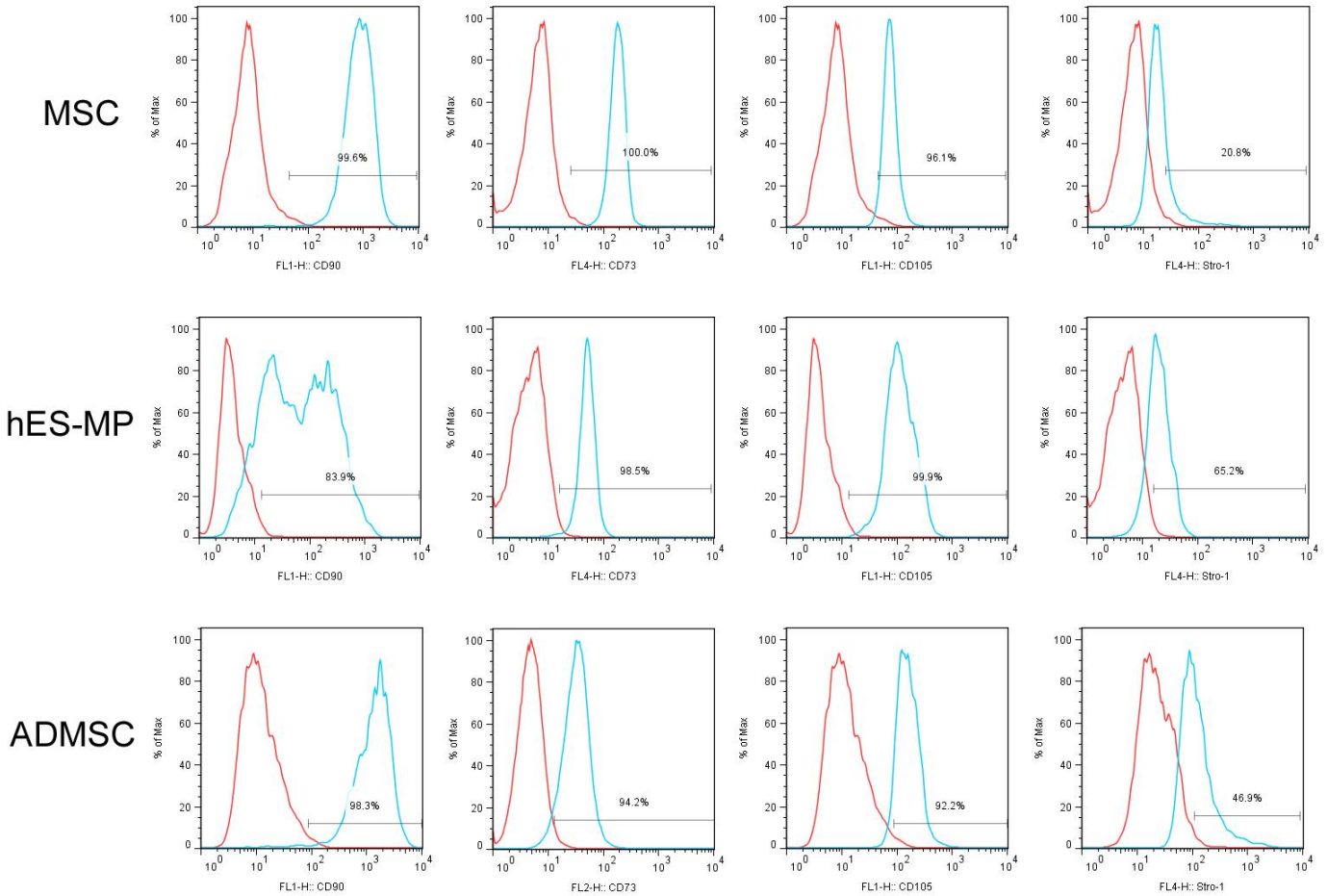

Figure 35: Flow cytomtery immunotyping.

Representative histograms show expression of surface markers associated with mesenchymal stem cells, expressed as a percentage of maximum. Red line - cells without antibody (negative) and blue line - cells with bound antibody (positive).

The MSC population is derived from bone marrow, which is a site of haematopoiesis and therefore contains haematopoietic stem cells. ADMSC, derived from adipose tissue is also a highly vascular tissue.

To examine the possibility of contamination with haematopoietic progenitors, each population was analysed for expression of markers associated with the haematopoietic lineage: CD34, CD14 and CD45. The percentage of positive cells expressing these surface markers, *versus* the mesenchymal associated markers: CD90, CD73, CD105 and Stro-1 are shown in Table 19 for each cell type.

Table 19: Percentage of cells expressing MSC or haematopoietic cell surface markers.

Cell type	Passage	CD90	CD73	CD105	Stro-1	CD34	CD14	CD45
MSC	P2	99.9	32	2.6	3.44	0.9	1.08	1.0
	P6	99.6	100	96.1	20.8	1.8	6.12	1.65
hES-MP	P8	83.9	98.5	99.9	65.2	40.9	78.5	N/ A
	P8 (Gelatin)	95.3	99.5	99.8	19.4	0.8	11.7	0.7
	P11	76	96.1	98.5	15.2	0.8	7.96	2.03
	P11 (Gelatin)	85.3	37.1	99.2	17	2.7	8.53	1.9
ADMSC	P1	98.3	98.2	92.2	46.9	9.5	15.8	5.5

N/A indicates this maker was not analysed.

hES-MP were originally established as a cell line grown on a gelatin substrate, although it was suggested that they could also be grown on uncoated tissue culture plastic (Karlsson et al. 2009). The cell line was therefore analysed after several passages on either 0.1% gelatin, or uncoated tissue culture plastic, to examine how the substrate influenced cell surface marker expression. Initially cells were then cultured on gelatin, as recommended by the supplier. A portion of these cells were transferred at P6 to culture on tissue culture plastic alone, to allow comparable results with MSC and ADMSC, which were routinely cultured on uncoated plastic. This change in culture conditions did not significantly affect the expression of CD90, CD73 and CD105 on hES-MP cells. However, hES-MP cultured on plastic did have higher Stro-1, CD34 and CD45 expression. The bimodal, CD90 positive, hES-MP population was gated according to

expression to determine whether gelatin or plastic was influencing CD90 expression. However, there was no significant difference in expression, between the subsets of CD90 between gelatin and plastic, as seen in Table 20.

Table 20: CD90 expression in hES-MP with dual populations.

Passage	**Expression**	**Percentage of CD90 positive cells (%)**	mean fluorescence intensity **(MFI)**
P8	CD90 low	46.4	30.2
	CD90 high	53.6	278.5
P11	CD90 low	25.5	21.2
	CD90 high	54.5	155.8
P8 (gelatin)	CD90 low	20.9	36
	CD90 high	79.1	209.2
P11 (gelatin)	CD90 low	32.8	30.0
	CD90 high	67.2	168.7

MSC did not express CD34, CD14 or CD45 in a significant proportion of cells at either P2 (<1.1%) or P6 (<6.13%). A high percentage of hES-MP expressed CD34 (40.9%) and CD14 (78.5%) at P8, when cultured on plastic; at P11, this was greatly reduced (0.803% and 7.96% respectively).

hES-MP had a higher percentage of cells expressing CD14 than MSC. Yet, there was no significant difference between cells cultured on plastic *vs.* gelatin with regard to CD34, CD14 and CD45 expression overall. ADMSC had a greater number of cells expressing CD34 (9.47%), CD14 (15.8%) and CD45 (5.48%) when compared to MSC.

The mean fluorescence intensity (MFI) was also examined, and was calculated by subtracting the median fluorescence intensity of the positive sample from the control sample (no antibody), and results are shown in Table 21. Under saturated conditions, MFI is directly related to the amount of bound antibody, and therefore the number of receptors per cell (Riquelme et al. 2006).

Table 21: Mean fluorescence intensity of surface markers on cells

Cell type	Passage	CD90	CD73	CD105	Stro-1	CD34	CD14	CD45
MSC	P2	1204.7	50.5	20.6	16.1	2.7	4	2.8
	P6	917.6	180.1	69.2	20.3	1.2	15.7	8.3
hES-MP	P8	137.5	47.3	128.5	16.5	22.5	14.6	N/ A
	P8 (Gelatin)	119.2	42.3	114.2	7.7	0	2.9	-0.4
	P11	86.9	29.7	65.9	6.25	0.18	4.6	0.5
	P11 (Gelatin)	105.7	29.8	81.7	10.9	1.1	3.4	-1.7
ADMSC	P1	1514.3	506.3	168.3	154.3	22.1	55.1	27.2

N/A indicates this maker was not analysed.

Significant differences in expression were observed, when compared to percentage expression. MSC had high mean fluorescence intensity (MFI) values for CD90, in both P2 and P6 (1204.7 and 917.6 respectively), P2 MSC displayed a MFI of 50.5 for CD73, and this was greater in in P6 (180.12). However, CD105 and Stro-1 were much lower (20.2 and 16.1 respectively). Haematopoietic markers CD34, CD45 and CD14 were low, with MFI values similar to hES-MP cultured on gelatin. hES-MP cultured on plastic (P8) had high MFI values for all haematopoietic markers, but this was not seen at the later passage (P11). A high percentage of hES-MP cells expressed CD90, CD73 and CD105. Yet, their MFI was considerably lower than MSC and ADMSC.

ADMSC displayed the highest MFI for all surface markers, with the exception of CD90, the MFI was greater than 2-fold higher than any other cell type. This could be due to larger cells binding more antibody, however when the population was divided according to size (FSC) and analysed, this was not proven.

To confirm that hES-MP had a mesenchymal stem cell phenotype they were also examined using markers associated with embryonic stem cells, shown below in Table 22. hES-MP displayed low expression, in a small

percentage of cells, of TRA1-60, TRA1-80, SSE1 and SSEA3. However SSEA4 expression was high, expressed by 83.5% of cells and had a MFI value at least 13.7–fold greater than any other hES associated marker.

Table 22: Embryonic stem cell associated marker expression in hES-MP.

Marker	Percentage of cells (%)	Mean fluorescence intensity (MFI)
TRA1-60	6.1	3.1
TRA1-81	2.6	0.41
SSEA1	1.23	0.1
SSEA3	3.51	3.1
SSEA4	83.5	101.19

To determine localisation of staining, and confirm flow cytometry results, cells were stained for CD105 and Stro-1 at several passages.

All cell types expressed CD105 and Stro-1 throughout culture on tissue culture plastic, in standard growth medium, MSC (P1-P4) hES-MP (P7-P15) and ADMSC (P2-P12).

Figure 36 shows the distribution of CD105 and Stro-1 staining for each cell type, representative of the level of staining seen at each passage.

MSC showed CD105 positive staining throughout the cell surface, but the strongest staining was detected near the nucleus. Stro-1 expression in MSC was similar to CD105, but was not detected in all cells. The majority of hES-MP cells expressed CD105 and the staining was similar in intensity compared with MSC. Stro-1 staining however, was much weaker in intensity and yet most cells showed positive expression. CD105 expression in ADMSC was noticeably different to hES-MP and MSC (distribution of staining was consistent across the cell surface) and there was also a clear difference in levels of expression between cells, with some cells much brighter than others. A large proportion ADMSCs expressed Stro-1, and the staining also appeared to be much brighter than in hES-MP and MSC.

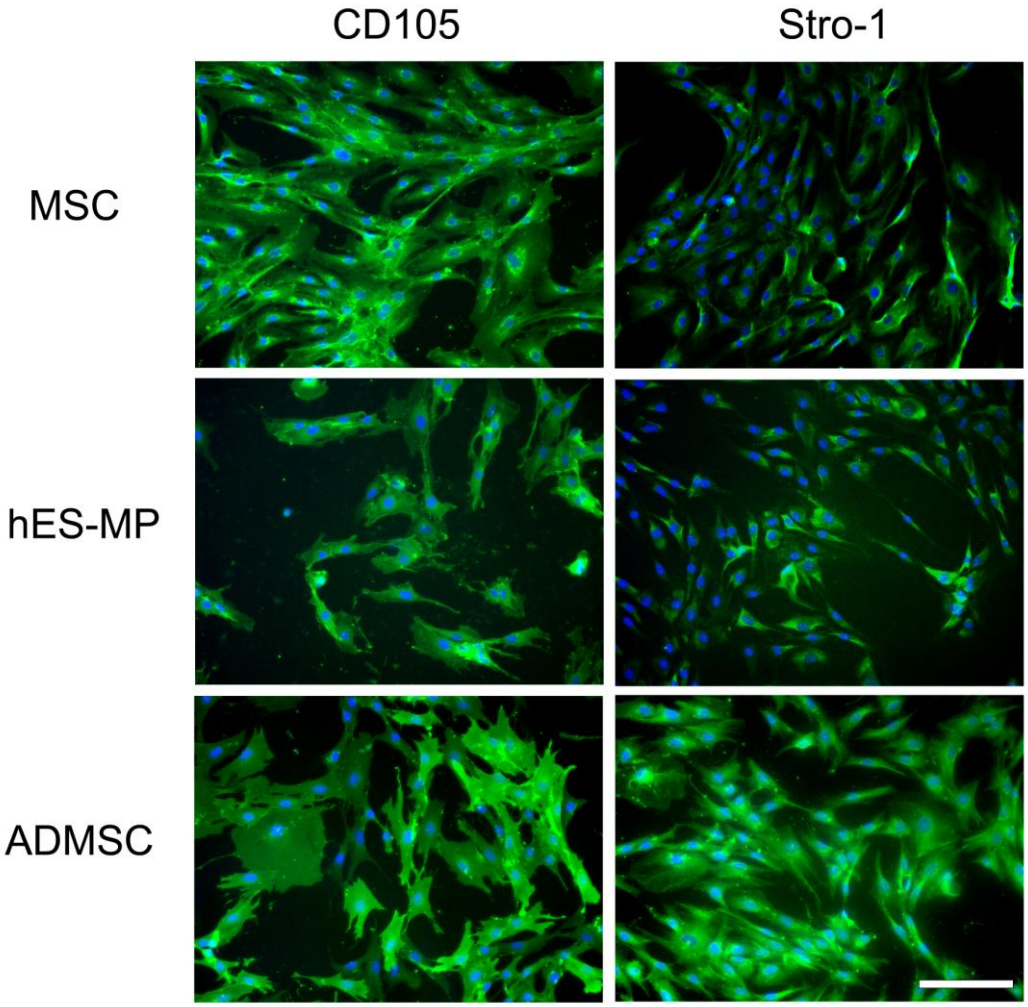

Figure 36: CD105 and Stro-1 immunostaining of MSC, hES-MP and ADMSC.

Repsesentative staining of cells in culture. Scale bar represents 100 μm.

4.2.4 Transcription factor expression

Each cell type was analysed using semi quantitative PCR to measure transcription factor expression in undifferentiated cells; cells were cultured in standard growth media, with no additional supplementation. For each gene analysed, expression was normalised to β2 microglobulin (*B2M*) expression in the same cell type, and these normalised levels are shown in Figure 37. MSC expressed all genes analysed at lower levels than *B2M*, except from *CD105* (1.12-fold). The osteogenic associated transcription factors *RUNX2* and *OSX* were the highest out of the lineage specific genes (0.58 and 0.53 respectively). *SOX9*, *ACAN* (Aggrecan) and *PPARG* were expressed at levels lower than 0.36-fold, significantly lower than B2M ($p<2x10^{-6}$).

hES-MP expressed the highest levels of lineage specific markers out of all cell types analysed, with the exception of *PPARG*, which was 0.87-fold less than ADMSC. hES-MP also expressed significantly lower levels of *CD105* (0.59-fold) compared with MSC ($p=0.0001$) and ADMSC ($p=0.00001$). Expression of both *RUNX2* and *SOX9* in hES-MP was high; significantly greater than in MSC and ADMSC ($p<0.00004$). *OSX* levels in hES-MP were also higher than in MSC (1.27-fold), and (2.18-fold) in ADMSC ($p=0.00004$). *ACAN* and *PPARG* expression were not significantly different in any cell type.

ADMSC expressed high levels of *CD105* (1.18-fold), and low levels of lineage specific makers. *RUNX2*, *OSX* and *ACAN* expression levels were all lower than in any of the other cell types. *SOX9* was significantly lower than in hES-MP ($p=0.0004$) but not significantly different to MSC ($p=0.31$). ADMSC expressed the highest levels of *PPARG* but this was not statistically significant.

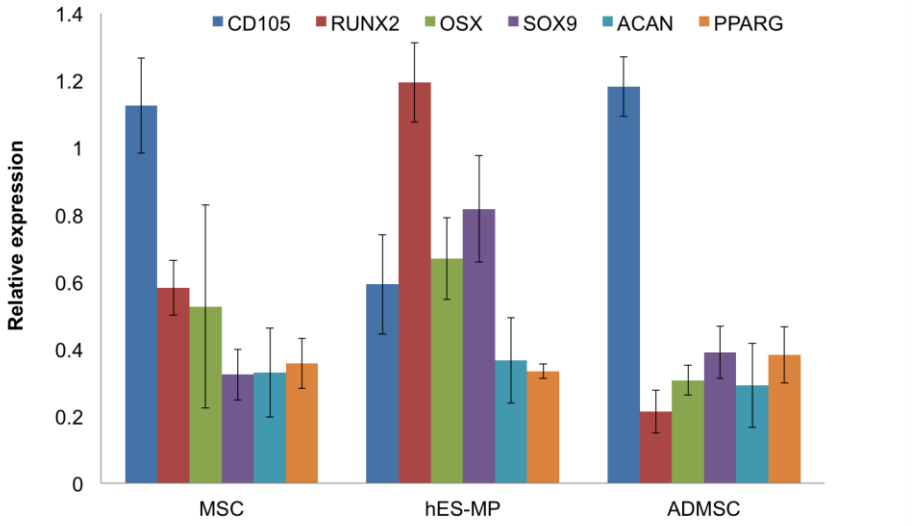

Figure 37: Transcription factor and gene expression in undifferentiated cells.

Relative expression of lineage associated genes, representative of cells at different passages, each sample was run in duplicate.

4.2.5 Multipotency

By definition a stem cell must possess two qualities, self renewal and potency *or* 'the ability to give rise to differentiated cell types' (Kolf, Cho & Tuan 2007a; Pittenger 1999; Nombela-Arrieta et al. 2011; Chamberlain et al. 2007; Crisan et al. 2008; Barry & J. M. Murphy 2004; Boyd et al. 2009; Haasters et al. 2009; Yoshimura et al. 2006; Jack et al. 2002). To confirm the cells used in this thesis were multipotent, each cell type was cultured for up to 21 days in standard growth medium or in lineage specific differentiation medium, and differentiation along adipogenic, osteogenic and chondrogenic lineages investigated.

Adipogenic differentiation was induced in all cells types through the addition of 1-methyl-3-isobutylxanthine, dexamethasone, insulin and indomethacin to standard growth medium. In MSC, adipogenic induction was apparent by Day 14, when lipid–rich vacuoles within the cells appeared, see Figure 38 (A). hES-MP differentiated into adipocytes and after only 7 days lipid vacuoles were detected, then by Day 14 strong staining for lipid droplets was observed (E). ADMSC were also induced to

form adipocytes; lipids were detected as early as Day 7, and continued to accumulate in culture over two weeks (I).

In the presence of β-glycerophosphate, ascorbic acid and dexamethasone, cells underwent osteogenic differentiation. All cells acquired an osteoblastic morphology and up-regulated alkaline phosphatase activity, as seen in Figure 38. Alkaline phosphatase staining was detected in MSC after 7 days in osteogenic medium and continued to increase in intensity and area over 21 days (B). hES-MP rapidly produced alkaline phosphatase, observed as early as 24 hours in culture with osteogenic medium; which continued to increase over time, Figure 38shows staining at 21 days (F). The strongest alkaline phosphatase staining was seen on Days 14 and 21, in ADMSC confirming these cells were also differentiating into osteoblasts (J).

Under osteogenic culture conditions cells also produced a mineralised matrix as detected by the Von Kossa stain (Chamberlain et al. 2007; Kossa 1901; Haasters et al. 2009; Yoshimura et al. 2006; Pittenger 1999). This was detected in MSC, as early as Day 14, and on Day 21 mineralisation was widespread and darker staining was observed in areas, suggesting bone nodule formation see Figure 38 (C). hES-MP rapidly formed a mineralised matrix, which was detected as early as Day 7. Staining increased in intensity and area up to 21 days (G), where its was more disperse, when compared to the staining seen with MSC. No staining was observed in ADMSC until Day 14, where it covered roughly 50 % of the culture dish. On Day 21, a greater area of mineralisation was detected (K) and was darker and more widespread than staining seen with MSC, and hES-MP.

Chondrogenic differentiation was initiated when cells were cultured in the absence of fetal bovine serum with the addition of transforming growth factor–β, dexamethasone, insulin, L-ascorbic acid, sodium pyruvate, transferrin, and proline, Differentiation along the chondrogenic lineage was detected by Safranin-O staining which detects glycosaminoglycans, shown in Figure 38. Cells cultured in chondrogenic medium condensed to form spheres and occasionally detached from the tissue culture plastic after two to three weeks, therefore staining and images were taken before this

occurred. MSC differentiated in culture and stained positively with Safranin-O by Day 14 (D). Differentiation in hES-MP occurred much more rapidly, and strong positive staining was seen on Day 7 (H). ADMSC differentiated and stained positively after Day 14 (L).

As differentiation along the three lineages proceeded, cells appeared healthy and no signs of apoptosis or necrosis were observed. In each culture, cells appeared to progress along the desired lineage and multiple lineages were not present, based on phenotypic characterisation and histological analysis. Cells cultured in standard growth medium did not stain positively for lipid droplets, alkaline phosphatase Safranin-O or Von Kossa.

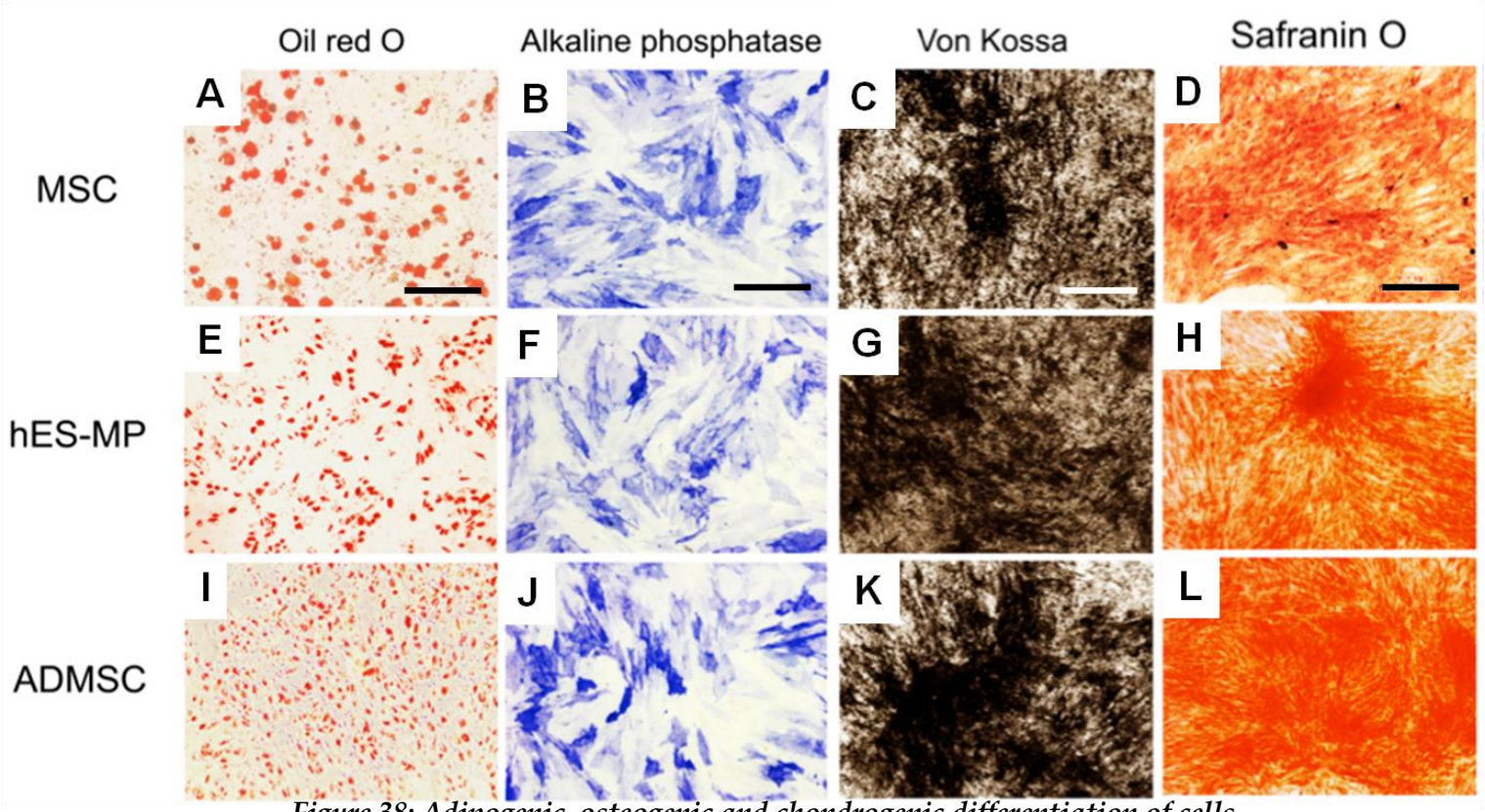

Figure 38: Adipogenic, osteogenic and chondrogenic differentiation of cells.

Oil Red O staining - adipogenic differentiation, alkaline phosphatase staining - osteogenic differentiation, Safranin O staining - chondrogenic differentiation and von kossa staining- bone nodule formation, in MSC, hES-MP and ADMSC, Scale bars represents 200 µm.

To confirm lineage restriction, RNA was collected, prior to differentiation and at 7, 14 and 21 days during differentiation; and used to amplify expressed transcripts involved in adipogenic (*PPARG*), osteogenic (*RUNX2, COL1A1, ALPL, BGLAP*) and chondrogenic differentiation (*SOX9, ACAN, COL2A1*), these transcripts were analysed by semi quantitative PCR and are shown in Figure 39.

PPARG is a regulator of adipogenic differentiation, promoting adipogenesis, and preventing osteogenesis (Augello et al. 2010; Kolf, Cho & Tuan 2007b). *PPARG* was expressed by MSC, hES-MP and ADMSC as they differentiated along the adipogenic lineage. Expression levels of *PPARG* transcription levels were highest in hES-MP and in ADMSC at Day 7, whereas in MSC expression was highest on Day 14 (8.9-, 15-, and 7.2-fold greater than on Day 0 respectively).

RUNX2 expression is be both necessary and sufficient to direct MSC towards the osteoblast lineage (Pittenger 1999; Ziros et al. 2008; Shui et al. 2003). *RUNX2* expression was highest in all cell types after 7 days of osteogenic differentiation; when it was expressed at significantly higher levels in both MSC ($p=0.02$) and ADMSC ($p=0.0004$) when compared with hES-MP. (*RUNX2* was significantly higher in ADMSC than MSC ($p=0.005$)). *RUNX2* levels reached a 16.5-fold increase in MSC, 27.2-fold in ADMSC and 1.7-fold in hES-MP (relative to Day 0). After Day 7 levels decreased, and were not significantly different between each cell type.

Collagen type I, constitutes 90% of the total organic extracellular matrix in mature bone, and is synthesised by pre-osteoblasts and mature osteoblasts (Dominici et al. 2006; Reffitt et al. 2003). In MSC, *COL1A1* was increased 1.6- fold on Day 7 and up to 4.2-fold (greater than Day 0) on Day 14. Expression in hES-MP peaked later, at Day 14 (2.4-fold, relative to Day 0) then decreased 1.8-fold on Day 21.

ADMSC expressed the highest levels of *COL1A1*, and expression was significantly greater than MSC and hES-MP at each time point ($p\leq0.017$). On Day 7, *COL1A1* reached 8.2-fold (greater than Day 0) then continued to increase to 12.5-fold (greater than Day 0) on Day 14 and remained high at Day 21.

Alkaline phosphatase (*ALPL*) is expressed by mature osteoblasts, and is thought to play a vital role in mineralisation (Barry & J. M. Murphy 2004; E. Golub 2007). *ALPL* levels steadily increased over time in each cell type. Initially ADMSC expressed the highest levels of *ALPL*, significantly higher than MSC ($p=0.02$). Levels of *ALPL* increased in ADMSC and remained significantly higher than MSC at all time points ($p\leq0.03$). hES-MP also expressed greater *ALPL* than MSC (relative to B2M), but did not reach significance until Day 21 ($p=0.01$).

Osteocalcin is the most bone specific protein produced by mature osteoblasts (Dominici et al. 2006; Malaval et al. 2005), and is encoded by the *BGLAP* gene. In all cell types *BGLAP* expression was low on Day 7, and increased, on days 14 and 21. In MSC, *BGLAP* increased rapidly (0.3-fold) on Day 14 and (8.8-fold) on Day 21. hES-MP followed a similar trend, levels were low on Day 14 then increased to the highest level on Day 21. This expression was significantly lower than ADMSC at the same time point ($p=0.002$). ADMSC expression of *BGLAP* was significantly higher than MSC at all time points ($p\leq0.01$); and also had the greatest expression of *BGLAP* overall, on days 14 (15.8) and 21 (25.3).

All genes associated with chondrocytes were elevated as each cell type underwent chondrogenic differentiation.

The only transcription factor, shown to be required for the initiation of cartilage differentiation during embryogenesis is *SOX9* (Kolf, Cho & Tuan 2007a; Kulyk & J. Franklin 2000). *SOX9* expression was elevated in MSC and ADMSC on Day 7, when levels were 3-fold (MSC) and 5.8-fold (ADMSC) greater than Day 0. On Day 7, *SOX9* expression in ADMSC was significantly higher than in MSC ($p=0.04$), and hES-MP ($p=0.01$). Expression of *SOX9* in hES-MP increased later, on Day 14 where it reached 3.2. Unlike MSC, both ADMSC and hES-MP continued to express *SOX9* on Day 21 (2.1- and 2.3-fold, greater than Day 0).

Aggrecan is a major component of cartilage and encoded by the gene *ACAN* (Dominici et al. 2006; Barry et al. 2001). Expression levels of *ACAN* were high on Day 7 in all cell types; MSC, ADMSC and hES-MP (3-, 8.6-, and 15.7-fold, greater than Day 0). *ACAN* was expressed in hES-MP, at levels significantly greater than ADMSC ($p=0.01$) and MSC ($p=0.003$). On Day 14 *ACAN* levels in MSC and ADMSC greatly decreased. In hES-MP

however, it remained significantly greater than MSC ($p=0.0005$) and ADMSC ($p=0.0006$) at 5.8. By Day 21 *ACAN* levels decreased (ADMSC 1.3-fold) or were undetectable (MSC and hES-MP).

Collagen type II (encoded by the gene *COL2A1*) is the major component of hyaline and articular cartilage (Kolf, Cho & Tuan 2007b; Barry et al. 2001; Chamberlain et al. 2007; Crisan et al. 2008; Vodyanik et al. 2010; Haasters et al. 2009; Sanchez-Guijo et al. 2009; Yoshimura et al. 2006; Kozhevnikova et al. 2008; Jack et al. 2002; Dominici et al. 2006; Ohgushi et al. 2005; Orciani et al. 2010). *COL2A1* expression in MSC increased on Day 7 and 14 were it reached 6-fold greater than Day 0, then decreased on Day 21 3.3-fold. hES-MP expression of *COL2A1* followed a similar trend, and was not significantly different to either MSC or ADMSC on Day 14 ($p\geq0.93$). On Day 21 however, *COL2A1* expression was 6.3-fold, significantly greater than MSC ($p=0.015$), and ADMSC expressed the highest levels of *COL2A1* on days 7 and 21, where they were significantly greater than MSC ($P\leq0.0007$) and hES-MP ($p\leq0.0016$). On Day 21 *COL2A1* expression reached 19.4, 5.8-fold greater than MSC, and 3.1-fold greater than hES-MP.

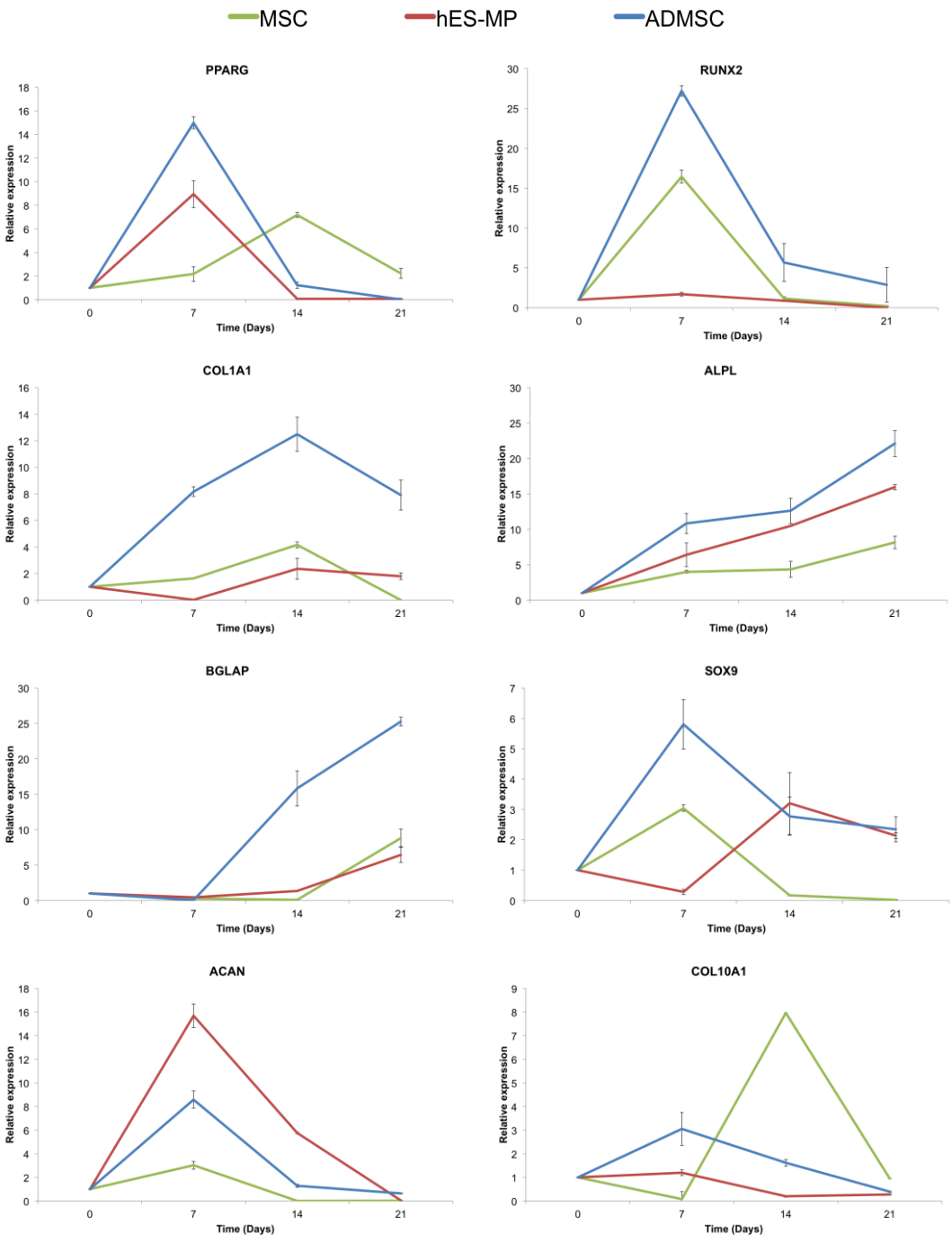

Figure 39: Lineage specific semi quantitative PCR.

mRNA levels of genes of interest and are represented as level of expression normalised to beta-2 microglobulin and to Day 0. For MSC three donors were used, for ADMSC two donors were used and each sample was run in duplicate.

4.2.6 CD90 analysis

The bimodal population of CD90 positive hES-MP detected by flow cytometry was sorted by FACS, and examined for differences in transcription factor expression prior to and after 1 week of culture.
Morphologically cells appeared very different in culture, shown in
Figure 40. The CD90^{high} cells were small, with a pronounced nucleus and appeared proliferate at a greater rate, whereas CD90 ^{low} cells were longer, more fibroblast-like and had a slower rate of proliferation.

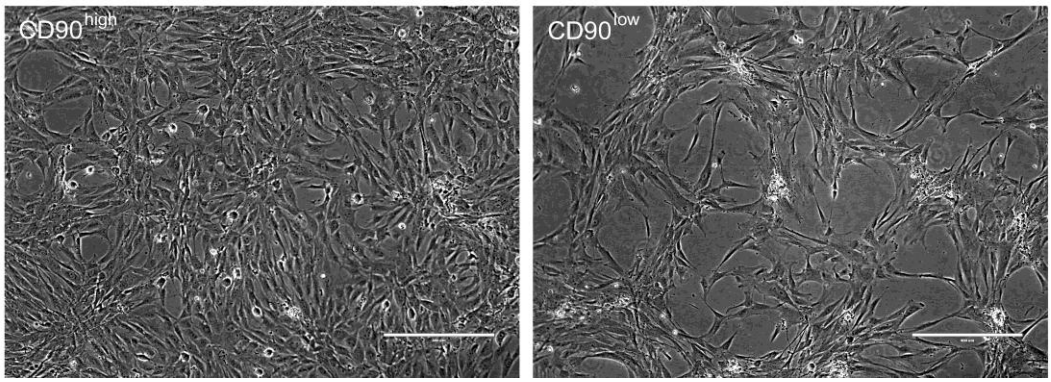

Figure 40: Morphology of sorted CD90 ^{high} and CD90 ^{low} hES-MP.

Representative morphology of hES-MP after sorting and 1 week of culture, scale bar represents 400 μm.

To examine possible differences in multipotency, RNA from cells was collected, reverse transcribed and analysed by semi quantitative PCR for transcription factors associated with each lineage and the results are shown in
Figure 41. Immediately after sorting, CD90 high cells expressed significantly more PPARG ($p=0.00008$), RUNX2 ($p=0.000001$) and SOX9 ($p= 0.0002$) than CD90 low cells. After 1 week in culture, levels of PPARG, RUNX2, and SOX9, in CD90 high remained significantly greater than in CD90 low cells, ($p=0.002$, 0.0006, and 0.0000003 respectively). At both time points RUNX2 was expressed at higher levels than B2M, but this was not statistically significant ($p>0.8$).

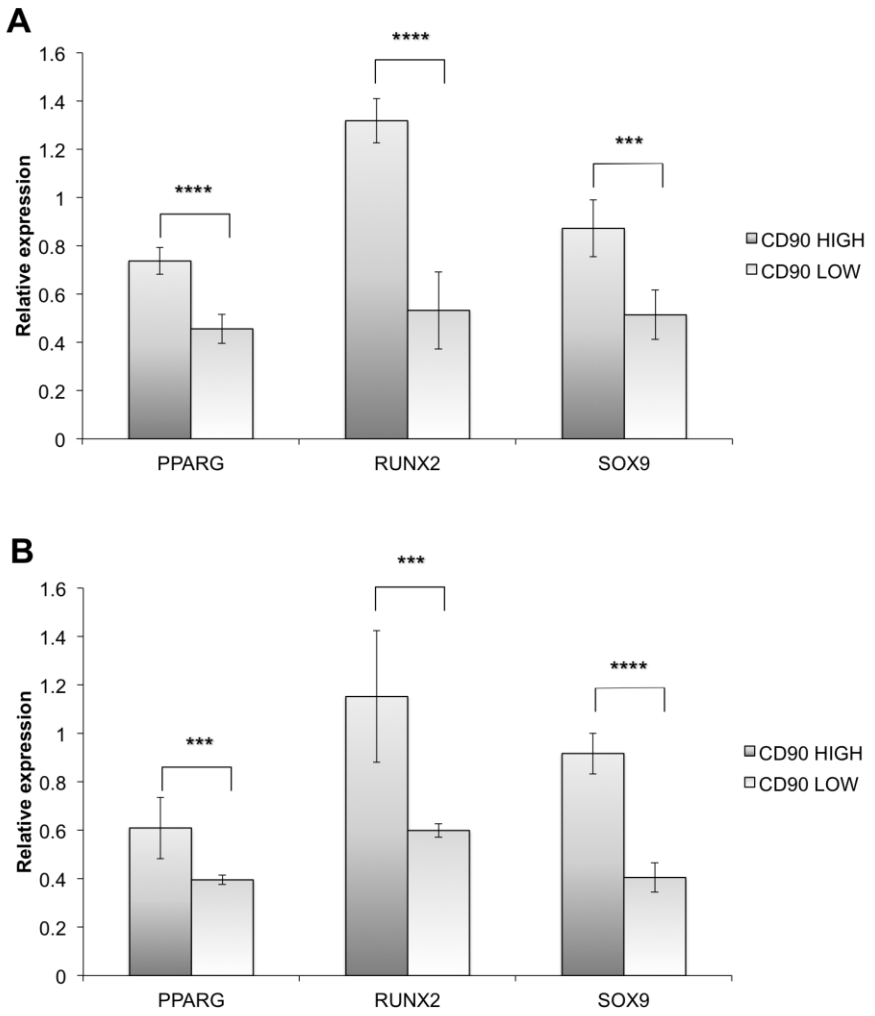

Figure 41: Transcription factor analysis of CD90 ^{high} and CD90 ^{low} hES-MP.

*(A) Cells immediately after sorting, (B) cells after 1 week in culture. Two samples of each cell population were analysed and run in duplicate Gene expression was normalised to Beta-2-microglobulin in each sample, and transcription factors involved in adipogenic (PPARG), osteogenic (RUNX2) and chondrogenic differentiation (SOX) were analysed. Key: ns (P>0.05), * (P≤ 0.05), ** (P≤ 0.01), *** (P≤ 0.001), **** (P ≤ 0.0001).*

4.3 Discussion

The aims of this chapter were to characterise the undifferentiated cells and to determine their differentiation capacity. This is the first time MSC, hES-MP and ADMSC have been characterised and analysed together. The results indicate similarities and differences in the morphology, proliferation, surface marker expression and multipotency of these cell populations.

Despite isolation from different sources, MSC and ADMSC appeared homogenous in size, shape and had very similar morphology, an observation that has been described previously (Kolf, Cho & Tuan 2007b; Kern et al. 2006; Chamberlain et al. 2007; Crisan et al. 2008; Barry & J. M. Murphy 2004; Boyd et al. 2009; Haasters et al. 2009; Kozhevnikova et al. 2008; Pittenger 1999; Jack et al. 2002; Dominici et al. 2006; Orciani et al. 2010). A common origin of multipotent adult stem cells was proposed by one group (Chamberlain et al. 2007; Crisan et al. 2008; Kolf, Cho & Tuan 2007b; Barry & J. M. Murphy 2004; Boyd et al. 2009; Haasters et al. 2009; Kozhevnikova et al. 2008; Pittenger 1999; Yoshimura et al. 2006; Blitterswijk et al. 2007; Foster et al. 2005; Jack et al. 2002; Dominici et al. 2006; Orciani et al. 2010), which could explain these similarities. hES-MP however, appeared to be more a more heterogeneous population of cells, which is likely due to the bimodal population of CD90 positive cells.

Proliferation analysis revealed significant differences in doubling rates; ADMSC proliferated at a rate two-fold greater than MSC, and significantly greater than hES-MP. The lower rate of proliferation seen in MSC may be due to donor age, a relationship which has been described by several groups (Kolf, Cho & Tuan 2007b; Stenderup et al. 2003; Vodyanik et al. 2010; Phinney et al. 1999; Jack et al. 2002; Mendes et al. 2002; Tare et al. 2012; Muschler et al. 2006). This has been further confirmed by studies that have examined proliferation of bone marrow derived MSC and adipose derived MSC (ADMSC) isolated from the same patient, and found no significant differences in growth kinetics (Crisan et al. 2008; Schäffler & Büchler 2007; Boyd et al. 2009; De Ugarte et al. 2003; Jack et al. 2002). The high variance in doubling times of hES-MP may also be a result of the

bimodal CD90 population, as CD90 ^{low} cells were observed to have a much slower rate of proliferation.

Flow cytometry results demonstrated MSC expressed surface makers commonly associated with mesenchymal stem cells (CD90, CD73, CD105). However, expression of the colony forming associated marker, Stro-1 was expressed by less than 25% of MSC, detected by flow cytometry. Stro-1 is a contentious MSC marker for several reasons, described previously.
Haematopoietic progenitor markers CD34, CD14 and CD45, were expressed in a small percentage of MSC, and overall expression of these markers in MSC was lower than in hES-MP and ADMSC. MFI values for mesenchymal associated markers were high in MSC; in particular CD90, and CD73 were greater than in hES-MP; indicating a greater number of receptors per cell.

hES-MP were more heterogeneous for expression of mesenchymal markers, CD90, CD73, CD105 and Stro-1, with expression varying significantly between passages.
MIP results also demonstrated hES-MP did not express the same levels of surface antigens as MSC, and MIP values were significantly lower for all mesenchymal markers. One passage of hES-MP (P8, cultured on plastic) also expressed significant levels of the CD34, and CD14. These commonly used markers of the haematopoietic lineage (Chamberlain et al. 2007; Kolf, Cho & Tuan 2007b; Haasters et al. 2009; Barry & J. M. Murphy 2004; Pittenger 1999; Boyd et al. 2009; Yoshimura et al. 2006; Crisan et al. 2008), which were not evaluated in the original paper (Nombela-Arrieta et al. 2011; Karlsson et al. 2009; Kolf, Cho & Tuan 2007b; Chamberlain et al. 2007; Crisan et al. 2008; Barry & J. M. Murphy 2004; Boyd et al. 2009; Haasters et al. 2009; Yoshimura et al. 2006; Pittenger 1999; Jack et al. 2002). Embryonic markers TRA1-60, TRA1-80, SSE1 and SSEA3, were not detected at significant levels, consistent with results from Karlsson *et al*. Inconsistent with this study was SSEA4 expression, previously thought to be an embryonic stem cell marker (Chamberlain et al. 2007; Barraud et al. 2006; Haasters et al. 2009; Yoshimura et al. 2006; Pittenger 1999). However, more recent studies have shown that SSEA4 also identifies bone marrow derived MSC (Oishi & Ito-Dufros 2006; Gang et al. 2007), which may explain this

ambiguity. Although not analysed here, it would be interesting to investigate the expression of SSEA4 on MSC and ADMSC.

Results here have shown ADMSC to have a similar immune phenotype to MSC, an observation reflected in data from a number of papers (Kolf, Cho & Tuan 2007b; Kuznetsov et al. 1997; Filshie et al. 1998; Nuttall et al. 1998; Gronthos 1999; Park & Oreffo 1999; Pittenger 1999; Erices et al. 2000; Simmons & Torok-Storb 1991a; Simmons & Torok-Storb 1991b; Haynesworth et al. 1992; Galmiche et al. 1993; Simmons et al. 1994; Rickard et al. 1996; Gronthos et al. 1997; Bruder et al. 1997).

ADMSC were highly homogenous, as evidenced by a clear, compact shift in relative fluorescence of surface markers associated with mesenchymal stem cells (CD90, CD73, CD105), and the MFI for each of these markers was highest out of all cell types, suggesting they have greater expression of the cell surface markers, per cell. However, MFI was not calculated under saturated conditions, as would be required to verify these results. A higher proportion of ADMSC expressed haematopoietic markers CD34, CD14 and CD45, compared to MSC, but given the vascularity of adipose tissue, this was not surprising, and was only detected at early passages.

Transcription factor expression was analysed to determine levels of gene expression in undifferentiated cells, and to indicate whether cells may be pre-committed to a certain lineage. In MSC and ADMSC lineage associated transcription factors and gene expression were lower than the housekeeping gene, B2M, suggesting lineage associated genes are transcribed at very low levels.
In hES-MP however, expression of osteoblast-associated transcription factor *RUNX2* and chondrogenic related transcription factor *SOX9* was higher than both *B2M* and *CD105* expression. This elevated *RUNX2* expression was noted by the group who derived hES-MP however, was not identified as a pontetial issue (Barry et al. 1999; de Peppo, Svensson, et al. 2010b). The increased levels of lineage related genes suggest that individual cells are expressing multiple transcription factors, at higher levels compared to MSC and ADMSC, or indicative of a subpopulation of pre-committed cells. CD90 analysis suggests that in fact this may be due to the

population of CD90 ^{high} cells that are expressing high levels of lineage specific transcription factors.

In addition to the identification of MSC based on plastic adherence, morphology or molecular characteristics, is to identify MSC populations is by their multilineage capacity *in vitro*. Results from histochemical staining and gene expression demonstrate each cell type was capable of differentiating along three distinct lineages, indicating each cell population was multipotent. Cells were supplemented with soluble factors known to direct cell fate and analysed over 21 days, which is a commonly used and widely recognised time frame for adipogenic, chondrogenic and osteogenic differentiation.

MSC differentiated along each lineage, as evidenced by histological analysis. Multiple lineages did not appear to be present, and was conformed by real time PCR. Differentiation occurred at a slightly slower rate in MSC, when compared to ADMSC and hES-MP, as evidenced by later gene expression and histological staining. The lower rate of proliferation associated with MSC in this study may have impacted upon the rate at which cells differentiate. Yet, during chondrocyte differentiation MSC had the greater levels of *SOX9* on Day 7 compared to hES-MP and had the highest relative levels of *COL10A1* over 21 days.

hES-MP were shown to differentiate along adipo- osteo- and chondrogenic lineages in the original research paper. However, Karlsson et al. reported results after longer culture in supplemented medium, adipogenic differentiation (25 days), Chondrogenic differentiation (6 weeks) and osteogenic differentiation (5 weeks). Furthermore, analysis of differentiation consisted solely of histochemical staining and did not include gene expression analysis (Banas et al. 2007; Karlsson et al. 2009; Mitchell et al. 2005). These are the first results to combine both histochemistry and gene expression of hES-MP in one study.

Previous studies have demonstrated that ADMSC are capable of differentiation along the three lineages examined here (Simmons & Torok-Storb 1991b; Hui et al. 2005; Im et al. 2005), and some cases were shown to be inferior to MSC, which was not observed here. Results from PCR and histology demonstrated ADMSC differentiated rapidly along the three

lineages and had the highest expression of adipogenic transcription factor *PPARG*, and osteoblast related genes *RUNX2*, *COL1A1*, and *BGLAP*.

MSC

Whilst MSC may represent the most clinically relevant source of stem cells to study osteogenic differentiation they have several drawbacks: (1) the cells used in this thesis were obtained from patients who had damaged bone or cartilage as a result of disease; (2) there was a limited supply of samples and often small volumes of tissue; (3) unsorted MSC derived from bone marrow may contain a heterogeneous population of cells; (4) variability between patient tissue samples, was noted, with regard to MSC number and expansion potential. Despite these drawbacks, MSC were readily expanded, and morphologically appeared to be healthy.

The only criterion for selection was plastic adherence, and MSC were not enriched or sorted according to surface markers. Nevertheless, MSC were relatively homogenous, as evidenced by morphology, flow cytometry and only slight heterogeneity was detected in immunostaining.

Transcription factor and gene expression results suggest MSC were not pre-committed to a specific lineage, and were capable of differentiating into multiple cell types, indicating a truly multipotent population.

A common and major drawback of studies utilising primary cells is donor variability. MSC displayed high donor variability with regard to CD73, CD105 and Stro-1 staining as detected by flow cytometry. However, significant variance between donors was not found in immunostaining, transcription factor expression or differentiation potential.

Despite several disadvantages, MSC remain the most extensively studied, characterised, and most clinically relevant source of cells to examine osteogenic differentiation *in vitro*. Recently, Prochymal® (remestemcel-L), was approved for the treatment of acute graft-*vs*-host disease (GvHD) in children (Gronthos et al. 2003; Osiris 2013).

hES-MP

hES-MP were derived, and first characterised in 2009 to overcome the drawbacks associated with primary MSC. hES-MP claim to have no donor

variability, exhibit a more extensive proliferative capacity, and represent a more homogenous source of multipotent stem cells (Peister 2004; Karlsson et al. 2009). Results shown here are in agreement with these previous reports, which suggest hES-MP resemble MSC, with regard to surface marker expression, and multipotency. However, several notable differences were observed.

CD90 was consistently expressed by a high percentage of hES-MP throughout culture, however, a dual population was observed at several passages. Analysis of the CD90 positive population revealed two distinct sub-populations, which once sorted and analysed were very different. CD90 ^{high} cells appeared to be more differentiated- expressing significantly higher lineage specific markers than CD90 ^{low} cells, in particular *RUNX2*. This elevated expression of *RUNX2* was also noted in transcription factor analysis of the unsorted population.

Until now, a bimodal distribution of CD90 in mesenchymal stem cells has not been described or investigated. CD90 is widely regarded to be a marker expressed by undifferentiated cells (Chamberlain et al. 2007; Kolf, Cho & Tuan 2007a; Dominici et al. 2006) and even in cancer stem cells (Péault et al. 2007; Parry & Engh 2012). However, one study has described expression of CD90 in cells of the osteoblast lineage. Furthermore, has demonstrated that CD90 expression is altered during differentiation: CD90 expression was maximal at the earliest stage of osteoblast maturation, during the proliferative phase, and then declined as the cells matured (Pittenger 1999; X. D. Chen et al. 1999). This observation is in agreement with results shown here, with CD90 ^{high} cells expressing the early osteoblast marker *RUNX2*.

Although hES-MP were shown to contain this subpopulation of pre-committed cells, the total population still possessed the ability to differentiate into multiple lineages; suggesting that CD90 ^{low} cells are multipotent.

hES-MP were recommended to be cultured on 0.1% gelatin, which is thought to enhance attachment and proliferation of cells (Toma et al. 2001; Chai & Leong 2007). However, once transitioned from gelatin to plastic, hES-MP attached strongly to PL and proliferation rates, although not quantified, did not appear to be significantly affected.

hES-MP were shown to differentiate rapidly into adipocytes, osteoblasts and chondrocytes, notably faster than MSC. This may be due to the origin of the MSC in this study (from mature, diseased patients) or due to hES-MP possessing a greater proliferative capacity.

Despite several drawbacks, hES-MP were readily expandable, and did not rely on surgical operations, or involve lengthy extraction procedures. Although these cells are unlikely to be used in the clinical setting, due to their derivation from embryonic tissue, they represent a valuable tool to study osteogenic differentiation *in vitro*.

ADMSC

Bone marrow derived mesenchymal stem cells hold great potential for use in tissue regeneration and repair. However, there are practical issues, which have limited clinical use; including low yield, the need for expansion, and significant morbidity imposed on the donor. As such interest has rapidly increased identifying MSC from alternate sources, such as adipose tissue. The ADMSC used here were isolated from the stromal vascular fraction of lipoaspirate or from whole fat, using an established extraction procedure (Zuk et al. 2001; Crisan et al. 2008). Representing a less painful, alternative source of highly proliferative cells.
Transcription factor analysis revealed undifferentiated ADMSC and MSC had similar gene expression profiles. This is in agreement with multiple studies, which suggest ADMSC and MSC display similar expression profiles based on mRNA analyses (Gronthos 2000; Gimble et al. 2007). Overall, undifferentiated ADMSC expressed lower levels of lineage specific markers than MSC and hES-MP, suggesting ADMSC may represent a population of less committed cells.

ADMSC were first shown to be multipotent in 2001 (Scherjon et al. 2004; Zuk et al. 2001), and since then have been differentiated into multiple cell types, including cardiac, neuronal, and pancreatic lineages (Erices et al. 2000; Locke et al. 2011; Strem et al. 2005). Here we demonstrated ADMSC could be successfully differentiated along adipo- osteo- and chondrogenic lineage, as evidenced from histology and real time PCR. ADMSC expressed

high levels of lineage specific markers once committed to each cell type, and genes specific to the osteoblast lineage were expressed at significantly greater levels in ADMSC, compared to both MSC and hES-MP.

ADMSC were notably more proliferative than MSC, this may be due to the lower donor age and health status. Due to relative ease of extraction, expansion potential, and similar characteristic to MSC, ADMSC represent an attractive, alternative source of cells to study osteogenic differentiation. The MFI for each of these markers was highest out of all cell types, suggesting they have greater expression of cell surface markers, per cell. Immunostaining confirmed this, where uniform, intense, CD105 staining was observed. Although a higher proportion of ADMSC expressed haematopoietic markers CD34, CD14 and CD45 compared to MSC, but given the vascularity of adipose tissue, this is not surprising, and was only detected at early passages.

In conclusion, each cell type has its own advantages and disadvantages to study osteogenic differentiation *in vitro*, and is summarised in Table 23.

Table 23: Advantages and disadvantages of each cell type.

	MSC	**hES-MP**	**ADMSC**
Availability	+	+++	++
Clinical relevance	+++	+	+++
Proliferation capacity	+	++	+++
Differentiation potential	++	++	+++
Donor varaibility	++	N/A	++
Ethical issues	N/A	++	N/A
Heterogeneity	+	++	+
Characterised	+++	+	++

CHAPTER FIVE: OSTEOGENIC EFFECT OF SUBSTRATES ON MESENCHYMAL STEM CELLS

5.1 Introduction

Bone tissue engineering, which utilises the endogenous bone remodeling capacity within the patient, offers a proof of principle that holds out the promise that more active regenerative strategies can result in complete regeneration of bone and restoration of its function.

Currently, bone tissue engineering involves the transplantation of graft materials combined with cells. Calcium phosphate based bone grafts are used to fill small bone defects and in spinal fixation. In the form of porous granules, these materials are commonly mixed with autologous bone marrow to form a cohesive graft (Gronthos, D. M. Franklin, et al. 2001a; K A Hing 2005).

Bone marrow contains a source of multipotent stem cells (MSC) that can be expanded and differentiated along a restricted set of lineages *in vitro* (Guilak et al. 2005; Muschler et al. 1997; Zhang et al. 2011); for example, the addition of β-glycerophosphate, ascorbic acid and dexamethasone results in commitment to the osteoblast lineage. This is a complex, highly regulated process involving the parallel and sequential expression of lineage specific genes. An essential transcription factor controlling this process is RUNX2, which is believed to be both necessary and sufficient to direct MSC toward the osteoblast lineage (Crisan et al. 2008; Ziros et al. 2008; Shui et al. 2003). RUNX2 acts by binding to a regulatory element found in the promoter of all major osteoblast genes, including *COL1A1* (collagen type I) (Wang et al. 2008; Komori 2010) and *BGLAP* (osteocalcin) (Pera et al. 2000; Makita et al. 2008). The proteins associated with these genes, amongst others, are secreted by osteoblasts and are incorporated into osteoid, the organic phase of bone (de Peppo, Sjovall, et al. 2010a; Glimcher 1984). Alkaline phosphatase is produced, initially in parallel with osteoid production, then declining as matrix mineralisation occurs (Karlsson et al. 2009; Stein et al. 1990), in which calcium phosphate crystals are deposited to form the mineral phase of bone (Karlsson et al. 2009; Zhao et al. 2007). Osteoblasts

that are left behind during osteoid production are then encased in the mineralised osteoid, cease proliferation and become terminally differentiated osteocytes, which express DMP1 (dentin matrix acidic phosphoprotein 1)(Riquelme et al. 2006; Dallas & Bonewald 2010).

Soluble osteogenic factors are an excellent tool to study osteogenesis *in vitro,* however they are unlikely to be practical in the clinical setting. An alternative approach is to use a scaffold or matrix engineered to provide cues for differentiation to eliminate the need for soluble factors.

Hydroxyapatite (HA) is currently used in fracture repair, spinal fixation and treatment of bone defects (Karin A Hing et al. 2007). HA is osteoconductive, and has been shown both to support bone formation *in vivo* (Bansal et al. 2009). Yet, it has poor degradation rates and in some cases is not completely remodeled (Habraken et al. 2007).

Clinical and *in vivo* studies have demonstrated that the incorporation of silicon, in the form of silicate, into the calcium phosphate lattice improves degradation rates, the quality of new bone formed, and rate of bone growth when compared to hydroxyapatite (Wheeler et al. 2007; Jenis & Banco n.d.; KA Hing et al. 2004b). However, is not clear whether the increased bone formation associated with these materials is the result of increased osteoblast activity or increased numbers of osteoblasts resulting from increased activation and differentiation of stem/ progenitor cells.

Most studies examining the osteogenic potential of bone grafts *in vitro* have used cells that are either immature osteoblasts or osteoblast-like cell lines (Dalby et al. 2006; Botelho et al. 2006; Rosa et al. 2003; Keeting et al. 1992). *In vivo* it is thought that MSC or progenitor cells are the first cell types to colonise a bone graft after implantation (Olivares-Navarrete et al. 2010).

Understanding the biological and physiological interaction between bone grafts and stem/ progenitor cells is critical to improving bone grafts and their successful incorporation (Kalfas 2001). Bone marrow derived mesenchymal stem cells (MSC) are though to be the most physiologically relevant cell type to investigate this interaction. However, extraction of these cells can be painful and often the population of cells has a limited expansion potential *in vitro*.

The unlimited proliferative and differentiation capacity of human embryonic stem cells has generated significant interest in bone tissue engineering (Bielby et al. 2004; Nieden et al. 2003; Sottile et al. 2003; Sinae

Kim et al. 2008). Yet, tumor formation and ethical debate over the origin of these cells has prevented their use in the clinical setting. One way of overcoming the associated risks of using pluripotent stem cells is to restrict their lineage capacity prior to implantation. hES-MP are a commercially available mesenchymal progenitor cell line, derived from human embryonic stem cells (hES); these cells possess the extensive capacity of hES but do not share the risk of teratoma formation (Karlsson et al. 2009). Consequently, human embryonic stem cell derived mesenchymal progenitors (hES-MP) are appealing alternatives to MSC in bone tissue engineering applications (de Peppo, Svensson, et al. 2010b). Furthermore, the use of a cell line removes potential issues associated with primary cells such as availability, donor variability and may also provide more reproducible results.

Adipose tissue has been the focus of much stem cell research, as it is an abundant and more accessible source of multipotent stem cells than bone marrow (Gimble & Guilak 2003). Recent studies have demonstrated that adipose derived mesenchymal stem cells (ADMSC) show similar characteristics and differentiation capacity, to those of bone marrow derived mesenchymal stem cells (Guilak et al. 2004; Gimble et al. 2007). This more accessible and abundant supply of primary multipotent cells, provides an excellent source of cells to study biomaterial-stem cell interactions.

Bone marrow derived MSC, hES-MP and ADMSC were selected to investigate whether the enhanced bone formation observed on silicate substituted calcium phosphate (Si-CaP) is the result of increased osteoblast differentiation or increased activation and differentiation of stem/ progenitor cells.

This chapter aims to firstly determine whether Si-CaP and HA can support differentiation of MSC in the presence of soluble osteogenic factors (+OS): and secondly, determine whether either substrate can initiate the differentiation of MSC, hES-MP and ADMSC in the absence of soluble osteogenic factors. In order to determine and quantify the degree of osteogenic differentiation upon both substrates, attachment, proliferation, gene expression, protein production, and mineralisation of extracellular matrix will be analysed.

5.2 Results

5.2.1 MSC

5.2.1.1 Osteogenic differentiation with soluble factors.

MSC were cultured on Si-CaP and HA in the presence of osteogenic media (OS), cells cultured on tissue culture plastic (PL) alone served as negative controls and cells on plastic in the presence of osteogenic media (PL+OS) were positive controls. Cells were cultured for up to 21 days and analysed for alkaline phosphatase expression, mineralisation and gene expression.

5.2.1.1.1 Alkaline phosphatase

Tissue non-specific alkaline phosphatase (ALP) is an enzyme produced by cells during osteogenesis (Malaval et al. 1994). To assess the degree of differentiation along the osteogenic pathway, ALP activity was calculated by measurement of the area of ALP positive staining cells after histochemical staining at different time points in culture, as described in materials and methods section 2.5.8.3. The percentage area of ALP staining on each substrate is shown in
Figure 42.

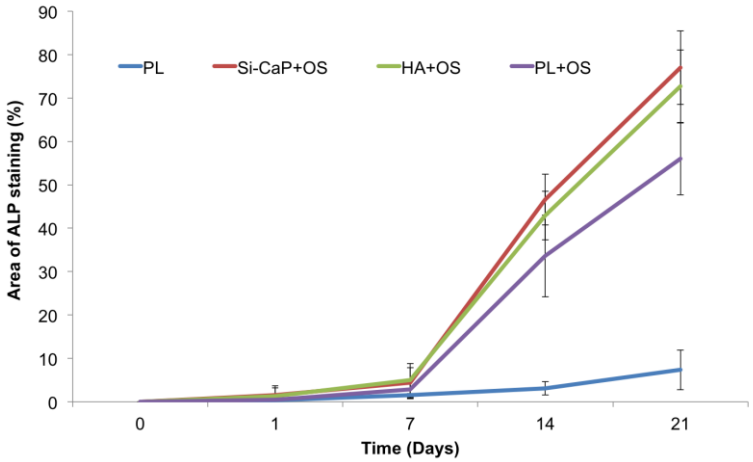

Figure 42: Area of alkaline phosphatase staining.

ALP activity of cells on substrates quantified by analysing the area of ALP positive cells using image analysis software and the mean area calculated per disc / well. The results represent the mean ± SD of three donors with samples run in triplicate.

ALP staining was limited in cells cultured on PL, and remained low at all time points. Cells cultured in the presence of osteogenic media (Si-CaP+OS, HA+OS and PL+OS) produced significant levels of ALP, and the ALP positive area increased over time. On Day 1 cells on Si-CaP+OS, HA+OS and PL+OS expressed detectable levels of ALP, and from Day 1 to 21 cells on Si-CaP+OS and HA+OS displayed significantly greater ALP activity than cells on PL+OS ($p<0.01$). ALP activity increased significantly on Si-CaP+OS, HA+OS and PL+OS on Day 14, while ALP activity on PL remained low. At this time point Si-CaP+OS and HA+OS were 1.39–fold and 1.28–fold higher than PL+OS respectively, and by Day 21 ALP activity on Si-CaP+OS and HA+OS were 1.37–fold and 1.30–fold greater than PL+OS. On days 7 to 21 ALP staining was significantly greater on both Si-CaP+OS and HA+OS when compared to PL+OS ($P<0.05$).

5.2.1.1.2 Mineralisation

To determine whether cells cultured on substrates in the presence of osteogenic supplementation were capable of producing a mineralised matrix, cultures were stained using the Von Kossa reagent. Areas of mineralisation were quantified as described in section 2.5.8.3 and the extent of mineralisation on the different substrates is shown in
Figure 43.
On Day 1 there was no detectable staining was observed on any substrate. On Day 7 there was no staining was seen on PL and PL+OS. However, a significant increase in staining on Si-CaP+OS and HA+OS was detected ($p<0.0307$). On Day 14 a rapid increase in area of mineralisation was detected on Si-CaP+OS, HA+OS and PL+OS, (increasing 9.9–fold, 6.5-fold and 49.9-fold respectively). This rate of mineralisation continued, and by Day 21 the greatest area of mineralisation was detected on Si-CaP+OS (77.6%). On HA+OS the area of mineralisation was also highest on Day 21, but peaked at 71.3% and on PL+OS reached 63.6%. At this final time point the area of mineralisation on both Si-CaP+OS and on HA+OS was significantly greater than PL+OS ($p>0.0098$).

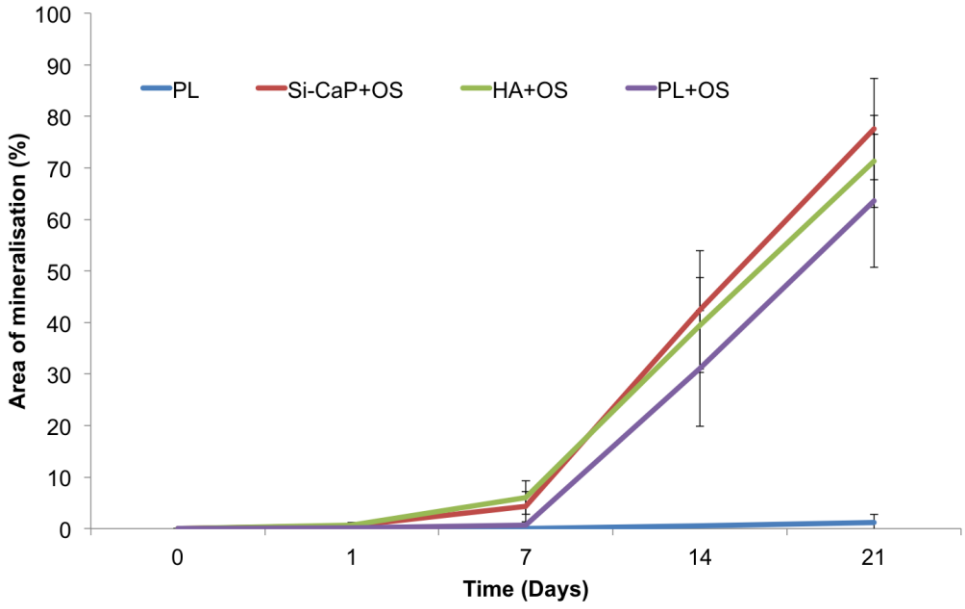

Figure 43: Area of mineralisation.

Mineralisation on substrates was measured by analysing the area of black deposits using image analysis software and the mean area covered was calculated per disc / well. The results represent the mean ± SD of three donors with samples run in triplicate.

5.2.1.1.3 Gene expression

To confirm that Si-CaP and HA were capable of supporting ostegenic differentiation, cells were cultured on substrates for up to 21 days in the presence of osteogenic supplementation and the transcription of selected osteoblast related genes was analysed. To account for differences in cell numbers on the various substrates, the expression levels were normalised to that of the house keeping gene β2 microglobulin; the normalised values for the expression of the selected osteoblast specific genes are shown in Figure 44.

RUNX2 expression increased in Si-CaP+OS, HA+OS and PL+OS on Day 1. Yet, expression on Si-CaP+OS, HA+OS increased to levels 2.14-fold and 2.13–fold greater than PL+OS respectively. On Day 7, *RUNX2* expression increased slightly on HA+OS (1.05-fold) and decreased on Si-CaP+OS (0.74-fold) and PL+OS (0.55-fold). On Day 14, *RUNX2* expression decreased

on Si-CaP+OS and HA+OS, but increased significantly on PL+OS to 2.32–fold greater than PL ($p=0.0059$). By 21 days in culture, levels of *RUNX2* expression decreased on Si-CaP+OS, HA+OS and PL+OS. Cells cultured on PL in the absence of soluble factors showed a slight increased in *RUNX2* expression over time, but remained lower than Si-CaP+OS, HA+OS up to 14 days.

COL1A1 expression increased rapidly on Si-CaP+OS on Day 1 and continued to increase over time, with highest levels on Day 21 where it was 2.69-fold greater than PL+OS. On HA+OS, *COL1A1* expression also increased over time but remained lower than Si-CaP+OS at all time points. *COL1A1* levels on HA+OS were higher than on PL+OS at all time points, and significantly so on days 7 ($p=0.002$) and 14 ($p=0.008$). On PL+OS *COL1A1* expression increased slightly on Day 1 then decreased 1.01–fold on Day 7, after which levels continued to increase peaking on Day 21. On PL *COL1A1* increased slightly (1.58-fold) on Day 7, but decreased on days 14 and 21 to levels significantly lower than on all other substrates ($p<0.01$).

Late stage marker *BGLAP*, expression began to increase on all substrates as early as Day 1 and continued to increase on both Si-CaP+OS and HA+OS until Day 14 where levels peaked at 1.31–fold and 1.14–fold greater then PL+OS. *BGLAP* expression on PL+OS decreased 0.83–fold on Day 7, then rapidly increased on Day 14 peaking at 1.58–fold greater than PL. On Day 21 levels decreased but remained higher than on Si-CaP+OS and HA+OS. On PL, *BGLAP* expression increased up to Day 14, but decreased on Day 21 to levels lower than on any other substrate.

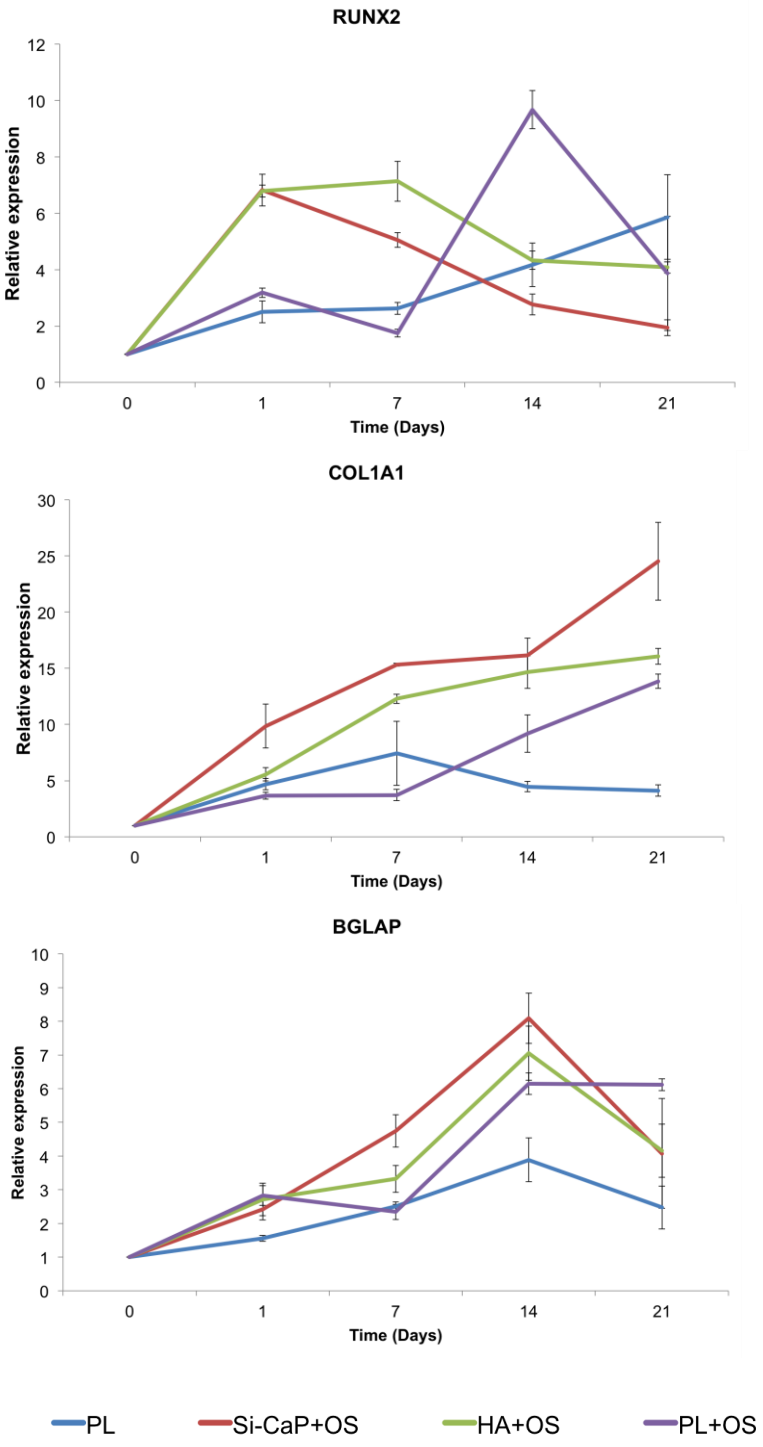

Figure 44: Real time gene expression profile of MSC on substrates.

mRNA levels of genes of interest and are represented as level of expression normalised to beta-2 microglobulin and to Day 0. Three donors were used, and each sample was run in duplicate.

5.2.1.2 Osteogenic differentiation in the absence of soluble factors

Initial results from ALP staining, mineralisation and gene expression suggest MSC were able to differentiate into osteoblasts on Si-CaP, HA and PL in the presence of osteogenic supplementation (+OS). MSC cultured on Si-CaP and HA rapidly differentiated into osteoblasts as evidenced by increased osteoblast related gene expression; enhanced production of ALP, and produced a greater area of mineralisation when compared to PL+OS. This augmented differentiation may be due to osteoinductive properties of theses calcium phosphate based substrates. To investigate this possibility the response of MSC in the absence of osteogenic supplementation was investigated.

5.2.1.2.1 Attachment

MSC were allowed to attach to each substrate over 8 hours. Every 2 hours, unbound cells were washed off and cells attached to the substrates were fixed, stained and counted. The average number of cells attached per mm^2 is shown in Figure 45.

The number of cells attached to all substrates increased with time and the number of cells attached to PL was greater than that obtained for HA at all time-points. The number of cells attached to Si-CaP were significantly lower than that on PL for time-points up to and including 6 hours. However, in the 6–8 hours time period there was a marked increase in the mean (±SD) number of cells attached to Si-CaP and by 8 hours the number of cells attached to this substrate was comparable to that for PL (129 ± 10.3 *vs.* 119 ± 8.6 cells/ mm^2; $p=0.222$). On HA, the rate of attachment showed the same time dependence as for Si-CaP, with a rapid increase in the number of cells attached at 6 and 8 hours. Significantly more cells attached to Si-CaP than to HA at 2 hours (32 ± 1.3 *vs.* 18 ± 0.8 cells/ mm^2; $p<0.05$) and at 8 hours (129 ± 10.3 *vs.*74 ± 2.3 cells/ mm^2; $p<0.05$).

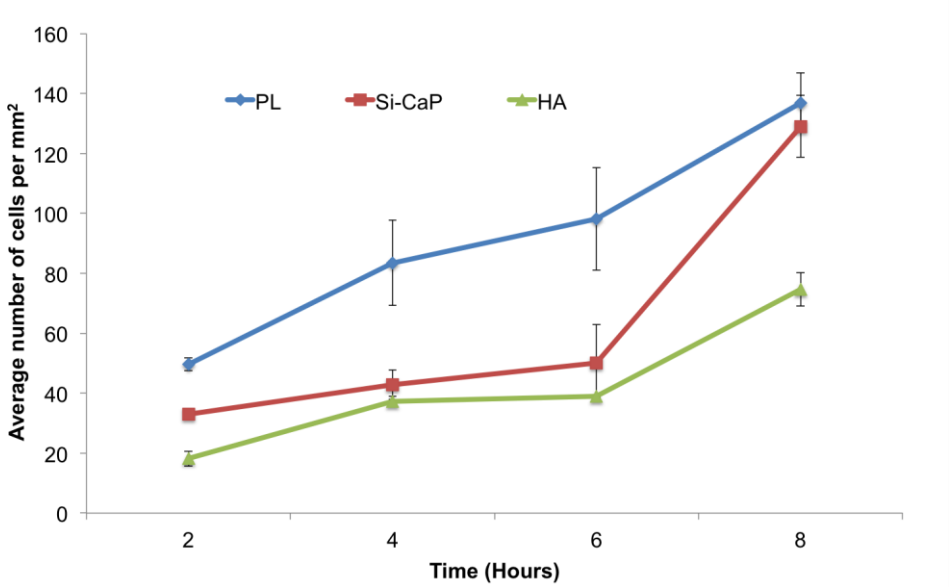

Figure 45: Attachment of MSC to substrates.

Number of cells attached to substrates over time normalised to surface area. The results represent the mean ± SD of three donors with samples run in triplicate

5.2.1.2.2 Proliferation

Bone marrow derived MSC were seeded onto scaffolds and allowed to proliferate over 21 days. At regular intervals, cells on scaffolds were fixed, stained and counted. The average number of cells attached per mm^2 was calculated and is shown in Figure 46. A time dependent increase in cell number for cultures on Si-CaP, HA, PL and PL+OS was observed up to 21 days. On Day 1, cell number was similar for all substrates, after which cells proliferated at different rates on each substrate. The greatest increase in cell number over time was observed for cells cultured on PL without osteogenic media. The addition of osteogenic factors led to a decrease in the growth rate, with cell density being significantly lower for PL+OS than for PL at all time-points after Day 1. However, this difference only achieved statistical significance on days 7 and 14 ($p=0.02$ and $p=0.03$, respectively). Cells cultured on Si-CaP and HA showed a similar growth curve to cells on PL+OS; cell numbers on both Si-CaP and HA were lower than PL at all time-points but the difference between Si-CaP and HA did not achieve statistical significance ($p>0.19$).

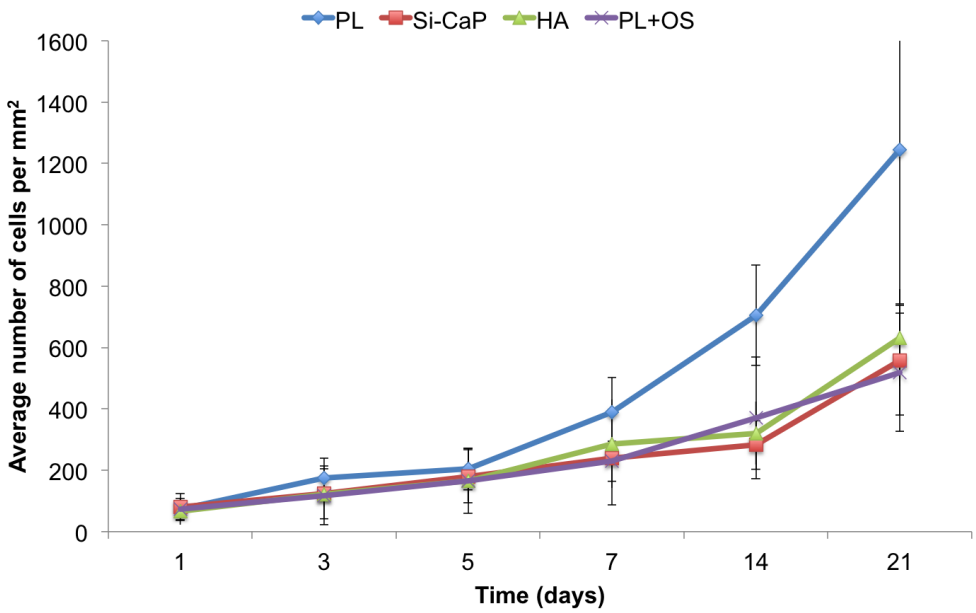

Figure 46: Proliferation of MSC on substrates.

Cell proliferation over time on substrates, normalised to surface area. The results represent the mean ± SD of three donors, with five samples run per donor.

5.2.1.2.3 Gene expression

Culturing MSC on different substrates for up to 21 days resulted in differential expression of osteoblast specific genes. To account for differences in cell numbers on the various substrates, the expression levels were normalised to the house keeping gene β2 microglobulin and the normalised values for the expression of a range of MSC and osteoblast specific genes are shown in Figure 47.

Endoglin (*CD105*) is a cell surface receptor commonly associated with MSC, and it decreases in expression as these cells differentiate. *CD105* expression decreased on Si-CaP and PL+OS, but did not change significantly on HA and PL. Expression of *CD105* was significantly reduced on Si-CaP and PL+OS on Day 7 and remained lower than PL at all time points thereafter. Cells cultured on HA expressed lower levels on Day 1 than compared to all other substrates; but did not decrease over time, and remained at similar levels to PL on Day 21.

RUNX2 has a key role in osteoblast differentiation. It binds to the promoters of a number of osteoblast specific genes including collagen type 1 and osteocalcin, inducing their expression. *RUNX2* expression was upreguated in cells cultured on Si-CaP, HA and PL+OS. High expression was observed earlier in cells cultured on Si-CaP and HA, compared to PL+OS. *RUNX2* levels were highest on Day 1 for both Si-CaP and HA, where they were 1.6- and 1.4-fold greater than PL respectively. Cells on PL+OS demonstrated a high level of *RUNX2* expression much later, on Day 14, where they reached 1.8-fold greater than PL.

Parathyroid hormone receptor 1 (*PTH1R*) expression is associated with endochondral ossification and plays a vital role in calcium homeostasis in bone (Alonso et al. 2011; McCauley et al. 1996). PTH1R expression is associated with a mature, cuboidal cell, and is expressed as osteoblastic cells differentiate (McCauley et al. 1996). *PTH1R* was upregulated on Si-CaP, HA and PL+OS however, the timing of expression was different on each substrate. Initially cells on Si-CaP expressed high levels of *PTH1R*, followed by PL+OS, then HA. Cells on Si-CaP significantly upregulated *PTH1R* expression on Days 1 and 7: 1.8- and 3.6-fold greater than PL. However, cultures on HA and PL+OS demonstrated the greatest levels of expression on Day 21, 2.4– and 5.6- fold greater than PL respectively. Cells on PL did not show any increase in *PTH1R* expression over 21 days.

An early marker of osteoblast differentiation and a reporter of osteoblast activity, Collagen type I (*COL1A1*) was increased in cells on Si-CaP, HA and PL+OS. *COL1A1* expression peaked at different time points on each substrate, first on Si-CaP, then HA and much later PL+OS. In cells on Si-CaP, *COL1A1 was* highly upregulated on Day 7, 3.9-fold greater than PL. On HA *COL1A1* expression was highest at Day 14, 2.5-fold greater than PL. Levels of *COL1A1* in cultures on PL+OS increased from Day 14 and but peaked later on Day 21, to 2.6-fold greater than PL. Expression of *COL1A1* was maintained at a low level in cells cultured on PL.

Osteocalcin (*BGLAP*) is a late marker of osteoblast differentiation, expressed at the onset of mineralisation. There were no significant differences in *BGLAP* expression on any of the substrates. Cells cultured on

Si-CaP, showed the greatest expression of *BGLAP* on Day 14, however this increase did not reach statistical significance (P=0.988).

Dentin matrix acidic phosphoprotein 1 is encoded by the *DMP1* gene and thought to be restricted to mineralised tissue (Kalajzic et al. 2004), where it is produced by terminally differentiated osteoblasts (Toyosawa et al. 2001). *DMP1* expression was low in cells on all substrates on Days 1 to 14 however, on Day 21 expression greatly increased in cells on Si-CaP (5.5-fold), HA (5.1-fold) and PL+OS (7.8-fold). Cells on PL expressed low levels of *DMP1*, less than 1-fold increase, on Day 21, and was significantly lower than cells on Si-CaP (p=0.03), HA (P=0.03) and PL+OS (P=0.003).

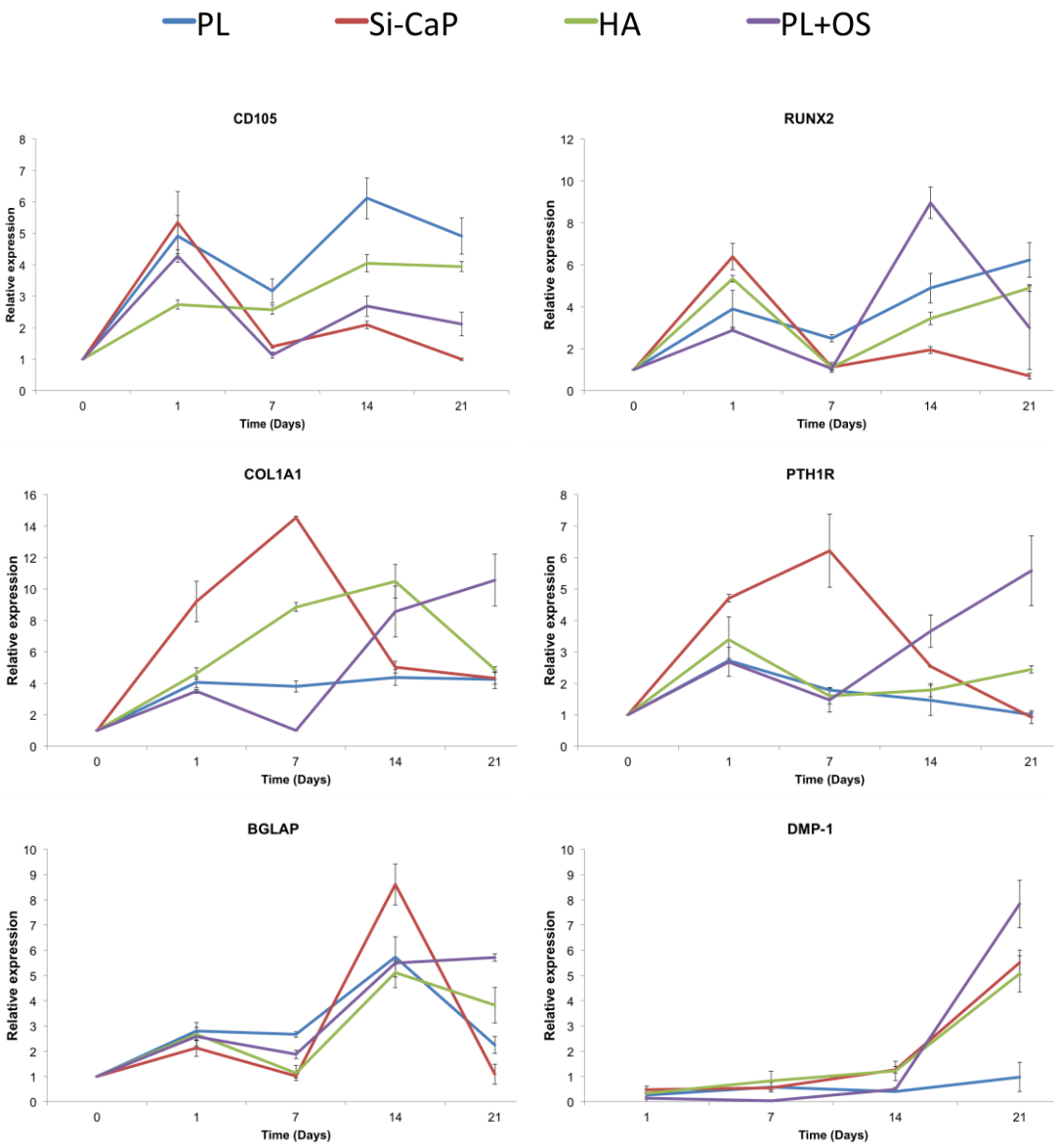

Figure 47: Real time gene expression profile of MSC on substrates.

Data are mRNA levels of genes of interest and are represented as level of expression normalised to beta-2 microglobulin and to Day 0. Three donors were used, and each sample was run in duplicate

5.2.1.2.4 Protein production

To confirm gene expression correlated with protein production, cells were immunostained for three key osteoblast proteins, RUNX2, collagen type I, and osteocalcin.

RUNX2 was detected via immunohistochemistry in cells cultured on PL+OS, Si-CaP and HA and is shown in Figure 48. Cells cultured on PL+OS expressed nuclear RUNX2 on days 7 and 14. Cells grown on Si-CaP and on HA showed the same nuclear pattern of RUNX2 expression on Day 7. However, on Days 14 and 21 RUNX2 appeared to be present also in the cytoplasm, although RUNX2 protein expression was predominantly nuclear (in approximately 91% and 87% of cells cultured on Si-CaP and on HA, respectively). RUNX2 was not detected in cells from any of the PL samples.

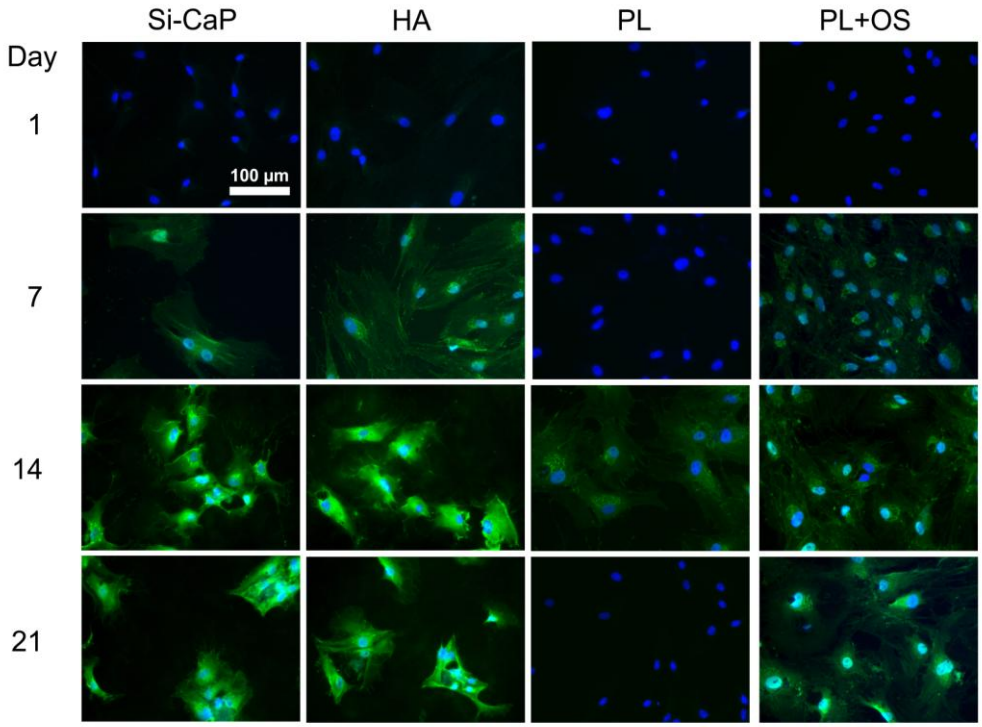

Figure 48: RUNX2 immunostaining of MSC on substrates.

RUNX2 (green) and DAPI (blue) Scale bar represents 100µm.

Collagen type I protein expression in cells cultured on the various substrates on days 1, 7, 14 and 21 is shown in
Figure 49. Collagen type I protein was detected as early as Day 1 in cells cultured on Si-CaP and HA, with expression increasing in intensity until Day 21. Collagen type 1 was detected in cells cultured on PL and PL+OS at all time-points; however, its expression was less intense and less widespread compared with that of cells grown in Si-CaP and HA.

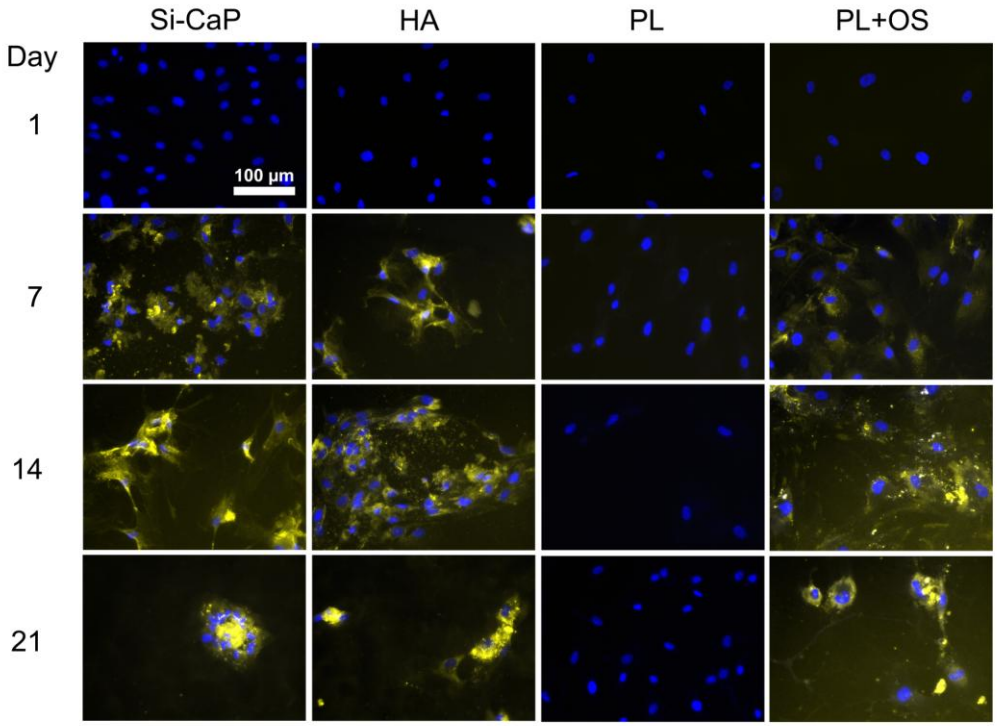

Figure 49: Collagen type I immunostaining of MSC on substrates.

Collagen type I (yellow) and DAPI (blue) Scale bar represents 100µm.

Osteocalcin staining, shown in
Figure 50, was not detected in cells on any substrate on Day 1. On Day 7 faint staining was seen in cells cultured on PL+OS, but not on Si-CaP, HA or PL. By Day 14 however, there was strong staining in cells on Si-CaP, HA and PL+OS, the majority of staining was cytoplasmic, yet in some cells nuclear staining was also detected. On days 14 and 21 no osteocalcin staining was observed in cells on PL. On PL+OS on Day 21 osteocalcin intense staining was detected in approximately 90% of the cells and in some areas small, punctate, extracelluar staining was seen. On HA and Si-CaP cytoplasmic and nuclear staining was detected in the majority of cells.

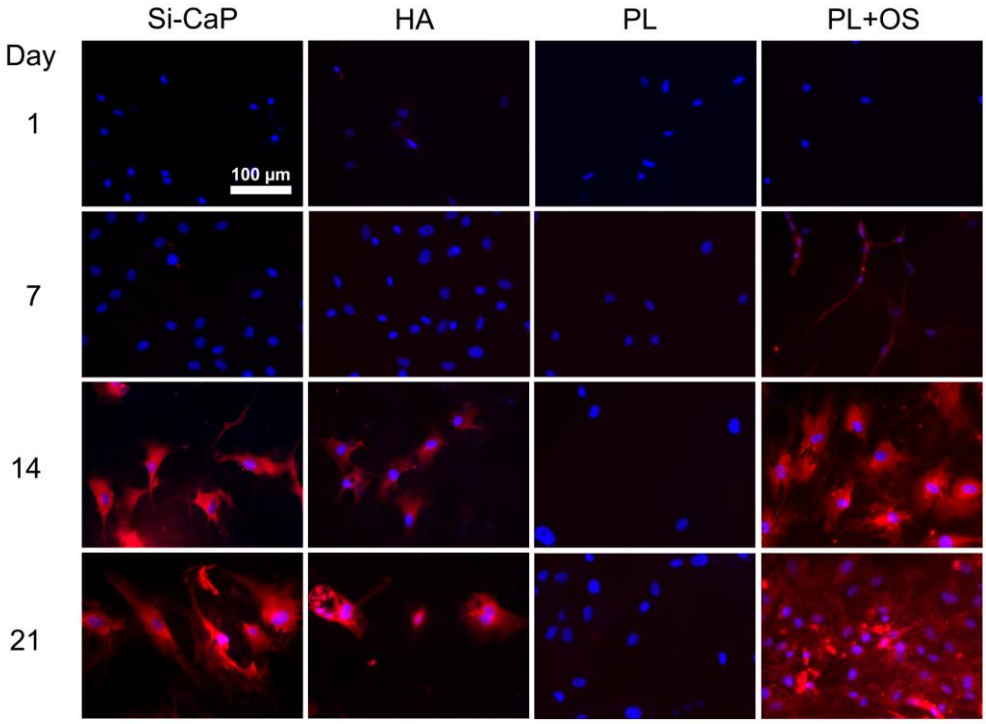

Figure 50: Osteocalcin immunostaiing of MSC on substrates.

Osteocalcin (red) and DAPI (blue) Scale bar represents 100µm

5.2.1.2.5 Alkaline phosphatase

The ALP positive area was low on cells cultured on plastic alone (PL), but was strongly 'induced' in PL+OS cultures, In contrast to cells maintained on PL alone, cells cultured on Si-CaP and HA in the absence of osteogenic supplements showed intense widespread positive staining for ALP, as shown in Figure 51. The area of staining was quantified and the average area of staining on each substrate is shown in Figure 52.

Cell numbers and ALP staining were comparable for cells cultured on Si-CaP, HA and PL+OS. The ALP activity on PL was lower, even though cell numbers were similar. The ALP positive fraction was significantly increased on Si-CaP and HA compared with PL (42.9 ± 9.3 and 32.9 ± 6.7 *vs.* 6.3 ± 8.5 % total substrate area, respectively; $P<0.01$). There was no statistically significant difference between the ALP activity of cells cultured

on Si-CaP versus HA; there was also no significant difference between either of these versus the positive control, cells cultured on PL+OS.

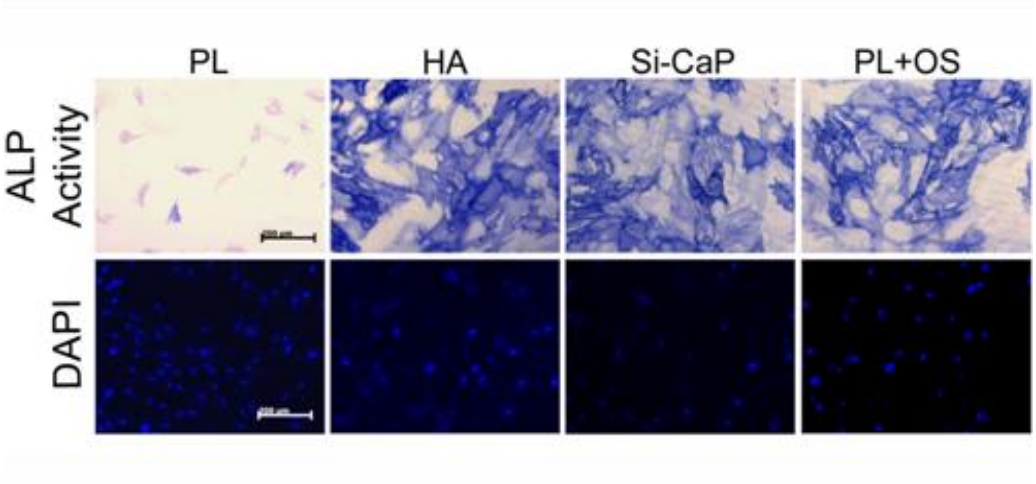

Figure 51: Alkaline phosphatase staining on substrates.

Staining of differentiating cells on substrates at Day 21 (upper panels), lower panel shows nuclear stain (DAPI) of same area to show cell density. (Scale bar represents 200μm).

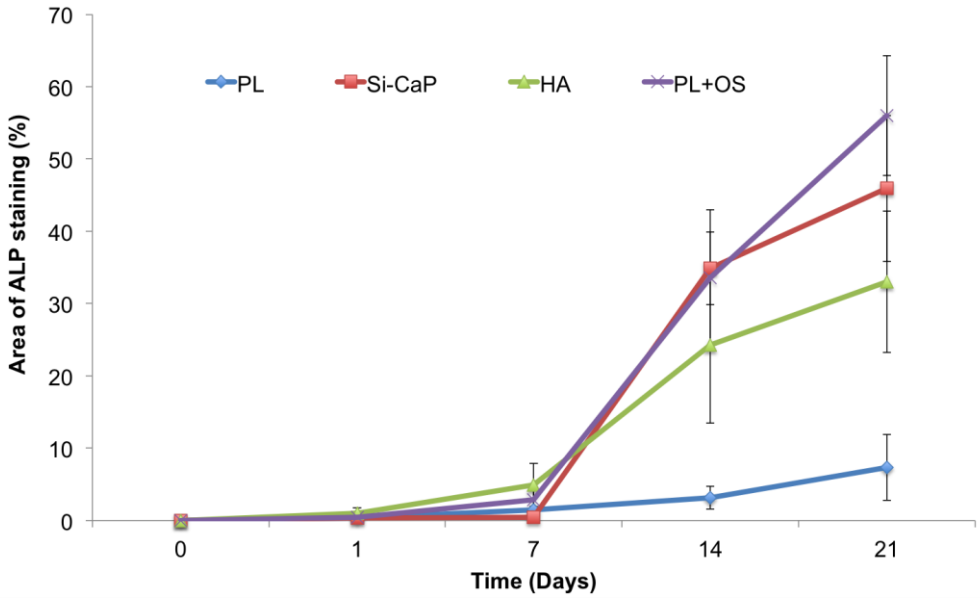

Figure 52: Area of alkaline phosphatase staining on substrates.

ALP activity of cells on substrates quantified by analysing the area of ALP positive cells using image analysis software and the mean area calculated per disk / well. The results represent the mean ± SD of three donors with samples run in triplicate.

3.4.2.1.1 Mineralisation

Areas of mineralisation were detected by staining using the von Kossa method, with black staining, indicating calcium deposits (shown in Figure 53). The staining was quantifed and the area of mineralisation on substrates is shown in Figure 54. The extent of mineralisation increased with time for all substrates except for PL, where no changes from baseline levels were observed. No significant increase in mineralised deposits on HA was detected until Day 14, at this time-point, the area covered with mineralised matrix was lower for HA when compared with Si-CaP (20.8 ± 8.2 % *vs.* 36.5 ± 12.3% total substrate area). In all substrates the area covered with mineralised matrix continued to increase up to the furthest time point at Day 21. At this time-point, the area of mineralisation on Si-CaP and HA was significantly greater than on PL (48.9 ± 14.5 and 42.5 ± 11.0 *vs.* 1.2 ± 0.2 % total substrate area, respectively; $p<0.05$ in both comparisons).

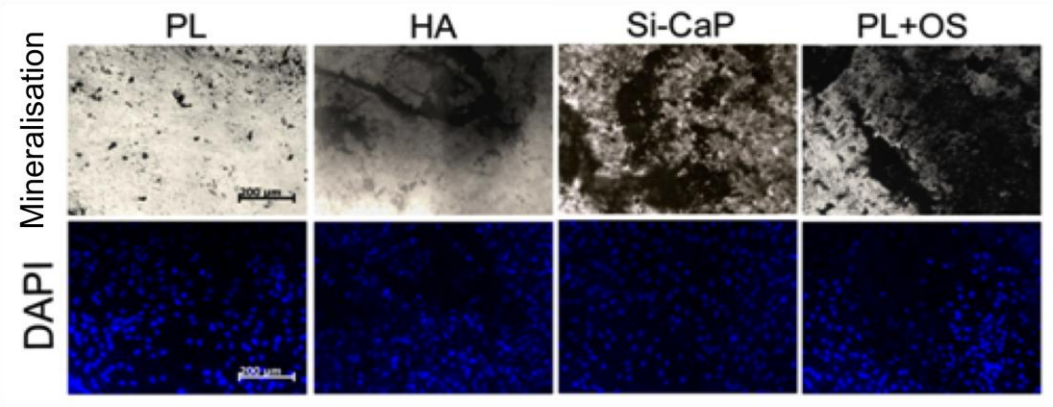

Figure 53: Von Kossa staining on substrates.

Staining of calcium deposits in mineralisation on substrates at Day 21(top panel), lower panel shows same fields with nuclear stain (DAPI) to show cell density (Scale bar represents 200μm).

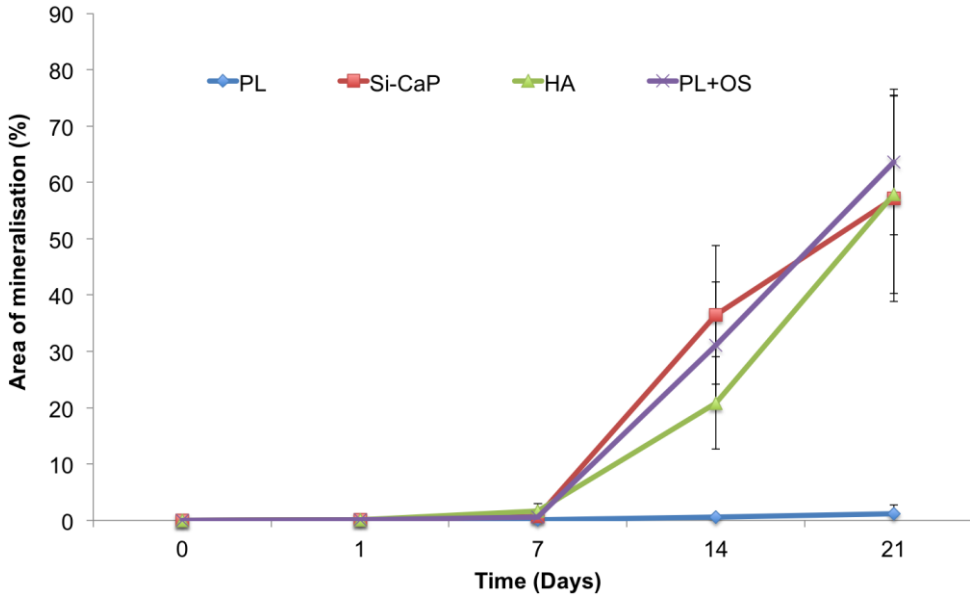

Figure 54: Area of mineralisation on substrates.

Mineralisation on substrates was measured by analysing the area of black deposits using image analysis software and the mean area covered was calculated per disk / well. The results represent the mean ± SD of three donors with samples run in triplicate.

5.2.2 hES-MP

5.2.2.1.1 Attachment

Cells attached to all substrates, increasing in a time dependent manner as shown in

Figure 55. Initially, at 2 hours, very few cells attached to all substrates: only 9.44 ± 4.03 cells per mm^2 attached to PL, more cells attached to Si-CaP and HA, 17.5 ± 3.2, and 12.7 ± 4.1 per mm^2 respectively. At this time, the number of cells attached to Si-CaP was significantly higher than on PL (P=0.006). At 4 hours post-seeding the number of cells attached to each substrate increased rapidly. On PL cell number increased 4.5-fold, to 43.2 cells per mm^2 and cell number on Si-CaP increased 2.9-fold and cell number on HA increased 2.8- fold, and cell number did not vary significantly between substrates. At 6 hours cell numbers on PL continued to increase, (71.5 ±12.9) significantly higher than cell number on both Si-CaP and HA (p=0.0001 and p=0.03 respectively). Average cell number on

Si-CaP did not increase at this point; instead it decreased from 50.6 to 50.1 per mm^2. On HA, cell number was lower than both Si-CaP and PL and increased on average by 0.4 cells per mm^2. At 8 hours post seeding average cell number again increased greatly on PL (73.7 ± 18.4). Cell number on Si-CaP and HA remained low on (55.5 ± 11.19, and 45.8 ± 9.9 respectively). At this final time point significantly more cells were attached to PL, compared with HA (p=0.01) yet cell number on PL did not vary significantly compared to Si-CaP.

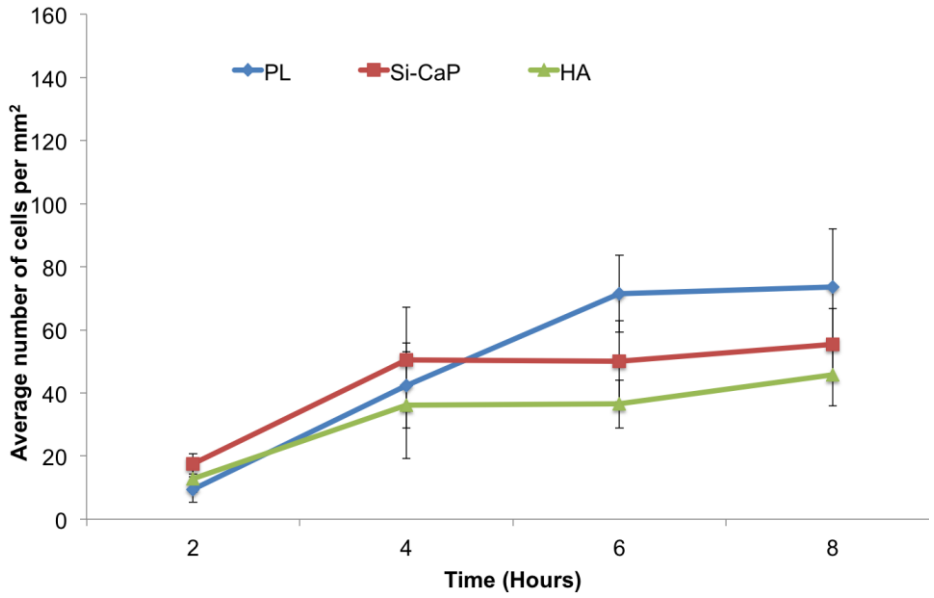

Figure 55: Attachment of hES-MP to substrates.

Number of cells attached to substrates over time normalised to surface area. The results represent the mean ± SD of cells at three different passages with samples run in triplicate.

5.2.2.1.2 Proliferation

On Day 1, cell numbers were similar on all substrates with no significant differences between PL, PL+OS, Si-CaP and HA (P> 0.78), as shown in Figure 56. On Day 3 cell number increased on all substrates, but did not differ significantly (P≥1). On PL, in the absence of osteogenic factors, cells proliferated rapidly, with cell number increasing over time, and by Day 5 cell number on PL was significantly higher than PL+OS (P=0.02). Average cell number was also high on Si-CaP, but did not reach statistical

significance. At Day 7 average cell number varied greatly between substrates: the greatest number of cells was seen on PL, and PL+OS had the least. Cells on PL continued to proliferate up to Day 21, where cell number reached its maximum, and was significantly greater than any other group ($P<10^{-7}$). PL+OS had the least number of cells from days 7 to 21. On Day the average cell number on HA and Si-CaP was similar, cell number on Si-CaP was higher than on HA on days 14 and 21, but did not vary significantly ($P> 0.2$). On Day 21, cell number on Si-CaP and HA was significantly greater than PL+OS ($P<0.02$) and significantly lower than PL ($P<0.001$).

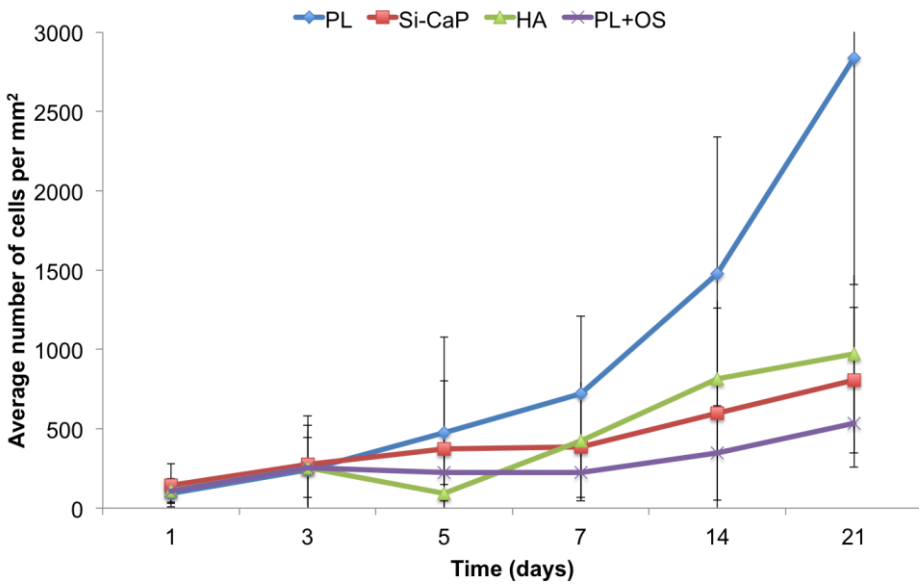

Figure 56: Proliferation of hES-MP on substrates.

Cell proliferation over time on substrates and on PL in OS media, normalised to surface area. The results represent the mean ± SD of cells at three different passages with five samples run per passage.

5.2.2.1.3Gene expression

CD105 expression in cells on PL was maintained at a relatively constant level in cells cultured on PL, and varied by only 1.27-fold over 21 days, (shown in Figure 57).
On Si-CaP, *CD105* expression was highest on Day 1, then decreased over time. Cells on PL+OS showed similar trend in expression, initially highest on Day 1, and then decreasing over time. On HA, *CD105* expression fluctuated, levels increased on Day 7, and then decreased on days 14 and 21.

hES-MP cultured on Si-CaP showed the highest *RUNX2* expression on Day 1, 16.1-fold greater than PL. After Day 1, *RUNX2* expression decreased gradually but on Day 21 remained higher than on PL. On HA *RUNX2* expression increased on Day 1 and was highest on Day 7, 19.2–fold greater than PL. On Day 14 expression decreased slightly, but remained at similar levels on Day 21. *RUNX2* expression on PL+OS initially decreased on Day 1, but increased significantly on Day 7, to 38.2-fold greater than PL; on days 14 and 21 *RUNX2* expression decreased, but remained higher than PL. hES-MP on PL, showed very little *RUNX2* expression and did not vary by more than 0.5–fold.

OSX expression on Day 1 was highest on Si-CaP (2.4-fold greater than PL). After Day 1, *OSX* levels decreased until Day 21, when *OSX* expression increased slightly. On HA, *OSX* expression was also greatest on Day 1 2.0–fold greater than PL, then decreased over time until Day 21 when levels increased slightly. On PL+OS, *OSX* expression decreased on Day 1 to 0.5–fold less than PL. Then on Day 7, levels increased to 10.2–fold greater than PL, decreased on Day 14, and remained at similar levels on Day 21. On PL *OSX* expression decreased 0.3–fold on Day 7, then gradually increased to 1.1–fold on Day 21.

COL1A1 expression increased on Si-CaP on Day 1, 4.3–fold greater than PL and continued to increase on Day 7, where it was highest and significantly greater than PL ($p=0.002$). On Day 14 *COL1A1* levels decreased, then increased slightly on Day 21 to levels significantly greater than PL ($p=0.04$).

On HA, *Col1A1* expression peaked later, on Day 14 6.2–fold greater than PL. Expression then decreased on Day 21, to 3.0–fold greater than PL, when it was significantly greater than PL ($p=0.02$). *Col1A1* expression on PL+OS increased gradually on days 1 and 7, then decreased slightly on day 14 yet was still 5.1–fold greater than PL. On Day 21 expression increased to levels significantly greater than on any other substrate. On PL *COL1A1* expression did not vary significantly, and was consistently lower than on all other substrates.

Expression of *BGLAP* was detected as early as Day 1 on PL+OS where expression reached 3.8–fold greater than PL. Levels of *BGLAP* continued to increase on PL+OS, Si-CaP and HA until Day 21, when the greatest expression was seen. Compared to PL at this time point *BGLAP* levels were 4.1-fold greater on Si-CaP, 4.6–fold on HA and on 6.2–fold PL+OS compared to PL. *BGLAP* expression increased on PL over time and reached 2.0-fold on Day 21, but was significantly lower than on any other substrate ($p<0.004$).

DMP1 was not expressed at significant levels on any substrate until Day 21. At this time point cells cultured on Si-CaP, HA and PL+OS expressed significant levels of *DMP1*: 26.7-fold, 38.7-fold and 43.4–fold greater than PL respectively, ($p<0.002$). On PL cells did not express high levels of *DMP1*. A slight increase was seen on Day 7 however this was not significantly different to any other substrate at the same time ($p>0.8$).

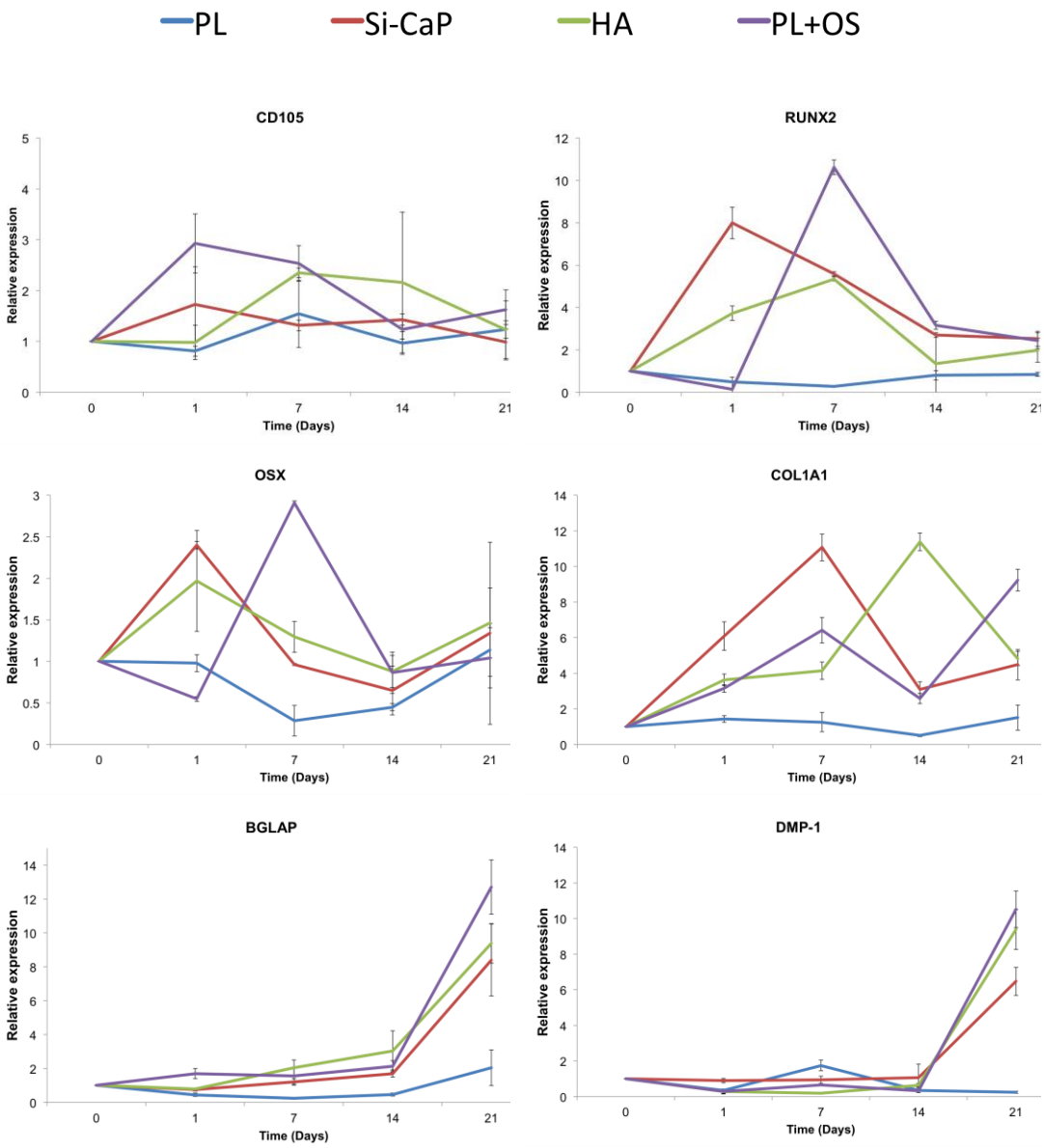

Figure 57: Real time gene expression profile of hES-MP on substrates.

Data are mRNA levels of genes of interest and are represented as level of expression normalised to beta-2 microglobulin and to Day 0. Cells at three different passages were used, and each sample was run in duplicate.

5.2.2.1.4 Protein production

RUNX2 was detected by immunostaining in cells cultured on substrates, over 21 days, and is shown in
Figure 58. On Si-CaP cells expressed RUNX2, as early as Day 1 where staining was bright and seen in the majority of cells. RUNX2 was observed throughout the cell, but the strongest staining was seen in the nucleus. Similar levels of RUNX2, were observed at days 7 and 14, however, by Day 21 expression was largely cytoplasmic, with few cells having nuclear staining. Cells cultured on HA, also displayed RUNX2 positive staining on Day 1, but again this was largely cytoplasmic. By Day 7, strong nuclear staining was detected in roughly half of the cells, then after 14 days localisation was similar to cells on Si-CaP, with the majority of cells displaying cytoplasmic staining. RUNX2 was detected at low levels in hES-MP cultured on PL, and appeared to increase in intensity over time up to 21 days. Very few cells had nuclear staining and in most cases cells expressed low levels in the cytoplasm. Cells cultured on PL+OS had strong nuclear and cytoplasmic staining on Day 1. Over time, less nuclear staining was detected, and cytoplasmic RUNX2 was observed.

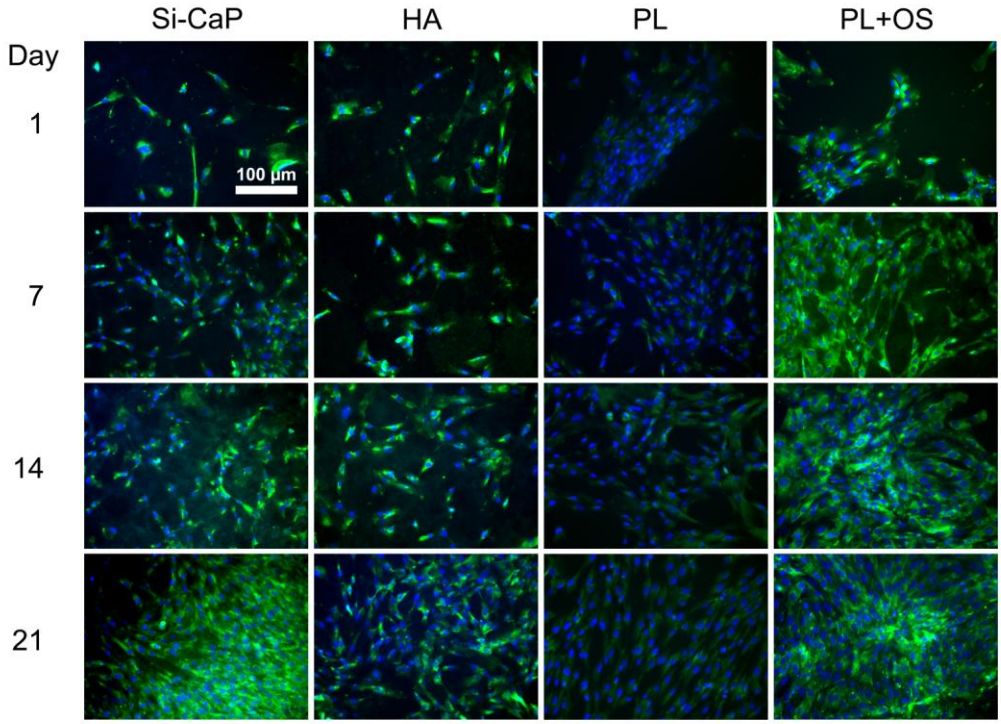

Figure 58: RUNX2 immunostaining of hES-MP on substrates.

RUNX2 (green) and DAPI (blue) Scale bar represents 100μm.

Figure 59 shows Collagen type I immunostaining of cells cultured on each substrate over 21 days. On Day 1 collagen type I staining was not detected on any substrates. Yet by Day 7, extracellular collagen staining was seen on Si-CaP, HA and PL+OS. On Si-CaP and HA collagen staining was widely dispersed, but intense in certain areas. ON PL+OS staining was also widespread, but appeared to be more filamentous. Intense, similar staining was observed on Si-CaP, and PL+OS on days 14 and 21 and became more widespread and significantly brighter at each time point. Staining on HA appeared to localised to certain areas, in the form of nodules, or aggregates. No mature collagen type I staining was observed on PL at any time point.

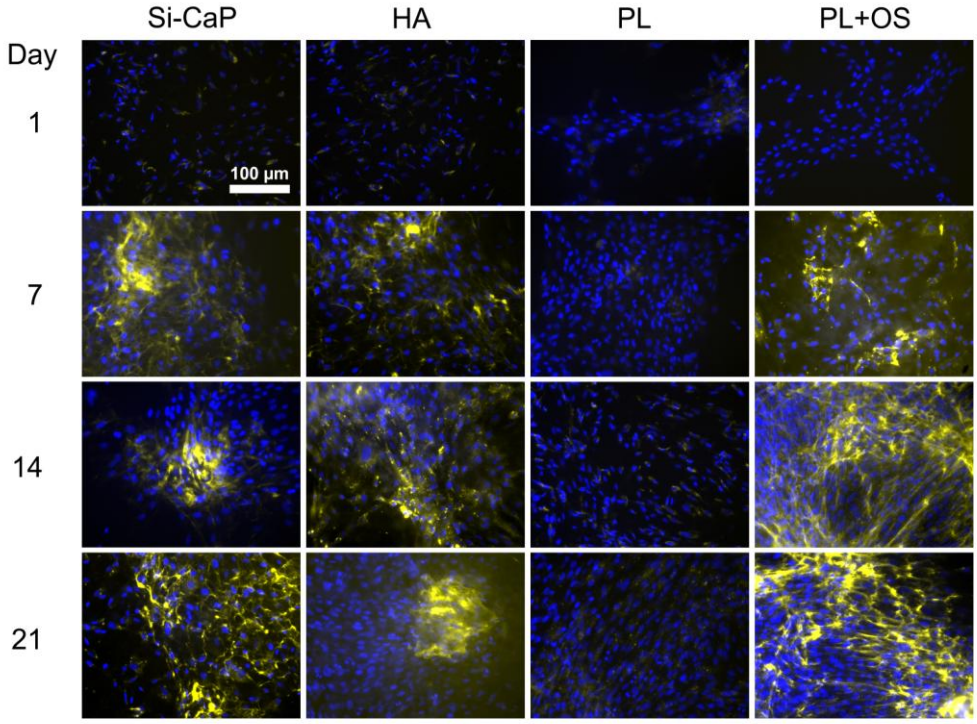

Figure 59: Collagen type I immunostaining of hES-MP on substrates.

Collagen type I (yellow) and DAPI (blue) Scale bar represents 100μm.

On Day 1, very little osteocalcin staining was detected on HA, PL and PL+OS as shown in

Figure 60. However, strong staining was seen in several cells on Si-CaP, this staining increased in intensity over time and by Day 21 staining was widespread and notably brighter is certain cells. Cells on HA also showed intense osteocalcin staining, which increased over time however, staining was more punctate and less evenly distributed throughout the cells, this was most apparent on days 7 and 14. On Day 21 staining appeared to be extracellular, filamentous, and disorganised. Cells on PL, did not express osteocalcin to the same extent as cells on Si-CaP, HA and PL+OS, however some weak staining was detected on Day 14, this was relatively weak, but was similar in localisation to staining seen on HA. Cells cultured on PL+OS showed weak staining up to Day 21, when staining was intense. Both punctate and cytoplasmic staining was observed, as seen in HA and Si-CaP respectively.

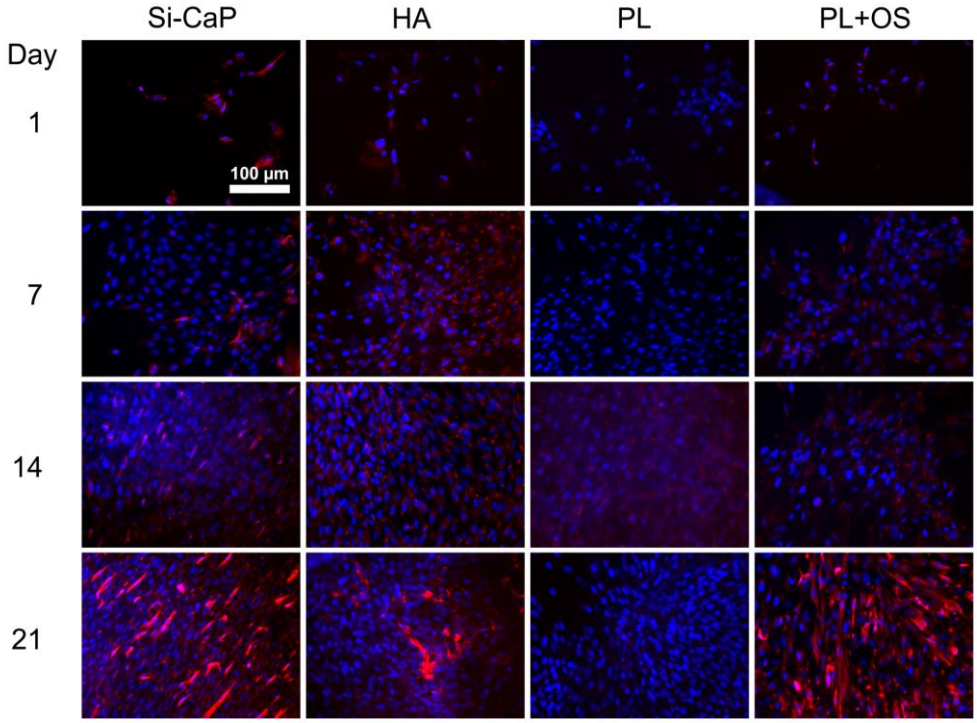

Figure 60: Osteocalcin immunostaining of hES-MP on substrates.

Osteocalcin (red) and DAPI (blue) Scale bar represents 100µm.

5.2.2.1.5 hES-MP alkaline phosphatase activity

ALP activity in cells cultured on all substrates was measured over 21 days as before and is shown in

Figure 61. Detectable levels of ALP were observed as early as Day 1 in hES-MP cultured on all substrates, and at this time there was no significant difference between ALP activity on any substrate ($p>0.85$). On Day 7, ALP activity increased rapidly on Si-CaP (7.3-fold), HA (6.8-fold) and on PL+OS (5.8-fold). At this time, there was significant variance between ALP activity at different passages, as evidenced by large error bars. On Day 7, ALP activity was significantly higher on Si-CaP than any other substrate ($p<0.04$). ALP levels on Day 7 were also high on HA, significantly greater than on PL+OS ($p=0.023$). On Day 14, ALP activity on PL+OS increased to 44.1%, higher but not significantly different to Si-CaP ($p=0.25$) and HA ($p=0.30$). ALP activity on Si-CaP and PL+OS increased on Day 21 and peaked at 51.2% and 53.1% respectively. ALP activity on HA only increased slightly to 41.6%, significantly lower than both Si-CaP ($p<0.0001$) and PL+OS ($p<0.0001$). Cells on PL showed continued low-level ALP activity, and peaked on Day 21 at 8.64%. ALP produced on PL, did not vary considerably between passages, and the error bars show the wide standard deviation seen within the same samples.

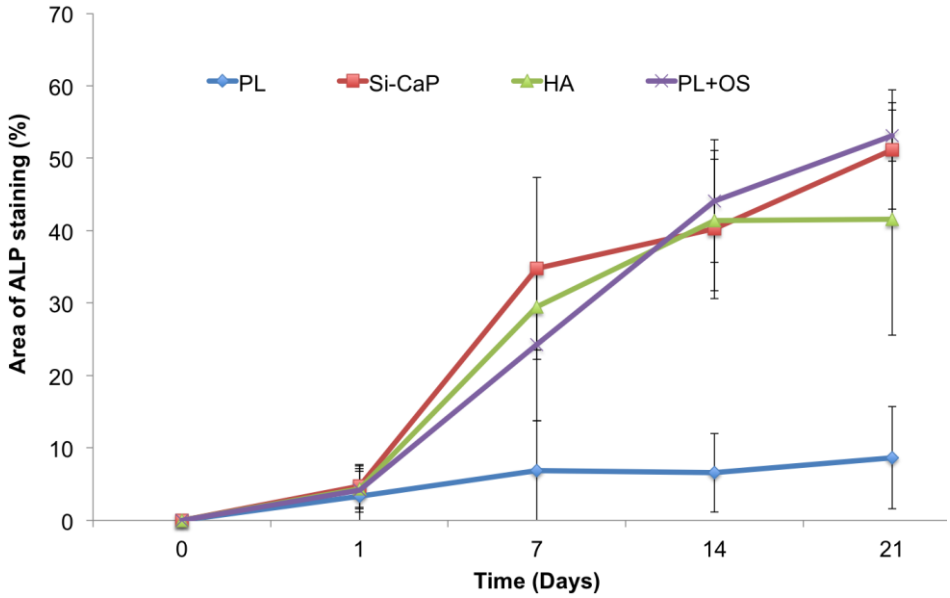

Figure 61: Area of alkaline phosphatase on substrates.

ALP activity of cells on substrates quantified by analysing the area of ALP positive cells using image analysis software and the mean area calculated per disk / well. The results represent the mean ± SD of cells at three different passages with samples run in triplicate.

5.2.2.1.6 Mineralisation

Cells cultured on PL, did not produce a mineralised matrix (shown in Figure 62), and no significant staining was observed over 21 days. However, a mineralised matrix was formed on Si-CaP, HA and PL+OS, and the area of mineralisation increased over time. On Day 7, a significant difference between cells on PL and cells on PL+OS, SiCaP and HA was detected ($p<0.00001$) and by Day 14 Si-CaP and HA, had very similar areas of mineralisation 39.2% and 39.3% respectively. Mineralisation on PL+OS was slightlylower, 35.5%, but not significantly so ($p> 0.34$). On Day 21 area of mineralisation increased on PL+OS, to 74.4%, significantly higher than all other substrates ($p>0.0004$). Mineralisation on Si-CaP covered a greater area (65.7%) than HA (63.0%), yet did not vary significantly ($p=0.433$).

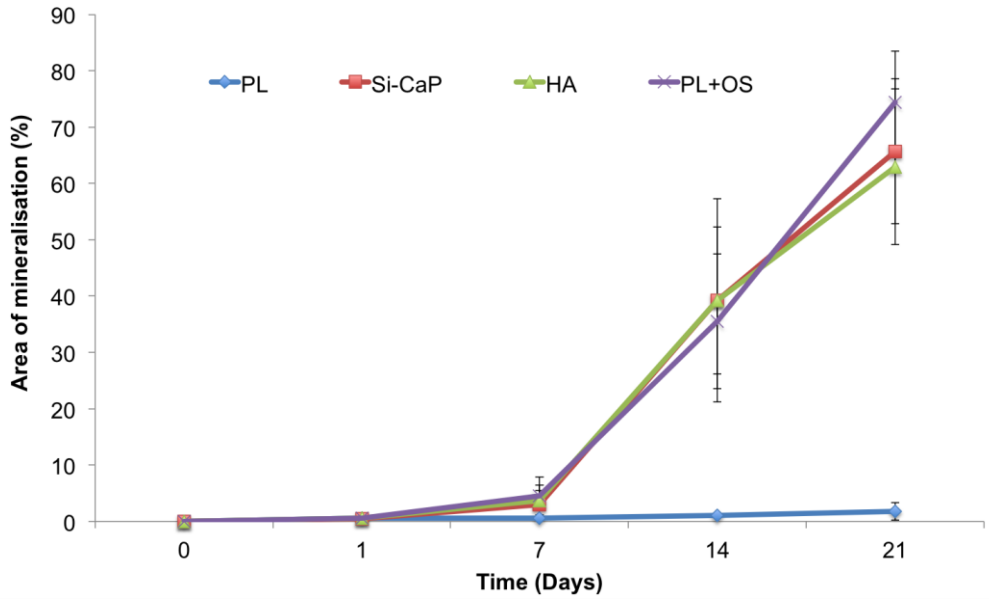

Figure 62: Area of mineralisation on substrates.

Mineralisation on substrates was measured by analysing the area of black deposits using image analysis software and the mean area covered was calculated per disk / well. The results represent the mean ± SD of cells at three different passages with samples run in triplicate.

5.2.3 ADMSC

5.2.3.1.1 Attachment

ADMSC attached to all substrates and average cell number increased over time, as shown in

Figure 63. At 2 hours post seeding there were significantly more cells attached to PL, compared to Si-CaP (P= 0.007) and HA (P=0.003). At this time point the average number of cells attached to HA was greater than on Si-CaP but the difference was not statistically significant (34.74 ± 9.3 *Vs.*32 ± 7.4 respectively, p=0.73). At 4 hours, the number of cells attached to HA increased 1.6-fold, and was (1.17-fold) higher than on Si-CaP. Yet, this did not reach statistical significant – in fact the average number of cells attached to Si-CaP did not vary significantly to HA at any time point (p>0.7). On PL the number of cells attached continued to increase, and at 6 hours remained significantly higher than both HA and Si-CaP (P < 0.02). By 8 hours post seeding similar number of cells were seen attached and there

was no significant difference between attachment each of the substrates (P > 0.054).

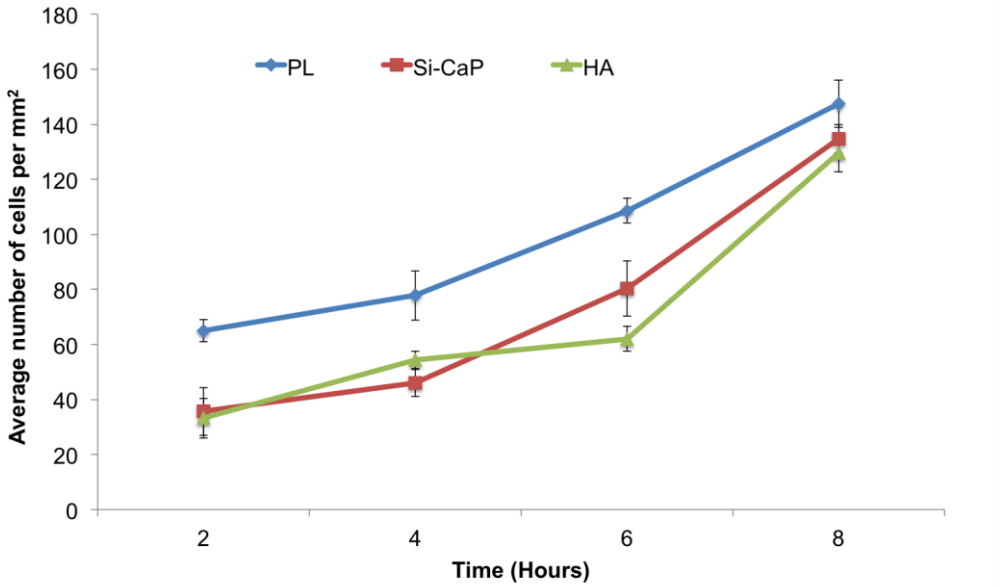

Figure 63: Attachment of ADMSC on substrates.

Number of cells attached to substrates over time normalised to surface area. The results represent the mean ± SD of two donors with samples run in triplicate.

5.2.3.1.2 Proliferation

Cell number on all materials was similar on Day 1 then increased over time, as shown in Figure 64. Cell number on PL, increased at near exponential rate up to Day 14 then slowed on Day 21. On Day 3, cell number was comparable on all substrates with the exception on PL+OS, HA and Si-CaP where cell number was significantly lower then PL (P=0.04). On Day 5 cell number increased on all substrates and did not vary significantly between substrates. However, on Day 7 cell number on PL was significantly higher than HA (P=0.02), Si-CaP (P=0.0006) and PL+OS (P= 0.02). This trend continued to Day 21, where cell number on PL was 0.8-fold greater than any on other substrate.

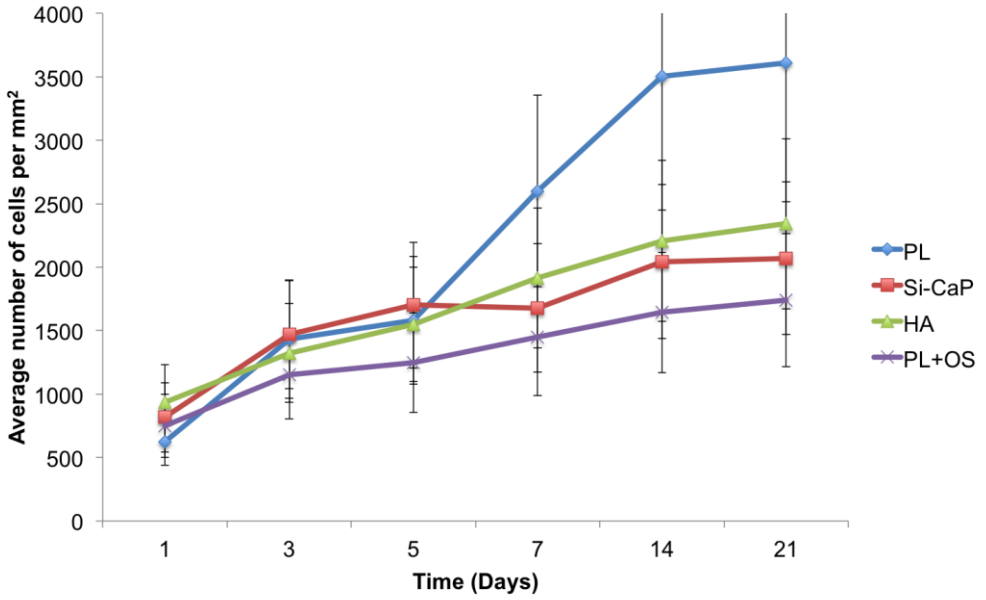

Figure 64: Proliferation of ADMSC on substrates.

Cell proliferation over time on substrates and on PL in OS media, normalised to surface area. The results represent the mean ± SD of two donors, with five samples run per donor.

5.2.3.1.3 Gene expression

ADMSC gene expression was analysed and is shown in **Error! Reference source not found.**. Mesenchymal associated *CD105* expression detected on all substrates and decreased over time and expression levels varied by less than 1-fold over 28 days in culture. *CD105* expression was highest in cells cultured on PL at all time points, but decreased slightly over 28 Day in culture. Expression of *CD105* in cells cultured on PL+OS, Si-CaP and HA decreased more significantly over time. On Si-CaP and HA, expression of CD105 decreased more rapidly compared to PL+OS. On Day 7 levels of *CD105* were 2- and 3-fold lower on HA and Si-CaP respectively compared to PL+OS. At 14 days *CD105* expression increased slightly on Si-CaP and HA, at Day 21 a similar increase was seen on PL+OS, after which expression continued to decrease over time. This small increase was the only time point where expression on PL was not significantly higher than PL+OS ($p=0.22$). *CD105* expression on Si-CaP and HA was significantly lower than PL at all time points ($p<0.00001$). At 28 days transcript levels in cells on Si-CaP were similar to PL+OS and levels of expression on HA were

significantly lower than on PL+OS ($p<0.0001$). Expression of *RUNX2* on substrates varied greatly over time. On PL+OS *RUNX2* expression was highest at Day 7, where it was 22-fold higher than on PL. After Day 7 *RUNX2* expression on PL+OS decreased to levels not significantly different to PL ($p>0.2$). RUNX2 expression on Si-CaP and HA followed a similar trend, peaking on Day 1, and then decreasing over time. On Day 1 expression on Si-CaP was 10.7 –fold and HA 8.1–fold higher than PL. After Day 1, *RUNX2* expression on HA decreased but remained higher than PL until Day 21. On Si-CaP *RUNX2* levels decreased after Day 1, but again were higher than on PL up to Day 28.

OSX expression was highest on PL+OS at Day 1, where it was 22.6 –fold higher than on any other substrate. After Day 1 *OSX* expression on PL+OS decreased over time, but remained higher than on any substrate. On Si-CaP and HA, *OSX* expression was highest on Day 7 (10.9 –fold and 8.3 –fold higher than PL respectively). On Si-CaP, *OSX* decreased on Day 21 and on Day 28 remained low. Levels of *OSX* decreased on Day 14 on HA, and also remained low thereafter. Cells cultured on PL did not express significant levels of OSX and did not increase by more than 1.8-fold over culture.

COL1A1 expression was consistently low on PL, but increased over time on Si-CaP, HA and PL+OS. On Days 1 and 7 expression levels were similar on all substrates, and did not vary significantly ($p>0.9$). On Day 14, *COL1A1* expression increased gsignificantly on Si-CaP, HA and PL+OS (15.8-fold 14.4–fold and 23.0–fold greater than PL respectively). On Day 21 *COL1A1* levels decreased slightly in Si-CaP, and PL+OS. On Day 28 *COL1A1* expression increased on Si-CaP and was 1.2–fold higher than PL+OS, expression levels on HA also continued to increase over time and on Day 28 there was no significant difference between Si-CaP, HA and PL+OS ($p>0.8$).

Expression of *BGLAP* on PL+OS was low until Day 21, when it increased rapidly (23.7-fold greater than on PL). Cells on Si-CaP showed similar expression of BGLAP, and levels increased alongside PL+OS on Day 21, and did not vary significantly ($p>0.9$). On HA *BGLAP* expression was much lower on Day 21, but 8.6–fold greater than PL. By Day 28, *BGLAP* expression on HA increased to similar levels to Si-CaP and PL+OS. On PL *BGLAP* expression increased, but significantly lower than on any other substrate ($p<0.01$).

In cells cultured on PL+OS, *DMP1* expression was detected as early as Day 14, and continued to increase up to Day 28, when it reached 24.5–fold greater than PL. *DMP1* expression on Si-CaP and HA was similar and not detected until Day 21, where levels were 8.9-fold and 8.4–fold greater than PL respectively. Expression of *DMP1* continued to increase on Si-CaP and HA, and on Day 28 was not significantly different to PL+OS. Cells on PL did not produce significant levels of *DMP1* and expression varied by less than 0.6-fold.

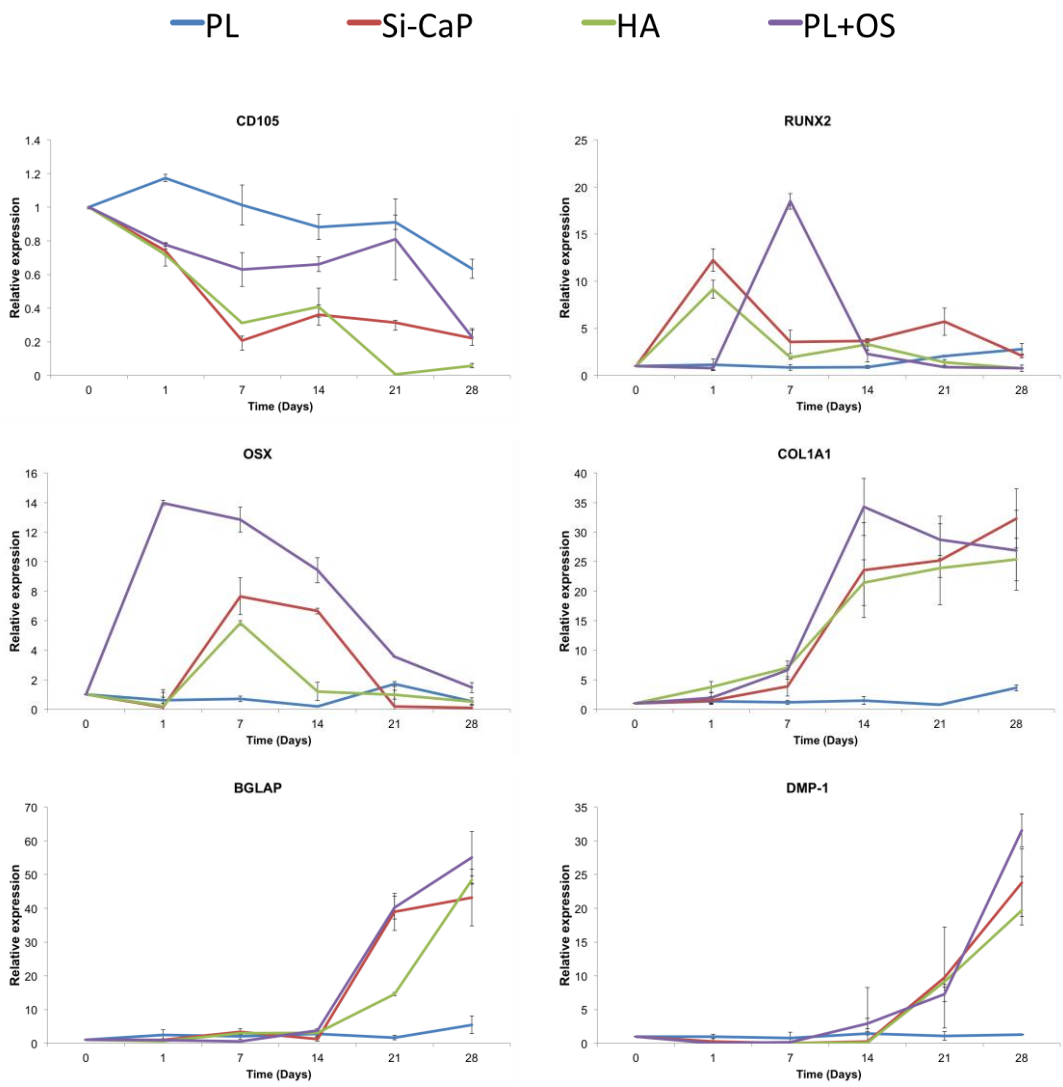

Figure 65: Real time gene expression profile of ADMSC on substrates.

Data are mRNA levels of genes of interest and are represented as level of expression normalised to beta-2 microglobulin and to Day 0. Two donors were used, and each sample was run in duplicate.

5.2.3.1.4 Protein production

RUNX2 was detected by immunohistochemistry over 21 days in culture and is and is shown in

Figure 66. RUNX2 staining was observed in cells cultured on HA and was strongest on days 1 and 7, where its localisation was similar to Si-CaP. However, on Day 14 staining was much weaker on HA, compared to Si-CaP. No staining was seen at any time points in cells cultured on PL, although similar numbers of cells were observed. On Day 1 no RUNX2 staining was detected on PL+OS. On Day 7 however, strong nuclear RUNX2 staining was observed throughout the majority of cells. By Day 14 staining was weak and localised to the cytoplasm of few cells, and by Day 21 no RUNX2 staining was not detectable.

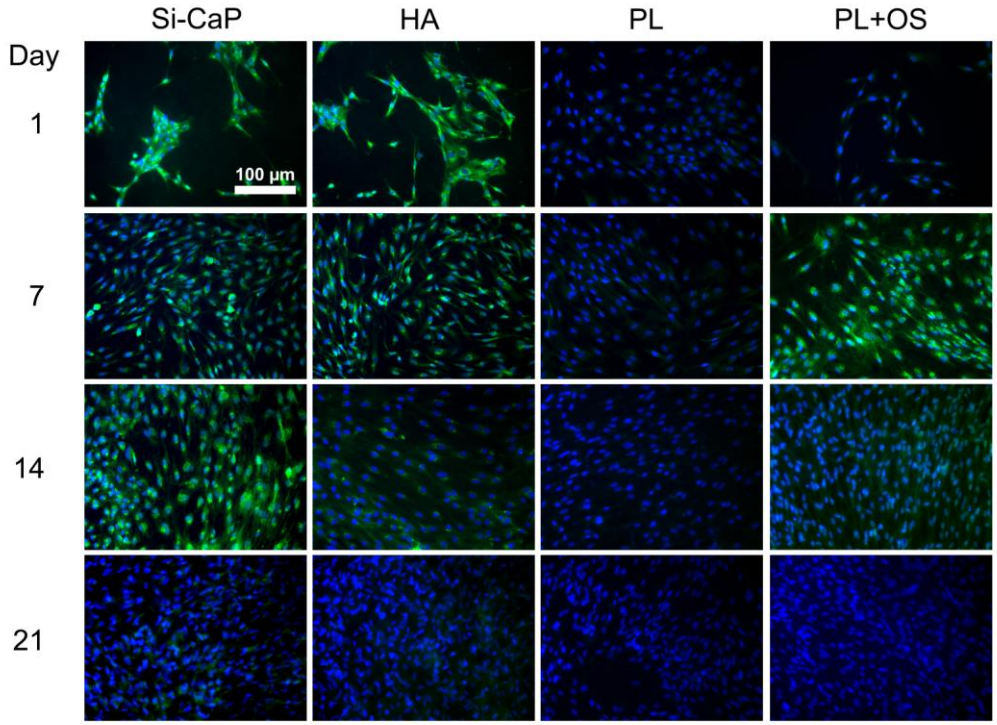

Figure 66: RUNX2 immunostaining of ADMSC on substrates.

RUNX2 (green) and DAPI (blue) Scale bar represents 100µm.

Collagen type I was detected by immunostaining in cells cultured on substrates over 21 days, as shown in Figure 67. Cells cultured on Si-CaP and HA showed undetectable staining on Day 1. But by Day 7 staining was detected in the cytoplasm of the majority of cells. The intensity of staining varied on Si-CaP and was notably brighter in a small proportion of cells. On HA on Day 14 more intense staining was detected and cells appeared to have aligned in one direction. On Si-CaP mature filamentous Collagen type I was detected in several areas, whilst the majority of cells still showed weaker cytoplasmic staining. Cells also appeared to be aligned in one direction and this was observed on several samples. Staining on Day 21, on Si-CaP was mostly extracellular; it was filamentous and appeared to be laid down in a woven fashion. On HA, similar staining was seen and was more intense in certain areas, and dispersed less evenly compared to Si-CaP. Cells on PL+OS also displayed weak cytoplasmic staining on Day 1 however; this was not seen at any time point thereafter. On days 7, 14 and 21 very intense staining was detected; this was exclusively filamentous and far brighter than the staining seen on Si-CaP and HA. No mature collagen staining was observed on PL at any time point.

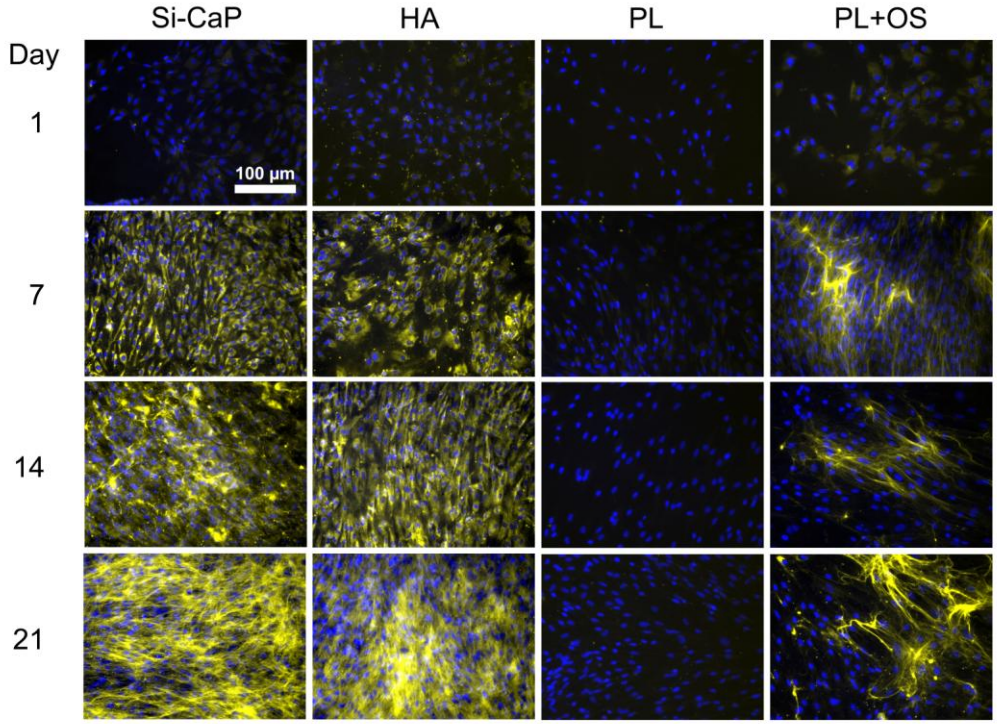

Figure 67: Collagen type I immunostaining of ADMSC on substrates.

Collagen type I (yellow) and DAPI (blue) Scale bar represents 100µm.

Osteocalcin staining was detected on Si-CaP, HA and PL+OS and is shown in Figure 68. On Day 1 very little staining was detected on Si-CaP, HA and PL+OS. Yet, by Day 7 staining was observed in the majority of cells on Si-CaP and was distributed throughout the cytoplasm. On HA, staining was more diffuse and expressed in roughly 50 % of cells. Cells on PL+OS displayed very different staining, which appeared to be localised in the cytoplasm, but was brightest at the cell periphery. Staining on Si-CaP, HA and PL+OS was more intense on days 14 and 21 again was very different on each substrate. On Si-CaP osteocalcin was detected throughout the cytoplasm, but also in large bundles or nodules, where staining was globular and intense. On HA staining was still cytoplasmic but much brighter and in some areas small punctate areas of intense staining was seen. Osteocalcin in cells on PL+OS, at Day 14, was similar to staining on Si-CaP at Day 7, and was detected in most cells. At Day 21 cells on PL+OS stained brightly for osteocalcin and again this was notably more intense around the cell periphery. On Si-CaP and HA staining was similar in distribution, and intensity. Intense, globular staining was seen in areas and was also still visible in the cytoplasm. Cells cultured on PL did not produce detectable levels of osteocalcin at any time point.

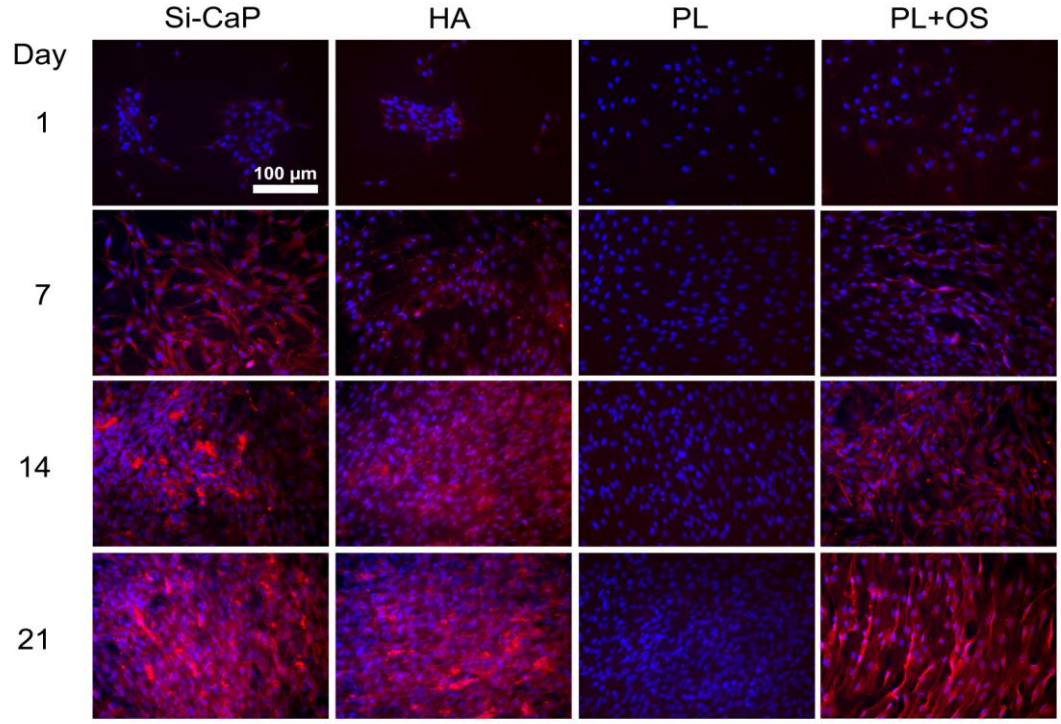

Figure 68: Osteocalcin immunostaining of ADMSC on substrates.

Osteocalcin (red) and DAPI (blue) Scale bar represents 100μm.

5.2.3.1.5 Alkaline phosphatase

The area of ALP staining was quantified as before (Figure 42) and is shown in

Figure 69. Initially, ADMSC on all substrates had similarly low levels of ALP activity. On Day 7, ALP activity increased greatly in cells cultured on Si-CaP, HA and PL+OS (5.1-fold, 4.5-fold and 8.2-fold respectively). ALP activity on PL remained low and was significantly lower than all other substrates ($p<0.00001$). ALP levels continued to increase on Si-CaP, HA and PL+OS on Day 14; where a particularly rapid increase in activity was detected in cells cultured on HA. However, levels did not vary significantly to Si-CaP ($p=0.21$) and PL+OS ($p=0.37$). On Day 21, ALP activity increased on all substrates and reached 47.6% on Si-CaP and 43.9% on HA; levels that did not vary significantly ($p=0.36$). PL+OS increased rapidly (2.6-fold) to 66.3%, significantly greater than HA, but not Si-CaP ($p= 0.02$ and $p>0.0001$ respectively). On PL ALP activity increased slightly on Day 21, but remained low (4.69 %).

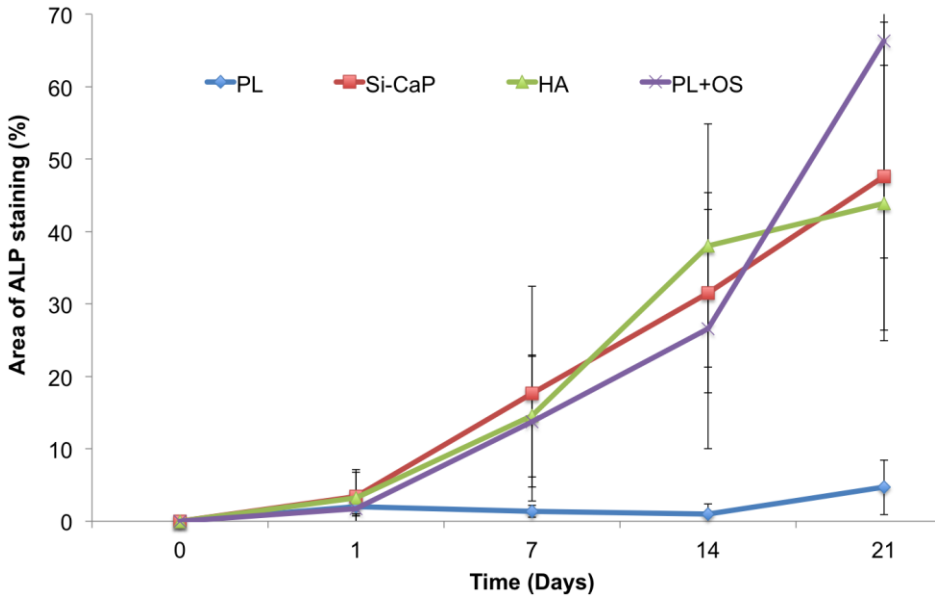

Figure 69: Area of alkaline phosphatase on substrates.

ALP activity of cells on substrates quantified by analysing the area of ALP positive cells using image analysis software and the mean area calculated per disk / well. The results represent the mean ± SD of two donors with samples run in triplicate.

5.2.3.1.6 Mineralisation

Production of a mineralised matrix was detected, quantified and is shown in Figure 43. Initally, no detectable mineralised matrix was seen, and on Day 7 less than 3 % of mineralisation was observed on any substrate. By Day 14 however, a rapid increase in area of mineralisation was detected on Si-CaP, HA and PL+OS (increasing 28–fold, 15-fold and 34-fold respectively). This rate of mineralisation then slowed, by Day 21, and at this time the greatest area of mineralisation was detected on PL+OS (67.21 %). On Si-CaP and HA the area of mineralisation was also highest on Day 21, but peaked at 56.28 % and 54.07 % respectively. At this point the area of mineralisation on Si-CaP and HA was not significantly different to PL+OS ($p>0.99$). Cells on PL did not produce appear to produce a mineralised matrix at any time point.

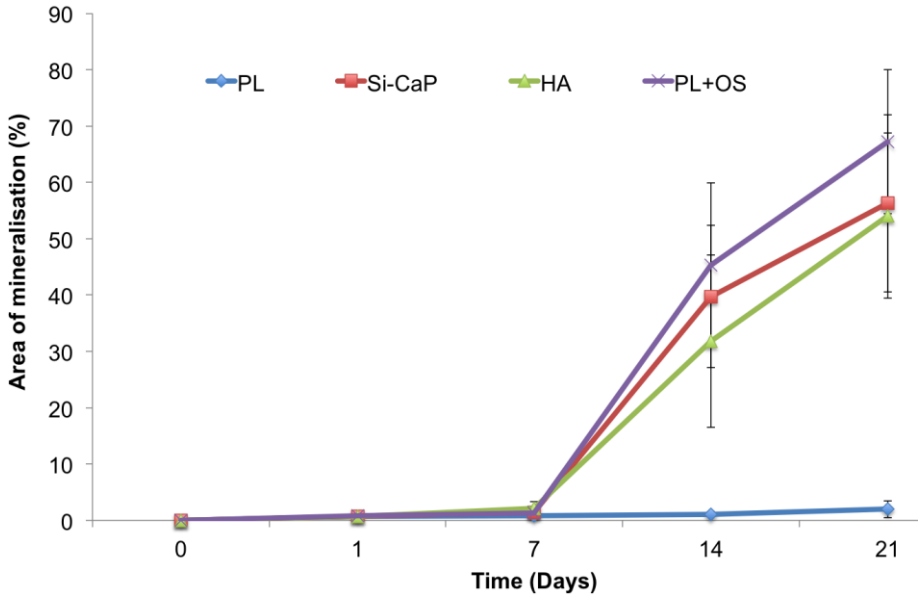

Figure 70: Area of mineralisation on substrates.

Mineralisation on substrates was measured by analysing the area of black deposits using image analysis software and the mean area covered was calculated per disk / well. The results represent the mean ± SD of three donors with samples run in triplicate.

5.3 Discussion

The results presented above show that different substrates can both support and induce mesenchymal stem cell differentiation into osteoblasts and can actively promote bone formation.
Previous studies have used either osteogenic supplementation alone or in combination with specific substrates, however here it was shown that the substrates alone were capable of differentiating mesenchymal stem cells into osteoblasts.

Osteogenic media commonly contains dexamethasone, ascorbic acid and β-glycerophosphate. Although these constituents are not specific to osteogenic differentiation (Pittenger 1999; Johnstone et al. 1998), each component has been shown to support osteogenic differentiation of mesenchymal stem cells *in vitro* (Nuttelman 2005).
Dexamethasone is a synthetic corticosteroid known to influence osteoblast gene expression (Viereck et al. 2002). *In vitro,* dexamethasone functions at several stages of osteogenic differentiation, upregulating the expression of *RUNX2,* and subsequently, osterix, osteocalcin, bone sialoprotein and alkaline phosphatase. Duration of supplementation is controversial, with various recommendations from different studies: some suggest it should be continuously present to prevent differentiation along alternative pathways and to ensure maximal osteoblastic differentiation, whereas others indicate continual supplementation to culture could have toxic effects and cause cell lysis (R. M. Porter et al. 2003b; Nuttelman 2005). This contradictory effect is thought to be due to the anti-proliferative effects of this corticoid (Jaiswal et al. 1998). The results shown here (Figure 46,
Figure 56 and Figure 64) reflect this anti-proliferative effect, and were clearly seen in each cell type when cultured on PL+OS.

Ascorbic acid is required to stabilise the collagen triple helix and to form intermolecular crosslinks within collagen (Murad et al. 1981). Although several studies suggest ascorbic acid can enhance collagen production (Aronow et al. 1990; Franceschi & Iyer 1992) and ALP activity (Franceschi et al. 2009) it does not actively drive osteogenic differentiation. Immunohistochemistry results clearly demonstrated collagen production is independent of ascorbic acid. However, clear differences in the structure of extracellular collagen type I were observed, in ADMSC in particular, suggesting ascorbic acid supplementation is required for optimal post translational modification.

βglycerophosphate is thought to promote osteogenic differentiation by providing a source of organic phosphate ions that act as a bone-like mineral phase *in vitro* (Chung et al. 1992). Both Si-CaP and HA will release ions *in vivo* and in culture, thus providing a source of phosphate, eliminating the need for βglycerophosphate. Calcium is also released from both substrates through dissolution, and regulates important cellular and molecular functions. Ca^{2+} has been demonstrated to positively influence osteoblast differentiation (Khoshniat et al. 2011) yet its exact role is not fully understood.

In combination, dexamethasone, ascorbic acid and βglycerophosphate are able to promote osteogenic differentiation of MSC, although each component cannot actively induce differentiation. It is therefore unclear exactly why these components drive osteogenic differentiation, and it is more likely these factors act synergistically to support the preferential differentiation along the osteogenic lineage.

Si-CaP and HA have been shown to direct osteogenic differentiation at a similar rate, through activation of the same genes as these osteogenic supplements. However, it is not clear whether these substrates are mimicking these supplements or are utilising alternative pathways. Many studies have examined how substrates can influence cell fate, yet the majority of these do so in the presence of soluble factors known to induce osteogenic differentiation (Müller et al. 2007), as a result it is unclear which

pathways are actually involved. A number of signaling pathways may be involved in substrate driven differentiation and these will be discussed in more detail in the next chapter.

Results shown here demonstrate both Si-CaP and HA support and actively direct differentiation of each type of multipotent cells *in vitro*. Previous results from multiple clinical (Jenis & Banco n.d.; Jenis & Banco 2008; Jenis 2010) and *in vivo* studies (A. E. Porter et al. 2003a; Patel et al. 2005; Wheeler et al. 2007) have demonstrated Si-CaP supports greater bone formation and enhanced bioactivity when compared to HA. Studies by different groups have examined silicon substitution with similar results; demonstrating silicon substituted calcium phosphates promote accelerated osteoblast differentiation (Ponader et al. 2008) and more rapid mineralisation than non-substituted controls (Thian et al. 2007).

The enhanced bioactivity of Si-CaP is thought to be due to the inclusion of silicate imparting improved physical properties to HA, which are described below.

- Silicate increases the rate of dissolution of calcium phosphate, providing an apatite layer *in vivo* or *in vitro*, which is known to increase the rate of mineralisation (A. E. Porter et al. 2003a; Patel et al. 2005).
- During dissolution silicate ions are released (Guth et al. 2006) which enhance osteoblast gene expression; protein production and can increase ALP levels (Reffitt et al. 2003).
- The addition of silicon into the calcium phosphate lattice alters grain size, causing chemical changes at the surface, which may lead to a change of the biological response (Botelho et al. 2005; A. E. Porter, Patel, et al. 2004b; A. E. Porter, Botelho, et al. 2004a; A. E. Porter et al. 2006).
- Due to altered surface chemistry Si-CaP is capable of adsorbing a greater quantity of protein when compared to both HA, which has been shown to increase cell attachment (Anselme 2000; Guth & Buckland 2005).

These properties appear to significantly impact cell response *in vitro*, and results shown in this chapter demonstrate that Si-CaP showed greater attachment than HA, for each cell type analysed. This preferential attachment, was has been previously linked to the micro- and macro-porosity of Si-CaP (K A Hing 2005), but more recently thought to be influenced by silicate dissolution from the graft (Guth, Campion, Buckland & Hing 2010a). Preferential silicate dissolution has been shown to enhance protein adsorption, and increase osteoblast attachment (Guth et al. 2006). As both substrates were in the form of dense discs, thus eliminating porosity, it is proposed that the dissolution of ions, and protein adsorption is also encouraging undifferentiated cells to attach to Si-CaP. On average, more cells attached to PL compared to Si-CaP and HA, this was observed for each cell type. However, after 8 hours the average cell numbers on Si-CaP and PL did not vary significantly.

Attachment or adhesion of cells to bone grafts is critical to their long-term integration, as contact with the graft will influence the cell's capacity to proliferate and differentiate. Cells attach to substrates via specific structures, known as focal adhesions, which are composed of receptors such as integrins and adapter proteins. The morphology and focal adhesions of cells attached to Si-CaP and HA are examined in the next chapter.

Once cells have attached to the surface of the substrate, the degree of cell colonisation is dependent on proliferation. The balance between proliferation and differentiation must be precisely regulated in order for a bone graft to successfully integrate with the surrounding tissue. If cells were to differentiate into committed cells upon attachment without any proliferation there may not be enough cells to form sufficient new bone without further recruitment from external sources. This may be relevant in therapeutic applications involving pre-seeded material grafts (Owen 1988). Conversely, if cells continually proliferate and do not differentiate there also will be a failure of new bone formation. In both cases this will lead to poor osseointegration and graft failure.

Similar trends in proliferation were seen for all cell types, on PL all cell types showed a simple exponential growth rate, increasing over time, whereas on Si-CaP and HA the rate of proliferation of all cell types decreased similarly, compared to cells on PL+OS, appearing to give a more linear growth rate compared to the exponential growth seen on PL. One interpretation of such a linear growth rate is that it reflects asymmetric division of stem cells, in which one committed cell and one daughter stem cell are produced at each division. Within the stem cell niche, cells undergo asymmetric cell divisions to balance proliferation and differentiation (D'Angelo et al. 2011). This form of differentiation on Si-CaP and HA is advantageous as it allows differentiation of committed cells in addition to providing a source of progenitors for further differentiation when required. One study has observed a similar decrease in proliferation rates of cells as they differentiate, and have proposed a similar mechanism (de Peppo et al. 2012). Cells cultured in differentiation media (PL+OS) doubled at an even slower rate, likely due to the anti-proliferative effects of dexamethasone, which is also consistent with a model in which differentiation of MSC starts as proliferation ceases.

The differentiation of stem cells along the osteogenic lineage proceeds through a series of defined stages and is marked by the changing expression of key genes and proteins as the cell moves down the differentiation pathway from a multipotent MSC to a terminally differentiated osteocyte, this process is shown in Chapter one, Figure 4.

In order to determine further differences between Si-CaP and HA, osteoblast related genes and key transcription factors were analysed.
Cells on Si-CaP showed a more rapid decrease in expression of *CD105* compared to HA, suggesting multipotency is lost as cells commit to the osteoblast lineage.
The most specific osteoblast associated transcription factor, controlling osteoblast commitment, differentiation and matrix mineralisation is RUNX2. In each cell type *RUNX2* gene expression was greater on Si-CaP compared to HA; ADMSC cultured on Si-CaP showed the greatest increase in *RUNX2* expression, which was significantly greater than on HA. These results were also reflected in protein levels detected by immunochemistry,

although RUNX2 protein was detected later than gene expression but was maintained until Day 21. This prolonged expression of RUNX2, has been shown to enhance osteogenic differentiation (Zhang et al. 2006). In MSC in particular, RUNX2 expression appeared to be both cytoplasmic and nuclear on Si-CaP and HA. Some transcription factors including RUNX2 can translocate from the nucleus to the cytoplasm. The cytoplasmic staining may indicate RUNX2 has already played its role in differentiation and gene expression, and has shuttled into the cytoplasm in its inactive form. However, some studies suggest this sub-nuclear localisation may be required for maximal transcriptional activity (Sunhwa Kim et al. 2003b; Pockwinse et al. 2005).

Expression of Parathyroid hormone 1 receptor (*PTH1R*) was detected in MSC and was also upregulated earlier on Si-CaP on day 7 compared to HA, indicating that cells on Si-CaP were differentiating at an increased rate.

In hES-MP and ADMSC expression of osterix (*OSX*) was analysed. *OSX* is a transcription factor which acts downstream of *RUNX2* it is essential for osteoblast differentiation. In both cell types, *OSX* levels were greater on Si-CaP compared to HA, thus supporting the trend of cells in Si-CaP differentiating at greater rate.

During osteoblast differentiation *RUNX2* and *OSX* upregulate osteoblast related genes including *COL1A1* and *BGLAP*. Collagen type I is the most abundant protein in bone, and production of this type of collagen peaks as cells become mature extracellular matrix-producing osteoblasts (Anselme 2000). In MSC, hES-MP and ADMSC, *COL1A1* gene expression on Si-CaP was upregulated earlier and to a greater extent to HA, and on both substrates increased gradually over time. In each cell type, collagen type I protein production reflected *COL1A1* gene expression; with the exception of MSC on Si-CaP: gene expression decreased on days 14 and 21, yet protein detected by immunocytochemistry, increased. This may be due to the level of translation and posttranslational processing required to produce stable collagen.

ADMSC showed the most extensive production of collagen type I, and on Si-CaP, and covered a greater area compared to HA. The structure of the

collagen appeared to be very different to that seen on PL+OS, which appeared brighter and denser. This may be due to the presence of ascorbic acid in the osteogenic media, which is thought to be required to crosslink and stabilise the triple helix (Aronow et al. 1990; Franceschi et al. 2009).
Osteocalcin or bone gamma-carboxyglutamic acid-containing protein (*BGLAP*) is a late stage osteoblast specific protein, produced only by mature osteoblasts prior to the onset of mineralisation (Marinucci et al. 2010). In MSC and ADMSC, *BGLAP* gene expression was higher on Si-CaP compared to HA. In hES-MP, *BGLAP* levels were slightly but not significantly higher on HA when compared to Si-CaP. The protein encoded by the *BGLAP* gene (osteocalcin), was detected in cells on both Si-CaP and HA, strong, cytoplasmic staining was seen, which closely reflected gene expression.

DMP1 gene expression was analysed to determine whether cells were capable of terminal differentiation along the osteoblast lineage into osteocytes. Osteocytes play a major role in bone remodeling, and are therefore essential for the long-term success of a bone graft. In each cell type *DMP1* expression was detected on both Si-CaP and HA. However, levels of *DMP1* were higher on Si-CaP in both MSC, and AMDSC, suggesting a greater number of osteocytes.

Results from gene expression and protein production demonstrate that cells were differentiating into osteoblasts on Si-CaP and HA. However, Si-CaP upregulated the osteoblast related genes *RUNX2, COL1A1* and *PTH1R* earlier than HA and PL+OS, suggesting that cells cultured on Si-CaP were differentiating along the osteoblast lineage at a greater rate compared to HA.

Alkaline phosphatase (ALP) is a commonly used early marker of osteoblast differentiation. ALP was strongly expressed in each cell type after culture on both Si-CaP and HA, suggesting both these substrates are capable of inducing differentiation into osteoblasts. All cell types had higher ALP activity on Si-CaP compared with HA; this was most obvious in the case of MSC, where ALP activity was greater than 10% higher on Si-CaP than on HA.

Alkaline phosphatase plays a crucial role in mineralisation as it functions to provide a source of inorganic phosphate required to form hydroxyapatite crystals (Bellows et al. 1991). For each cell type, the area of mineralisation was greater on Si-CaP to that on HA. In MSC and ADMSC levels of mineralisation were similar, whereas in hES-MP, the area of mineralisation was up to 10% greater on both Si-CaP and HA. These results demonstrate that both calcium-based materials initiated the formation of a mineralised matrix. Yet overall, Si-CaP was clearly shown to be more osteoinductive, initiating differentiation at an increased rate and to a greater extent than HA.

In the absence of soluble factors, multipotent stem cells cultured on tissue culture plastic, hydroxyapatite and silicate substituted calcium phosphate showed very different responses.

Tissue culture plastic (PL) is composed of polystyrene, a benzene containing polymer that is commonly modified to increase cell attachment (Steele et al. 1993). This can be achieved through the addition of oxygen containing groups to the polymer, creating a hydrophilic, negatively charged surface when medium is added (Ramsey et al. 1984; Amstein & Hartman 1975; M 1974). Treated PL supports cell attachment and proliferation, and is not designed to promote differentiation, as the results shown above demonstrate.

However, some cells can differentiate on PL without soluble factors, such as human embryonic stem cells (hES). In hES cultures, PL is commonly coated with Matrigel, proteins or substrates that mimic the extracellular matrix *in vivo*, to prevent differentiation. More recently, alternative coatings or treatments to apply to PL to maintain stem cell function have been the subject of investigation (Ramos-Ibeas et al. 2012; Rajaraman et al. 2012). These are designed to mimic stem cell niches, where cells are maintained in a multipotent or pluripotent state until differentiation is required. Conversely, biomaterials to support cell growth and differentiation for organ repair aim to mimic the desired tissue.

Many studies have exploited aspects of the desired *in vivo* environment to produce materials to direct cell fate without the need for soluble factors. The use of engineered substrates for culturing and differentiating cells has

significant advantages over the use of supplemented media, as it allows cell growth and development to be tailored to a specific application without the need to use expensive, or introduce potentially harmful chemicals into the body. However, the *in vivo* environment is extremely complex, and cells may encounter a variety of surfaces with different compositions, topographies, and nano-scale features, each of which has the potential to influence cell behavior and function. To understand how each of these factors can influence cell fate, a number of studies have designed materials to examine specific parameters such as; altered topography, defined surface chemistry, nano-scale features and the influence of protein composition.

Topography has been known to influence cells for over a century (Carrel & Burrows 1911) and can alter cell morphology, adhesion, motility, proliferation gene expression and protein production (McNamara et al. 2010). Due to advances in technology enabling precise manufacture and analysis of nano- patterned surfaces, the extent to which topography can alter cell fate has been understood only recently (J. Y. Lim et al. 2011).

The size and shape of topographical patterns appear to be critical for controlling cell fate. Substrates composed of poly (methyl methacrylate) with semi-disordered pits, 120 nm diameter and 100 nm deep, induce osteogenic differentiation of MSC (Dalby et al. 2007). Nanotubes between 70-100 nm in diameter enhanced cytoskeletal stress and induced osteogenic differentiation, when compared to tubes of 30 nm, which promoted proliferation (S. Oh et al. 2009). These studies suggest the topography regulates cell differentiation via controlled adhesion and enhanced cytoskeletal tension.

This theory was also examined in two separate studies, which utilised adhesive islands; cell fate was shown to be dependent upon the shape of island to which each cell could adhere. Star and rectangle shapes, encouraged cell spreading, and an increase in actin filament organisation promoted osteogenesis. Whereas shapes that promoted low contractility, such as flower-like or rounded shapes promoted adipogenic differentiation (McBeath et al. 2004; Kilian et al. 2010). Adipocytes are spherical in shape, as this provides the most efficient surface area to volume ratio for lipid storage, the smaller, rounded islands minimise cell spreading and

focal adhesion formation, and as a result the preferential spherical phenotype is maintained (S. Murphy et al. 2010).

The disordered nano-patterned substrates used by Dalby et al in the study mentioned above concluded that the extent of osteogenic differentiation was determined by the disorder of the pattern produced (Dalby et al. 2007). Regularly spaced pits or symmetrical patterns did not induce differentiation to the same extent as slightly disordered patterns (Dalby et al. 2007). This is reflected in the rate and extent of differentiation shown in this chapter, with Si-CaP promoting greater differentiation compared to HA, which could be due to the substitution of silicate into Si-CaP creating a disordered surface containing areas of negative and positive charge, whereas HA has a regular repeating pattern of calcium and phosphate ions. These topographical studies reflect the role of components of the native ECM, which is fibrillar and contains specific distributions of adhesive proteins. Although the surfaces of Si-CaP and HA discs do not contain significant areas of raised or patterned topography, a similar activation of osteogenic differentiation was observed. However, the surfaces of these substrates contain areas of both positive and negative charge, known to influence the distribution and conformation of proteins bound to the surface, and these may have a similar patterning effect as changes in surface topography.

Surface chemistry can readily be controlled and modified and has been shown to influence cell attachment (Tourniaire et al. 2006), differentiation (Hay et al. 2011) and to guide cell fate *in vitro* (Curran et al. 2006). Some studies have investigated alternate ionic substitutions in hydroxyapatites, such as strontium, zinc and magnesium with the aim to improve dissolution rates and bioactivity (S R Kim et al. 2003a; Ramaswamy et al. 2008; Fredholm et al. 2012). The silicon substitution in Si-CaP affects its surface charge, surface structure, and solubility, which can, in turn, result in changes in the biological performance *in vitro* and *in vivo*. The surface chemistry of HA and Si-CaP undergoes significant changes *in vivo*, as ions are released through dissolution, creating a biomimetic apatite like layer, which is known to encourage protein adsorption and osteogenic differentiation.

The surface energy of substrates can also directly influence protein adsorption and determine their structural arrangement, with differential protein adsorption detected on surfaces with positively and negatively charged surfaces (Anselme 2000).

The ECM is composed of a variety of proteins, an important part of the cellular microenvironment and plays a significant role in regulating cell adhesion, proliferation and differentiation (Mathews et al. 2012). As such significant effort has focused of ECM based scaffolds for bone repair. Studies have examined the effect of a variety of proteins on osteogenic differentiation and have utilised peptides to create substrates with greater bioactivity, with promising results (García & Reyes 2005; Badylak et al. 2009). Collagen type I and vitronectin have profound influences on mesenchymal stem cells, reducing proliferation rates and encouraging osteogenic differentiation (Mathews et al. 2012). Both of these proteins have been shown to bind *in vivo* and *in vitro* to HA and Si-CaP with high affinity (Botelho et al. 2011).

Substrates designed to induce osteogenic differentiation, through topological variation, the use of adhesive islands, altered surface chemistry and adsorption of proteins or peptides provide valuable tools to study osteogenic differentiation *in vitro*. However, they may not be suitable for clinical use *in vivo*. For example, it is relatively easy to manufacture in 2D nano-patterned surfaces on a small scale, such as is required for *in vitro* experiments, however producing large, complex 3D structures for major skeletal defects may not be cost effective or easy to manufacture (McMurray et al. 2011). However, recent advances in 3D printing may change this.

Calcium phosphate based substrates naturally incorporate a number of the desired aspects of the *in vivo* environment, and due to their similarity with the mineral phase of bone mimic the environment, which they aim to induce repair. As a result, these substrates have become clinically relevant. Whether combined with autologous cells or implanted alone, both HA and Si-CaP have the potential to direct osteogenic differentiation or multipotent cells without the need for soluble factors.

Results shown above demonstrate cells from bone marrow, adipose tissue and of embryonic origin are capable of osteogenic differentiation. Despite the efficient differentiation of hES-MP cells, there are still safety and ethical issues regarding the clinical use of these cells, which must be addressed before their clinical use. Bone marrow derived MSC are currently used as a source of multipotent cells for bone repair, however extraction is an invasive procedure, and both volume of tissue and number of multipotent cells obtained are often limited.

Adipose derived stem cells (ADMSC) showed comparable rates of attachment, differentiation and mineralisation to MSC, but demonstrated greater proliferation potential and more extensive, mature protein production on both HA and Si-CaP. Furthermore, autologous supply is not nearly as limited, multipotent cells much more frequent, surgery is still invasive (but may be preferred) and cells may be purified and stored for later use if needed. As a result it is suggested that ADMSC may represent a promising alternative source for cells for clinical bone repair.

This study is the first to compare the osteogenic differentiation of these three cell types, on Si-CaP and HA, in the absence of soluble osteogenic factors. The results clearly demonstrate these substrates are osteoinductive, and are capable of directing cell fate in a manner comparable to, or greater than osteogenic supplementation.

The implication of these findings for tissue engineering is clear, suggesting these substrates may be utilised to control stem cell fate *in vivo* and *in vitro* without the need for osteogenic supplementation.

CHAPTER SIX: CELL SUBSTRATE INTERACTIONS

6.1 Introduction

The development of successful biomaterials for bone tissue engineering is shifting towards substrates that mimic the natural extracellular matrix (ECM). Substrates that actively drive cellular differentiation and accurately mimic natural repair of tissues or organs remove the need for the supplementation of expensive, potentially harmful soluble factors.

In vivo cells interact closely with the extracellular matrix ECM, a heterogeneous milieu, a structurally organised network of biological macromolecules, which is subject to many physical forces (Nombela-Arrieta et al. 2011; Badylak et al. 2009; Kolf, Cho & Tuan 2007b; Chamberlain et al. 2007; Crisan et al. 2008; Barry & J. M. Murphy 2004; Boyd et al. 2009; Haasters et al. 2009; Yoshimura et al. 2006; Pittenger 1999; Jack et al. 2002). Due to the complexity of the ECM it is inherently difficult to determine its impact on cell behavior. As a result studies have examined individual aspects of the ECM in an attempt to understand its role in cell fate and differentiation (Chamberlain et al. 2007; Fisher et al. 2010; Haasters et al. 2009; Yoshimura et al. 2006; Pittenger 1999). Cell response to substrate compliance, composition, topography and physical forces have all been analysed with fascinating results. For example, matrix elasticity has been shown to differentiate mesenchymal stem cells into tissues that most closely resemble the mechanical properties of the polyacrylamide substrates to which they were attached (Engler et al. 2006). Matrix composition has also been shown to stimulate differentiation; when MSC adhered to vitronectin and collagen type I coated plates, they were induced to differentiate along the osteoblast lineage without the need for osteogenic supplementation (Salasznyk et al. 2004). Topography in the form of nano-patterned substrates, adhesive islands, micro-textured and surface roughness and physical forces including shear stress, mechanical loading and compression have all been shown to positively influence osteogenic differentiation (McNamara et al. 2010; Rosa et al. 2003; Kapur et al. 2003; Sun et al. 2012; Barrère et al. 2008).

These studies have provided significant insight into how cells 'sense' their environment and transduce this information into complex cellular responses. A common factor in such studies is the requirement of cellular adhesion. Cells initially 'attach' to surfaces and over the longer term 'adhere'. The adhesion phase is characterised by binding of integrins - the key receptor involved in linking cells to the ECM. Since their discovery over 25 years ago (Hynes 1987) they have become one of the best understood cell adhesion receptors.

Integrins are composed of two glycoprotein subunits, namely the αchain and βchain, which are non-covalently bound. The mammalian set of integrins is composed of 18 α and 8 β subunits, which assemble to form 24 distinct integrins. Individually integrin binding to the ECM is relatively weak however, ligand binding activates clustering of multiple integrins, which form a larger signaling complex. Within this complex, a variety of adapter proteins connect integrins to the cytoskeleton. These large clusters of integrins and signaling molecules form focal adhesion complexes, which are essential to cell adhesion (Eleniste & Bruzzaniti 2012). Shown below in Figure 71.

Focal adhesions can directly couple to the actin cytoskeleton, and allow information about the external environment to be transduced into the cell, activating intracellular signaling pathways involved in proliferation, migration, and differentiation (Giancotti 1999).

In bone, cells are in intimate contact with bone mineral and the variety of proteins secreted by osteoblasts. Studies mimicking this natural ECM produced by osteoblasts have shown demonstrated enhanced osteoblast differentiation and even activation of osteogenic lineage in MSC (Mathews et al. 2012; Florence Barrère 2006). The mineral phase of bone, composed of calcium phosphate in the form of hydroxyapatite, has also been shown to significantly impact cell behavior (Müller et al. 2007). However, cells are rarely in direct contact with hydroxyapatite instead interact with an adsorbed protein layer (both *in vivo* and *in vitro*) (Guth & Buckland 2005). The structure of calcium phosphates can be altered via ionic substitutions and these impact upon the type, amount and conformation of protein adsorbed, whilst this has been well documented (Botelho 2005), the interaction of MSC with this layer is not yet fully understood.

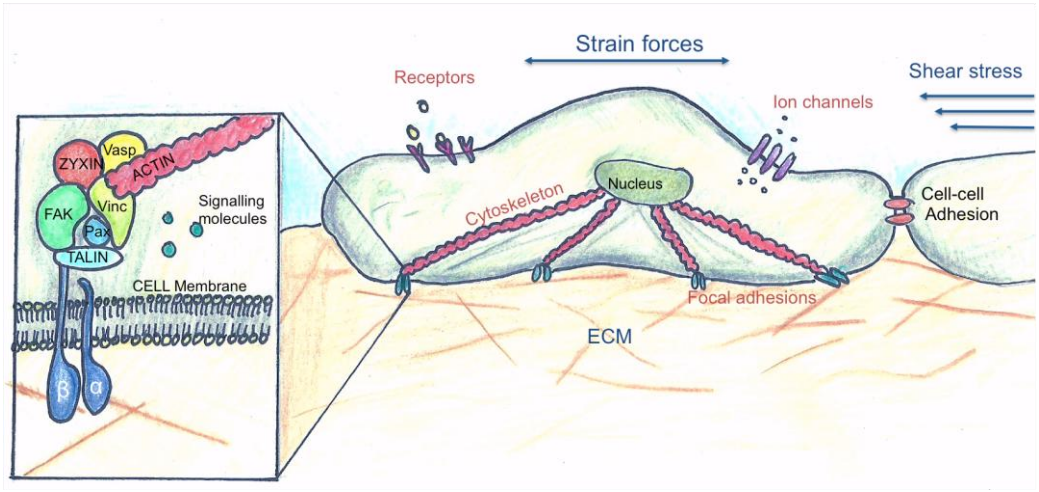

Figure 71: Biophysical forces and interactions of a stem cell and the extracelluar matrix.

Physical forces are written in blue and mechanical stimuli in red. Inset shows magnification of a focal adhesion, incuding a transmembrane heterodimeric integrin, paxillin (Pax), TALIN, focal adhesion kinase (FAK), vinculin (Vinc), ZYXIN, and vasodilator-stimulated phosphoprotein (VASP). Abbreviation: ECM, extracellular matrix. Adapted from (Sun et al. 2012).

This chapter aims to determine how multipotent stem cells interact with hydroxyapatite and silicate substituted calcium phosphate (and the adsorbed protein layer) through morphological analysis of the actin cytoskeleton and focal adhesion formation during adhesion and the expression of integrins during osteogenic differentiation.

6.2 Results

6.2.1 Commitment signals

To determine whether Si-CaP and HA were delivering discrete signals to direct differentiation along the osteogenic lineage or whether continuous contact with these substrates was required, the lineage capacity of cells (MSC) was analysed after culture for 24 hours on each substrate.
Cells were seeded onto Si-CaP, HA and on PL+OS and after 24 hours; non-adherent cells were removed and adherent cells re-plated onto PL with adipogenic, chondrogenic or osteogenic differentiation media. After 7, 14 and 21 days mRNA was collected and analysed for expression of lineage related genes. The results are shown below in Figure 72.
Cells that were cultured on Si-CaP and HA did not show expression of adipogenic transcription factor *PPARG* or the chondrogenic markers *SOX9* and *COL2A1*. Whereas cells cultured on PL+OS for 24 hours were not committed to the osteoblast lineage: cells expressed *PPARG* on days 7 and 21 after culture in adipogenic media, and *SOX9* and *COL2A1* in chondrogenic differentiation media. Cells cultured on all substrates showed expression of osteogenic markers *RUNX2* and *BGLAP*.

These results demonstrate that cells are committed to the osteoblast lineage within 24 hours, when cultured on Si-CaP and HA. This proves there must be a positive signalling event driving differentiation within this short period of time. PL+OS is known to favour osteogenic differentiation rather than actively induce it and that commitment to the osteoblast lineage under these conditions does not occur within 24 hours.

These results prompted the investigation into changes in morphology and possible signalling events that could occur within this short time period.

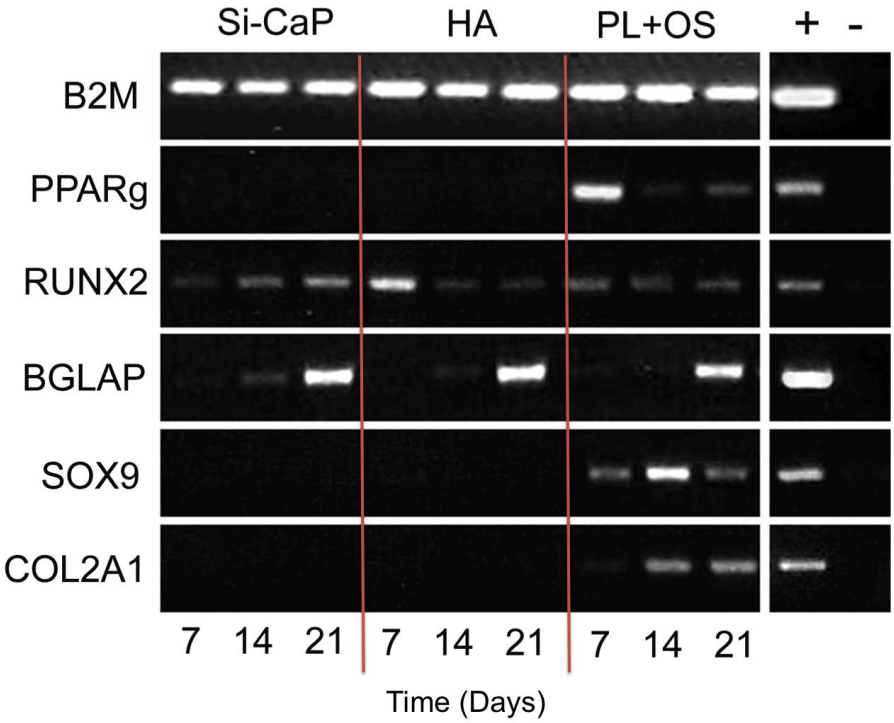

Figure 72: Commitment signals.

Cells were cultured on Si-CaP, HA or PL+OS for 24 hours then replated onto PL with adipogenic, osteogenic or chondrogenic media and cultured for up to 21 days. Abbreviations: B2M; beta-2-microglobulin, PPARG; Peroxisome proliferator-activated receptor gamma, RUNX2; Runt-related transcription factor 2, BGLAP; bone gamma-carboxyglutamic acid-containing protein, SOX9; SRY (sex determining region Y)-box 9, and COL2A1; collagen type 2 alpha 1, +; positive control (cDNA from primary bone cartilage and fat) and -; negative control (water instead of cDNA).

6.2.2 MSC morphology

To examine the cell morphology on each substrate, attached cells were immunostained for vinculin, a key protein in focal adhesions, and with a phalloidin conjugate to detect filamentous actin. Representative images of MSC vinculin and actin staining at 24 hours and 48 hours are shown inFigure 73 and Figure 74 respectively, where the vinuclin staining is shown in green and phalloidin in red. Cell nuclei were stained with the DNA intercalating dye DAPI, which appears blue.

At 24 hours MSC attached to Si-CaP had diverse morphology, cells varied in both size and shape see Figure 73. Several cells had defined focal adhesions and displayed strong actin staining. Cells were evenly dispersed at 24 hours; however, by 48 hours cells were clustered together. At this time, cells were more homogenous in size, yet cell shape was still varied, ranging from stellar-like to elongated cells. Vinculin staining was brighter throughout the cell, and the majority of cells had multiple, well defined focal adhesions. Actin staining was less intense than at 24 hours and was located around the edge of the cells.

MSC attached to HA at 24 hours were notably smaller than cells on Si-CaP, nonetheless there was still wide variation in cell shape. Focal adhesions were observed in most cells, and strong actin was detected in roughly 50% of the cells. Similar to Si-CaP, cells were evenly dispersed at 24 hours. At 48 hours post seeding a greater number of cells were detected and were packed close together. Vinculin staining was seen in multiple focal adhesions and filamentous actin fibers were observed throughout many cells. Overall, cells were homogenous in size and were morphologically similar to cells on Si-CaP.

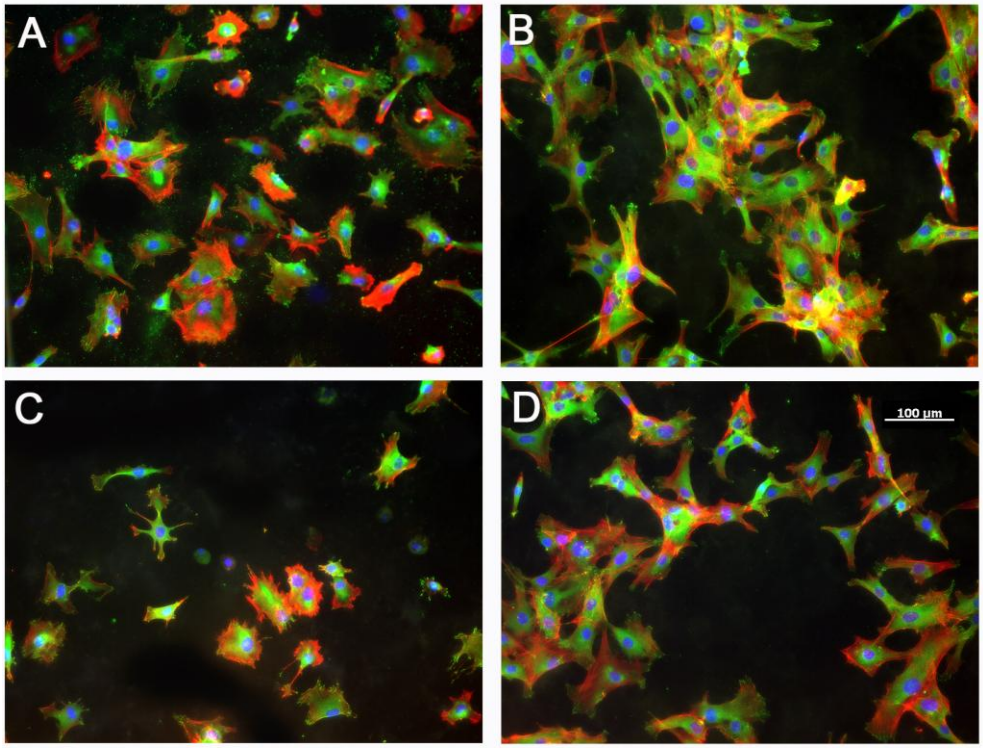

Figure 73: Actin and vinculin immunostaining of MSC on Si-CaP and HA, 24 and 48 hours after seeding.

(A) MSC on Si-CaP at 24 hours and (B) 48 hours, (C) MSC on HA at 24 hours and (D) 48 hours. Immunstined with Actin (Red) and Vinculin (Green) DAPI (blue), scale bar represents 100 µm.

Cells attached to PL+OS at 24 hours were larger than the cells seen on Si-CaP and HA at the same time see Figure 74. Prominent focal adhesions were detected and strong actin staining was seen around the cell edge. After 48 hours cells were more flattened and the actin fibers more organised.

At 24 hours post seeding on PL, most cells were small, fibroblast-like and had numerous, small, focal adhesions. Actin fibers were localised around the cell edge near the focal adhesions. Several cells were rounded up, without mature focal adhesions. By 48 hours, cells were more flattened, and cuboidal in shape, had distinct focal adhesions, and strong actin staining was detected around the edge of cell. At 48 hours cells were notably smaller than on PL+OS, HA and si-CaP at the same time point.

Morphology and staining varied between cells on each substrate. Cells were more flattened and hade distinct focal adhesions on PL and PL+OS at 24 hours, compared to cells on HA and Si-CaP. However, at 48 hours cells on Si-

CaP and HA were homogenous in shape and size, and on both substrates had strong vinculin staining, in the form of focal adhesions.

On PL and PL+OS at both time points cells were more heterogeneous in size and shape and did not change as significantly over time, compared to HA and Si-CaP.

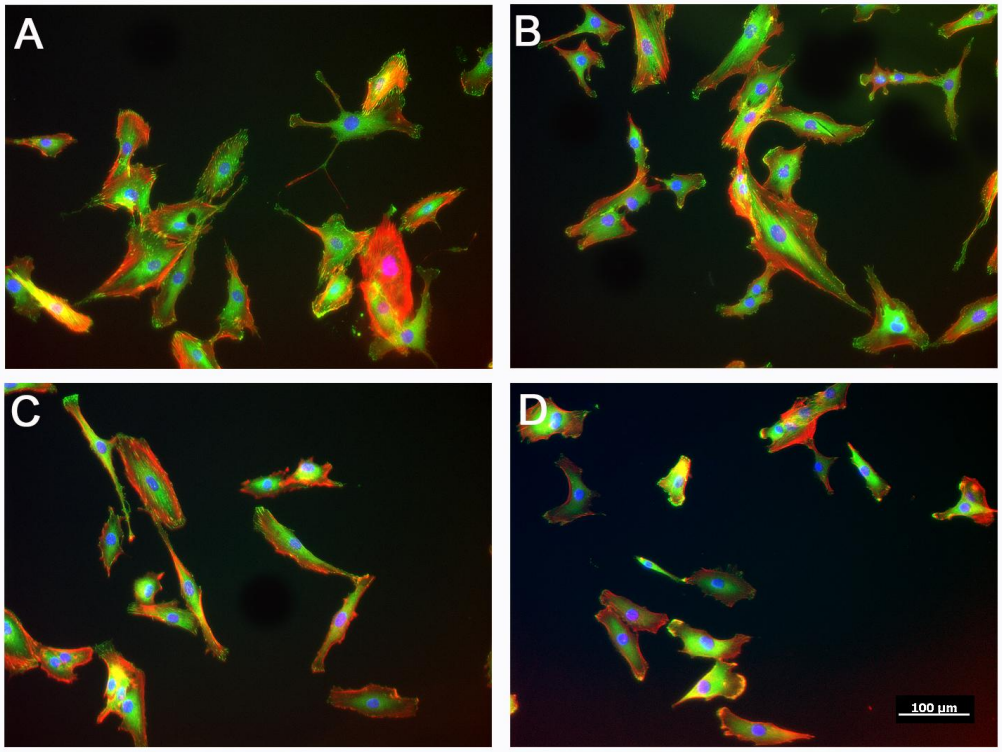

Figure 74: Actin and vinculin immunostaining of MSC on PL and PL+OS, 24 and 48 hours after seeding.

(A) MSC on PL+OS at 24 hours and (B) 48 hours, (C) MSC on PL at 24 hours and (D) 48 hours. Immunstined with Actin (Red) and Vinculin (Green) DAPI (blue), scale bar represents 100 µm.

6.2.3 hES-MP morphology

hES-MP attached to Si-CaP at 24 hours were heterogeneous in size and shape, some were elongated, fibroblast-like and others were very small, as shown in Figure 75.
Only a few cells appeared to have focal adhesions however, actin staining was seen in the majority of the cells. At 48 hours, less actin was detected, and staining was observed in few cells. Many cells had focal adhesion and appeared to be more flattened than at the previous time point. Cell size still varied and some very small cells were observed. Cells appeared to be tightly packed forming clusters of cells.

The majority of cells on HA, at 24 hours, were small, with multiple focal adhesion sites. Strong vinculin staining was detected throughout the cells and actin staining was seen, but did not appear organised into fibrils. The cells morphology did not change significantly at 48 hours post seeding. The majority of hES-MP were small and had little actin staining, however there were several larger cells, which displayed organised actin fibrils and multiple focal adhesions.

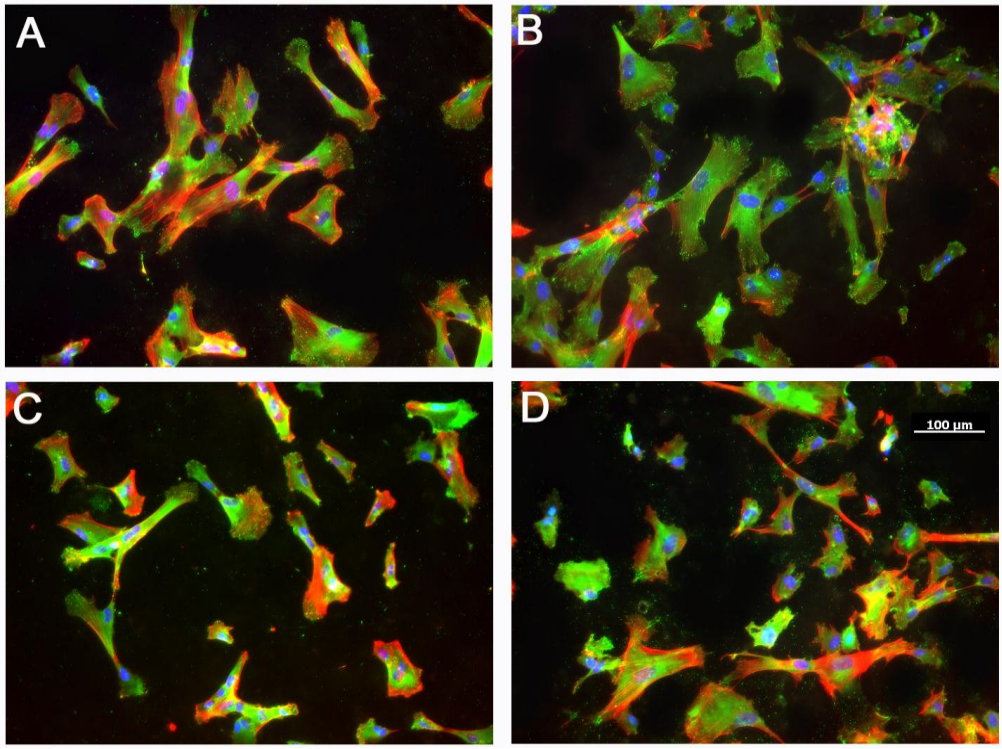

Figure 75: Actin and vinculin immunostaining of hES-MP on Si-CaP and HA, 24 and 48 hours after seeding.

(A) hES-MP on Si-CaP at 24 hours and (B) 48 hours, (C) hES-MP on HA at 24 hours and (D) 48 hours. Immunstined with Actin (Red) and Vinculin (Green) DAPI (blue), scale bar represents 100 µm.

The size and shape of cells on PL+OS was heterogeneous, see Figure 76; some cells were large and irregular, whereas others were much smaller and more uniform in shape. Strong vinculin staining was detected at the edge of many cells, and also across the cell body. Actin fibers were well defined and intensely stained. At 48 hours, cells were larger and contained more focal adhesions, throughout the cells, cells were wide and flattened but still varied in size and shape.

At 24 hours on PL, many cells were clustered close together and mostly elongated, and fibroblastic in morphology. Vinculin staining was detected throughout the cells, but few small focal adhesions were seen. Actin was intensely stained and arranged around the edges of the cells. At 48 hours, post seeding, significantly more, larger focal adhesions were seen and cells were slightly wider and more flattened out. Strong actin was seen near the focal adhesions and was largely filamentous.

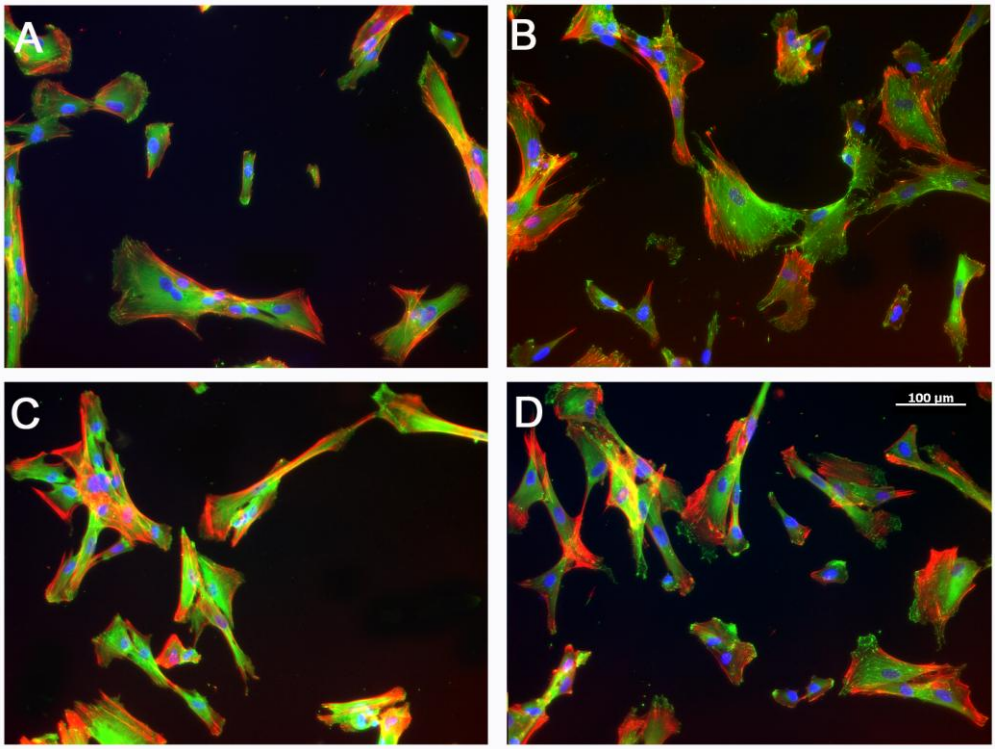

Figure 76: Actin and vinculin immunostaining of hES-MP on PL and PL+OS, 24 and 48 hours after seeding.

(A) hES-MP on PL+OS at 24 hours and (B) 48 hours, (C) hES-MP on PL at 24 hours and (D) 48 hours. Immunstined with Actin (Red) and Vinculin (Green) DAPI (blue), scale bar represents 100 µm.

6.2.4 ADMSC morphology

Cells on Si-Cap at 24 hours stained intensely with actin - filamentous strands were clearly visible, see Figure 77. The majority of cells were elongated, fibroblast-like and were homogenous in size, and had multiple small focal adhesions, as detected by vinculin staining. By 48 hours post seeding cells were wider and more flattened with larger, punctate focal adhesions. Cells showed differential staining of actin, either staining widely of having very little. Cells on HA at 24 hours were similar to cells on Si-CaP, at 24 hours, displaying intense, widespread actin staining. Cells also had few, small focal adhesions, and had less vinculin staining throughout the cell. By 48 hours cells were wider, had less actin staining, and had more, larger focal adhesions. Vinculin staining was also evident throughout the cells.

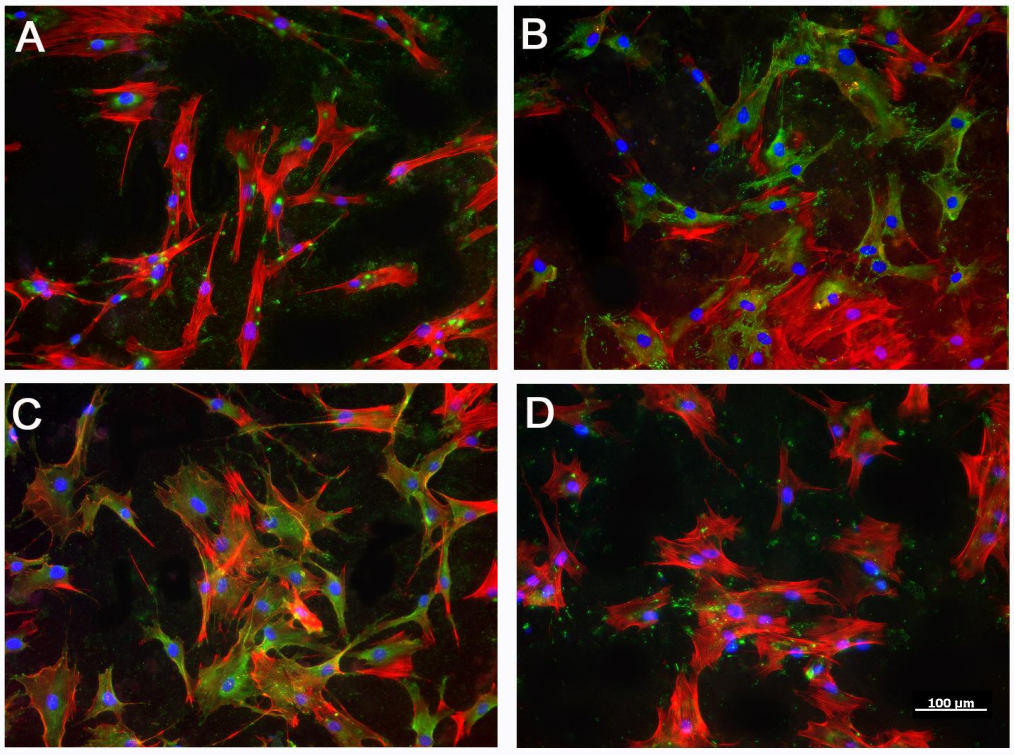

Figure 77: Actin and vinculin immunostaining of ADMSC on Si-CaP and HA, 24 and 48 hours after seeding.

(A) ADMSC on Si-CaP at 24 hours and (B) 48 hours, (C) ADMSC on HA at 24 hours and (D) 48 hours. Immunstined with Actin (Red) and Vinculin (Green) DAPI (blue), scale bar represents 100 µm

At 24 hours on PL+OS cells were wide (Figure 78), flattened and had intense actin staining, as seen on Si-CaP and HA. However, vinuclin staining was

more evident and larger focal adhesions were observed, in some case throughout the cell. At 48 hours post seeding, cells had significantly more, larger, focal adhesions. Although not present in some cells, strong actin staining was detected in other cells, closely related to the focl adhesions. Cells were spread out in a monolayer, and did not appear to overlap as seen in HA and Si-CaP.

Cells cultured on PL for 24 hours, had a wide, flattened morphology. Cells were relatively homogenous, and displayed intense actin staining, with little to no vnculin staining detected. Very few focal adhesions were seen and were very faint. At 48 hours post seeding, cells still had strong actin staining, but had larger, brighter focal adhesions, and appeared to grow in small clusters, unlike cells on PL+OS.

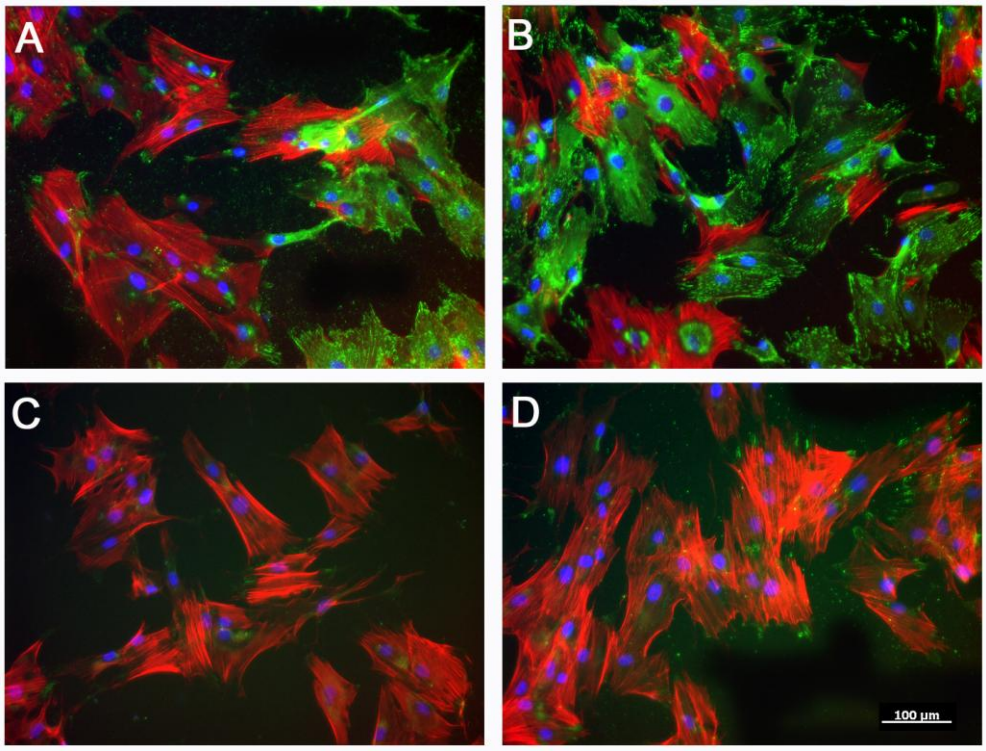

Figure 78: Actin and vinculin immunostaining of ADMSC on Si-CaP and HA, 24 and 48 hours after seeding.

(A) ADMSC on Si-CaP at 24 hours and (B) 48 hours, (C) ADMSC on HA at 24 hours and (D) 48 hours. Immunstined with Actin (Red) and Vinculin (Green) DAPI (blue), scale bar represents 100 µm

6.2.5 MSC integrin expression

Integrin expression in MSC was analysed over 21 days on each substrate and the relative expression of each subunit is shown in Figure 79 and Figure 80.
On Day 1, alpha 1 integrin (*ITGA1)* levels increased on Si-CaP and HA 1.3- and 1.5-fold, and expression remained at similar levels on Day 7 (5.3 ± 0.05, and 4.0 ± 0.06 respectively). On Day 14, levels of *ITGA1* on Si-CaP increased rapidly to 5.7-fold greater than PL and 3.0-fold greater than HA, by Day 21 levels of *ITGA1* were highest on Si-CaP (29.3 ± 0.14). *ITGA1* expression on HA also increased slightly on Day 14, but was at its highest on Day 21 (23.8 ± 0). *ITGA1* expression on PL+OS followed a similar trend, increasing over time and was highest on Day 21 (15.2 ± 2.2). *ITGA1* expression on PL remained constant, and did not increase above (1.9 ± 0.03).
On HA, alpha 2 integrin (*ITGA2)* expression increased over time in a linear fashion until Day 7 (7.7 ± 0.08), after which it decreased slightly but later increased on Day 21 to 7.97 ± 3.04. On Si-CaP *ITGA2* increased at a similar rate to HA up to Day 14, when it was 5.5-fold greater than PL+OS), on Day 21 levels increased to (20.5 ± 3.04) and was 2.6-fold greater than. *ITGA2* on PL+OS increased over time, dropping slightly on Day 7, and reaching its highest level on Day 21 (3.5 ± 0). On PL levels decreased slightly after Day 1, and remained low throughout culture.
Alpha 3 integrin (*ITGA3)* expression increased rapidly on Day 1 on HA and Si-CaP and (13.5 ± 0, and 11.6 ± 0.06 respectively). On Si-CaP *ITGA3* levels then decreased to 4.5 ± 0.07 on Day 7 and then further declined on Day 21 to 1.3 ± 0.01. On HA *ITGA3* levels decreased at a slower rate and remained 2.4-fold greater than Si-CaP on Day 7, after which expression levels decreased to 2.9 ± 0.01. On PL+OS expression of *ITGA3* decreased on Day 1 then increased over time and was highest on Day 21 at 4.6 ±0.4. On PL levels of *ITGA3* fluctuated over time but remained between 0.19 and 1.05 ± 0.01.
On Si-CaP, alpha 4 integrin (*ITGA4)* increased on Day 1 to 5.2 ± 0.08 and then decreased over time to 2.1 ± 0.02 on Day 21. On HA *ITGA4* expression was highest on Day 7 (3.1-fold less than Si-CaP) then decreased over time to 0.5 ± 0.02. On PL+OS *ITGA4* expression fluctuated between 0.5 and 1.1 ± 0.2. On PL *ITGA4* expression remained low at all time points and did not increase above 1, over 21 days.

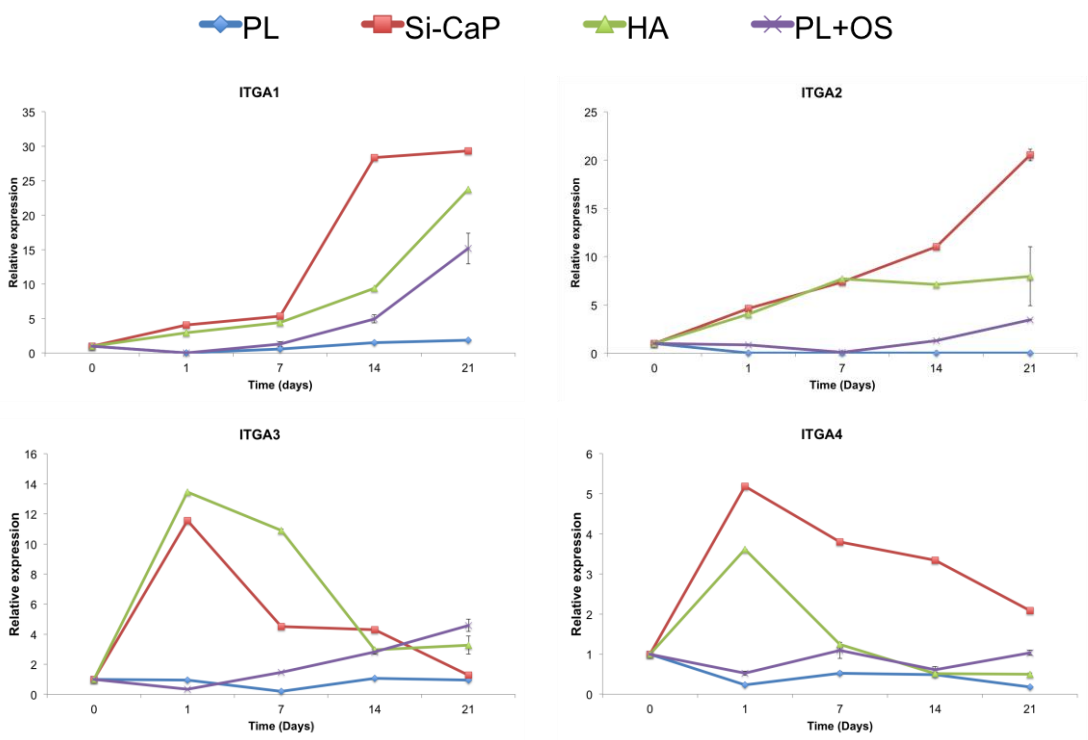

Figure 79:MSC integrin expression.

Data are mRNA levels of genes of interest and are represented as level of expression normalised to beta-2 microglobulin and to Day 0. Two donors were used, and each sample was run in duplicate

On Si-CaP, alpha 5 integrin (*ITGA5)* expression increased 26-fold on Day 1 to 26.2 ± 0.51 and then decreased on days 7 and 14, by Day 21 levels increased slightly to 4.6 ± 0.05. On HA *ITGA5* expression increased gradually (7-fold) over 14 days and on Day 21 was 11.9 ± 2.26. On PL+OS *ITGA5* also increased gradually over 21 days, increasing sharply on Day 7 (11.5-fold) and on Day 21 reached 11.9 ± 0.05. *ITGA5* expression on PL was highest on Day 1 (2.8 ± 0.73) then decreased over time.

Alpha V integrin (*ITGAV)* expression on Si-CaP followed a similar trend to *ITGA5*. *ITGAV* on Si-CaP was highest on Day 1 (46.5 ± 1.14) then decreased until Day 14, after which levels increased slightly to 12.0 ± 1.17 on Day 21. On HA, *ITGAV* levels reached 34.8 ± 0.87 on Day 7 and then decreased until Day 21 where expression was 0.06 ± 0.006. *ITGAV* expression on PL+OS was initially low (0.11 ± 0.005) then increased rapidly on days 14 and 21, reaching 41.9 ± 1.02 on Day 21. On PL *ITGAV* levels were less than 2.4 until Day 21 where expression increased 2.8-fold to 6.7 ± 0.13.

Expression of beta 1 integrin (*ITGB1)* on Si-CaP increased 25.6-fold on Day 1 and continued to increase to 54.8 ±0.27, on Day 14 where levels were highest, on Day 21 expression decreased 0.8-fold to 48.7 ±0.23. On HA, *ITGB1* expression increased 8.1-fold on Day 1, and continued to rise until Day 21 to 22.9 ± 1.46. *ITGB1* levels on PL+OS also increased over time, reaching highest levels on Day 21 (30.5 ±0.74). ON PL, expression of *ITGB1* remained relatively constant (between 0.33 and 1.04).

On Si-CaP, HA and PL+OS expression of beta 3 integrin (*ITGB3)* increased over time. On both HA and Si-CaP, *ITGB1* expression increased in a similar manner, with the greatest increase seen on Day 7, (1.01- and 1.07-fold) , levels then increased 1.46- and 1.40 fold on 14, and finally increasing to 22.6 ±0.22 and 22.4 ±0.44 Day 21. On PL+OS *ITGB1* expression was relatively low until Day 7, where levels increased 5.5-fold to reach 12.7 ± 1.62 on Day 14, after which increased 1.2-fold and reached 15.2 ± 0.22 on Day 21. On PL, *ITGB3* levels decreased slightly (0.01-fold) on Day 1 and remained less than 0.02 ±0.001 over 21 days.

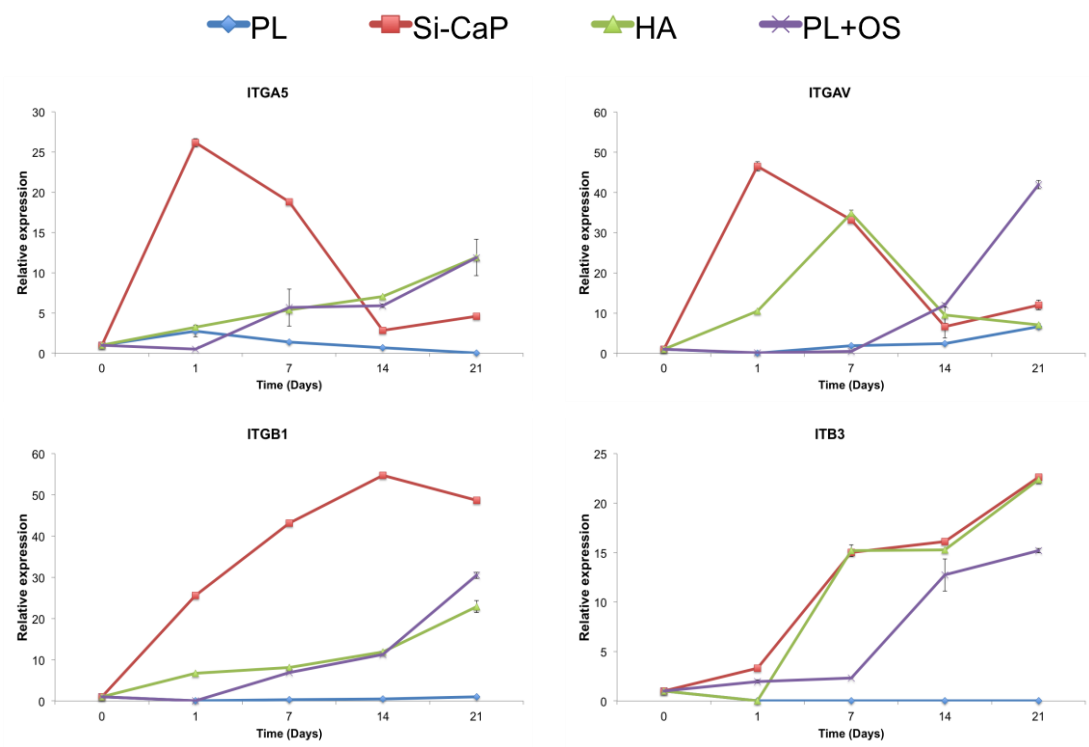

Figure 80: MSC integrin expression.

Data are mRNA levels of genes of interest and are represented as level of expression normalised to beta-2 microglobulin and to Day 0. Two donors were used, and each sample was run in duplicate

6.2.6 hES-MP integrin expression

ITGA1 expression on Si-CaP increased greatly over 14 days, (64-fold) then remained at a similar level on Day 21 (64.9 ± 3.81), shown inFigure 81. Expression of *ITGA1* on HA also increased over 21 days, and was highest on Day 21 (53.3 ± 2.87), but remained lower than Si-CaP at all time points. On PL+OS expression of *ITGA1* was low on days 1 and 7, then increased (15.2-fold) to 46.8 ± 0.23 then increased further on Day 21 to 53.9 ± 0.53. On PL *ITGA1* levels increased gradually over time (reaching 4.4 ± 0.04), but were lower than on all other substrates at all time points.

Expression of *ITGA2* on Si-CaP increased on Day 1 22.6-fold and continued to increase at a similar rate until Day 7, when levels were 1.04-fold greater

than HA and 95.7-fold greater than PL. On Day 14 *ITGA2* expression on Si-CaP increased to 44.6 ± 6.53 on Day 21 where levels were 1.18-fold greater than all other substrates. On HA *ITGA2* also increased in a time dependent manner, initially at a slow rate on days 1 and 7 (1.2-fold) however, on Day 14 expression increased 2.7-fold to 35.0 ± 0.34. On PL+OS *ITGA2* levels were low on Day 1 then increased on Day 7 to 8.53 ± 1.21, expression remained at a similar level on Day 14, then increased again on Day 21 to 12.91 ± 0.13. Expression of *ITGA2* on PL did not vary over 21 days remaining less than 1.

On HA, *ITGA3* expression increased 4.6-fold on Day 1 and continued to rise to 13.9 ± 0.41 on Day 7, where levels were greater than on any other substrate. On Day 14 *ITGA3* decreased to 7.4 ± 0.11 and by Day 21 was 0.92 ± 0.004. On Si-CaP *ITGA3* increased on days 1 and 7 (7.1-fold higher than on PL), on Day 14 levels dropped to 7.5 ± 0.04, then decreased further to 4.6 ± 0.02 on Day 21 (5.1-fold greater than HA). *ITGA3* on PL+OS initially decreased on Day 1 and then increased to 0.1 ± 0.01 on Day 7. By Day 14 levels of *ITGA3* decreased and then increased on Day 21 to 4.7 ± 0. On PL *ITGA3* expression decreased slightly (0.0001-fold) on Day 1, and remained low at all time points.

ITGA4 levels on Si-CaP and HA increased on Day 1 (4- and 4.6-fold respectively), and at this point *ITGA4* levels were at least 4-fold greater than PL and PL+OS. On Day 7 *ITGA4* expression on Si-CaP remained the same but decreased on HA (0.8-fold). *ITGA4* expression on Si-CaP decreased slightly on Day 14 to 0.82-fold less than on HA, after which levels of *ITGA4* on both Si-CaP and HA decreased. On PL+OS *ITGA4* expression decreased initially, and remained low until Day 21 when levels increased to 4.6 ± 0.06. On PL, *ITGA4* expression decreased on Day 1 and remained at similar levels at all other time points.

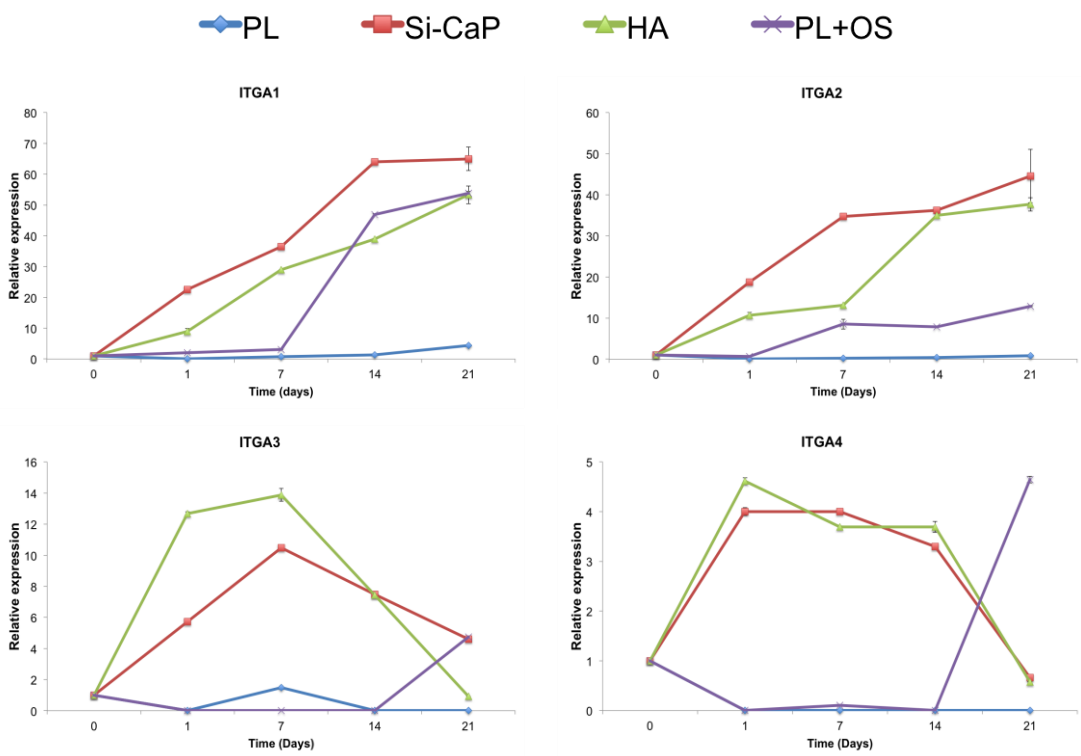

Figure 81: hES-MP integrin expression.

Data are mRNA levels of genes of interest and are represented as level of expression normalised to beta-2 microglobulin and to Day 0. Two donors were used, and each sample was run in duplicate

ITGA5 levels on Si-CaP increased on Day 1 to 25.4 ± 0.62, where expression was 136-fold greater than on any other substrate shown in Figure 82. Expression continued to increase on Day 7 to 36.9 ± 0.90 and then decreased on Day 14. By Day 21 levels of *ITGA5* were similar to Day 0 (0.16 ±0.001). On HA *ITGA5* did not increase until Day 7 (65.8-fold), after which levels increased at a similar rate to 23.9 ± 0.31 on Day 14, by Day 21 *ITGA5* levels decreased to 0.84 ± 0.01. On PL+OS *ITGA5* expression remained low, until Day 14, when it increased to 22.9 ± 0.89, on Day 21, levels decreased to 4.64 ± 0.07, similar to levels of *ITGA5* seen on Si-CaP and HA at this time. On PL expression increased slightly on Day 7, to 1.48 ± 0.10 but remained less than 1 at all other time points.

On Si-CaP and HA, levels of *ITGAV* increased over 14 days, reaching 48.7 ± 0.24 and 32.5 ± 2.7 respectively. Initially levels on Si-CaP increased at a

greater rate (21.3-fold) compared to HA (3.9-fold). Throughout culture, levels of *ITGAV* were consistently higher on Si-CaP than on HA. On Day 21, *ITGAV* on both HA and Si-CaP decreased, yet were both at least 10-fold greater than on PL. On PL+OS *ITGAV* expression initially, then increased to 3-.4 ± 0.3 on Day 7, levels remained high on Day 14 then increased further to 33.8 ± 0.05 on Day 21. On PL, *ITGAV* increased slightly on Day 7, but remained less than 0.6 at all other time points.

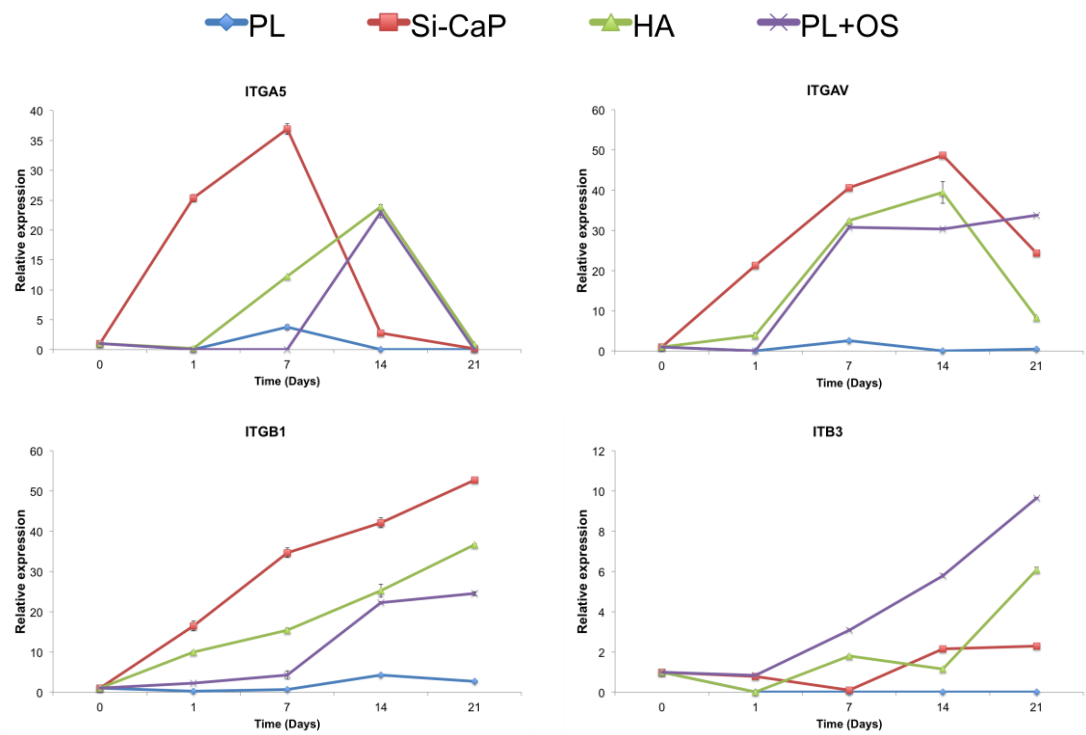

Figure 82: hES-MP integrin expression.

Data are mRNA levels of genes of interest and are represented as level of expression normalised to beta-2 microglobulin and to Day 0. Two donors were used, and each sample was run in duplicate

ITGB1 expression increased over time on PL+OS, Si-CaP and HA. On Si-Cap, levels of *ITGB1* were consistently higher than on all other substrates including HA, and by Day 21 Si-CaP was 1.43-fold greater than HA, and 19.9-fold greater than PL. On PL+OS expression of *ITGB1* was initially low (4.35 ± 0.03 until Day 7) then increased sharply on Day 14 (5.2-fold), after which the rate of expression slowed and was highest on Day 21 at 24.5 ± 0.48.

On PL, *ITGB1* also remained low until Day 14, where it increased slightly to 4.2 ± 0.02, but by Day 21 expression decreased to 2.65 ± 0.03.
ITGB3 expression on PL+OS increased 3.9-fold on Day 7, by Day 14 levels were greater than on any other substrate 5.8 ± 0.09, levels of *ITGB3* continued to increase, and were highest on Day 21 9.65 ± 0.05. On Si-CaP expression was also initially low, and decreased to 0.78 ± 0.01 on Day 7, however levels increased 21.7-fold on Day 14, and reached 2.29 ± 0 on Day 21. On HA, *ITGB3* decreased on Day 1 to 0.16 ± 0.004 and then increased, to 18-fold greater than Si-CaP on Day 7, by Day 14 levels of *ITGB3* decreased again then reached 6.08 ± 0.12 on Day 21. On PL, expression of *ITGB3* decreased on Day 1 and remained low thereafter.

6.2.7 ADMSC integrin expression

Expression of *ITGA1* increased in a linear fashion on Si-CaP on days 1 to 14, where levels reached 46.37 ± 0.23; on Day 21 expression decreased to 45.73 ± 0, shown in Figure 83. On HA *ITGA1* expression was low (less than 0) until Day 14 when it increased greatly to 18.07 ± 0.62. On Day 21 *ITGA1* increased 2.3-fold, but expression of *ITGA1* on HA remained lower than Si-CaP at all time points. A similar trend in expression was seen on PL+OS, initially low until Day 14 (27.3 ± 1.47) after which it increased to 63.14 ± 10.7 on Day 21, higher than on any other substrate. On PL expression of *ITGA1* remained less than 1 over 21 days.

On both HA and Si-CaP *ITGA2* expression increased at similar rates over 21 days, and reached levels of 32.33 ± 0.15 and 24 ± 0 on Day 21 respectively. At all time points cells on Si-CaP showed greater expression of *ITGA2* compared with HA and PL+OS. On PL+OS *ITGA2* expression did not increase until Day 21, where it reached 10.05 ± 2. On PL *ITGA2* expression increased on days 7 and 14 reaching 3.83 ± 0.34, on Day 21 levels decreased 0.

On PL expression of *ITGA3* did not vary by more than 0.5 and remained less than 1 at all time points after Day 0. On HA, *ITGA3* expression increased 5.1-fold on Day 1 (15.6-fold higher than any other substrate at this time). Expression levels decreased to 0.02 ± 0.001 on Day 14 and by Day 21 were 0. On Si-CaP *ITGA3* expression decreased initially to 0.33 ± 0.15, then increased

sharply on Day 7 to 10.53 ± 0.51 (1.8-fold higher than PL+OS). On days 14 and 21 expression decreased to 1.54 ± 0.02 and 0.18 ± 0.02 respectively. On PL+OS expression decreased on Day 1, then increased on Day 7, 28-fold. By Day 14 levels of *ITGA3* dropped slightly and then increased to 13.22 ± 0.26 on Day 21.

ITGA4 expression on Si-CaP increased on Day 1, 4.24-fold then decreased on Day 7 to 3.69 ± 0.05. On days 14 and 21 levels continued to decrease and were 1.25 ± 0.05 on Day 21. On HA, *ITGA4* expression followed a similar trend but peaked later, on Day 7 (3.49 ± 0.05). Levels decreased on Day 14, but were higher than on any other substrate at this time point, on Day 21 expression levels dropped to 1.11 ± 0.02. On PL+OS, *ITGA4* expression decreased on days 1 and 7, then increased to 0.95 ± 0.12 on Day 14, and peaked on Day 21 at 2.01 ± 0.11. *ITGA4* expression on PL, was lower than on PL+OS, yet followed a similar trend, decreasing initially, then increasing to 1.08 ± 0.24 on Day 21.

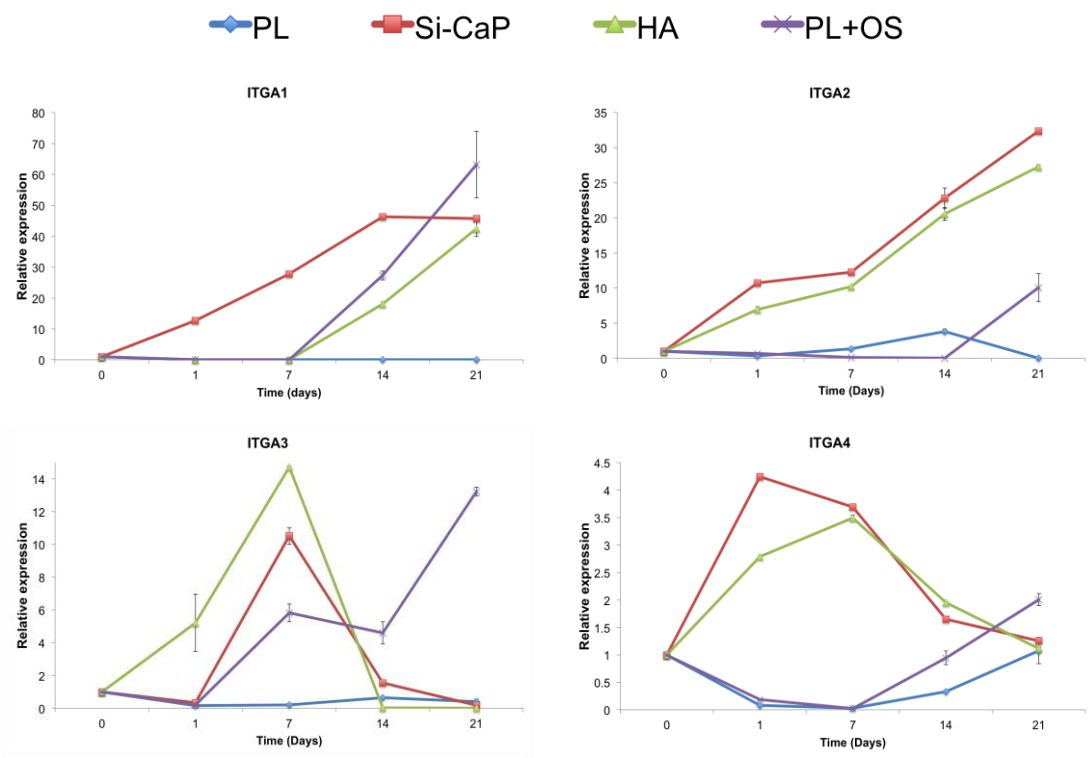

Figure 83: ADMSC integrin expression.

Data are mRNA levels of genes of interest and are represented as level of expression normalised to beta-2 microglobulin and to Day 0. Two donors were used, and each sample was run in duplicate

ITGA5 expression on Si-CaP and HA increased on Day 1 (25.5- and 6.7-fold), and levels continued to increase on Day 7, reaching 42.8 ± 1.04 and 21.5 ± 2.0 respectively, shown in Figure 84. At this point cells on both substrates had 4.17-fold greater *ITGA5* expression than PL and PL+OS. On Day 14 expression decreased to 5.8 ± 0.11 on HA and 10.7 ± 2.7 on Si-CaP. *ITGA5* expression on Day 21 decreased on Si-CaP to 2.98 ± 0.03, but increased on HA to 10.06 ± 0.19. On PL+OS expression initially increased 6-fold, then dropped to 5.83 ± 0.54 on Day 7. On Day 14 levels increased 7.3-fold and continued to increase to 25.19 ± 0.25 on Day 21. On PL expression of *ITGA5* fluctuated increasing on days 1 and 14, but decreasing on Day 7; expression remained between 5.8 and 0.5 at all time points.

Expression of *ITGAV* increased 35.9-fold on Si-Cap on Day 1, and then increased to 58.2 ± 2.9 on Day 7 (1.12-fold higher than on any substrates at any time point), on Day 14 levels decreased to 13.23 ± 1.6 then increased slightly on Day 21 to 18.0 ± 0.44. On PL+OS expression followed a similar trend, increasing on days 1 and 7, reaching 51.93 ± 5.08, then decreasing sharply on Day 14 to 0.52 ± 0.002 and then decreased further on Day 21 to 0. On HA, expression increased at a slower rate on Day 1 (3.75-fold) but increased rapidly on Day 7 to 49.87 ± 0.24. On Day 14 levels of *ITGAV* decreased to 10.41 ± 0.4 and remained at a similar level on Day 21. On PL *ITGAV* expression increased to 19.6 ± 0.1 on Day 7 then decreased on Day 14 to 2.0 ± 0.1, by Day 21 expression of *ITGAV* increased to 13.23.

On PL and PL+OS expression of *ITGB1* increased over time, reaching 15.19 ± 0.15 and 33.48 ± 0.32 respectively. On HA expression of *ITGB1* increased 3.95-fold then increased more gradually on days 7 and 14, to 13.55 ± 0.2 and 21.48 ± 0.31 respectively. By Day 21 expression increased slightly and was 1.58 –fold greater than PL, but 0.72-fold less than PL+OS. On Si-CaP expression increased rapidly (24.42-fold) on Day 1, then slowed to reach 25.82 ± 0.5 on Day 7. By Day 14, expression decreased to 17.45 ± 0.09, by Day 21 *ITGB1* expression increased sharply and reached 27.1 ± 0.13.

On PL+OS, ITGAB3 expression did not increase until Day 7, when it increased 3.42-fold to 5.08 ± 0.1. ITGAB3 levels continued to increase at a similar rate and by Day 21 reached 10.78 ± 1.26. On Si-Cap, *ITGB3* expression increased rapidly, 12-fold on Day 1 and then increased to 12.64 ±0.18, on Day 7. By Day 14 levels reached were 12.295- and 2.23-fold greater than PL and PL+OS respectively).the highest expression of *ITGB3* was seen on Si-Cap on Day 21 (18.32 ± 0). On HA, expression increased 5.5-fold on Day 1 and by Day 7 levels of *ITGB3* on HA were 1.13-fold higher than on any other substrate at this time point. On Day 14 expression increased to 16.25 ± 3.01, then decreased to 13.98 ± 0.27 on Day 21. Expression of *ITGB3* remained relatively constant On PL, between 1 and 1.07, over 21 days.

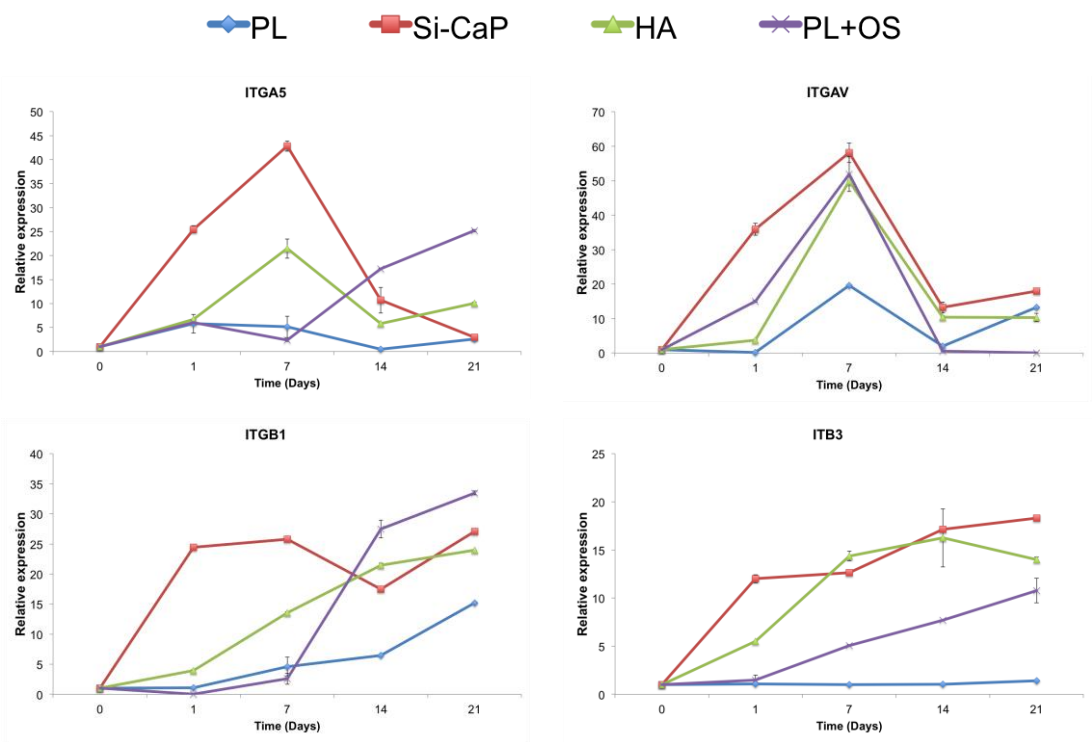

Figure 84: ADMSC integrin expression.

Data are mRNA levels of genes of interest and are represented as level of expression normalised to beta-2 microglobulin and to Day 0. Two donors were used, and each sample was run in duplicate

6.3 Discussion

Cell-substrate interactions are critical for the clinical success of a bone graft, as they determine integration with the host tissue. Early signals were shown to direct differentiation of uncommitted cells within 24 hours upon Si-CaP and HA. Further examination of the interactions between mesenchymal stem cells and these substrates demonstrated that the cells were morphologically distinct, and showed differential integrin expression profiles when compared to PL and PL+OS.

Morphology

Visualisation of cell morphology upon different substrates revealed distinct morphologies and differences in focal adhesion (FA) number, size, and distribution (visualised through vinculin staining) and in cytoskeletal organisation (visualised as actin staining). Whether *in vivo* or *in vitro*, cells are rarely in direct contact with substrates, but instead interact with an adsorbed protein layer. Nonetheless, the surface chemistry of the substrates determines the type, quantity and conformation of protein adsorbed. As a result, differences in adhesion and morphology may be ultimately attributed to the substrates' structure and composition.

Cells adhere to the protein layer via integrins; these receptors bind to specific motifs in proteins such as the RGD sequence found in fibronectin and collagen type I (Siebers et al. 2005). Integrins that are not bound to ECM ligands are generally distributed diffusely over the cell surface, and association with the actin cytoskeleton is only induced upon binding to a ligand. Once bound to the ECM, integrins cluster together into focal contacts, which are composed of cytoskeletal proteins, adapter molecules and kinases. Vinculin is a key component of focal adhesions; along with other adapter proteins it links integrins to the actin cytoskeleton, and functions to stabilse focal adhesions (Ziegler et al. 2006).
Vinculin staining was detected in all cell types on each substrate, yet the size and number of vinculin containing FAs varied on different substrates

between each cell type. MSC and hES-MP displayed similar patterns of staining, whereas while ADMSC showed a similar morphology to the other MSC types, yet the pattern of staining was clearly different; with vinculin staining localised to the cell periphery and and strong actin detected throughout the cells. In all cell types FA were smaller, and more numerous on Si-CaP and HA when compared to PL+OS and PL. Small FAs are indicative of motile cells (Anselme 2000) whereas larger more pronounced FAs, such as seen in ADMSC on PL+OS at 48 hours, suggest sessile cells.

The size and distribution of FAs regulate cell shape and spreading (C. S. Chen et al. 2003), which in turn have been shown to directly influence cell fate (Kilian et al. 2010; Sun et al. 2012). These results have been confirmed by several recent studies, which have manipulated cell shape through controlling the size and shape of adhesive islands. These studies demonstrated multipotent cells on adhesive islands will preferentially differentiate into osteoblasts if the island promotes cell spreading, for example larger islands with defined edges, whereas smaller islands with rounded edges induce an adipogenic phenotype (McBeath et al. 2004; Kilian et al. 2010). *In vivo*, adipocytes are spherical in shape, as this provides the most efficient surface area to volume ratio for lipid storage, the smaller, rounded islands minimise cell spreading and focal adhesion formation, and as a result the preferential spherical phenotype is maintained (S. Murphy et al. 2010).

The substrates examined in this chapter did not contain controlled adhesive areas; instead, adsorption of adhesive proteins was purely determined by the substrate's surface chemistry. Hydroxyapatite consists of a hexagonal arrangement of calcium (Ca^{2+}) and phosphate (PO_4^{3-}) ions around columns of monovalent hydroxyl (OH^-) ions. Whereas, the inclusion of silicate ions in silicate substituted calcium phosphate (Si-CaP) alters this well organised structure, which has been shown to enhance its bioactivity through increased dissolution rates and protein adsorption, which are known to occur after 24 hours in culture (Botelho 2005).

Results shown above show clear differences in cell morphology between 24 and 48 hours after cell seeding. Cell shape varied on each substrate, and at different time points but no substrate specific morphologies could be

identified. hES-MP were larger on Si-CaP than on HA, yet this was less apparent in the other cell types. Cells were notably larger and more flattened on Si-CaP and HA after 48 hours. However, on PL and PL+OS cells appeared to be of similar size at both time points.
The increased number of FAs and larger cells observed on Si-CaP, compared to HA, indicate greater sites of ligand binding, which may be due to adsorption of protein in a preferential conformation or due a greater quantity of adsorbed protein. This is consistence with previous studies comparing protein adsorption on Si-CaP and HA (Guth et al. 2011; Guth & Buckland 2005; Botelho et al. 2011; Guth, Campion, Buckland & Hing 2010a).

Focal adhesions not only anchor cells to proteins or substrates but, when coupled to the cytoskeleton, can also transfer force and regulatory signals between the ECM and the cell.
Cells transduce these signals through cell architecture, in a manner dependent upon tensional integrity or 'tensegrity' (C. S. Chen & Ingber 1999). A principal that is evident in the structural organisation of the musculoskeletal system and its components, down to single cells (Ingber 2010).
Cells attached to substrates via integrin clusters within FAs, these sites act as anchors, allowing cells to generate tension within the cytoskeleton through an actomysin filament sliding mechanism (C. S. Chen & Ingber 1999). This increases cytoskeletal stress, which has been shown to influence cell fate (McBeath et al. 2004).

In each cell type on Si-CaP and HA at 48 hours, cell morphology was similar; cells appeared to be stretched between areas of attachment, with areas of strong actin staining between focal adhesions. It is possible that the conformation of proteins, on HA and Si-CaP, are adsorbed in a particular distribution that encourages cells to generate cytoskeletal tension, acting as a regulator of transcription, driving cell fate.

Integrin signalling

Integrins represent a major family of transmembrane, cell-surface receptors, composed of non-covalently bound α and βsubunits (Ingber 2003). Each

subunit contains a large extracellular domain, a transmembrane region and a small intracellular region. The extracellular domain interacts directly with ECM proteins, such as fibronectin, laminin, vitronectin and collagen type I. The intracellular region interacts with signal transmission molecules and cytoskeletal proteins to regulate multiple cell functions, including; signal transduction, cytoskeletal remodeling, cell motility, migration, apoptosis, cell proliferation and cell adhesion (Clark & J. S. J. Brugge 1995; Giancotti 1999). As the key receptors connecting the cytoskeleton to the extracellular matrix (ECM), integrins play a critical role in bone formation and osteogenic differentiation.

Integrin expression in mesenchymal stem cells (Docheva et al. 2007) and in mature osteoblasts (Anselme 2000) has been well documented, yet the expression of integrins during osteoblast differentiation remains poorly understood. This is largely due to different detection methods resulting in contradictory results.

Fluorescence activated cell sorting (FACS) and flow cytometry are commonly used, and provide accurate and rapid results; immunocytochemistry and western blotting provide information regarding localisation and quantity of expression however these techniques are often unsuitable to analyse expression over time courses in culture. Although few studies have relied on RNA based detection, PCR provides inexpensive, readily reproducible, clear insight into gene expression levels.

Results from integrin gene expression analysis of 11 αand 8 βsubunits (shown here) revealed upregulation of α1, α2, α3, α4, α5, αV, β1 and β3 subunits in all three cell types analysed. No change (defined as a change of <1 relative expression units) was detected in α6, α7, α8, α10, α11, β2, β4, β5, β6, β7 and β8 integrins.

Expression of integrins varied between substrates, and significant differences were seen between expression on the calcium phosphate based substrates and on tissue culture plastic. In general subunit expression on PL did not vary significantly, on PL+OS integrin expression appeared lower and increased later on when compared to both Si-CaP and HA. Differences were also noted between Si-CaP and HA and the expression of all subunits, with the exception of α3, was higher and increased earlier on Si-CaP. The discrepancies observed in expression levels between the calcium phosphate

based substrates are of particular interest. The attachment of MSC is predominately mediated by β1 (Docheva et al. 2007). Expression of β1 was significantly higher on Si-CaP compared with HA up to day 7, which may explain the higher levels of attachment observed on Si-CaP in the previous chapter. Differences in integrin expression have also been shown to affect the timing and level of gene expression (Gronthos, Simmons, et al. 2001b; Hamidouche et al. 2009), which may explain the earlier, greater increase in osteoblast related genes RUNX2 and COL1A1, on Si-CaP when compared to HA.

Integrin expression levels varied significantly on Si-CaP and HA, yet the results from the previous chapter did not show such significant differences in levels of protein production or mineralisation. This may be attributed to the low sample number (n=2), however, expression in each cell type appeared very similar, suggesting these result may reflect true changes in integrin levels.

The initial expression of intgerins on each substrate is likely to be determined by the type of protein adsorbed onto the substrates surface. Both HA and Si-CaP have been shown to absorb fibronectin and vitronectin from fetal bovine serum (FBS) in culture media, which are recognised by α3β1, α4β1, α5β1 and αVβ3. Expression of these subunits were all upregulated on day 1 on both Si-CaP and HA, suggesting these proteins were adsorbed onto the surface of these substrates, providing initial sites of attachment for cells. The αVβ3 heterodimer also recognises the RGD sequence within bone sialoprotein and osteopontin- proteins secreted by osteoblasts. The expression of αV and β3 increased over time in each cell type, consistent with production of these osteoblast related genes. Collagen type I is recognised by α1β1 and α2β1, expression of these subunits also increased over time and reached the greatest levels on day 21. Collagen type I is not found in FBS but is secreted by mature osteoblasts, the timing of expression of these integrins is consistent with collagen type I production shown in the previous chapter.

Despite conflicting results from different studies, undifferentiated human MSC are generally thought to express α1, α2, α3, α4, α5, α6, α7, αv, β1, β3, and β5 whereas α1, α2, α3, α4, αv, β1, and β3 have been detected in osteoblasts. The results shown above are consistent with these results from other studies, and

although the β5 subunit was initially detected in each cell type prior to differentiation was not upregulated on any substrate.

Integrin expression is dynamic and alters in response to variety of factors. The composition and topography of orthopedic implants has been shown to impact cell adhesion and expression of integrin subunits in osteoblasts.

Osteoblast adhesion is greater on calcium phosphate based materials such as HA, when compared to on titanium (Kilpadi et al. 2001). Yet, integrin expression patterns on these substrates are quite similar: expression of α2, α3, α4, α6, αV, β1 and β3 subunits have been shown on titanium based alloys, whereas on cobalt-chrome-molybdenum alloys expression of α3, α6 and β3 subunits were not detected (R. K. Sinha & Tuan 1996). With the exception of α6 all of these subunits were detected in MSC, hES-MP and ADMSC on both Si-CaP and HA.

The surface topography of substrates is known to significantly affect cellular attachment, and behavior as discussed in the previous chapter. Yet, studies comparing integrin expression on surfaces with smooth and rough topographies have conflicting results. Integrins α3 and α6 were not detected in primary osteoblasts (R. K. Sinha & Tuan 1996), yet were found on U2OS (human osteosarcoma cell line) cells on rough titanium (P. J. ter Brugge, Dieudonne, et al. 2002a). In rat marrow cells α5 and α6 were upregulated (P. J. ter Brugge, Torensma, et al. 2002b) whereas in MG-63 (human osteosarcoma cell line) cells expression of α2, α3, α5, β1 and β3 were seen yet α6 was not detected (Lange et al. 2002). Difficulties in comparing expression in these studies arise from the use of different cell types, and substrate compositions. Differential integrin expression involved in cell attachment may also be attributed to differential protein adsorption, which can be influenced by topography. For example, altered topography can cause changes in surface wettability, impacting directly upon protein adsorption (Siebers et al. 2005).

Integrin expression is not only affected by quantity of protein but also the conformation and type of protein absorbed. On uncoated polystyrene, osteoblasts express subunits α2, α4, α6, αV, β1 and β3. When cultured on fibronectin coated polystyrene, α2, α6, and αv expression is lost and α3 and α5 are expressed. Osteoblasts on collagen type I coated polystyrene, express subunit α3 instead of subunit α6, and on laminin coated polystyrene α4, α6, αv,

and β1 subunits are expressed (R. K. Sinha & Tuan 1996).

These integrin subunits recognise specific sequences within these ECM proteins, and can impact on cell adhesion, and behavior. Irrespective of the composition of the substrate that is coated (glass, titanium, titanium alloy, or tissue culture polystyrene) fibronectin consistently increases adhesion, proliferation and differentiation of osteoblasts (Cowles et al. 2000; Siebers et al. 2005). Conversely, coating titanium with collagen type I did not increase proliferation or differentiation of osteoblasts (Becker et al. 2002). Whereas collagen type I coated polystyrene increased adhesion, spreading, and proliferation of osteoblasts and differentiation of MSC (Cowles et al. 2000; Salasznyk et al. 2004). Vitronectin has been shown to be a potent inducer of osteogenic differentiation in MSC (Salasznyk et al. 2004), yet a decrease in adhesion was seen in osteoprogenitors on vitronectin when compared to uncoated polystyrene (Verrier et al. 2002).

On Si-CaP and HA expression of integrin subunits that recognise fibronectin, vitronectin, laminin and collagen type I were upregulated, consistent with previous studies, which have confirmed the adsorption of these proteins *in vitro* onto these substrates (Guth et al. 2011; Guth & Buckland 2005; Botelho et al. 2011; Guth, Campion, Buckland & Hing 2010a).

Fibronectin, vitronectin, laminin and collagen type I all contain a binding sequence recognised by $\alpha v\beta 3$, known as the RGD sequence. In collagen type I, however, this site is only exposed after proteolytic processing (Davis 1992). The osteogenic effect of proteins containing the RGD sequence has been clearly shown, and research has shown increased biocompatibility of orthopedic implants by coating substrates with short peptides containing this sequence (Huang et al. 2003; Hersel et al. 2003; Kantlehner et al. 2000; Schliephake et al. 2002; Ferris et al. 1999). However, the biological activity of these short peptides is less than that of the whole protein, and over-coating of the substrates with peptides can lead to impaired motility (LeBaron & Athanasiou 2000). Therefore substrates such as Si-CaP and HA, that encourage adsorption of complete proteins onto their surfaces naturally, may be preferential to utilising such peptides.

The majority of these results focused on observational integrin expression in mature osteoblasts or cell lines. However, integrin expression can be highly

dynamic, changing as adsorbed proteins are degraded or replaced by other proteins, secreted by osteoblasts. Studies examining the requirement of certain integrins during osteogenic differentiation have provided more relevant data with regard to improving and understanding bioactivity of current bone graft substrates.

A comprehensive study on MSC showed α5 was essential during dexamethasone induced osteogenic differentiation; forced expression of α5 promoted differentiation, while silencing of the *ITGA5* gene prevented differentiation, and priming of α5β1 was sufficient to drive osteogenic differentiation (Hamidouche et al. 2010). However, others have shown that osteogenic differentiation on calcium phosphate and titanium based substrates is dependent upon expression of the α2β1 integrin heterodimer (Lu & Zreiqat 2010; Olivares-Navarrete et al. 2008).
Possibly the most essential integrin subunit involved in osteogenic differentiation is β1, which is the major subunit involved in both substrate driven and osteogenic supplement driven differentiation (Müller et al. 2007; R. K. Sinha & Tuan 1996; Anselme 2000).
The significant increase in β1 on both Si-CaP and HA suggest it is likely the key integrin subunit involved in initiating substrate driven differentiation.

To confirm the role of β1 in osteogenic differentiation, it could then be blocked using a integrin neutralising antibody, such as the one used by Lu and Zreiquat (Lu & Zreiqat 2010). The α subunits known to form heterodimers with β1 could also be overexpressed, blocked and analysed to determine the key combination of subunits involved.

Once the key integrins involved were identified osteogenic differentiation could be initiated through priming the integrins using a similar monoclonal antibody used by Hamidouche et al (Hamidouche et al. 2009).

Determining key integrins involved in substrate driven differentiation could enable better design of biomaterials for bone repair, through improved design of substrates or development of small molecules to activate the required integrins. The use of such substrates or molecules may be used to promote differentiation of MSC in skeletal disorders or injuries where recruitment or differentiation of MSC is compromised.

CHAPTER SEVEN: GENERAL CONCLUSIONS AND FUTURE DIRECTIONS

This thesis examined the hypothesis that the superior bone formation associated with Si-CaP is a result of activating the osteogenic differentiation of mesenchymal stem cells.

Si-CaP and HA were used for *in vitro* testing in the form of dense discs, which were manufactured to eliminate porosity as a potential factor that may influence cell response; as a result the only significant variable between the materials was their different surface chemistries. The manufacture of dense discs was optimised with regard to multiple physical properties and production yield. Several critical parameters determining the physical properties of dense discs were identified including (powder weight, pressure applied, calcination, lubrication and sintering temperature). The recommended final parameters allowed discs to be manufactured to be <0.16 % porous..
Mesenchymal stem cells from three different sources (bone marrow, embryonic stem cells, and adipose tissue) were chosen for analysis and although were shown to display differences in morphology, proliferation, heterogeneity, and surface marker expression profiles, possessed similar differentiation capacities.

Bone marrow derived MSC may represent the most biologically relevant stem cell to examine osteogenic differentiation, however were limited in number and supply, had relatively low proliferation capacity and detectable donor variability. Mesenchymal progenitors derived from embryonic stem cells (hES-MP) represent a far more abundant supply of multipotent cells, with significant proliferation capacity yet may not be clinically relevant due to legal and ethical issues. Furthermore, it was demonstrated that hES-MP are heterogeneous; containing a subpopulation of committed progenitor cells. Adipose derived stem cells (ADMSC) displayed similar characteristics to MSC, but possessed greater expansion

potential, greater availability and as such may represent an attractive clinical alternative to bone marrow derived MSC.

Si-CaP and HA were shown to support attachment, proliferation and induce osteogenic differentiation of MSC, hES-MP and ADMSC in the absence of osteogenic supplementation. Rates of differentiation were comparable to cells cultured on tissue culture plastic with soluble factors known to drive osteogenic differentiation.

Each cell type differentiated along the osteoblast lineage as evidenced by upregulation of osteoblast related genes (*RUNX2, OSX, COL1A1, BGLAP* and *DMP1*), increased protein production (RUNX2, collagen type I, and osteocalcin), an increase in alkaline phosphatase activity, and production of a mineralised matrix.

ADMSC showed comparable rates of attachment, differentiation and mineralisation to MSC and hES-MP; but demonstrated greater proliferation potential and more extensive, mature protein production on both HA and Si-CaP. As a result it is suggested that ADMSC are a promising source of multipotent cells for clinical bone repair.

Greater attachment, proliferation, gene expression, protein production alkaline phosphatase and mineralisation were detected on Si-CaP when compared to HA, in each cell type. Suggesting the superior bone formation seen with Si-CaP *in vivo* may be a result of increased rates of differentiation of multipotent stem cells.

The inclusion of silicate in the calcium phosphate lattice has been previously shown to enhance dissolution rates, and encourage preferential adsorption of proteins when compared to stoichiometric HA (Botelho 2005). Cells adhere to these proteins adsorbed onto bone grafts via integrins, which are known to regulate cell behavior through bi-directional signalling (Siebers et al. 2005).

To determine whether Si-CaP and HA were eliciting their ostogenic effect via these receptors, integrin expression was analysed. An upregulation in

expression of α1, α2, α3, α4, α5, αV, β1 and β3 subunits was detected. These subunits recognise binding sequences within fibronectin, vitronectin, laminin and collagen type I, proteins known to positively influence osteogenic differentiation (Salasznyk et al. 2004; Müller et al. 2007). These results suggest integrin signaling may be implicated in the substrate driven differentiation observed on Si-CaP and HA.

The intracellular signalling pathways involved in substrate driven osteogenic differentiation remain unclear, largely due to the lack of research in this area but also differences in the proposed pathways involved.
The ERK1/ 2 pathways is known to be key mechanotransduction pathway in activating cellular responses to mechanical stimuli (Sun et al. 2012) and has been shown to be involved in osteoblast survival, proliferation and differentiation (Salazar & Ohneda 2012).

Culture of cells upon substrates in the presence of selective MEK inhibitor U0126 (Favata 1998) may determine if the MAPK/ ERK pathway is involved. However, due to the complexity of signalling cascades, it is possible that one pathway may compensate for inhibition of another.

An alternative approach would be to use a microarray designed to detect known molecules involved in intracellular signalling pathways or cell lineage specification (Arrayit Corporation ARYC - Pathways™ 1993).

Protein adsorption on Si-CaP and HA has been previously examined in several comprehensive studies (Guth & Buckland 2005; Guth et al. 2011; Botelho et al. 2011; Botelho et al. 2004), and as such was not examined in this thesis. However, it may be pertinent to analyse protein adsorption with regard to integrin expression and examine how proteins synthesised by osteoblasts influence their subsequent behaviour.

Topography in the form of porosity has been shown to impact upon protein adsorption and significantly cell behavior (K A Hing 2005). As Si-CaP and HA are clinically used in the form of porous micro-granules. It may also be relevant to examine the differentiation of multipotent stem

cells upon these substrates in this porous form. However, several issues regarding cell imaging and detachment are likely to complicate analysis of the substrates in this format.

Morphologically cells on Si-CaP and HA were very different to those cultured on PL and PL+OS. The presence of directionally aligned actin fibers and small focal adhesions on Si-CaP and HA suggests cell may be tensionally strained upon these substrates.

Increased cellular tension is known to positively influence osteogenic differentiation, and can result from regulating adhesion (McBeath et al. 2004; Kilian et al. 2010), shear stress, (Kapur et al. 2003) and mechanical loading (S.-M. Lim et al. 2012).

In microgravity, such as in space flight, bone density is lost due to lack of mechanical loading (Bikle & Halloran 1999). It would be interesting to determine whether the differentiation observed on Si-CaP and HA would be influenced in microgravity. Examining the mechanism through which this tensional strain induces differentiation may provide insight into improving bone health during space flight.

In conclusion, the directed differentiation observed on Si-CaP and HA not only provides significant implications for improving bone graft design and subsequent repair, but also may hold the answers to questions further afield.

APPENDIX

Macros used to count cell number and area of staining run on Image J

A. Cell counter macro

```
setAutoThreshold("Default dark");
/ / run("Threshold...");
setThreshold(57, 255);
run("Convert to Mask");
run("Analyze Particles...", "size=10-1000 circularity=0.00-1.00 show=Ellipses display summarize in_situ");
```

B. Area quantification macro

```
run("8-bit");
/ / run("Threshold...");
setAutoThreshold("Default dark");
setThreshold(0, 128);
run("Convert to Mask");
run("Analyze Particles...", "size=0-Infinity circularity=0.00-1.00 show=Nothing display summarize");
```

REFERENCES

Abell, A., Willis, K. & Lange, D., 1999. Mercury Intrusion Porosimetry and Image Analysis of Cement-Based Materials. *Journal of colloid and interface science*, 211(1), pp.39–44.

Akao, M., Aoki, H. & Kato, K., 1981. Mechanical properties of sintered hydroxyapatite for prosthetic applications. *Journal of Materials Science*, 16(3), pp.809–812.

Albrektsson, T. & Johansson, C., 2001. Osteoinduction, osteoconduction and osseointegration. *European spine journal : official publication of the European Spine Society, the European Spinal Deformity Society, and the European Section of the Cervical Spine Research Society*, 10 Suppl 2, pp.S96–101.

Alford, A.I. & Hankenson, K.D., 2006. Matricellular proteins: Extracellular modulators of bone development, remodeling, and regeneration. *Bone*, 38(6), pp.749–757.

Alonso, V. et al., 2011. A naturally occurring isoform inhibits parathyroid hormone receptor trafficking and signaling. *Journal of Bone and Mineral Research*, 26(1), pp.143–155.

Amstein, C.F. & Hartman, P.A., 1975. Adaptation of plastic surfaces for tissue culture by glow discharge. *Journal of Clinical Microbiology*, 2(1), p.46.

Anon, *Office for National Statistics*, Office for National Statistics, Government Buildings, Cardiff Rd, Newport NP10 8XG, info@ons.gov.uk.

Anselme, K., 2000. Osteoblast adhesion on biomaterials. *Biomaterials*, 21(7), pp.667–681.

Arinzeh, T.L. et al., 2005. A comparative study of biphasic calcium phosphate ceramics for human mesenchymal stem-cell-induced bone formation. *Biomaterials*, 26(17), pp.3631–3638.

Aronow, M.A. et al., 1990. Factors that promote progressive development of the osteoblast phenotype in cultured fetal rat calvaria cells. *Journal of Cellular Physiology*, 143(2), pp.213–221.

Arrayit Corporation ARYC - Pathways™, 1993. Arrayit Corporation ARYC - Pathways™ Focused Human Genome Microarray Products. *arrayit.com*. Available at: http:/ / arrayit.com/ Products/ DNA_Microarrays/ Microarrays/ microa rrays.html [Accessed October 23, 2012].

Atilgan, S. et al., 2007. An experimental comparison of the effects of

calcium sulfate particles and beta-tricalcium phosphate/ hydroxyapatite granules on osteogenesis in internal bone cavities. *Biotechnology & Biotechnological Equipment*, 21(2), pp.205–210.

Augello, A., Kurth, T.B. & De Bari, C., 2010. Mesenchymal stem cells: a perspective from in vitro cultures to in vivo migration and niches. *Eur Cell Mater*, 20, pp.121–133.

B, A., D, B. & J, L., 2001. *Molecular Biology of the Cell* 3rd ed, new york: Garland publishing Inc.

Badylak, S.F., Freytes, D.O. & Gilbert, T.W., 2009. Extracellular matrix as a biological scaffold material: Structure and function. *Acta Biomaterialia*, 5(1), pp.1–13.

Bagi, C.M., 2005. Targeting of therapeutic agents to bone to treat metastatic cancer. *Advanced Drug Delivery Reviews*, 57(7), pp.995–1010.

Balamurugan, A. et al., 2008. Suitability evaluation of sol–gel derived Si-substituted hydroxyapatite for dental and maxillofacial applications through in vitro osteoblasts response. *Dental Materials*, 24(10), pp.1374–1380.

Banas, A. et al., 2007. Adipose tissue-derived mesenchymal stem cells as a source of human hepatocytes. *Hepatology*, 46(1), pp.219–228.

Bansal, S. et al., 2009. Evaluation of hydroxyapatite and beta-tricalcium phosphate mixed with bone marrow aspirate as a bone graft substitute for posterolateral spinal fusion. *Indian journal of orthopaedics*, 43(3), pp.234–239.

Barraud, P. et al., 2006. In vitro characterization of a human neural progenitor cell coexpressing SSEA4 and CD133. *Journal of neuroscience research*, 85(2), pp.250–259.

Barrère, F. et al., 2008. Advanced biomaterials for skeletal tissue regeneration: Instructive and smart functions. *Materials Science and Engineering: R: Reports*, 59(1), pp.38–71.

Barry, F. et al., 2001. Chondrogenic differentiation of mesenchymal stem cells from bone marrow: differentiation-dependent gene expression of matrix components. *Experimental Cell Research*, 268(2), pp.189–200.

Barry, F.P. & Murphy, J.M., 2004. Mesenchymal stem cells: clinical applications and biological characterization. *The International Journal of Biochemistry & Cell Biology*, 36(4), pp.568–584.

Barry, F.P. et al., 1999. The monoclonal antibody SH-2, raised against human mesenchymal stem cells, recognizes an epitope on endoglin (CD105). *Biochemical and Biophysical Research Communications*, 265(1), pp.134–139.

Becker, D.D. et al., 2002. Proliferation and differentiation of rat calvarial osteoblasts on type I collagen-coated titanium alloy. *Journal of*

Biomedical Materials Research Part A, 59(3), pp.516–527.

Bellows, C.G., Aubin, J.E. & Heersche, J.N., 1991. Initiation and progression of mineralization of bone nodules formed in vitro: the role of alkaline phosphatase and organic phosphate. *Bone and mineral*, 14(1), pp.27–40.

Bellows, C.G., Heersche, J.N. & Aubin, J.E., 1990. Determination of the capacity for proliferation and differentiation of osteoprogenitor cells in the presence and absence of dexamethasone. *Developmental biology*, 140(1), pp.132–138.

Benayahu, D. et al., 1989. Bone marrow-derived stromal cell line expressing osteoblastic phenotype in vitro and osteogenic capacity in vivo. *Journal of Cellular Physiology*, 140(1), pp.1–7.

Benoit, D.S.W. et al., 2008. Small functional groups for controlled differentiation of hydrogel-encapsulated human mesenchymal stem cells. *Nature Materials*, 7(10), pp.816–823.

Bentmann, A. et al., 2010. Circulating fibronectin affects bone matrix, whereas osteoblast fibronectin modulates osteoblast function. *Journal of Bone and Mineral Research*, 25(4), pp.706–715.

Bielby, R.C. et al., 2004. In vitro differentiation and in vivo mineralization of osteogenic cells derived from human embryonic stem cells. *Tissue Engineering*, 10(9-10), pp.1518–1525.

Bikle, D.D. & Halloran, B.P., 1999. The response of bone to unloading. *Journal of Bone and Mineral Metabolism*, 17(4), pp.233–244.

Bjerre, L. et al., 2008. Flow perfusion culture of human mesenchymal stem cells on silicate-substituted tricalcium phosphate scaffolds. *Biomaterials*, 29(17), pp.2616–2627.

Blitterswijk, C., Boer, J. & Bruijn, J., 2007. A rapid and efficient method for expansion of human mesenchymal stem cells. *Tissue …*.

Block, J.E., 2005. The role and effectiveness of bone marrow in osseous regeneration. *Medical hypotheses*, 65(4), pp.740–747.

Blunn, G., Biopsy Assessment of Actifuse™ Synthetic Bone Graft at One Year Post Lumbosacral Fusion Surgery. *apatech.com*

.

Bonewald, L.F., 2006. Mechanosensation and Transduction in Osteocytes. *BoneKEy osteovision*, 3(10), pp.7–15.

Botelho, C., 2005. *Silicon-substituted hydroxyapatite for biomedical applications*, Thesis.

Botelho, C.M. et al., 2004. Effect of Human Serum Proteins on Pure Hydroxyapatite and Silicon Substituted Hydroxyapatatite: AFM and SEM Studies. *Materials Science Forum*, 455-456, pp.378–382.

Botelho, C.M. et al., 2011. Effect of Protein Adsorption onto the Dissolution of Silicon-Substituted Hydroxyapatite. *Journal of Encapsulation and Adsorption Sciences*, 1(4), pp.72–79.

Botelho, C.M. et al., 2006. Human osteoblast response to silicon-substituted hydroxyapatite. *Journal of Biomedical Materials Research Part A*, 79(3), pp.723–730.

Botelho, C.M. et al., 2005. In Vitro Analysis of Protein Adhesion to Phase Pure Hydroxyapatite and Silicon Substituted Hydroxyapatite. *Key Engineering Materials*, 284-286, pp.461–464.

Botelho, C.M. et al., 2002. Structural analysis of Si-substituted hydroxyapatite: zeta potential and X-ray photoelectron spectroscopy. *Journal of Materials Science: Materials in Medicine*, 13(12), pp.1123–1127.

Boyan, B., 1996. Role of material surfaces in regulating bone and cartilage cell response. *Biomaterials*, 17(2), pp.137–146.

Boyd, N.L. et al., 2009. Human Embryonic Stem Cell–Derived Mesoderm-like Epithelium Transitions to Mesenchymal Progenitor Cells. *Tissue Engineering Part A*.

Bruder, S.P. et al., 1997. Monoclonal antibodies reactive with human osteogenic cell surface antigens. *Bone*, 21(3), pp.225–235.

Brugge, ter, P.J., Dieudonne, S. & Jansen, J.A., 2002a. Initial interaction of U2OS cells with noncoated and calcium phosphate coated titanium substrates. *Journal of Biomedical Materials Research Part A*, 61(3), pp.399–407.

Brugge, ter, P.J., Torensma, R., et al., 2002b. Modulation of Integrin Expression on Rat Bone Marrow Cells by Substrates with Different Surface Characteristics. *Tissue Engineering Part A*, 8(4), pp.615–626.

Caetano-Lopes, J., Canhão, H. & Fonseca, J.E., 2007. Osteoblasts and bone formation. *Acta reumatológica portuguesa*, 32(2), p.103.

Campion, C.R. et al., 2011. Increasing strut porosity in silicate-substituted calcium-phosphate bone graft substitutes enhances osteogenesis. *Journal of biomedical materials research. Part B, Applied biomaterials*, 97(2), pp.245–254.

Camplejohn, K.L. & Allard, S.A., 1988. Limitations of safranin “O” staining in proteoglycan-depleted cartilage demonstrated with monoclonal antibodies. *Histochemistry*, 89(2), pp.185–188.

Cantatore, F.P. et al., 2004. Osteocalcin synthesis by human osteoblasts from normal and osteoarthritic bone after vitamin D3 stimulation. *Clinical rheumatology*, 23(6), pp.490–495.

Caplan, A.I., 1991. Mesenchymal stem cells. *Journal of orthopaedic research*, 9(5), pp.641–650.

Carlisle, E.M., 1972. Silicon: an essential element for the chick. *Science*, 178(4061), pp.619–621.

Carrel, A. & Burrows, M.T., 1911. Cultivation in vitro of malignant tumors. *The Journal of Experimental Medicine*.

Chai, C. & Leong, K.W., 2007. Biomaterials approach to expand and direct differentiation of stem cells. *Molecular therapy : the journal of the American Society of Gene Therapy*, 15(3), pp.467–480.

Chamberlain, G. et al., 2007. Concise Review: Mesenchymal Stem Cells: Their Phenotype, Differentiation Capacity, Immunological Features, and Potential for Homing. *Stem Cells*, 25(11), pp.2739–2749.

Chang, Y.L., Stanford, C.M. & Keller, J.C., 2000. Calcium and phosphate supplementation promotes bone cell mineralization: Implications for hydroxyapatite (HA)-enhanced bone formation. *Journal of biomedical materials research*, 52(2), pp.270–278.

Chen, C.S. & Ingber, D.E., 1999. Tensegrity and mechanoregulation: from skeleton to cytoskeleton. *Osteoarthritis and cartilage*, 7(1), pp.81–94.

Chen, C.S. et al., 2003. Cell shape provides global control of focal adhesion assembly. *Biochemical and Biophysical Research Communications*, 307(2), pp.355–361.

Chen, X.D. et al., 1999. Thy-1 antigen expression by cells in the osteoblast lineage. *Journal of Bone and Mineral Research*, 14(3), pp.362–375.

Chou, Y.-F. et al., 2004. The effect of pH on the structural evolution of accelerated biomimetic apatite. *Biomaterials*, 25(22), pp.5323–5331.

Chung, C.H. et al., 1992. Mechanism of action of beta-glycerophosphate on bone cell mineralization. *Calcified Tissue International*, 51(4), pp.305–311.

Civitelli, R., 2008. Cell-cell communication in the osteoblast/ osteocyte lineage. *Archives of Biochemistry and Biophysics*, 473(2), pp.188–192.

Clark, E.A.E. & Brugge, J.S.J., 1995. Integrins and signal transduction pathways: the road taken. *Science*, 268(5208), pp.233–239.

Combes, C. & Rey, C., 2002. Adsorption of proteins and calcium phosphate materials bioactivity. *Biomaterials*, 23(13), pp.2817–2823.

Courteney-Harris, R.G., Kayser, M.V. & Downes, S., 1995. Comparison of the early production of extracellular matrix on dense hydroxyapatite and hydroxyapatitecoated titanium in cell and organ culture. *Biomaterials*, 16(6), pp.489–495.

Cowles, E.A., Brailey, L.L. & Gronowicz, G.A., 2000. Integrin-mediated signaling regulates AP-1 transcription factors and proliferation in osteoblasts. *Journal of biomedical materials research*, 52(4), pp.725–737.

Crisan, M. et al., 2008. A perivascular origin for mesenchymal stem cells in multiple human organs. *Cell stem cell*, 3(3), pp.301–313.

Curran, J.M., Chen, R. & Hunt, J.A., 2006. The guidance of human mesenchymal stem cell differentiation in vitro by controlled modifications to the cell substrate. *Biomaterials*, 27(27), pp.4783–4793.

D'Angelo, F. et al., 2011. Mechanotransduction: Tuning Stem Cells Fate. *Journal of Functional Biomaterials*, 2(2), pp.67–87.

D'Ippolito, G. et al., 1999. Age-Related Osteogenic Potential of Mesenchymal Stromal Stem Cells from Human Vertebral Bone Marrow. *Journal of Bone and Mineral Research*, 14(7), pp.1115–1122.

Dalby, M.J. et al., 2006. Osteoprogenitor response to semi-ordered and random nanotopographies. *Biomaterials*, 27(15), pp.2980–2987.

Dalby, M.J. et al., 2007. The control of human mesenchymal cell differentiation using nanoscale symmetry and disorder. *Nature Materials*, 6(12), pp.997–1003.

Dallas, S.L. & Bonewald, L.F., 2010. Dynamics of the transition from osteoblast to osteocyte. *Annals of the New York Academy of Sciences*, 1192(1), pp.437–443.

Damen, J.J. & Cate, Ten, J.M., 1992. Silica-induced precipitation of calcium phosphate in the presence of inhibitors of hydroxyapatite formation. *Journal of Dental Research*, 71(3), pp.453–457.

Danen, E.H. et al., 1995. Requirement for the synergy site for cell adhesion to fibronectin depends on the activation state of integrin alpha 5 beta 1. *The Journal of biological chemistry*, 270(37), pp.21612–21618.

Datta, H.K. et al., 2008. The cell biology of bone metabolism. *Journal of Clinical Pathology*, 61(5), pp.577–587.

Davis, G.E.G., 1992. Affinity of integrins for damaged extracellular matrix: alpha v beta 3 binds to denatured collagen type I through RGD sites. *Biochemical and Biophysical Research Communications*, 182(3), pp.1025–1031.

de Jong, W.F., 1926. La Substance Minérale Dans les Os. *Recueil des Travaux Chimiques des Pays-Bas*, 45(6), pp.445–448.

de Peppo, G.M. et al., 2012. Free-form-fabricated commercially pure Ti and Ti6Al4V porous scaffolds support the growth of human embryonic stem cell-derived mesodermal progenitors. *The Scientific World Journal*, 2012, p.646417.

de Peppo, G.M., Sjovall, P., et al., 2010a. Osteogenic Potential of Human Mesenchymal Stem Cells and Human Embryonic Stem Cell-Derived Mesodermal Progenitors: A Tissue Engineering Perspective. *Tissue Engineering Part A*, 16(11), pp.3413–3426.

de Peppo, G.M., Svensson, S., et al., 2010b. Human embryonic mesodermal progenitors highly resemble human mesenchymal stem cells and display high potential for tissue engineering applications. *Tissue Engineering Part A*, 16(7), pp.2161–2182.

De Ugarte, D.A. et al., 2003. Comparison of Multi-Lineage Cells from Human Adipose Tissue and Bone Marrow. *Cells Tissues Organs*, 174(3), pp.101–109.

Dick, H.M. & Strauch, R.J., 1994. Infection of Massive Bone Allografts. *Clinical orthopaedics and related research*, 306, p.46.

Dinopoulos, H., Dimitriou, R. & Giannoudis, P.V., 2012. Bone graft substitutes: What are the options? *The surgeon : journal of the Royal Colleges of Surgeons of Edinburgh and Ireland*.

Docheva, D. et al., 2007. Human mesenchymal stem cells in contact with their environment: surface characteristics and the integrin system. *Journal of cellular and molecular medicine*, 11(1), pp.21–38.

Dominici, M. et al., 2006. Minimal criteria for defining multipotent mesenchymal stromal cells. The International Society for Cellular Therapy position statement. *Cytotherapy*, 8(4), pp.315–317.

Drosse, I.I. et al., 2008. Tissue engineering for bone defect healing: an update on a multi-component approach. *Audio, Transactions of the IRE Professional Group on*, 39 Suppl 2, pp.S9–20.

Ducheyne, P. & Qiu, Q., 1999. Bioactive ceramics: the effect of surface reactivity on bone formation and bone cell function. *Biomaterials*, 20(23-24), pp.2287–2303.

Ducheyne, P., Radin, S. & King, L., 1993. The effect of calcium phosphate ceramic composition and structure onin vitro behavior. I. Dissolution. *Journal of Biomedical Materials Research Part A*, 27(1), pp.25–34.

Duivenvoorden, W., Middleton, A. & Kinrade, S.D., 2008. Divergent effects of orthosilicic acid and dimethylsilanediol on cell survival and adhesion in human osteoblast-like cells. *Journal of Trace Elements in Medicine and Biology*, 22(3), pp.215–223.

Dyson, M., 1983. Stimulation of bone repair by ultrasound. *Ultrasound in medicine & biology*.

Eleniste, P.P. & Bruzzaniti, A., 2012. Focal adhesion kinases in adhesion structures and disease. *Journal of signal transduction*, 2012, p.296450.

Engler, A.J. et al., 2006. Matrix Elasticity Directs Stem Cell Lineage Specification. *Cell*, 126(4), pp.677–689.

Erices, A., Conget, P. & Minguell, J.J., 2000. Mesenchymal progenitor cells in human umbilical cord blood. *British Journal of Haematology*, 109(1), pp.235–242.

Favata, M.F., 1998. Identification of a Novel Inhibitor of Mitogen-activated Protein Kinase Kinase. *Journal of Biological Chemistry*, 273(29), pp.18623–18632.

Feng, J.Q. et al., 2006. Loss of DMP1 causes rickets and osteomalacia and identifies a role for osteocytes in mineral metabolism. *Nature genetics*, 38(11), pp.1310–1315.

Ferris, D.M. et al., 1999. RGD-coated titanium implants stimulate increased bone formation in vivo. *Biomaterials*, 20(23-24), pp.2323–2331.

Filshie, R.J. et al., 1998. MUC18, a member of the immunoglobulin superfamily, is expressed on bone marrow fibroblasts and a subset of hematological malignancies. *Leukemia : official journal of the Leukemia Society of America, Leukemia Research Fund, U.K*, 12(3), pp.414–421.

Fisher, O.Z. et al., 2010. Bioinspired Materials for Controlling Stem Cell Fate. *Accounts of Chemical Research*, 43(3), pp.419–428.

Florence Barrère, C.A.V.B.K. de G., 2006. Bone regeneration: molecular and cellular interactions with calcium phosphate ceramics. *International Journal of Nanomedicine*, 1(3), p.317.

Foster, L.J. et al., 2005. Differential expression profiling of membrane proteins by quantitative proteomics in a human mesenchymal stem cell line undergoing osteoblast differentiation. *Stem Cells*, 23(9), pp.1367–1377.

Franceschi, R.T. & Iyer, B.S., 1992. Relationship between collagen synthesis and expression of the osteoblast phenotype in MC3T3-E1 cells. *Journal of Bone and Mineral Research*, 7(2), pp.235–246.

Franceschi, R.T., Iyer, B.S. & Cui, Y., 2009. Effects of ascorbic acid on collagen matrix formation and osteoblast differentiation in murine MC3T3-E1 cells. *Journal of Bone and Mineral Research*, 9(6), pp.843–854.

Fredholm, Y.C. et al., 2012. Influence of strontium for calcium substitution in bioactive glasses on degradation, ion release and apatite formation. *Journal of the Royal Society, Interface / the Royal Society*, 9(70), pp.880–889.

Fujita, R. et al., 2003. Ultrastructure of ceramic-bone interface using hydroxyapatite and beta-tricalcium phosphate ceramics and replacement mechanism of beta-tricalcium phosphate in bone. *Tissue and Cell*, 35(6), pp.427–440.

Furuse, A., 1989. Volume measuring apparatus and method.

Galmiche, M.C. et al., 1993. Stromal cells from human long-term marrow cultures are mesenchymal cells that differentiate following a vascular smooth muscle differentiation pathway. *Blood*, 82(1), pp.66–76.

Gang, E.J. et al., 2007. SSEA-4 identifies mesenchymal stem cells from bone marrow. *Blood*, 109(4), pp.1743–1751.

Gans, C. & Northcutt, R.G., 1983. Neural Crest and the Origin of Vertebrates: A New Head. *Science*, 220(4594), pp.268–273.

García, A.J. & Reyes, C.D., 2005. Bio-adhesive surfaces to promote osteoblast differentiation and bone formation. *Journal of Dental Research*, 84(5), pp.407–413.

Giancotti, F.G., 1999. Integrin Signaling. *Science*, 285(5430), pp.1028–1033.

Giannoudis, P.V. & Einhorn, T.A., 2009. Bone morphogenetic proteins in musculoskeletal medicine. *Injury*, 40 Suppl 3, pp.S1–3.

Giannoudis, P.V., Dinopoulos, H. & Tsiridis, E., 2005. Bone substitutes: an update. *Injury*, 36 Suppl 3, pp.S20–7.

Gibson, I., Huang, J. & Best, S., 2009. Enhanced in vitro cell activity and surface apatite layer formation on novel silicon-substituted hydroxyapatites. In The 12th International Symposium on Ceramics in Medicine. (pp. 191 - 194).

Gibson, I.R., Best, S.M. & Bonfield, W., 1999. Chemical characterization of silicon-substituted hydroxyapatite. *Journal of Biomedical Materials Research Part A*, 44(4), pp.422–428.

Gimble, J.M. & Guilak, F., 2003. Adipose-derived adult stem cells: isolation, characterization, and differentiation potential. *Cytotherapy*, 5(5), pp.362–369.

Gimble, J.M., Katz, A.J. & Bunnell, B.A., 2007. Adipose-derived stem cells for regenerative medicine. *Circulation research*, 100(9), pp.1249–1260.

Glimcher, M.J., 1984. Recent studies of the mineral phase in bone and its possible linkage to the organic matrix by protein-bound phosphate bonds. *Philosophical transactions of the Royal Society of London. Series B, Biological sciences*, 304(1121), pp.479–508.

Golub, E., 2007. alkaline phosphatase bone essential for mineralisation enzyme that phosphatase - Google Search. *Current Opinion in Orthopaedics*.

Golub, E.E. & Boesze-Battaglia, K., 2007. The role of alkaline phosphatase in mineralization. *Current Opinion in Orthopaedics*, 18, pp.444–448.

Gronthos, S., 2000. Postnatal human dental pulp stem cells (DPSCs) in vitro and invivo. *Proceedings of the National Academy of Sciences*, 97(25), pp.13625–13630.

Gronthos, S. & Zannettino, A.C.W., 2008. *Mesenchymal Stem Cells* D. J. Prockop, B. A. Bunnell, & D. G. Phinney, eds., Totowa, NJ: Humana Press.

Gronthos, S. et al., 1997. Integrin Expression and Function on Human Osteoblast-like Cells. *Journal of Bone and Mineral Research*, 12(8), pp.1189–1197.

Gronthos, S. et al., 2003. Molecular and cellular characterisation of highly purified stromal stem cells derived from human bone marrow. *Journal of cell science*, 116(9), pp.1827–1835.

Gronthos, S. et al., 1994. The STRO-1+ fraction of adult human bone marrow contains the osteogenic precursors. *Blood*, 84(12), pp.4164–4173.

Gronthos, S., Franklin, D.M., et al., 2001a. Surface protein characterization of human adipose tissue-derived stromal cells. *Journal of Cellular Physiology*, 189(1), pp.54–63.

Gronthos, S., Simmons, P.J., et al., 2001b. Integrin-mediated interactions between human bone marrow stromal precursor cells and the extracellular matrix. *Bone*, 28(2), pp.174–181.

Gronthos, S.E.A., 1999. Differential Cell Surface Expression of the STRO-1 and Alkaline Phosphatase Antigens on Discrete Developmental Stages in Primary Cultures of Human Bone Cells. pp.1–10.

Guilak, F. et al., 2004. Adipose-derived adult stem cells for cartilage tissue engineering. *Biorheology*, 41(3-4), pp.389–399.

Guilak, F. et al., 2005. Clonal analysis of the differentiation potential of human adipose-derived adult stem cells. *Journal of Cellular Physiology*, 206(1), pp.229–237.

Gundle, R. & Joyner, C., 1995. Human bone tissue formation in diffusion chamber culture in vivo by bone-derived cells and marrow stromal fibroblastic cells. *Bone*.

Guth, K. & Buckland, T., 2005. Protein adsorption and early osteoblastic behavior on phase pure hydroxyapatite (HA) and silicon substituted hydroxyapatite (SiHA). In 19th European Conference on Biomaterials, Sorrento, Italy.

Guth, K. et al., 2011. Effects of serum protein on ionic exchange between culture medium and microporous hydroxyapatite and silicate-substituted hydroxyapatite. *Journal of Materials Science: Materials in Medicine*, 22(10), pp.2155–2164.

Guth, K., Buckland, T. & Hing, K.A., 2006. Silicon dissolution from microporous silicon substituted hydroxyapatite and its effect on osteoblast behaviour. *Key Engineering Materials*, 309, pp.117–120.

Guth, K., Campion, C., Buckland, T. & Hing, K.A., 2010a. Effect of Silicate-Substitution on Attachment and Early Development of Human Osteoblast-Like Cells Seeded on Microporous Hydroxyapatite Discs. *Advanced Engineering Materials*, 12(1-2), pp.B26–B36.

Guth, K., Campion, C., Buckland, T. & Hing, K.A., 2010b. Surface Physiochemistry Affects Protein Adsorption to Stoichiometric and Silicate-Substituted Microporous Hydroxyapatites U. Krupp, ed. *Advanced Engineering Materials*, 12(4), pp.B113–B121.

Haasters, F. et al., 2009. Morphological and immunocytochemical characteristics indicate the yield of early progenitors and represent a quality control for human mesenchymal stem cell culturing. *Journal of anatomy*, 214(5), pp.759–767.

Habraken, W.J.E.M., Wolke, J.G.C. & Jansen, J.A., 2007. Ceramic composites as matrices and scaffolds for drug delivery in tissue engineering. *Advanced Drug Delivery Reviews*, 59(4-5), pp.234–248.

Hamidouche, Z. et al., 2010. Crosstalks between integrin alpha 5 and IGF2/ IGFBP2 signalling trigger human bone marrow-derived mesenchymal stromal osteogenic differentiation. *BMC Cell Biology*, 11(1), p.44.

Hamidouche, Z. et al., 2009. Priming integrin 5 promotes human mesenchymal stromal cell osteoblast differentiation and osteogenesis. *Proceedings of the National Academy of Sciences*, 106(44), pp.18587–18591.

Hao, J. et al., 2004. Differential expression patterns of the dentin matrix proteins during mineralized tissue formation. *Bone*, 34(6), pp.921–932.

Hay, D.C. et al., 2011. Unbiased screening of polymer libraries to define novel substrates for functional hepatocytes with inducible drug metabolism. *Stem Cell Research*, 6(2), pp.92–102.

Haynesworth, S.E., Baber, M.A. & Caplan, A.I., 1992. Cell surface antigens on human marrow-derived mesenchymal cells are detected by monoclonal antibodies. *Bone*, 13(1), pp.69–80.

Hemler, M.E., 1999. Integrins. In T. Sasaki et al., eds. *Guidebook to the Extracellular Matrix, Anchor, and Adhesion Proteins*. Sambrook and Tooze Publication at Oxford University Press, Oxford, pp. 196–212.

Hench, L.L. et al., 1971. Mechanisms of interfacial bonding between ceramics and bone. *Journal of Biomedical Materials Research Part A*, 2, pp.485–418.

Hersel, U., Dahmen, C. & Kessler, H., 2003. RGD modified polymers: biomaterials for stimulated cell adhesion and beyond. *Biomaterials*, 24(24), pp.4385–4415.

Hing, K A, 2005. Bioceramic bone graft substitutes: influence of porosity and chemistry. *International journal of applied ceramic technology*, 2(3), pp.184–199.

Hing, K A et al., 2004a. Bone development is sensitive to silicon level in substituted apatites. *7th World Biomaterials Congress - 2004*.

Hing, K A et al., 1998. Effect of variation in Ca: P ratio on cellular response of primary human osteoblast-like cells to hydroxyapatite-based ceramics. In BIOCERAMICS-CONFERENCE. BIOCERAMICS- …, pp. 293–296.

Hing, K A et al., 2005. Microporosity enhances bioactivity of synthetic bone

graft substitutes. *Journal of Materials Science: Materials in Medicine*, 16(5), pp.467–475.

Hing, KA et al., 2004b. Silicate substitution alters the progression of bone apposition within porous hydroxyapatite bone graft substitutes. *Trans 50th A Meeting …*.

Hing, Karen A et al., 2001. Influence of Phase Purity on the in Vivo Response to Hydroxyapatite. *Key Engineering Materials*, 192-195, pp.373–376.

Hing, Karin A et al., 2006. Effect of silicon level on rate, quality and progression of bone healing within silicate-substituted porous hydroxyapatite scaffolds. *Biomaterials*, 27(29), pp.5014–5026.

Hing, Karin A, Wilson, L.F. & Buckland, T., 2007. Comparative performance of three ceramic bone graft substitutes. *The spine journal : official journal of the North American Spine Society*, 7(4), pp.475–490.

Huan, Z. & Chang, J., 2009. Novel bioactive composite bone cements based on the beta-tricalcium phosphate-monocalcium phosphate monohydrate composite cement system. *Acta Biomaterialia*, 5(4), pp.1253–1264.

Huang, H. et al., 2003. Enhanced osteoblast functions on RGD immobilized surface. *The Journal of oral implantology*, 29(2), pp.73–79.

Hui, J.H.P. et al., 2005. Comparative Study of the Ability of Mesenchymal Stem Cells Derived from Bone Marrow, Periosteum, and Adipose Tissue in Treatment of Partial Growth Arrest in Rabbit. *Tissue Engineering*, 11(5-6), pp.904–912.

Huibregtse, B.A. et al., 2000. Effect of age and sampling site on the chondro-osteogenic potential of rabbit marrow-derived mesenchymal progenitor cells. *Journal of orthopaedic research : official publication of the Orthopaedic Research Society*, 18(1), pp.18–24.

Hunter, G.K., Kyle, C.L. & Goldberg, H.A., 1994. Modulation of crystal formation by bone phosphoproteins: structural specificity of the osteopontin-mediated inhibition of hydroxyapatite formation. *Biochemical Journal*, 300(Pt 3), p.723.

Hynes, R.O., 1987. Integrins: a family of cell surface receptors. *Cell*, 48(4), p.549.

Im, G.-I., Shin, Y.-W. & Lee, K.-B., 2005. Do adipose tissue-derived mesenchymal stem cells have the same osteogenic and chondrogenic potential as bone marrow-derived cells? *Osteoarthritis and cartilage*, 13(10), pp.845–853.

Ingber, D.E., 2010. From cellular mechanotransduction to biologically inspired engineering: 2009 Pritzker Award Lecture, BMES Annual Meeting October 10, 2009. *Annals of Biomedical Engineering*, 38(3), pp.1148–1161.

Ingber, D.E.D., 2003. Tensegrity I. Cell structure and hierarchical systems biology. *Journal of cell science*, 116(Pt 7), pp.1157–1173.

Jack, A., Emery, P. & McGonagle, D., 2002. Isolation and characterization of bone marrow multipotential mesenchymal progenitor cells. *Arthritis & …*.

Jaiswal, N. et al., 1998. Osteogenic differentiation of purified, culture-expanded human mesenchymal stem cells in vitro. *Journal of Cellular Biochemistry*, 64(2), pp.295–312.

Jenis, L., 2010. Efficacy of silicate-substituted calcium phosphate ceramic in posterolateral instrumented lumbar fusion. *Spine*.

Jenis, L.G. & Banco, R.J., 2008. Clinical and radiographic evaluation of silicate-substituted calcium phosphate ceramic in posterolateral lumbar spinal fusion: one & two year results

. non-published study report prepared by ApaTech. Copyright ApaTech.

Jenis, L.G. & Banco, R.J., CLINICAL AND RADIOGRAPHIC EVALUATION OF SILICATE-SUBSTITUTED CALCIUM PHOSPHATE CERAMIC IN POSTEROLATERAL LUMBAR SPINAL.

Jenis, L.G. & Banco, R.J., Clinical Experience With ActifuseTM Synthetic Bone Graft In Posterolateral Lumbar Fusion.

Johnstone, B. et al., 1998. In vitro chondrogenesis of bone marrow-derived mesenchymal progenitor cells. *Experimental Cell Research*, 238(1), pp.265–272.

Joung, Y.K., Bae, J.W. & Park, K.D., 2008. Controlled release of heparin-binding growth factors using heparin-containing particulate systems for tissue regeneration. *Expert opinion on drug delivery*, 5(11), pp.1173–1184.

Juang, H., 1996. Effect of calcination on sintering of hydroxyapatite. *Biomaterials*, 17(21), pp.2059–2064.

Kalajzic, I. et al., 2004. Dentin matrix protein 1 expression during osteoblastic differentiation, generation of an osteocyte GFP-transgene. *Bone*, 35(1), pp.74–82.

Kalfas, I.H., 2001. Principles of bone healing. *Neurosurgical focus*, 10(4), pp.1–4.

Kamalia, N. et al., 1992. Dexamethasone recruitment of self-renewing osteoprogenitor cells in chick bone marrow stromal cell cultures. *Blood*, 79(2), pp.320–326.

Kannan, S. et al., 2008. Ionic substitutions in biphasic hydroxyapatite and beta-tricalcium phosphate mixtures: Structural analysis by rietveld refinement. *Journal of the American Ceramic Society*, 91(1), pp.1–12.

Kantlehner, M. et al., 2000. Surface coating with cyclic RGD peptides stimulates osteoblast adhesion and proliferation as well as bone formation. *Chembiochem : a European journal of chemical biology*, 1(2), pp.107–114.

Kapur, S., Baylink, D.J. & Lau, K.-H.W., 2003. Fluid flow shear stress stimulates human osteoblast proliferation and differentiation through multiple interacting and competing signal transduction pathways. *Bone*, 32(3), pp.241–251.

Karageorgiou, V. & Kaplan, D., 2005. Porosity of 3D biomaterial scaffolds and osteogenesis. *Biomaterials*, 26(27), pp.5474–5491.

Karlsson, C. et al., 2009. Human embryonic stem cell-derived mesenchymal progenitors—Potential in regenerative medicine. *Stem Cell Research*, 3(1), pp.39–50.

Katagiri, T. & Takahashi, N., 2002. Regulatory mechanisms of osteoblast and osteoclast differentiation. *Oral diseases*, 8(3), pp.147–159.

Keating, J.F. & McQueen, M.M., 2001. Substitutes for autologous bone graft in orthopaedic trauma. *The Journal of bone and joint surgery. British volume*, 83(1), pp.3–8.

Keeting, P.E. et al., 1992. Zeolite A increases proliferation, differentiation, and transforming growth factor beta production in normal adult human osteoblast-like cells in vitro. *Journal of Bone and Mineral Research*, 7(11), pp.1281–1289.

Kern, S. et al., 2006. Comparative Analysis of Mesenchymal Stem Cells from Bone Marrow, Umbilical Cord Blood, or Adipose Tissue. *Stem Cells*, 24(5), pp.1294–1301.

Khoshniat, S. et al., 2011. Phosphate-dependent stimulation of MGP and OPN expression in osteoblasts via the ERK1/ 2 pathway is modulated by calcium. *Bone*, 48(4), pp.894–902.

Kilian, K.A. et al., 2010. Geometric cues for directing the differentiation of mesenchymal stem cells. *Proceedings of the National Academy of Sciences*, 107(11), pp.4872–4877.

Kilpadi, K.L., Chang, P.L. & Bellis, S.L., 2001. Hydroxylapatite binds more serum proteins, purified integrins, and osteoblast precursor cells than titanium or steel. *Journal of biomedical materials research*, 57(2), pp.258–267.

Kim, S R et al., 2003a. Synthesis of Si, Mg substituted hydroxyapatites and their sintering behaviors. *Biomaterials*, 24(8), pp.1389–1398.

Kim, Sinae et al., 2008. In vivo bone formation from human embryonic stem cell-derived osteogenic cells in poly(d,l-lactic-co-glycolic acid)/ hydroxyapatite composite scaffolds. *Biomaterials*, 29(8), pp.1043–1053.

Kim, Sunhwa et al., 2003b. Stat1 functions as a cytoplasmic attenuator of Runx2 in the transcriptional program of osteoblast differentiation. *Genes & Development*, 17(16), pp.1979–1991.

Kolf, C.M., Cho, E. & Tuan, R.S., 2007a. Biology of adult mesenchymal stem cells: regulation of niche, self-renewal and differentiation. *Arthritis research & therapy*, 9(204), p.7.

Kolf, C.M., Cho, E. & Tuan, R.S., 2007b. Mesenchymal stromal cells. Biology of adult mesenchymal stem cells: regulation of niche, self-renewal and differentiation. *Arthritis research & therapy*, 9(1), p.204.

Komori, T., 2010. Regulation of bone development and extracellular matrix protein genes by RUNX2. *Cell and Tissue Research*, 339(1), pp.189–195.

Komori, T., 2006. Regulation of osteoblast differentiation by transcription factors. *Journal of Cellular Biochemistry*, 99(5), pp.1233–1239.

Kossa, von, J., 1901. Ueber die im Organismus künstlich erzeugbaren Verkalkungen. *Beitr Path Anat*, 29, pp.163–202.

Kozhevnikova, M.N., Mikaelyan, A.S. & Starostin, V.I., 2008. Comparative immune-phenotypic and functional characteristics of mesenchymal stromal cells from definitive and transitory hematopoietic organs. 422(1), pp.363–365.

Krane, S.M., 1977. Paget's Disease of Bone. *Clinical orthopaedics and related research*, 127, p.24.

Kulyk, W. & Franklin, J., 2000. ScienceDirect.com - Experimental Cell Research - Sox9 Expression during Chondrogenesis in Micromass Cultures of Embryonic Limb Mesenchyme. *Experimental Cell Research*.

Kumar, D. et al., 2010. Polarization of hydroxyapatite: Influence on osteoblast cell proliferation. *Acta Biomaterialia*, 6(4), pp.1549–1554.

Kurata, K. et al., 2007. Role of mechanically damaged osteocytes in the initial phase of bone remodeling. In International Journal of Fatigue. pp. 1010–1018.

Kuznetsov, S.A. et al., 1997. Single-colony derived strains of human marrow stromal fibroblasts form bone after transplantation in vivo. *Journal of Bone and Mineral Research*, 12(9), pp.1335–1347.

Lange, R.R. et al., 2002. Cell-extracellular matrix interaction and physico-chemical characteristics of titanium surfaces depend on the roughness of the material. *Biomolecular Engineering*, 19(2-6), pp.255–261.

Langstaff, S. et al., 2001. Resorbable bioceramics based on stabilized calcium phosphates. Part II: evaluation of biological response. *Biomaterials*, 22(2), pp.135–150.

Lavery, K. et al., 2009. New insights into BMP-7 mediated osteoblastic

differentiation of primary human mesenchymal stem cells. *Bone*, 45(1), pp.27–41.

LeBaron, R.G. & Athanasiou, K.A., 2000. Extracellular Matrix Cell Adhesion Peptides: Functional Applications in Orthopedic Materials. *Tissue Engineering*, 6(2), pp.85–103.

Legato, Legato™ Synthetic Bone Graft. *pioneersurgical.com*. Available at: http:/ / www.pioneersurgical.com/ index.php?option=com_content&view=article&id=106&Itemid=147 [Accessed July 20, 2012].

LeGeros, R.Z. et al., 2003. Biphasic calcium phosphate bioceramics: preparation, properties and applications. *Journal of Materials Science: Materials in Medicine*, 14(3), pp.201–209.

Li, J.K.-J. et al., 2006. Comparison of ultrasound and electromagnetic field effects on osteoblast growth. *Ultrasound in medicine & biology*, 32(5), pp.769–775.

Lim, J.Y. et al., 2011. Optimizing the osteogenic potential of adult stem cells for skeletal regeneration. *Journal of orthopaedic research*, 29(11), pp.1627–1633.

Lim, S.-M. et al., 2012. RhoA-induced cytoskeletal tension controls adaptive cellular remodeling to mechanical signaling. *Integrative biology : quantitative biosciences from nano to macro*, 4(6), pp.615–627.

Liu, Q. et al., 2008. A comparative study of proliferation and osteogenic differentiation of adipose-derived stem cells on akermanite and beta-TCP ceramics. *Biomaterials*, 29(36), pp.4792–4799.

Liu, X. & Ei-Ghannam, A., 2010. Effect of processing parameters on the microstructure and mechanical behavior of silica-calcium phosphate nanocomposite. *Journal of Materials Science: Materials in Medicine*, 21(7), pp.2087–2094.

Locke, M., Feisst, V. & Dunbar, P.R., 2011. Concise review: human adipose-derived stem cells: separating promise from clinical need. *Stem Cells*, 29(3), pp.404–411.

Lu, Z. & Zreiqat, H., 2010. Beta-tricalcium phosphate exerts osteoconductivity through α2β1 integrin and down-stream MAPK/ ERK signaling pathway. *Biochemical and Biophysical Research Communications*, 394(2), pp.323–329.

Lucarelli, E. et al., 2004. Bone reconstruction of large defects using bone marrow derived autologous stem cells. *Transfusion and apheresis science : official journal of the World Apheresis Association : official journal of the European Society for Haemapheresis*, 30(2), pp.169–174.

M, H., 1974. Plasma Treatment of Solid Materials. In J. R. Hollahan & T. A. Bell, eds. *Techniques and Applications of Plasma Chemistry*. New York: John Wiley and Sons, pp. 113–147.

Mackie, E.J., 2003. Osteoblasts: novel roles in orchestration of skeletal architecture. *The International Journal of Biochemistry & Cell Biology*, 35(9), pp.1301–1305.

Maegawa, N. et al., 2007. Enhancement of osteoblastic differentiation of mesenchymal stromal cells cultured by selective combination of bone morphogenetic protein-2 (BMP-2) and fibroblast growth factor-2 (FGF-2). *Journal of tissue engineering and regenerative medicine*, 1(4), pp.306–313.

Makita, N. et al., 2008. Two of four alternatively spliced isoforms of RUNX2 control osteocalcin gene expression in human osteoblast cells. *Gene*, 413(1-2), pp.8–17.

Malaval, L. et al., 1994. Cellular expression of bone-related proteins during in vitro osteogenesis in rat bone marrow stromal cell cultures. *Journal of Cellular Physiology*, 158(3), pp.555–572.

Malaval, L. et al., 2005. Cellular expression of bone-related proteins during in vitro osteogenesis in rat bone marrow stromal cell cultures. *Journal of Cellular Physiology*, 158(3), pp.555–572.

Malfait, F. et al., 2007. Three arginine to cysteine substitutions in the pro-alpha (I)-collagen chain cause Ehlers-Danlos syndrome with a propensity to arterial rupture in early adulthood. *Human mutation*, 28(4), pp.387–395.

Marie, P.J., 2008. Transcription factors controlling osteoblastogenesis. *Archives of Biochemistry and Biophysics*, 473(2), pp.98–105.

Marie, P.J. & Kassem, M., 2011. Extrinsic mechanisms involved in age-related defective bone formation. *The Journal of clinical endocrinology and metabolism*, 96(3), pp.600–609.

Marinucci, L. et al., 2010. Effects of hydroxyapatite and Biostite on osteogenic induction of hMSC. *Annals of Biomedical Engineering*, 38(3), pp.640–648.

Marsh, J.L., 2003. Principles of bone grafting: non-union, delayed union. *Surgery (Oxford)*, 21(9), pp.213–216.

Mason, C., 2007. Regenerative Medicine 2.0. *Regenerative medicine*, 2(1), pp.11–18.

Massagué, J., 1998. TGF-βsignal transduction. *Annual review of biochemistry*, 67(1), pp.753–791.

Mastrogiacomo, M. et al., 2006. Role of scaffold internal structure on in vivo bone formation in macroporous calcium phosphate bioceramics. *Biomaterials*, 27(17), pp.3230–3237.

Mathews, S. et al., 2012. Extracellular matrix protein mediated regulation of the osteoblast differentiation of bone marrow derived human mesenchymal stem cells. *Differentiation; research in biological diversity*.

Mazziotti, G. et al., 2006. Glucocorticoid-induced osteoporosis: an update. *Trends in endocrinology and metabolism: TEM*, 17(4), pp.144–149.

McBeath, R. et al., 2004. Cell shape, cytoskeletal tension, and RhoA regulate stem cell lineage commitment. *Developmental cell*, 6(4), pp.483–495.

McCauley, L.K. et al., 1996. PTH/ PTHrP receptor is temporally regulated during osteoblast differentiation and is associated with collagen synthesis. *Journal of Cellular Biochemistry*, 61(4), pp.638–647.

McMurray, R., Dalby, M.J. & Gadegaard, N., 2011. Nanopatterned Surfaces for Biomedical Applications. In Biomedical Engineering, Trends in Materials Science, InTech.

McNamara, L.E. et al., 2010. Nanotopographical control of stem cell differentiation. *Journal of tissue engineering*, 2010, p.120623.

Mendes, S.C. et al., 2002. Bone Tissue-Engineered Implants Using Human Bone Marrow Stromal Cells: Effect of Culture Conditions and Donor Age. *Tissue Engineering*, 8(6), pp.911–920.

Mikami, Y. et al., 2008. Dexamethasone promotes DMP1 mRNA expression by inhibiting negative regulation of Runx2 in multipotential mesenchymal progenitor, ROB-C26. *Cell biology international*, 32(2), pp.239–246.

Mitchell, J.B. et al., 2005. Immunophenotype of Human Adipose-Derived Cells: Temporal Changes in Stromal-Associated and Stem Cell–Associated Markers. *Stem Cells*, 24(2), pp.376–385.

Murad, S. et al., 1981. Regulation of collagen synthesis by ascorbic acid. *Proceedings of the National Academy of Sciences of the United States of America*, 78(5), pp.2879–2882.

Murphy, S., Martin, S. & Parton, R.G., 2010. Quantitative analysis of lipid droplet fusion: inefficient steady state fusion but rapid stimulation by chemical fusogens. *PLoS ONE*, 5(12), p.e15030.

Muschler, G.F. et al., 2006. Age-and gender-related changes in the cellularity of human bone marrow and the prevalence of osteoblastic progenitors. *Journal of orthopaedic research*, 19(1), pp.117–125.

Muschler, G.F., Boehm, C. & Easley, K., 1997. Aspiration to obtain osteoblast progenitor cells from human bone marrow: the influence of aspiration volume. *The Journal of bone and joint surgery. American volume*, 79(11), pp.1699–1709.

Muzzarelli, R.A.A., 2009. Chitins and chitosans for the repair of wounded skin, nerve, cartilage and bone. *Carbohydrate Polymers*, 76(2), pp.167–182.

Müller, P. et al., 2007. Calcium phosphate surfaces promote osteogenic differentiation of mesenchymal stem cells. *Journal of cellular and*

molecular medicine, 12(1), pp.281–291.

Nabavi, N. et al., 2011. Effects of microgravity on osteoclast bone resorption and osteoblast cytoskeletal organization and adhesion. *Bone*, 49(5), pp.965–974.

Nair, M.B. et al., 2008. A triphasic ceramic-coated porous hydroxyapatite for tissue engineering application. *Acta Biomaterialia*, 4(1), pp.173–181.

Nakashima, K. et al., 2002. The novel zinc finger-containing transcription factor osterix is required for osteoblast differentiation and bone formation. *Cell*, 108(1), pp.17–29.

NHS, 2012a. Organ Donation and Transplantation - Activity figures for the UK. *organdonation.nhs.uk*. Available at: http:/ / www.organdonation.nhs.uk/ ukt/ statistics/ downloads/ weekly _stats.pdf [Accessed July 9, 2012a].

NHS, 2012b. Osteoporosis - NHS Choices. *nhs.uk*. Available at: http:/ / www.nhs.uk/ conditions/ osteoporosis/ pages/ introduction.asp x [Accessed August 13, 2012b].

Nicoll, S.B.S. et al., 1997. In vitro release kinetics of biologically active transforming growth factor-beta 1 from a novel porous glass carrier. *Biomaterials*, 18(12), pp.853–859.

Nieden, zur, N.I., Kempka, G. & Ahr, H.J., 2003. In vitro differentiation of embryonic stem cells into mineralized osteoblasts. *Differentiation; research in biological diversity*, 71(1), pp.18–27.

Noble, B.S., 2008. The osteocyte lineage. *Archives of Biochemistry and Biophysics*, 473(2), pp.106–111.

Nombela-Arrieta, C., Ritz, J. & Silberstein, L.E., 2011. The elusive nature and function of mesenchymal stem cells. *Nature Publishing Group*, 12(2), pp.126–131.

Nuttall, M.E. et al., 1998. Human trabecular bone cells are able to express both osteoblastic and adipocytic phenotype: implications for osteopenic disorders. *Journal of Bone and Mineral Research*, 13(3), pp.371–382.

Nuttelman, C.R., 2005. *Osteogenic poly(ethylene glycol)-based hydrogels for three-dimensional human mesenchymal stem cell culture and bone regeneration*. Chemical engineering.

Ogose, A. et al., 2006. Histological assessment in grafts of highly purified beta-tricalcium phosphate (OSferion) in human bones. *Biomaterials*, 27(8), pp.1542–1549.

Oh, G.-J. et al., 2010. Sintering behavior and mechanical properties of zirconia compacts fabricated by uniaxial press forming. *The Journal of Advanced Prosthodontics*, 2(3), p.81.

Oh, S. et al., 2009. Stem cell fate dictated solely by altered nanotube

dimension. *Proceedings of the National Academy of Sciences of the United States of America*, 106(7), pp.2130–2135.

Ohgushi, H. et al., 2005. Tissue engineered ceramic artificial joint—ex vivo osteogenic differentiation of patient mesenchymal cells on total ankle joints for treatment of osteoarthritis. *Biomaterials*, 26(22), pp.4654–4661.

Oishi, K. & Ito-Dufros, Y., 2006. Angiogenic potential of CD44+ CD90+ multipotent CNS stem cells in vitro. *Biochemical and Biophysical Research Communications*, 349(3), pp.1065–1072.

Oktar, F.N., 2007. Microstructure and mechanical properties of sintered enamel hydroxyapatite. *Ceramics international*, 33(7), pp.1309–1314.

Olivares-Navarrete, R. et al., 2010. Direct and indirect effects of microstructured titanium substrates on the induction of mesenchymal stem cell differentiation towards the osteoblast lineage. *Biomaterials*, 31(10), pp.2728–2735.

Olivares-Navarrete, R. et al., 2008. Integrin 2 1 plays a critical role in osteoblast response to micron-scale surface structure and surface energy of titanium substrates. *Proceedings of the National Academy of Sciences*, 105(41), pp.15767–15772.

Orciani, M. et al., 2010. Functional characterization of calcium-signaling pathways of human skin-derived mesenchymal stem cells. *Skin pharmacology and physiology*, 23(3), pp.124–132.

Osiris, 2013. Osiris Therapeutics Inc. | Prochymal - The World's First Approved Stem Cell Therapy. *osiris.com*. Available at: http:/ / www.osiris.com/ [Accessed June 18, 2012].

Owen, M., 1988. Marrow stromal stem cells. *Journal of cell science Supplement*.

Palumbo, C., Palazzini, S. & Marotti, G., 1990. Morphological study of intercellular junctions during osteocyte differentiation. *Bone*, 11(6), pp.401–406.

Pampena, D.A. et al., 2004. Inhibition of hydroxyapatite formation by osteopontin phosphopeptides. *Biochem. J*, 378(Pt 3), pp.1083–1087.

Papachroni, K.K. et al., 2009. Mechanotransduction in osteoblast regulation and bone disease. *Trends in Molecular Medicine*, 15(5), pp.208–216.

Park, S. & Oreffo, R., 1999. Interconversion potential of cloned human marrow adipocytes in vitro. *Bone*.

Parry, P.V. & Engh, J.A., 2012. CD90 is Identified as a Marker for Cancer Stem Cells in High-Grade Gliomas Using Tissue Microarrays. *Neurosurgery*, 70(4), pp.N23–4.

Patel, N. et al., 2002. A comparative study on the in vivo behavior of hydroxyapatite and silicon substituted hydroxyapatite granules. *Journal*

of Materials Science: Materials in Medicine, 13(12), pp.1199–1206.

Patel, N. et al., 2005. In vivo assessment of hydroxyapatite and silicate-substituted hydroxyapatite granules using an ovine defect model. *Journal of Materials Science: Materials in Medicine*, 16(5), pp.429–440.

Pattanayak, D.K. et al., 2005. Synthesis and evaluation of hydroxyapatite ceramics. *Trends in Biomaterials and Artificial Organs*, 18(2).

Peister, A., 2004. Adult stem cells from bone marrow (MSCs) isolated from different strains of inbred mice vary in surface epitopes, rates of proliferation, and differentiation potential. *Blood*, 103(5), pp.1662–1668.

Pera, M.F., Reubinoff, B. & Trounson, A., 2000. Human embryonic stem cells. *Journal of cell science*, 113(1), pp.5–10.

Péault, B. et al., 2007. Stem and Progenitor Cells in Skeletal Muscle Development, Maintenance, and Therapy. *Molecular therapy : the journal of the American Society of Gene Therapy*, 15(5), pp.867–877.

Phinney, D.G. et al., 1999. Donor variation in the growth properties and osteogenic potential of human marrow stromal cells. *Journal of Cellular Biochemistry*, 75(3), pp.424–436.

Pietak, A.M. & Sayer, M., 2006. Functional atomic force microscopy investigation of osteopontin affinity for silicon stabilized tricalcium phosphate bioceramic surfaces. *Biomaterials*, 27(1), pp.3–14.

Pietak, A.M. et al., 2007. Silicon substitution in the calcium phosphate bioceramics. *Biomaterials*, 28(28), pp.4023–4032.

Pittenger, M.F., 1999. Multilineage Potential of Adult Human Mesenchymal Stem Cells. *Science*, 284(5411), pp.143–147.

Pockwinse, S.M. et al., 2005. Microtubule-dependent nuclear-cytoplasmic shuttling of Runx2. *Journal of Cellular Physiology*, 206(2), pp.354–362.

Ponader, S., Brandt, H. & Vairaktaris, E., 2008. In vitro response of hFOB cells to pamidronate modified sodium silicate coated cellulose scaffolds. *Colloids and Surfaces B: …*.

Pontier, C. et al., 2001. About the use of stoichiometric hydroxyapatite in compression–incidence of manufacturing process on compressibility. *European journal of pharmaceutics and biopharmaceutics*, 51(3), pp.249–257.

Porter, A.E. et al., 2003a. Comparison of in vivo dissolution processes in hydroxyapatite and silicon-substituted hydroxyapatite bioceramics. *Biomaterials*, 24(25), pp.4609–4620.

Porter, A.E. et al., 2006. The structure of the bond between bone and porous silicon-substituted hydroxyapatite bioceramic implants. *Journal of Biomedical Materials Research Part A*, 78(1), pp.25–33.

Porter, A.E., Botelho, C.M., et al., 2004a. Ultrastructural comparison of

dissolution and apatite precipitation on hydroxyapatite and silicon-substituted hydroxyapatite in vitro and in vivo. *Journal of Biomedical Materials Research Part A*, 69(4), pp.670–679.

Porter, A.E., Patel, N., et al., 2004b. Effect of sintered silicate-substituted hydroxyapatite on remodelling processes at the bone-implant interface. *Biomaterials*, 25(16), pp.3303–3314.

Porter, R.M., Huckle, W.R. & Goldstein, A.S., 2003b. Effect of dexamethasone withdrawal on osteoblastic differentiation of bone marrow stromal cells. *Journal of Cellular Biochemistry*, 90(1), pp.13–22.

Quaglia, F., 2008. Bioinspired tissue engineering: the great promise of protein delivery technologies. *International Journal of Pharmaceutics*, 364(2), pp.281–297.

Rajaraman, G. et al., 2012. Optimization and Scale-up Culture of Human Endometrial Multipotent Mesenchymal Stromal Cells: Potential for Clinical Application. *Tissue engineering. Part C, Methods*.

Ramaswamy, Y. et al., 2008. Biological response of human bone cells to zinc-modified Ca-Si-based ceramics. *Acta Biomaterialia*, 4(5), pp.1487–1497.

Ramos-Ibeas, P. et al., 2012. Maintenance of Pluripotency in Mouse Stem Cells: Use of Hyaluronan in the Long-Term Culture. *Stem Cells and Cancer Stem Cells, Volume 7*, pp.123–133.

Ramsey, W.S. et al., 1984. Surface treatments and cell attachment. *In Vitro Cellular & Developmental Biology-Plant*, 20(10), pp.802–808.

Reffitt, D.M. et al., 2003. Orthosilicic acid stimulates collagen type 1 synthesis and osteoblastic differentiation in human osteoblast-like cells in vitro. *Bone*, 32(2), pp.127–135.

Reid, J.W. et al., 2006. Synthesis and characterization of single-phase silicon-substituted αtricalcium phosphate. *Biomaterials*, 27(15), pp.2916–2925.

Rickard, D.J. et al., 1996. Isolation and characterization of osteoblast precursor cells from human bone marrow. *Journal of Bone and Mineral Research*, 11(3), pp.312–324.

Riquelme, B.D. et al., 2006. A simple method for quantifying high density antigens in erythrocyte membrane by flow cytometry. *Journal of Biochemical and Biophysical Methods*, 68(1), pp.31–42.

Robbins & Cotran, 1974. Tissue Renewal, Regeneration, and Repair. In *Pathologic basis of disease*. ELSEVIER.

Robison, R., 1923. The Possible Significance of Hexosephosphoric Esters in Ossification. *Biochem. J*, 17(2), pp.286–293.

Rodan, G.A., 1992. Introduction to bone biology. *Bone*, 13, pp.S3–S6.

Rodríguez-Lorenzo, L.M., Vallet-Regí, M. & Ferreira, J.M., 2001. Fabrication of hydroxyapatite bodies by uniaxial pressing from a precipitated powder. *Biomaterials*, 22(6), pp.583–588.

Rosa, A.L., Beloti, M.M. & van Noort, R., 2003. Osteoblastic differentiation of cultured rat bone marrow cells on hydroxyapatite with different surface topography. *Dental materials : official publication of the Academy of Dental Materials*, 19(8), pp.768–772.

Rungruang, P., Grady, B.P. & Supaphol, P., 2006. Surface-modified calcium carbonate particles by admicellar polymerization to be used as filler for isotactic polypropylene. *Colloids and Surfaces A: Physicochemical and Engineering Aspects*, 275(1-3), pp.114–125.

Salasznyk, R.M. et al., 2004. Adhesion to Vitronectin and Collagen I Promotes Osteogenic Differentiation of Human Mesenchymal Stem Cells. *Journal of Biomedicine and Biotechnology*, 2004(1), pp.24–34.

Salazar, G.T. & Ohneda, O., 2012. Review of biophysical factors affecting osteogenic differentiation of human adult adipose-derived stem cells. *Biophysical Reviews*, pp.1–18.

Sanchez-Guijo, F.M. et al., 2009. Multiparametric comparison of mesenchymal stromal cells obtained from trabecular bone by using a novel isolation method with those obtained by iliac crest aspiration from the same subjects. *Cell and Tissue Research*, 336(3), pp.501–507.

Schade, V.L. & Roukis, T.S., 2008. Percutaneous bone marrow aspirate and bone graft harvesting techniques in the lower extremity. *Clinics in podiatric medicine and surgery*, 25(4), pp.733–42– x.

Schäffler, A. & Büchler, C., 2007. Concise Review: Adipose Tissue-Derived Stromal Cells—Basic and Clinical Implications for Novel Cell-Based Therapies. *Stem Cells*, 25(4), pp.818–827.

Scherjon, S.A. et al., 2004. Isolation of mesenchymal stem cells of fetal or maternal origin from human placenta. *Stem Cells*, 22(7), pp.1338–1345.

Schimandle, J.H. & Boden, S.D., 1997. Bone substitutes for lumbar fusion:present and future. *Operative Techniques in Orthopaedics*, 7(1), pp.60–67.

Schliephake, H. et al., 2002. Effect of RGD peptide coating of titanium implants on periimplant bone formation in the alveolar crest. An experimental pilot study in dogs. *Clinical oral implants research*, 13(3), pp.312–319.

Schulmerich, M.V., 2008. *Subsurface and transcutaneous Raman spectroscopy, imaging, and tomography*, ProQuest.

Schwarz, K. & Milne, D.B., 1972. Growth-promoting effects of silicon in rats. *Nature*, 239(5371), pp.333–334.

Shapiro, F., 2008. Bone development and its relation to fracture repair. The role of mesenchymal osteoblasts and surface osteoblasts. *European Cells and Materials*, 15, pp.53–76.

Shi, D., 2004. *Biomaterials and Tissue Engineering*, Springer.

Shui, C. et al., 2003. Changes in Runx2/ Cbfa1 expression and activity during osteoblastic differentiation of human bone marrow stromal cells. *Journal of Bone and Mineral Research*, 18(2), pp.213–221.

Siebers, M.C. et al., 2005. Integrins as linker proteins between osteoblasts and bone replacing materials. A critical review. *Biomaterials*, 26(2), pp.137–146.

Sikavitsas, V.I., Temenoff, J.S. & Mikos, A.G., 2001. Biomaterials and bone mechanotransduction. *Biomaterials*, 22(19), pp.2581–2593.

Simmons, P.J. & Torok-Storb, B., 1991a. CD34 expression by stromal precursors in normal human adult bone marrow. *Blood*, 78(11), pp.2848–2853.

Simmons, P.J. & Torok-Storb, B., 1991b. Identification of stromal cell precursors in human bone marrow by a novel monoclonal antibody, STRO-1. *Blood*, 78(1), pp.55–62.

Simmons, P.J. et al., 1994. Isolation, characterization and functional activity of human marrow stromal progenitors in hemopoiesis. *Progress in clinical and biological research*, 389, pp.271–280.

Sims, N.A. & Gooi, J.H., 2008. Bone remodeling: Multiple cellular interactions required for coupling of bone formation and resorption. *Seminars in Cell & Developmental Biology*, 19(5), pp.444–451.

Sinha, A. et al., 2001. Development of calcium phosphate based bioceramics. *Bulletin of Materials Science*, 24(6), pp.653–657.

Sinha, R.K. & Tuan, R.S., 1996. Regulation of human osteoblast integrin expression by orthopedic implant materials. *Bone*, 18(5), pp.451–457.

Sokolsky-Papkov, M. et al., 2007. Polymer carriers for drug delivery in tissue engineering. *Advanced Drug Delivery Reviews*, 59(4), pp.187–206.

Sottile, V., Thomson, A. & McWhir, J., 2003. In VitroOsteogenic Differentiation of Human ES Cells. *Cloning and Stem Cells*, 5(2), pp.149–155.

Steele, J.G. et al., 1993. Polystyrene chemistry affects vitronectin activity: An explanation for cell attachment to tissue culture polystyrene but not to unmodified polystyrene. *Journal of Biomedical Materials Research Part A*, 27(7), pp.927–940.

Stein, G.S., Lian, J.B. & Owen, T.A., 1990. Relationship of cell growth to the regulation of tissue-specific gene expression during osteoblast differentiation. *FASEB journal : official publication of the Federation of*

American Societies for Experimental Biology, 4(13), pp.3111–3123.

Stenderup, K. et al., 2003. Aging is associated with decreased maximal life span and accelerated senescence of bone marrow stromal cells. *Bone*, 33(6), p.919.

Strem, B.M. et al., 2005. Multipotential differentiation of adipose tissue-derived stem cells. *The Keio journal of medicine*, 54(3), pp.132–141.

Sun, Y., Chen, C.S. & Fu, J., 2012. Forcing stem cells to behave: a biophysical perspective of the cellular microenvironment. *Annual review of biophysics*, 41, pp.519–542.

SunMax, SunMax Biotechnology Co., Ltd.-Sunmax Collagen Bone Graft Matrix. *taiwantrade.com.tw*. Available at: http:/ / www.taiwantrade.com.tw/ sunmaxbiotech/ products-detail/ en_US/ 679643 [Accessed July 20, 2012].

Tamai, M., Isama, K. & Nakaoka, R., 2007. Synthesis of a novel b-tricalcium phosphate/ hydroxyapatite biphasic calcium phosphate containing niobium ions and evaluation of its osteogenic properties. *Journal of Artificial Organs*.

Tang, X.L., Xiao, X.F. & Liu, R.F., 2005. Structural characterization of silicon-substituted hydroxyapatite synthesized by a hydrothermal method. *Materials Letters*, 59(29-30), pp.3841–3846.

Tare, R.S. et al., 2012. Isolation, differentiation, and characterisation of skeletal stem cells from human bone marrow in vitro and in vivo. *Methods in molecular biology (Clifton, N.J.)*, 816, pp.83–99.

Tate, M.L.M.K. et al., 2004. The osteocyte. *The International Journal of Biochemistry & Cell Biology*, 36(1), pp.1–8.

Theill, L.E., Boyle, W.J. & Penninger, J.M., 2002. RANK-L and RANK: T cells, bone loss, and mammalian evolution. *Annual review of immunology*, 20, pp.795–823.

Theoleyre, S. et al., 2004. The molecular triad OPG/ RANK/ RANKL: involvement in the orchestration of pathophysiological bone remodeling. *Cytokine & Growth Factor Reviews*, 15(6), pp.457–475.

Thian, E.S. et al., 2007. Silicon-substituted hydroxyapatite: the next generation of bioactive coatings. *Materials Science and Engineering: C*, 27(2), pp.251–256.

Tolar, J., Teitelbaum, S.L. & Orchard, P.J., 2004. Osteopetrosis. *The New England journal of medicine*, 351(27), pp.2839–2849.

Toma, J., Akhavan, M. & Fernandes, K., 2001. Isolation of multipotent adult stem cells from the dermis of mammalian skin. *Nature cell biology*.

Tourniaire, G. et al., 2006. Polymer microarrays for cellular adhesion. *Chemical Communications*, (20), pp.2118–2120.

Toyosawa, S. et al., 2001. Dentin matrix protein 1 is predominantly expressed in chicken and rat osteocytes but not in osteoblasts. *Journal of Bone and Mineral Research*, 16(11), pp.2017–2026.

Tremoleda, J.L. et al., 2008. Bone Tissue Formation from Human Embryonic Stem Cells In Vivo. *Cloning and Stem Cells*, 10(1), pp.119–132.

Valerio, P. et al., 2004. The effect of ionic products from bioactive glass dissolution on osteoblast proliferation and collagen production. *Biomaterials*, 25(15), pp.2941–2948.

van Meekeren, J., 1730. *Heel-en geneeskonstige aenmerkingen*, Amsterdam: Herm. Kentlink.

Verrier, S.S. et al., 2002. Function of linear and cyclic RGD-containing peptides in osteoprogenitor cells adhesion process. *Biomaterials*, 23(2), pp.585–596.

Vico, L., Lafage-Proust, M.H. & Alexandre, C., 1998. Effects of gravitational changes on the bone system in vitro and in vivo. *Bone*, 22(5 Suppl), pp.95S–100S.

Viereck, V. et al., 2002. Differential regulation of Cbfa1/ Runx2 and osteocalcin gene expression by vitamin-D3, dexamethasone, and local growth factors in primary human osteoblasts. *Journal of Cellular Biochemistry*, 86(2), pp.348–356.

Vodyanik, M.A. et al., 2010. A Mesoderm-Derived Precursor for Mesenchymal Stem and Endothelial Cells. *Stem Cell*, 7(6), pp.718–729.

Wang, Y. et al., 2008. Embryonic stem cell-specific microRNAs regulate the G1-S transition and promote rapid proliferation. *Nature genetics*, 40(12), pp.1478–1483.

Washburn, E.W., 1921. Note on a Method of Determining the Distribution of Pore Sizes in a Porous Material. *Proceedings of the National Academy of Sciences of the United States of America*, 7(4), p.115.

Weiner, S. & Traub, W., 1986. Organization of hydroxyapatite crystals within collagen fibrils. *FEBS letters*, 206(2), pp.262–266.

Wheeler, D.L. et al., 2007. Efficacy of silicated calcium phosphate graft in posterolateral lumbar fusion in sheep. *The spine journal : official journal of the North American Spine Society*, 7(3), pp.308–317.

Williams, D.F., 2008. On the mechanisms of biocompatibility. *Biomaterials*, 29(20), pp.2941–2953.

Wolff, J., 1870. Uber die innrer Architektur der knochen und ihre Bedeutung furdie Fragen vom Knochenwachsthum. *Virchows Arch. Path. Anat. Physiol*, 50, pp.389–450.

Wolff, J. & Wessinghage, D., 1991. *Das Gesetz der Transformation der Knochen*, Schattauer.

Wong, J.C.Y. et al., 2010. Definitive endoderm derived from human embryonic stem cells highly express the integrin receptors alphaV and beta5. *Cell adhesion & migration*, 4(1), pp.39–45.

Wu, C. et al., 2008. Incorporation of titanium into calcium silicate improved their chemical stability and biological properties. *Journal of Biomedical Materials Research Part A*, 86A(2), pp.402–410.

Xu, X. et al., 2011. Hydroxylation of recombinant human collagen type I alpha 1 in transgenic maize co-expressed with a recombinant human prolyl 4-hydroxylase. *BMC biotechnology*, 11, p.69.

Xynos, I.D. et al., 2001. Gene-expression profiling of human osteoblasts following treatment with the ionic products of Bioglass® 45S5 dissolution. *Journal of biomedical materials research*, 55(2), pp.151–157.

Yamaguchi, A., Komori, T. & Suda, T., 2000. Regulation of osteoblast differentiation mediated by bone morphogenetic proteins, hedgehogs, and Cbfa1. *Endocrine reviews*, 21(4), pp.393–411.

Yaszemski, M.J. et al., 1996. Evolution of bone transplantation: molecular, cellular and tissue strategies to engineer human bone. *Biomaterials*, 17(2), pp.175–185.

Yavropoulou, M.P. & Yovos, J.G., 2008. Osteoclastogenesis--current knowledge and future perspectives. *Journal of musculoskeletal & neuronal interactions*, 8(3), pp.204–216.

Yoshimura, K. et al., 2006. Characterization of freshly isolated and cultured cells derived from the fatty and fluid portions of liposuction aspirates. *Journal of Cellular Physiology*, 208(1), pp.64–76.

You, L.L. et al., 2008. Osteocytes as mechanosensors in the inhibition of bone resorption due to mechanical loading. *Bone*, 42(1), pp.172–179.

Zhang, X. et al., 2006. Runx2 overexpression enhances osteoblastic differentiation and mineralization in adipose--derived stem cells in vitro and in vivo. *Calcified Tissue International*, 79(3), pp.169–178.

Zhang, X. et al., 2011. The Nell-1 growth factor stimulates bone formation by purified human perivascular cells. *Tissue Engineering Part A*, 17(19-20), pp.2497–2509.

Zhao, G. et al., 2007. Requirement for both micron- and submicron scale structure for synergistic responses of osteoblasts to substrate surface energy and topography. *Biomaterials*, 28(18), pp.2821–2829.

Ziegler, W.H., Liddington, R.C. & Critchley, D.R., 2006. The structure and regulation of vinculin. *Trends in Cell Biology*, 16(9), pp.453–460.

Zimmer, Zimmer News Market Bone Graft Substitute for Spinal Indications. *zimmer.com*. Available at: http:/ / www.zimmer.com/ z/ ctl/ op/ global/ action/ 1/ id/ 196/ templat

e/ MP [Accessed July 20, 2012].

Zippel, N., Schulze, M. & Tobiasch, E., 2010. Biomaterials and Mesenchymal Stem Cells for Regenerative Medicine. *Recent Patents on Biotechnology*, 4(1), pp.1–22.

Ziros, P.G., Basdra, E.K. & Papavassiliou, A.G., 2008. Runx2: of bone and stretch. *The International Journal of Biochemistry & Cell Biology*, 40(9), pp.1659–1663.

Zou, S. et al., 2009. The effects of silicate ions on human osteoblast adhesion, proliferation, and differentiation. *Journal of biomedical materials research. Part B, Applied biomaterials*, 90(1), pp.123–130.

Zuk, P.A. et al., 2001. Multilineage cells from human adipose tissue: implications for cell-based therapies. *Tissue Engineering*, 7(2), pp.211–228.